A comprehensive CRISPR-Cas9 toolkit for *Bacillus subtilis*: development for biomanufacturing applications

by

Adam Westbrook

A thesis
presented to the University of Waterloo
in fulfillment of the
thesis requirement for the degree of
Doctor of Philosophy
in
Chemical Engineering

Waterloo, Ontario, Canada

Examining committee membership

The following served on the Examining Committee for this thesis. The decision of the Examining Committee is by majority vote.

External Examiner	Yen-Han Lin Professor (Chemical Engineering)
Supervisor(s)	C. Perry Chou Professor (Chemical Engineering) Murray Moo-Young Distinguished Professor Emeritus (Chemical Engineering)
Internal Member	William Anderson Professor (Chemical Engineering) Marc Aucoin Associate Professor (Chemical Engineering)
Internal-external Member	Matthew Scott Associate Professor (Applied Mathematics)

Author's Declaration

This thesis consists of material all of which I authored or co-authored: see Statement of Contributions included in the thesis. This is a true copy of the thesis, including any required final revisions, as accepted by my examiners.

I understand that my thesis may be made electronically available to the public.

Statement of Contributions

I am the sole author of Chapters 1-5, 7, and 8.

Chapter 6 was co-authored with Xiang Ren.

Abstract

Bacillus subtilis is a model Gram-positive GRAS organism sought after for its robust growth characteristics in inexpensive media, genetic tractability, and ability to secrete products into the extracellular environment. Although *B. subtilis* has gained widespread acceptance as an industrial workhorse for the production of low-cost enzymes, issues with protein degradation and misfolding, and plasmid instability have hindered its status as a recombinant protein expression host. Efforts aimed at resolving these issues have been partially successful, although strain development to this end has occurred on an insignificant scale relative to *Escherichia coli.* Accordingly, advanced genetic tools are needed to accelerate the progression of *B. subtilis* towards full industrial utility. The recently developed clustered regularly interspaced short palindromic repeat (CRISPR)-Cas9 (CRISPR-associated (protein) 9) system has revolutionized genetic manipulation and genome-scale interrogation of gene function across the spectrum of life. CRISPR-Cas9 systems have been developed for established industrial organisms such as *E. coli* and *Saccharomyces cerevisiae*, and are highly amenable to scalable strain construction. This thesis encompasses the development of a CRISPR-Cas9 toolkit for *B. subtilis*, and its application to strain engineering for the production of value-added biologicals.

We first developed and validated a CRISPR-Cas9 toolkit facilitating simplified genome editing and transcriptional interference in *B. subtilis*. To exploit the simplicity of the Cas9-targeting synthetic guide RNA (gRNA), a novel gRNA transcription cassette was constructed that performed equally well compared with the native CRISPR RNA (crRNA)/*trans*-activating crRNA (tracrRNA) targeting system. To facilitate gRNA eviction and, in turn, continuous editing in the same background, the counter-selectable marker *mazF* was successfully employed. Multiplexing was subsequently evaluated and although efficiency was acceptable, it was deemed

too low to accommodate higher order multiplexing. Consequently, editing templates required for double-strand break (DSB) repair were evaluated to determine optimal homology length (HL) and appropriate format to enhance editing efficiency, and subsequent multiplexing under optimized conditions was highly efficient. Transcriptional interference, i.e. CRISPR interference (CRISPRi), was also demonstrated, resulting in high-level repression of gene expression comparable to that reported for CRISPR-Cas9 systems developed for other organisms.

Upon validating the CRISPR-Cas9 toolkit, we applied CRISPRi to enhance heterologous hyaluronic acid (HA) production in strains of *B. subtilis* via engineering of the cell membrane. Membrane cardiolipin (CL) levels were first enhanced in previously engineered HA-producing strains by overexpressing components of the CL biosynthesis pathway. CRISPRi was then applied to redistribute CL along the lateral membranes of CL-overproducing mutants via repression of the expression of the cell division initiator protein FtsZ, resulting in significant improvements to the HA titer and molecular weight (MW). Moreover, removal of phosphatidylethanolamine and neutral glycolipids from the membrane of HA-producing *B. subtilis* via inactivation of *pssA* and *ugtP*, respectively, has suggested the lipid dependence for functional expression of the hyaluronan synthase from *Streptococcus equisimilis* (SeHAS).

CRISPRi was also applied to reduce the expression of *pfkA* or *zwf*, whose respective gene products are enzymes at the branchpoints of glycolysis and the pentose phosphate pathway opposing cell wall biosynthesis, in HA-producing *B. subtilis*, leading to substantial improvements to the HA titer with a concomitant decrease in the MW. On the other hand, multiplexed repression of both *pfkA* and *zwf* expression resulted in significant increases to the HA titer and modest enhancements to the MW. Moreover, the addition of exogenous HA monomers, i.e. glucuronic acid (GlcUA) and *N*-acetyl-glucosamine (GlcNAc), to *B. subtilis*

cultures markedly improved the HA MW but decreased the HA titer, providing insights into the mechanism of HA biosynthesis by SeHAS in *B. subtilis*.

We also explored the application of hydrocarbons and perfluorocarbons as potential oxygen vectors to address the innate oxygen limitation associated with microbial cultures for HA production. Out of seven compounds evaluated in a preliminary screening, significant improvements to the HA titer and/or cell density were observed in cultures containing *n*-heptane, *n*-hexadecane, perfluoromethyldecalin, and perfluoro-1,3-dimethylcyclohexane. Adjustments to the vector concentration, timing of vector addition, and the agitation rate resulted in further enhancements to the HA titer, and the results suggest that certain vectors may alter the functional expression of SeHAS in *B. subtilis*, and that higher shear rates may be beneficial for HA production.

Finally, the capacity of the toolkit was fully assessed through a second case study in which *B. subtilis* strains were engineered for L-valine overproduction. The native L-valine biosynthetic pathway was engineered to relieve transcriptional and allosteric regulation in the presence of excess amino acids, leading to substantial improvements to the L-valine titer, compared to the wild-type strain. Further investigation revealed that pyruvate availability and competing amino acid biosynthesis limited L-valine overproduction in *B. subtilis*, and strain engineering to simultaneously resolve these bottlenecks resulted in an ~50-fold increase in the L-valine titer, relative to the wild-type strain. Through this case study, recombination was identified as the step that limits toolkit performance, leading to the identification of potential strategies to overcome this limitation.

Collectively, we have developed a comprehensive and highly effective CRISPR-Cas9 toolkit for *B. subtilis*, and have extensively demonstrated its utility for advanced strain engineering in biomanufacturing applications. Moreover, we have developed novel HA-producing strains of *B. subtilis* that may be of industrial value, and have provided valuable insight into the application of oxygen vectors to mitigate oxygen limitation in microbial cultures

for HA production. Lastly, we have tested the limits of our toolkit through the construction of L-valine-overproducing *B. subtilis* strains, resulting in a potentially industrially relevant production platform for this niche amino acid, and identification of the bottleneck limiting toolkit performance. Thus, it is anticipated that the CRISPR-Cas9 toolkit described herein will be an invaluable resource for scalable strain construction at the academic and industrial levels.

Keywords: CRISPR, *Bacillus subtilis*, hyaluronic acid, L-valine, membrane engineering, metabolic engineering, synthetic biology

Acknowledgements

I am eternally grateful to have Professors C. Perry Chou and Murray Moo-Young as my PhD supervisors. Their guidance, support, and wisdom have been absolutely critical for my development as a graduate student and engineer. Professor Chou has bestowed the values of meticulousness, efficiency, and modesty upon me, and I have an immense desire to follow in his footsteps as a true academic in every sense of the word. Professor Moo-Young is a shining example of how the pioneering spirit and devoted work ethic can achieve anything, and I am very fortunate to have been his student.

I am greatly indebted to my committee members – Professors Marc Aucoin and William Anderson from the Department of Chemical Engineering, and Professor Matthew Scott from the Department of Applied Mathematics - for attending my comprehensive examination and defense, and providing valuable feedback on my work. I am also honoured to have Professor Yen-Han Lin from the University of Saskatchewan serve as my external examiner, and am grateful for the time and expertise contributed by him.

I am also grateful for the financial support from the Natural Sciences and Engineering Research Council (NSERC) of Canada, and to the Government of Ontario and University of Waterloo for financial support through the Ontario Graduate Scholarship (OGS) program.

I would also like to acknowledge the hard-working staff and faculty members of the Department of Chemical Engineering, especially Rose Guderian, Judy Caron, Liz Bevan, Ingrid Sherrer, Pauline Ferfolja, Rick Hecktus, Bert Habicher, and Ravindra Singh.

I have been fortunate to work with many personally and professionally supportive colleagues in our research group. In particular, Fan Li and Michael Pyne provided invaluable training and technical discussions that contributed to the development of this thesis, and Xiang

Ren worked tirelessly on our many collaborations together that culminated in this work. I would also like to thank the many diligent co-op students and volunteers that have worked in our laboratory. In particular, Jaewon Oh was an impressively dedicated and talented student with whom I was lucky enough to work with and befriend.

Last, but certainly not least, I thank my Mother and Father for their love, patience, and emotional and financial support. My beloved sister Jennifer whom is my best friend, and has always encouraged and supported me in life and work. Of course, I owe so much to my better half, Huayu, who so understands the long hours spent working and occasional single-mindedness of my academic pursuit. She has made me a stronger person, and I cannot imagine approaching what lies ahead without her by my side.

To my Mother, Father, Jennifer, and Huayu.

Table of Contents

List of figures

List of tables

List of abbreviations

AHAS	acetohydroxy-acid synthase
ALS	acetolactate synthase
asRNA	antisense RNA
BCAA	branched-chain amino acid
2,3-BDO	2,3-butanediol
CL	cardiolipin
CRE	catabolite repression element
CRISPR	clustered regularly interspaced palindromic repeats
CRISPRi	CRISPR interference
DO	dissolved oxygen
DR	direct repeat
DSB	double-stranded break
dsDNA	double-strand DNA
gDNA	genomic DNA
GRAS	Generally Recognized as Safe
HA	hyaluronic acid
HAS	hyaluronan synthase
HPLC	high-performance liquid chromatography
HR	homologous recombination
KD	knock-down
KI	knock-in
KO	knockout
LB	lysogeny broth
MW	molecular weight
ORF	open reading frame
OTR	oxygen transfer rate
OUR	oxygen uptake rate
PAM	protospacer adjacent motif
PPP	pentose phosphate pathway
SeHAS	HAS from *Streptococcus equisimilis*
ssDNA	single-strand DNA
STR	stirred-tank reactor
tracrRNA	trans-activating CRISPR RNA

Chapter 1

Introduction

Industrial bioprocesses centered on microbial hosts often rely on the model organisms *Escherichia coli* and *Bacillus subtilis* due to their well characterized genomes, excellent growth characteristics in inexpensive media, and capacity for high-level protein production [1, 2]. As of 2011, 66 out of 211 biopharmaceuticals receiving regulatory approval in the United States and European Union were produced in *E. coli*, while the remainder were expressed in eukaryotic cell lines [3]. These statistics reflect the continuing dependence on *E. coli* as the default prokaryotic expression host for recombinant therapeutic protein production, despite the fact that *B. subtilis* presents many advantages over its Gram-negative counterpart. *B. subtilis* is capable of growing on a wide range of carbon sources, can readily secrete proteins into the extracellular environment and has been granted a 'Generally Recognized as Safe (GRAS)' designation by the Food and Drug Administration (FDA), USA. In contrast, common industrial *E. coli* strains cannot metabolize cost-effective carbon sources such as sucrose [4], and cells must be disrupted and debris separated from the expressed protein, a limitation that is exacerbated by the release of endotoxins into the product [2]. In addition to possessing desirable traits for protein expression, *B. subtilis* is an ideal candidate for production of biopolymers and biofuels. High-level production of hyaluronic acid (HA), a valuable therapeutic biopolymer, has been achieved with *B. subtilis* in a minimal medium supplemented with sucrose [5], whereas comparatively low titers were obtained with *E. coli* using a rich medium supplemented with glucose and HA precursors [6]. Moreover, *B. subtilis* exhibits improved tolerance to butanol compared to *E. coli* and *Saccharomyces cerevisiae* [7].

In addition to the potential cost savings associated with less expensive media components and simplified downstream product purification, and the ease of regulatory approval due to GRAS status, domesticated strains of *B. subtilis* are amenable to genetic manipulation. Commonly used auxotrophic strains develop a naturally competent state for DNA uptake and, in general, *B. subtilis* contains an efficient recombination system such that genome engineering is relatively straightforward [8]. However, the development of stable industrial strains is lagging behind the efforts applied to *E. coli*, such that certain issues continue to hamper protein expression in *B. subtilis*. Proteolytic degradation and protein misfolding, and limited availability of stable expression vectors have limited the acceptance of *B. subtilis* as a recombinant protein expression host [2, 9], relegating it to the production of low cost industrial enzymes (e.g. proteases and amylase) that are often naturally secreted [2, 10]. Furthermore, advanced genetic tools required for scalable strain development are lagging behind established industrial production hosts such as *E. coli* and *S. cerevisiae* [11, 12].

Currently, markerless genome engineering strategies employed in *B. subtilis* rely on self-evicting counter-selectable markers, e.g. *mazF* [13] and *upp* [14], and site specific recombination systems such as Cre/*loxP* [15] and FLP/*FRT* [16]. While these approaches are appropriate for lab-scale strain construction, they provide low editing efficiencies (in the case of counter-selection alone) and/or are not conducive to multiplexing (i.e. editing multiple targets simultaneously), hindering their application to industrial strain construction. CRISPR (clustered regularly interspaced palindromic repeats)-Cas (CRISPR-associated (proteins)) systems are adaptive prokaryotic viral defense mechanisms first described in *E. coli* in 1987 [17], although more than two decades passed before their function was demonstrated *in vivo* [18]. Identification of the minimal type II CRISPR-Cas9 system of *Streptococcus pyogenes* has significantly

expanded the capacity for genome editing in established industrial workhorses and genetically intractable organisms alike. CRISPR-Cas9 systems have been developed for *E. coli* [19, 20] and *S. cerevisiae* [21, 22], facilitating simple continuous (i.e. sequential) multiplexing in these organisms. In addition, the CRISPR-Cas9 system has been extended to transcriptional modulation (CRISPR interference; CRISPRi) through a catalytically inactive variant of Cas9 (dCas9) [23].

This thesis investigates the development of a CRISPR-Cas9 toolkit for comprehensive genetic engineering of *B. subtilis*, and its application to strain construction for the production of value-added biologicals. The development of CRISPR-Cas9 systems for *E. coli* and *S. cerevisiae* has demonstrated the potential of this technology for industrial strain construction, and the performance of these systems serve as metrics for the evaluation of the toolkit. Once the functionality of the toolkit has been demonstrated, it will be utilized for advanced strain engineering through a case study of HA production to enhance the molecular weight (MW) and titer. As HA production in *B. subtilis* is an industrially important process and central theme of this investigation, the application of potential oxygen vectors to mitigate the inherent oxygen limitation observed in microbial HA production cultures will also be explored. Finally, the toolkit will be applied to a second case study of L-valine overproduction through advanced genome engineering strategies that will test the limits of toolkit performance, while resulting in the construction of potentially industrially useful L-valine-overproducing strains of *B. subtilis.* Collectively, the CRISPR-Cas9 toolkit should be an invaluable tool for the scalable construction of *B. subtilis* strains for biomanufacturing or academic studies of the complex regulatory architecture possessed by this model bacterium. Moreover, this investigation may result in the

generation of novel and industrially relevant strains of *B. subtilis* capable of high-level HA or L-valine production.

1.1 Research objectives

The primary objectives of this research can be described as follows:

1. Develop a CRISPR-Cas9 toolkit for comprehensive engineering of *B. subtilis*. This objective includes the design and construction of all necessary DNA elements and base strains required to implement CRISPR-Cas9 genome editing and CRISPRi in *B. subtilis*, and the evaluation of toolkit performance for single and multiplexed gene mutations and insertions, continuous editing, and transcriptional interference.
2. Apply the toolkit to a case study of heterologous HA production in engineered *B. subtilis*. This objective includes the construction and evaluation of HA-producing control strains used to establish protocols for HA quantification and MW determination, and serve as a baseline with which to compare novel mutants. Employ CRISPRi to alter the distribution of cardiolipin (CL) in the cell membrane to improve the functional expression of the hyaluronan synthase of *Streptococcus equisimilis* (SeHAS), or to divert carbon flux from central metabolic pathways toward cell wall biosynthesis and, in turn, HA production with the ultimate goal of enhancing the HA titer and MW.
3. Evaluate hydrocarbons and perfluorocarbons as potential oxygen vectors to enhance oxygen transfer in cultures of HA-producing *B. subtilis*. This objective includes a preliminary screening of three hydrocarbons and flour perfluorocarbons for their impact on culture performance, and the selection of two or three compounds for further characterization. Assess the effects of vector concentration and timing of addition, and

agitation rate on culture performance, and the influence of vectors on the overall mass transfer coefficient (k_La).

4. Apply the toolkit to a case study of L-valine overproduction in engineered *B. subtilis*. Engineer the native L-valine biosynthetic pathway to relieve various levels of transcriptional and allosteric regulation resulting from the presence of excess amino acids. Investigate potential bottlenecks hindering L-valine overproduction, and combinatorial genome modifications to further improve L-valine overproduction. Establish the limitation(s) of the toolkit.

1.2 Thesis organization

This thesis is comprised of a literature review presented as Chapter 2, and five original research manuscripts corresponding to Chapters 3-7. Chapters 3, 4, and 6 have been published, Chapter 5 has been submitted for publication, and Chapter 7 is in preparation.

Chapter 2 provides a comprehensive summary of five subjects relevant to the development of this thesis: 1) the progress made toward developing *B. subtilis* as a biomanufacturing platform; 2) the development of the naturally competent state for DNA transformation, and markerless genome engineering strategies prior to the advent of CRISPR-Cas9 technology; 3) the functionality of the CRISPR-Cas9 system, and its application to genome editing and transcriptional interference; 4) the function and lipid dependence of streptococcal hyaluronan synthase (HAS), and progress made toward engineering bacteria for heterologous HA production; and 5) the mechanisms by which oxygen vectors enhance mass transfer between gas and aqueous phases, and their application to real and simulated bacterial cultivations.

Chapter 3 outlines the design, construction, and validation of the CRISPR-Cas9 toolkit. Upon construction of the toolkit components, the editing efficiencies of single gene mutations and insertions, and the capacity for continuous editing and multiplexing were evaluated. Editing template homology length size and type were subsequently investigated, leading to significant improvements to multiplexing efficiency, and transcriptional interference via dCas9 (i.e. CRISPRi) was demonstrated with high efficiency.

Chapter 4 details the construction and culture performance of HA-producing strains of *B. subtilis* in which the membrane CL content and spatial distribution have been altered to improve the functional expression of SeHAS. Significant improvements to the HA titer and MW were obtained, indicating that engineering of the cell membrane is an effective approach to enhance heterologous HA production in *B. subtilis* expressing HAS from group C streptococci.

Chapter 5 outlines the construction and culture performance of HA-producing strains of *B. subtilis* in which carbon flux was diverted from central metabolism into HA biosynthesis. CRISPRi was employed to reduce the expression of enzymes at the branch points of the pentose phosphate pathway (PPP) and glycolysis with cell wall biosynthesis to increase carbon flux through the HA biosynthetic pathway (i.e. an extension of cell wall biosynthesis). This metabolic engineering strategy resulted in significant improvements to the HA titer and modest enhancements to the MW.

Chapter 6 investigates hydrocarbons and perfluorocarbons as potential oxygen vectors to improve mass transfer in HA production cultures. After a preliminary screening of seven compounds, *n*-heptane, *n*-hexadecane, and perfluoromethyldecalin were selected for further characterization based on their relative cost and impact on culture performance. Manipulating

culture parameters led to further improvements to the HA titer, and provided insight into the effect of certain vectors on the functional expression of SeHAS.

Chapter 7 outlines the construction and culture performance of L-valine-overproducing strains of *B. subtilis*. The native L-valine biosynthetic pathway was engineered to relieve transcriptional and allosteric regulation in amino acid-containing medium, resulting in significantly improved L-valine production compared to the wild-type strain. Moreover, potential bottlenecks limiting L-valine overproduction in *B. subtilis* are identified, leading to markedly enhanced culture performance.

Lastly, Chapter 8 provides a summary of the work performed throughout the entirety of this thesis. Recommendations and potential avenues for future research are provided as a guide to further enhance toolkit performance, and improve the production capacity of HA-producing and L-valine-overproducing strains developed herein.

Chapter 2

Literature review

2.1 Developing *B. subtilis* as a biomanufacturing platform

B. subtilis is a rod-shaped endospore-forming soil bacterium which has been extensively studied, leading to its status as the model Gram-positive organism [24]. The naturally competent state developed by domesticated strains, presence of an efficient recombination system, and development of replicating *E. coli-B. subtilis* shuttle vectors led to the early application of recombinant DNA technology in *B. subtilis*. However, issues with protein and plasmid instability have limited the use of *B. subtilis* to academic pursuits, or production of inexpensive industrial enzymes (most of which are endogenous or are native to other *Bacillus* species) [2, 10].

2.1.1 Strategies for enhancing recombinant protein expression

Much has been accomplished in addressing extracellular proteolysis in *B. subtilis* cultures. In an early study, the disruption of genes expressing extracellular neutral (*nprE*) and serine (*aprE*) proteases resulted in a 97% reduction in extracellular protease activity (strain DB104) relative to the parental strain (DB101), with the *aprE* mutation accounting for 61% of the reduction in activity [25]. Further efforts to reduce proteolysis in *B. subtilis* cultures resulted in strain WB800 (Δ*nprE*, Δ*nprB*, Δ*aprE*, Δ*epr*, Δ*mpr*, Δ*bpr*, Δ*vpr*, Δ*wprA*) which possesses less than 0.5% of the extracellular protease activity of DB101 [26]. However, mutation (or knockout; KO) of *nprE* and *aprE* resulted in a 5-fold increase in the extent of cell lysis in DB104 (relative to *B. subtilis* 168) upon entry to stationary phase [27] (combined mutations to *nprB*, *epr*, *mpr*, and *bpr* had a marginal effect on lysis), demonstrating that these proteases play a major role in regulating autolytic proteins. The severe cell lysis observed is a concern when expressing

recombinant proteins as intracellular proteases are released (along with other internal molecules), potentially causing product degradation and contamination.

Protein misfolding (i.e. inclusion body formation) has been addressed in a few studies in which native molecular chaperones (i.e. the GroEL/ES complex and DnaK) were coexpressed with single chain antibody (SCA) fragments leading to marked improvements in expression of functional SCA fragments. Mutation of *hrcA*, encoding a common repressor of both the *groES-groEL* and *dnaK* (*grpE-dnaK-dnaJ-prmA-rsmE-mtaB*) operons, and combined overexpression of the extracytoplasmic molecular chaperone *prsA* resulted in significant improvements to functional expression of both antidigoxin [28] and MH-1 (fibrin-specific monoclonal antibody) [26] SCA fragments in protease deficient strains (*wprA* mutation was required in the latter case). However, the resources invested in establishing *B. subtilis* as a recombinant protein expression host pale in comparison to the decades spent developing *E. coli* as the preeminent bacterium for protein expression [29].

2.1.2 The development of [conditionally] stable expression vectors

The establishment of stable replicating vectors has been a significant challenge in *B. subtilis*. Segregational instability (i.e. the loss of the plasmid from the cell) and structural instability (i.e. rearrangements in the plasmid sequence) of replicating plasmids has been widely reported [30-33], and has been largely attributed to the mode of replication. The rolling circle method of replication entails nicking of the sense origin of replication (Sori) by a plasmid-encoded replication protein, leaving a 3'–OH group used as a primer for leading strand synthesis [34]. The newly synthesized sense strand and parental antisense RNA (asRNA) strand form a double-strand DNA (dsDNA) replicate, leaving the displaced parental sense strand behind as a

single-strand DNA (ssDNA) intermediate [35]. The ssDNA intermediate poses several issues: 1) the asRNA ori (ASori) present on the displaced strand (required for conversion to dsDNA) is not entirely compatible between organisms potentially leading to accumulation of the ssDNA intermediate [32]; 2) recombination is strongly stimulated between direct repeats (DRs) as short as 9 base pairs (bp) in ssDNA intermediates (particularly when DRs flank inverted repeats) causing structural instability [30, 31]; and 3) the resulting unstable ssDNA structures lead to the accumulation of high MW linear DNA that impedes host fitness [30].

The theta mode of replication entails melting of the parental plasmid strands and coupled continuous and discontinuous synthesis of the leading and lagging strands, respectively, such that ssDNA intermediates are avoided, and segregational and structural stability are significantly improved [34]. Theta-replicating vectors have been isolated from strains of *B. subtilis* [36-38], and one in particular (i.e. pBS72) has been used to construct the pHT *E. coli-B. subtilis* shuttle vector series for stable protein expression [9, 39]. Subsequent optimization of promoter elements led to pHT vectors which can facilitate protein expression levels reaching 30% of total cellular protein [40], which is still moderate compared to protein fractions obtained in *E. coli* (up to 50%) [41]. Unfortunately, the stability of theta-replicating vectors is dependent on the effect on host fitness imposed by the proteins expressed [42], which has also been observed by us when expressing recombinant proteins required for HA production. Accordingly, more effort is required to elucidate the complex regulatory architecture of this organism to enable inactivation or stimulation of stress responses that may affect genetic stability [43].

2.2 Genetic manipulation in *B. subtilis*

2.2.1 Transition to the naturally competent state

Most commonly used strains of *B. subtilis* are derivatives of strain 168, the first auxotrophic strain (unable to synthesize tryptophan) observed to be naturally competent [44]. The competent state develops in a fraction of the cell population (5-20%) at the end of exponential growth [8, 45] through a complex regulatory network initiated by the competence transcription factor ComK [45, 46]. During exponential growth, the repressor MecA binds to ComK inhibiting its activity. The competence quorum-sensing mechanism is activated late in exponential growth by a downshift in nutrient availability, inducing expression of the derepressor ComS [47, 48]. ComS binds to MecA, releasing ComK which results in upregulated expression of more than 100 genes [45, 46]. As many of these genes are not required for transformation, it was proposed that competence is only one aspect of the physiological state induced by ComK, which was speculated to be a global adaptation to stress (termed the K-state) enabling repair of cellular DNA and acquisition of new genetic elements to enhance cell fitness [45, 49]. Nonetheless, genes involved in the synthesis of DNA transport machinery (i.e. the *comE*, *comF*, and *comG* operons and *comC*), and those involved in DNA metabolism, repair and recombination (e.g. *nucA*, *addAB* and *recA*) are upregulated by ComK [45, 46, 50, 51].

2.2.2 DNA uptake and fate in the cytosol

DNA transport begins with binding of dsDNA to the cell surface via ComEA and subsequent fragmentation by the endonuclease NucA [52]. DNA accessibility to ComEA relies on the pseudopilins ComGC (the major ComG pseuodpilin), ComGD, ComGE and ComGG which are believed to modify the cell wall (perhaps by opening channels) exposing ComEA [53]. ComGA is an ATPase required for assembly of the ComG pseudopilus (and binding of DNA to the cell), and prevents cell growth and division during competence prior to ComK depletion [54].

In addition, ComC, a prepilin peptidase, and BdbD and BdbC (protein oxidoreductases) are required for ComG pseudopilus maturation [52]. Once bound by ComEA and fragmented by NucA, the dsDNA is converted to ssDNA by an unknown enzyme, and one strand is translocated into the cytosol (the other is degraded and released from the cell) through the ComEC membrane permease [55], a process mediated by the ATPase ComFA [56]. The DNA uptake machinery appears to be static, localizing at the cell poles, with the exception of ComEA which can colocalize with the stationary uptake apparatus or remain mobile [55]. It is believed that the mobility of ComEA enables DNA capture for later transport to the cytosol [55], although the static nature of the ComG pseudopilus required for DNA binding to ComEA complicates the matter. Another explanation for ComEA mobility is saturation of polar ComEA binding sites due to its abundance relative to other uptake proteins [54], or perhaps the ComG pseudopilus causes a global shift in cell wall structure to enable uniform DNA binding across the membrane for delayed transport to the cytosol.

Once ssDNA reaches the cytosol, ssDNA binding proteins (i.e. SsbA or SsbB) protect it from exonucleolytic degradation. SsbA and SsbB perform similar functions in the recruitment of the primary recombination protein RecA to ssDNA via mediators RecO and DprA through independent pathways [57, 58]. DprA and RecO are important factors in homologous recombination (HR) as they facilitate RecA filamentation onto protein-coated ssDNA, modulate RecA-mediated strand exchange, and promote annealing of complementary DNA strands [57-59]. It is believed that the path taken for HR depends largely on which protein (i.e. SbsA or SbsB) is bound to the incoming ssDNA [57], with DprA and RecO preferentially interacting with SsbB- and SsbA-bound ssDNA, respectively [57, 58]. SsbA and SsbB protect transformed ssDNA from degradation, remove DNA secondary structure, prevent unnecessary binding of

RecA to ssDNA, and enable DprA/RecO-mediated single-strand annealing (SSA) by RecA [58, 60]. *In vitro* experiments indicate that RecA-ATP (ATP is a cofactor for RecA although dATP is preferred) will nucleate and polymerize onto naked ssDNA, albeit with low efficiency, and ultimately catalyze strand exchange [61]. However, SsbA-ssDNA and SsbB-ssDNA complexes are unavailable to RecA [60, 61], which requires either a RecO-ssDNA-SsbA or RecO-SsbA-ssDNA-SsbB complex to efficiently carry out its functions [60]. The same concept applies to DprA except that it preferentially associates with SsbB, and either RecO or DprA can mediate RecA-ATP nucleation of the SsbA-ssDNA-SsbB complex [57].

2.2.3 Transformation and markerless recombineering strategies

The preferred method of DNA transformation in *B. subtilis* is via natural competence, although other methods are employed such as protoplast transformation, electroporation, transduction, and conjugation depending on strain compatibility. Transformation of genomic DNA (gDNA), a highly efficient process known as congression, is commonly performed to transfer genetic markers between isogenic strains, and is particularly useful for natural transformation of poorly transformable strains [8]. High efficiency transformation of *B. subtilis* for chromosomal integration ($\geq 10^3$ colony forming units [CFU] μg^{-1} DNA) has been reported using natural competence, for example [15, 62, 63], and artificially induced competence by overexpression of ComK [64], or coexpression of ComK and ComS [65]. Integration cassettes minimally consist of a selection marker flanked by two homology lengths (HL) corresponding to a target in the chromosome, facilitating HR by a double cross-over integration event. Single cross-over integration events also occur by a Campbell-like mechanism, however, these insertions are significantly less stable resulting in spontaneous chromosomal pop-out [66].

Integration cassettes are often constructed as plasmids which replicate in *E. coli* (for cloning purposes) but not in *B. subtilis*, ensuring that transformation results in HR [8]. Transformation can also be achieved with PCR products, although efficiency is expectedly higher for linearized plasmids [64]. Transformation efficiency is highly dependent on HL size [15] and a minimum length of 400-500 bp is thought to be a requirement for double cross-over recombination to occur in *B. subtilis* [14].

The flexibility afforded by markerless genome engineering strategies is essential for the development of laboratory and commercial strains. A common approach has been the application of counter-selectable markers, such as *upp* [14, 64], *blaI* [67] and *mazF* [13], flanked by short direct repeats (DR) to promote auto-eviction of the selection/counter-selection cassettes by single-crossover recombination. *upp* encodes a uracil-phosphoribosyltransferase, which converts uracil to UMP, and can also metabolize the toxic pyrimidine analog 5-fluorouracil (5FU) into 5-fluoro-dUMP, a potent inhibitor of the thymidylate synthetase [14]. [14]. A cassette composed of *upp* and a selection marker (Phleo^R, imparting phleomycin resistance) flanked by two DRs was cloned between HLs, yielding a HL5'-DR-*upp*-Phleo^R-DR-HL3' counter-selectable integration cassette (designated as *upp*-CS). In an *upp* null background, the *upp*-CS cassette was transformed into *B. subtilis* yielding a Phleo^R, 5FU sensitive (5FU^S) strain with the desired mutation. Subsequent growth in non-select (i.e. antibiotic-free) media for ~24 h enables automatic eviction of the *upp*-CS cassette, yielding Phleo^S, 5FU^R colonies (at low 5FU concentration, 10 μM) [14]. Similarly, the promoter of *lysA*, encoding a diaminopimelate decarboxylase needed for lysine synthesis in *B. subtilis*, was replaced with the *blaP* (encoding β-lactamase) promoter (P_{blaP}) from *Bacillus licheniformis*, and *blaI* (encoding the repressor of P_{blaP}) was used as the counter-selectable marker (cells having lost the *blaI*-CS cassette were

selected on lysine deficient minimal media) [67]. *mazF*, an endoribonuclease and part of the *mazEF* toxin-antitoxin module from *E. coli*, was applied as an inducible counter-selectable marker (i.e. cells having lost the *mazF*-CS cassette were resistant to the inducer) using the same approach [13], and has the distinct advantage of requiring no conditional genetic background. While these methods are simple to use, the editing efficiencies are relatively low (25-50% of counter-selected mutants lose the selection marker) and conditional genetic backgrounds are required in most cases. Site-specific recombination via the Cre/*loxP* [15] and FLP/*FRT* [16] systems has also been successfully applied to markerless recombineering in *B. subtilis* with a generally higher efficiency (~90%) than self-evicting counter-selection cassettes. The viral Cre recombinase catalyzes reciprocal site-specific recombination between two *loxP* sites in the absence of any host cofactors or accessory proteins, excising DNA sequences internal to the convergently oriented *loxP* sites [15]. A selection marker (e.g. Spc^R, imparting spectinomycin resistance) flanked by mutant *lox* sites (*lox71*/*lox66*) was cloned between HLs yielding a HL5'-*lox77*-Spc^R-*lox66*-HL3' cassette [15]. Chromosomally expressed Cre was induced to evict the Spc^R cassette, leaving behind a poorly recognized double mutant *lox72* site, which minimizes chromosomal instability in the presence of Cre. The FLP/*FRT* recombination system (*S. cerevisiae*) was applied in a similar manner [16], and while mutant *FRT* sites have been established [68], they are often not applied due to the low frequency of unwanted recombination events [69]. Additionally, ssDNA recombineering mediated by the λ-Red phage β-recombinase of *E. coli*, for which the Cre/*loxP* system and counter-selectable hen egg white lysozyme (*hewl*) were used in combination to enhance marker eviction frequency, provided a high editing efficiency [70]. However, site-specific recombination systems are not particularly conducive to

multiplexing given the requirement for multiple selection (and potentially counter-selection) markers and the subsequent tedious screening needed to confirm their absence.

2.3 CRISPR-Cas9 as a powerful tool for genome editing and transcriptional modulation

CRISPRs were originally observed in *E. coli* and had been described as a series of short DRs separated by 32 bp inserts [17]. Early predictions were made about the possible role of CRISPR-Cas systems in DNA repair [71] or gene regulation [72]. However, subsequent studies revealed that spacer sequences matched those of viral genomes and plasmids, and that *cas* genes encode proteins with putative helicase and nuclease domains [73, 74], leading to the concept that CRISPR-Cas systems might be an adaptive defense mechanism in which asRNAs serve as record of prior invasions. Their function was demonstrated experimentally by bacteriophage challenge of a WT strain of *Streptococcus thermophilus* possessing CRISPR loci, resulting in phage-resistant mutants in which additional spacers bearing complementarity to the invading phage DNA were acquired [18]. Type I, II, and III CRISPR-Cas systems have been identified (each containing multiple subsets), and are highly diverse in genetic structure (i.e. sequences of CRISPR repeats and *cas* genes, and *cas* operon arrangement) and mechanism (i.e. RNA processing, RNA-protein assembly, and targeting) [75], although the basic process of spacer acquisition to achieve immunity is conserved [76]. The type II CRISPR-Cas9 system derived from *S. pyogenes* has been extensively characterized and exploited for genetic engineering due to its simplicity relative to other identified CRISPR-Cas systems [77].

2.3.1 Functionality of the CRISPR-Cas9 system

In the CRISPR-Cas9 system (as in other type II systems), CRISPR arrays (CRISPRa) containing target-specific protospacers flanked by short DRs are transcribed as immature CRISPR-targeting RNAs (pre-crRNAs). A trans-activating crRNA (tracrRNA) is also transcribed and forms a duplex with the pre-crRNA via complementarity to the DRs. To target Cas9, the pre-crRNA/tracrRNA duplex must be processed by host endoribonuclease RNase III [78], a process requiring Cas9 to presumably bind and position the duplex to enable cleavage [76]. Cas9 remains bound to the mature crRNA/tracrRNA duplex after cleavage by RNase III [79], yielding a catalytically active Cas9-RNA complex due to conformational changes in Cas9 upon RNA binding [80] (*apo*-Cas9 will bind, but not cleave, DNA non-specifically [81]). In type I and II systems, site-specific binding and cleavage occur based on complementary base-pairing between the target and protospacer, and the presence of a recognition sequence adjacent to the 3' end of the base pairing region known as the protospacer adjacent motif (PAM) [79]. The PAM site (NGG for *S. pyogenes* Cas9) is located on the non-targeting strand, i.e. the strand opposite to that which complements the protospacer, and is not included in the protospacer sequence. Cas9-RNA target location occurs through random three-dimensional collisions with DNA, and targeting proceeds through binding of PAM sites and interrogation of adjacent DNA for protospacer complementarity [81]. A fully complementary 12 bp seed region at the 3' end of the protospacer is necessary for efficient Cas9-RNA binding and cleavage of the target [82], and mismatches in the two bp adjacent to the PAM site results in complete loss of Cas9-RNA activity [81]. Unwinding of the dsDNA target by Cas9-RNA begins at the PAM site and proceeds toward the distal end of the base pairing region [81]. Base pairing between the protospacer and target strand generates a RNA-DNA duplex, facilitating R-loop formation for Cas9 cleavage [83]. Cas9 contains two nuclease domains responsible for cleavage of respective DNA stands: the HNH-

and RuvC-like domains cleave the target and non-target strands, respectively [79, 80]. The end result is a blunt-ended double-stranded break (DSB) in the target DNA three bp upstream of the PAM site (Figure 2.1). The high specificity of CRISPR-induced DSBs enables efficient selection of mutants that evade DNA cleavage via HR of exogenous donor DNA, or editing templates. More recently, the synthetic guide RNA (gRNA) comprised of a protospacer, a Cas9-binding hairpin (CBH) and a transcriptional terminator has been used in place of the native targeting crRNA/tracrRNA duplex, further simplifying application of the CRISPR-Cas9 system [79].

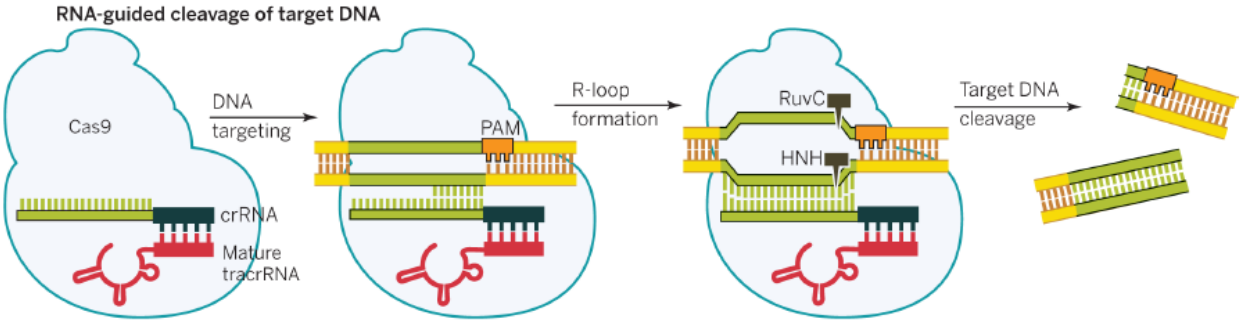

Figure 2.1. DNA cleavage by Cas9 with the crRNA/tracrRNA duplex. Adapted from [77].

2.3.2 Application of the CRISPR-Cas9 system to genome editing

The CRISPR-Cas9 system has been widely adopted for genome editing as Cas9 is the only Cas protein required for DNA targeting and cleavage (a common feature of type II systems), and Cas9 recognizes a short PAM sequence increasing the number of potential targets in a given genome. At around the same time, genome editing in human cell lines was reported in two independent studies [84, 85]. Using a human-codon optimized version of Cas9 (*S. pyogenes*) targeted by gRNAs, the activity of a chromosomally inserted inactive green fluorescent protein (GFP) was restored in human embryonic kidney cells (HEK293T) by HR of an exogenous editing template, with editing efficiencies of up to 8% [84]. In the same study, multiplexing was

demonstrated by targeting two sites (separated by 19 bp) in the AAVS1 locus, resulting in excision of the internal sequence and repair by nonhomologous end joining (NHEJ). In addition, an integration cassette containing functional GFP was delivered to the AAVS1 locus although efficiency was not reported. Similar observations were made in the other study, in which the functionality of a human-compatible version of Cas9 derived from *S. thermophiles* was also verified, although gRNA performance was inferior to the native crRNA/tracrRNA duplex [85]. At the same time, the CRISPR-Cas9 system was first applied to bacterial genome editing in *Streptococcus pneumoniae* and *E. coli* [82]. gDNA was isolated from *S. pneumoniae* strain crR6, which contains the heterologous CRISPR-Cas9 system from *S. pyogenes* that targets a sequence in bacteriophage ϕ8232.5 (*S. pyogenes*), and transformed by congression into two strains bearing either the intact viral target sequence ($R6^{8232.5}$), or the sequence carrying a mutation in the PAM site ($R6^{370.1}$) inserted to the *srtA* locus. Unexpectedly [at the time], a small number of $R6^{8232.5}$ mutants survived CRISPR-mediated cleavage by acquisition of the WT *srtA* gene by a double cross-over recombination event. In the same study, plasmids expressing Cas9 (pCas9) and the CRISPRa (pCRISPR) were used for ssDNA recombineering in *E. coli* strain HME63, which expresses the λ-Red γ, β and exo proteins, resulting in an editing efficiency of 65%. These were the first demonstrations that simultaneous transformation of CRISPR-Cas9 machinery and an editing template for DSB repair (or avoidance if HR happens first) could result in the selection of mutants with a desired mutation in the absence of a selectable marker.

Subsequent systems developed for *E. coli* and *S. cerevisiae* focused on enhancing continuous multiplexing capability for scalable strain construction. In a two plasmid system designed for *E. coli*, the λ-Red system, Cas9 (*S. pyogenes*) and an inducible gRNA targeting the pMB1 ori (pMB1-gRNA) were constructed in a vector containing a temperature sensitive ori

(pCas), while the gRNA(s) and editing template(s) were included in a second plasmid containing a pMB1 ori (pTargetT) [20]. High multiplexing efficiency was obtained for two KOs (*maeA* and *maeB*; 97%), although efficiency dropped markedly for three simultaneous mutations, likely due to the third target selected (*cadA*; discussed in section 4.1.7). High editing efficiency was also obtained for insertions up to 4.5 kb (75%). Elimination of the pTargetT vectors was accomplished by induction of the pMB1-gRNA and pCas was eliminated via growth at a non-permissive temperature. However, inclusion of the editing templates in the pTargetT vectors limited the capacity of the system to three simultaneous KOs due to complications with cloning. A subsequent study employed a similar plasmid system except that editing templates were delivered as independent linear fragments [19]. High editing efficiencies were obtained for dual KOs (83%) with ssDNA, and single dsDNA insertions (or knock-ins; KI) up to 3 kb (≥59%). A system developed for *S. cerevisiae* made use of an ultrahigh copy vector to express all CRISPR-Cas9 elements, including the editing template which was constructed as part of the CRISPRa [22]. High multiplexing efficiency was obtained (up to 100% depending on PAM site selection) for up to three targets, although four days of continuous growth was required to achieve acceptable efficiency. In addition, a counter-selectable marker was included in the single plasmid system, although the capacity of the system for continuous editing was not evaluated. Finally, a subsequent study employed gap repair, a form of *in vivo* HR in which plasmids are constructed by simultaneously transforming inserts bearing homology to a plasmid backbone (all linear components), for gRNA delivery, achieving multiplexing efficiencies of 64 and 27% for three and five KOs, respectively, in *S. cerevisiae* [21]. Moreover, a total of 11 genes were simultaneously inserted (via six editing templates) across three genomic loci (requiring nine recombination events) with an editing efficiency of 4.2%, resulting in a muconic acid producing

strain. Only one day of growth after transformation was required in this system, although editing template HLs were 10-fold longer than those used in the prior study in *S. cerevisiae* [22]. Cas9 was chromosomally expressed and editing templates were transformed as individual fragments. Beyond the aforementioned work, the CRISPR-Cas9 system has proven an indispensable tool for simple and precise genome editing in bacteria [86-89], yeast [90] and higher eukaryotes, for example [91-94].

Table 2.1. Summary of CRISPR-Cas9 systems developed for *E. coli* and *S. cerevisiae*

Organism	Cas9 expression	gRNA or crRNA\tracrRNA	KI efficiency (%) / insert size (kb)	KO efficiency (%) / no. targets	editing template format / HL (bp)	Ref.
E. coli	plasmid	gRNA	92 / 1.3 75 / 4.5	97 / 2 47 / 3	plasmid / 250-550	[20]
E. coli	plasmid	gRNA	90 / 2 59 / 3	83[a] / 2 23[a] / 3	linear / 300-500	[19]
S. cerevisiae	plasmid	crRNA\tracrRNA	N/A	87[b] / 3 100[c] / 3	plasmid / 50	[22]
S. cerevisiae	chromosome	gRNA[d]	4.2 / 24[e]	64 / 3 27 / 5	linear / 500	[21]

a) KO performed with ssDNA; b) four days of cultivation required to obtain efficiency; c) six days of cultivation required to obtain efficiency; d) system not designed for continuous editing; e) six fragments inserted over three loci requiring nine simultaneous recombination events

2.3.3 Application of CRISPRi to transcriptional modulation

The utility of the CRISPR-Cas9 system extends beyond the capacity for chromosomal modification as an efficient means of metering transcription. A Cas9 variant (dCas9), exhibiting loss of endonucleolytic activity, through mutations to the HNH- and RuvC-like domains, while retaining DNA-binding capability (causing physical interruption of RNA polymerase) has recently been exploited as a transcriptional repressor, facilitating highly specific and reversible modulation of gene expression [23]. RNA-mediated regulatory mechanisms such as *cis*-acting

riboswitches [95], and asRNAs with [96, 97] or without [98, 99] recruiting motifs for proteins promoting hybridization have been successfully developed. While considerable transcriptional control can be achieved with these strategies, inherent complexities such as the requirement for upstream sequence modifications to the targeted gene, and extensive screening of endogenous regulatory RNAs and evaluation of synthetic constructs have limited their utility in tailoring gene expression. On the other hand, CRISPRi provides excellent transcriptional control, while being simple to implement and easily transferrable to any organism in which the CRISPR-Cas9 system is functional. CRISPRi was first demonstrated in *E. coli* using an inducible version of dCas9, resulting in up to 300-fold repression of the monomeric red fluorescent protein (mRFP) [23]. 1000-fold repression was achieved when two gRNAs targeted the mRFP coding sequence simultaneously, and multiplexed repression of two reporters was demonstrated. gRNAs targeting the nontemplate DNA strand demonstrated effective gene silencing (or knock-down; KD), while those targeting the template strand provided marginal repression (repression via promoter targeting was strand independent). Additionally, modest repression levels were observed in the same study for HEK293 cells using human-compatible dCas9. Subsequent efforts to improve CRISPRi performance in mammalian cells focused on developing dCas9 fusions with repressive chromatin modifier domains (e.g. the Krüppel-associated box; KRAB), or transcription activators such as VP16 [100]. dCas9-KRAB fusions resulted in substantial improvements to repression levels, and transcriptional activation via dCas9-VP64 (four VP16 molecules) was also successful. Since these pioneering studies were published, CRISPRi has been successfully applied to genome-scale transcriptional repression [101] and activation [101, 102] for interrogation of gene function in human cell lines, as well as to metabolic engineering of *E. coli* [103].

2.4 HA production in bacteria

HA is a high-value biopolymer used in a broad range of applications such as abdominal, pelvic and opthalmic surgeries; viscosupplement injections for osteoarthritis treatment; and various health, food and cosmetic products [104, 105]. The current US market for HA is estimated to exceed $1 billion annually and is expected to increase quickly due to the escalating demand for viscosupplements and dermal fillers [105]. HA is a linear, unbranched polysaccharide composed of alternating *N*-acetyl-glucosamine (GlcNAc) and glucuronic acid (GlcUA) monomers, reaching up to 8 MDa in size [5]. High MW HA (>1.8 MDa) possesses an enhanced capacity to retain water, a desirable characteristic for biomedical applications [106]. Traditionally, HA was extracted from avian and mammalian sources, although microbial synthesis (primarily using *Streptococcus* sp.) has become increasingly common [5, 105]. Extraction from animal tissue is costly and the resulting products may cause allergic reactions or viral infections. Moreover, HA produced from *Streptococcus* sp. may contain exotoxins inherent to these pathogenic species [5]. Accordingly, the adoption of GRAS designated organisms to HA biomanufacturing processes is an attractive option.

2.4.1 The function and phospholipid dependence of streptococcal hyaluronan synthases

HA is naturally synthesized by certain pathogenic bacteria including Lancefield group A [107] and C [108] streptococci (Gram-positive), and Type A *Pasteurella multocida* (Gram-negative) [109], in addition to many eukaryotes (and the odd virus). Streptococcal and eukaryotic HAS have been designated as Class I HAS as they are integral membrane proteins with similar predicted topology and contain a single glycosyltransferase 2 (GT2) family module [110]. In contrast, the *P. multocida* HAS (PmHAS) is a peripheral membrane protein containing two GT2

modules [111], and is the only Class II HAS identified to date [112]. The overall topology of the HAS from *S. pyogenes* (SpHAS) was deduced experimentally, and is proposed to contain four transmembrane domains, 2 membrane-associated regions and an intracellular catalytic domain [113]. Other Class I HAS topologies are expected to be similar based on comparative sequence analysis, although eukaryotic HAS (HAS1, HAS2 and HAS3) are predicted to contain two additional transmembrane domains [114]. Streptococcal HAS, like most other Class I HAS, alternately add uridine diphosphate (UDP)-GlcNAc and UDP-GlcUA to the reducing end of the growing HA chain, such that the UDP sugars are acceptors rather than donors [110]. The relatively small size and few transmembrane domains of Streptococcal HAS suggest that it could not facilitate pore formation for translocation of the growing HA chain [115]. This theory was supported by the observation that mutation of a component of an ABC transporter complex reduced HA capsule size in *S. pyogenes*, suggesting that additional proteins may assist translocation [116]. However, recent work showed that SeHAS could release a small fluorescent dye (Cascade Blue; CB) from inside liposomes, and that mutations to one of its transmembrane domains (which decreased enzyme activity and HA MW in an earlier study) resulted in reduced CB efflux [117] (a similar independent study released at the same time corroborated this observation [118]). Furthermore, it was suggested that disruption of ABC transporters could lead to accumulation of cytoplasmic UDP, inhibiting HAS activity via substrate inhibition [117], and that CL may assist HAS in creating an internal pore-like passage for translocation [119]. Finally, pore formation is likely necessary to constrain the growing HA chain as it transiently dissociates from the HAS during each monomer addition cycle [117], considering that Class I HAS are strictly processive [115]. Accordingly, a single HAS protein appears to produce HA

autonomously, a process requiring as many as seven different functions to initiate and elongate the HA chain, and subsequently extrude it across the membrane [115].

The dependence of SpHAS activity on its orientation with CL was first demonstrated when the activity of solubilized SpHAS recovered from membrane preparations was recovered upon treatment with CL [120]. More than a decade passed before active SpHAS and SeHAS were observed to be ~23 kDa larger than the purified enzymes, both of which were inactive (~47.8 kDa each) [119]. Based on the estimated size difference, it was proposed that ~16 CL molecules must interact with a single SpHAS or SeHAS protein, and that loss of even a single molecule can cause enzyme inactivation. Subsequent work demonstrated that other anionic phospholipids could stimulate SpHAS and SeHAS activity, albeit less effectively than CL, and that respective enzymes responded very differently to each compound [121]. For example (comparisons are relative to pure HAS), phosphatidylserine increased SpHAS activity 2.5-fold while increasing SeHAS activity 6-fold, while phosphatidic acid slightly inhibited SpHAS and provided similar stimulation to SeHAS activity as phosphatidylserine. Furthermore, bovine CL was shown to stimulate HAS activity more effectively than *E. coli* CL (1.3- and 2-fold for SpHAS and SeHAS, respectively), demonstrating that the composition of CL fatty acyl chains (four in total) is also important. Later investigations confirmed that tetraoleoyl-CL, containing unsaturated 18:1(Δ9) oleoyl chains, stimulates SeHAS activity considerably (1.5-fold increase relative to bovine CL), and that saturated CL chains do not stimulate SeHAS activity [122, 123].

2.4.2 Metabolic engineering for HA production

While a considerable amount of effort has been applied to developing bioprocesses for endogenous HA production via exotoxin-free strains of group C streptococci [105], this review

focuses on production of HA in recombinant strains which are non-native producers, although a few highlights are provided for the sake of comparison. Through optimization of media components, a titer of 7 g/L and MW of 5.9 MDa was achieved in a non-hemolytic, hyaluronidase-negative (an enzyme degrading HA) strain of *Streptococcus* (*Streptococcus* sp. ID9102) obtained through chemical mutagenesis [124]. Similar titers (6-7 g/L) and MW of 3.2 MDa were achieved using a non-hemolytic, hyaluronidase-negative *S. equisimilis* strain (KFCC 10830; also obtained with mutagenesis), through optimization of culture conditions [125]. Production of HA in a recombinant host was first demonstrated in *B. subtilis* [5], leading to the exploration of heterologous HA production in several other bacteria. As both *Streptococcus* sp. and *B. subtilis* are Gram-positive, HA biosynthesis pathways can be readily adapted to achieve production in *B. subtilis* (Figure 2.2) [5]. HA production is a metabolically demanding process requiring 2 mol of glucose, 5 mol of nucleoside triphosphates and 1 mol acetyl-coA for every polymer subunit (i.e. -GlcUA-GlcNAc-) synthesized [5]. HA-producing streptococci have evolved a dedicated expression system to address this issue, which entails expression of *has* genes to maintain suitable precursor flux during HA capsule formation. In addition to *hasA* (encoding HAS), *S. pyogenes* expresses *hasB* (*tuaD*), encoding a UDP-glucose 6-dehydrogenase, and *hasC* (*gtaB*), encoding a UTP-glucose-1-P uridylyltransferase [126], while *S. equisimilis* also expresses *hasD* (*gcaD*), encoding a UDP-GlcNAc pyrophosphorylase (*B. subtilis* homologues are in parentheses) [5]. For heterologous production of HA in *B. subtilis*, SeHAS was expressed due to its enhanced rate of polymerization relative to SpHAS [108], and an extra copy of *tuaD* was constitutively expressed as the expression of native *tuaD* is repressed in the presence of phosphates [127], a common component of *B. subtilis* media formulations. Accordingly, constitutive coexpression of *seHas* and *tuaD* resulted in significant HA production in *B. subtilis*,

and expression of *gtaB* or *gcaD* provided moderate enhancements to the titer which was in the multi-gram per liter range (MW of 1.1-1.2 MDa; all genes expressed chromosomally) [5]. A subsequent study reported that coexpression of *hasA* and *tuaD* led to an improved HA titer compared to coexpression of *hasA* and *hasB* (*has* genes from group C *Streptococcus* sp.) in *B. subtilis* [128]. In addition, coexpression of *vhb*, encoding bacterial hemoglobin from *Vitreoscilla* (VHb), provided a further 1.8-fold increase in the HA titer. Finally, chromosomal expression of the Class II HAS from *P. multocida* (*pmHas*), in combination with *tuaD* and *gtaB* expressed from a plasmid, resulted in high HA titers (up to 6.8 g/L) and MWs (up to 5.4 MDa) [129]. MW was observed to decline between 36 h and 48 h which was observed in the initial study based on the drop in relative viscosity with time [5]. Finally, the coexpression of *szHas* (encoding HAS from *S. zooepidemicus*; SzHAS), *tuaD*, *gtaB*, *glmS* (encoding L-glutamine-D-fructose-6-phosphate amidotransferase; GlmS), *glmM* (encoding phosphoglucosamine mutase; GlmM), and *gcaD* improved the HA titer by ~30% (2.8 g/L) in shake flask cultures, compared to the coexpression of only *szHas* and *tuaD*, or *szHas* and *gcaD*, without improving the MW [130]. In the same study, reducing the expression of *pfkA* (encoding 6-phosphofructokinase; PfkA), via replacement of the native ATG start codon with TTG, further increased the HA titer by 18% (3.2 g/L).

HA production has also been investigated in the Gram-positive bacterium *Lactococcus lactis*, leading to the same observation that GlcUA availability was limiting synthesis [131]. Plasmid-based expression of *hasA* (*has* genes from group C *Streptococcus* sp.) alone resulted in a very low HA titer (80 mg/L), while coexpression of *hasB* increased the titer 8-fold (shake flasks). A subsequent study exploiting *L. lactis* reported that coexpression of *hasC* (*has* genes from group C *Streptococcus* sp.) resulted in 2- to 3-fold increases in the HA titer compared to

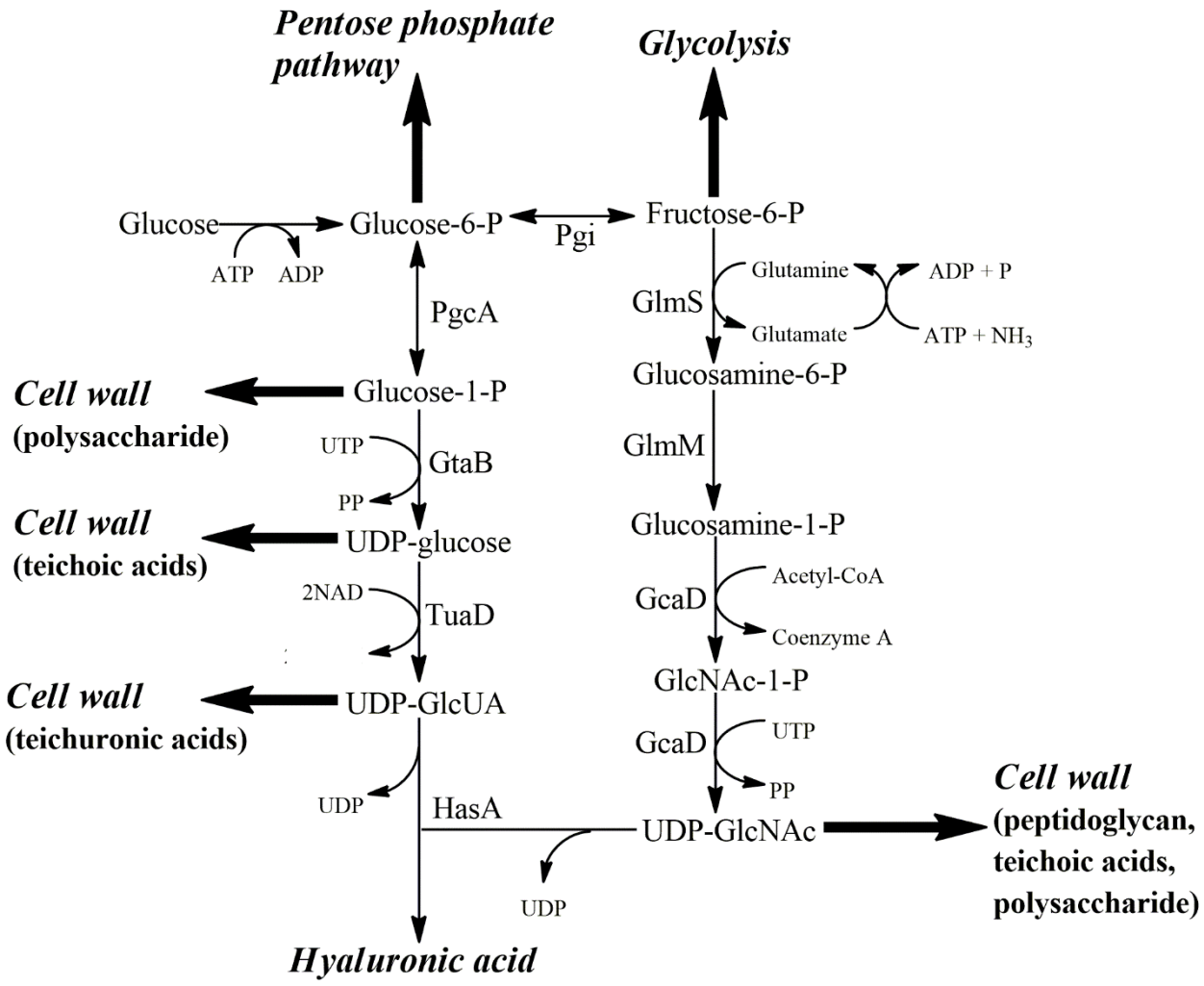

Figure 2.2. HA biosynthetic pathway in *B. subtilis*. TuaD, UDP-glucose 6-dehydrogenase; HasA, hyaluronan synthase; Pgi, glucose-6-P isomerase; PgcA, phosphoglucomutase; GlmS, glutamine-fructose-6-P amidotransferase; GtaB, UTP-glucose-1-P uridylyltransferase; GlmM, phosphoglucosamine mutase; GcaD, UDP-GlcNAc pyrophosphorylase. Adapted from [5].

coexpression of *hasA* and *hasB* without *hasC* (all genes were expressed from the same plasmid used in the previous study) [132]. The HA titer and MW reached 1.8 g/L and 2.8 MDa, respectively, in a batch stirred-tank reactor (STR) cultivation. HA production in *Streptomyces albulus* has also been demonstrated, although due to the high GC content of its genome, it was necessary to codon-optimize *seHas* and replace Lys residues flanking the transmembrane domains with Arg residues, resulting in $hasA_m$ [133]. Plasmid-based expression of $hasA_m$ and

endogenous *udgA* (*hasB*), *glmU* (*hasD*) and *gtaB* (*hasC*) resulted in a titer of 6.2 g/L and MW of 2.2 MDa in a batch STR cultivation (coexpression of only $hasA_m$ and *udgA* reduced the titer). The desirable HA production characteristics observed for *S. albulus* were attributed to the enhanced ATP pools generated during native polylysine production. Gram-negative bacteria have also been exploited as HA production platforms. Expression of plasmid-borne *spHas* and *E. coli* homologues *ugD* (*hasB*) and *galF* (*hasC*) led to a very low titer (48 mg/L). Replacement of *spHas* with codon-optimized *seHas* increased the titer to 160 mg/L, while removing *galF* from the operon, surprisingly, increased the titer to 196 mg/L in shake flask cultures (MW of 0.5 MDa) [134]. Furthermore, as observed in all Gram-positive species, GlcUA was the limiting factor for HA production in *E. coli* such that exclusion of *ugD* led to no appreciable HA being produced. Significantly improved HA production was achieved with *E. coli* by expressing *pmHas* and the *E. coli* K5 homologue *kfiD* (*hasB*). The titer reached 2.7 g/L in fed-batch cultures and could be increased to 3.7 g/L with GlcNAc supplementation (MW of 1.5 MDa) [6]. The authors of the aforementioned study originally designed the expression system used in *E. coli* for HA production in *Agrobacterium* sp., and the HA titer and MW reached 220 mg/L and 2.2 MDa, respectively, in shake flask cultures of *Agrobacterium* sp., although GlcNAc supplementation was necessary [135]. Based on the results summarized here (and personal experience), it appears that mating Gram-negative and Gram-positive organisms with corresponding HAS is ideal to promote productivity and strain stability. We observed that PmHAS is not stable in *B. subtilis*, even when expressed as a chromosomal insert from promoters of varying strength, such that a viable industrial bioprocess is currently not feasible with this host/HAS coupling.

Table 2.2. Summary of strain characteristics and heterologous HA production in cultures of engineered bacteria. All Class I HAS are from group C *Streptococcus* sp.

Organism	HAS	Expression system	Titer (g/L)	MW (MDa)	Cultivation mode	Ref.
B. subtilis	Class I	chromosomal (*hasA-hasB-hasC*)	N/A	1.2	STR	[5]
B. subtilis	Class I	chromosomal (*hasA-hasB-vgb*)	1.8	N/A	flask	[128]
B. subtilis	Class II	chromosomal (*hasA-hasB*[a]*-hasC*[a])	3.4[b] / 6.8[c]	5.43[b] / 4.55[c]	flask	[129]
L. lactis	Class I	plasmid (*hasA-hasB*)	0.64	N/A	flask	[131]
L. lactis	Class I	plasmid (*hasA-hasB-hasC*)	1.8	2.8	STR	[132]
S. albulus	Class I[d]	plasmid (*hasA-hasB-hasC-hasD*)	6.2	2.2	STR	[133]
E. coli	Class I	plasmid (*hasA-hasB*)	0.2	0.5	flask	[134]
E. coli	Class II	plasmid (*hasA-hasB*)	3.7[e]	1.5	STR	[6]
Agrobacterium sp.	Class II	plasmid (*hasA-hasB*)	0.22[e]	2.2	flask	[135]

a) expressed from plasmid; b) after 36 h cultivation; c) after 48 h cultivation; d) enzyme modified as described in text; e) GlcNAc supplementation required

2.5 Oxygen vectors

Oxygen vectors are water-immiscible compounds possessing a greater capacity to dissolve oxygen compared to water. Hydrocarbons [136-139], perfluorocarbons [140-142], vegetable oil [143], and silicone oil [139, 144] can enhance oxygen transfer in microbial cultivations, while insoluble polymers such as silicone rubber [139, 145], nylon [145], glass beads [145], Hytrel [139], Kraton [139], Desmopan [139, 144], and Elvax [144] are examples of solid oxygen vectors.

2.5.1 Mechanism of oxygen transfer in microbial cultures

In the context of a system containing a dispersed phase (liquid vector), continuous phase (aqueous media), gas phase (air) and suspended bacterial cells, there are five possible pathways for oxygen transfer from gas bubbles to bacterial cells (Figure 2.3). Liquid vectors are often categorized based on their propensity to form droplets (non-spreading) or films (spreading) when

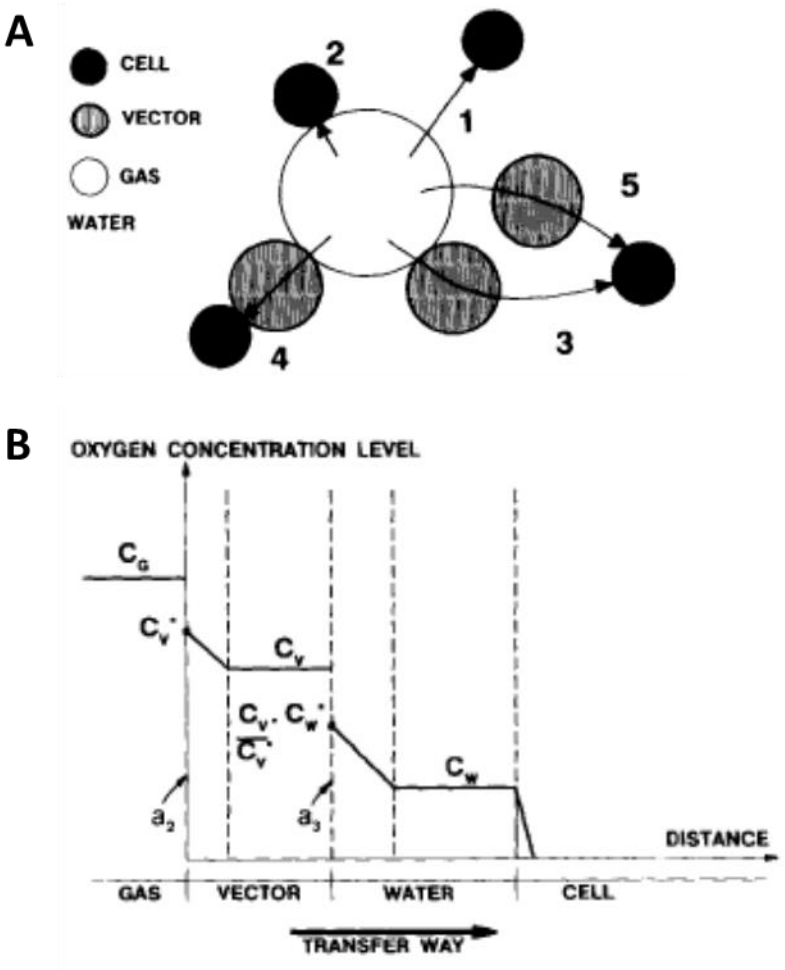

Figure 2.3. Oxygen transfer in microbial cultures containing oxygen vectors. A) Possible pathways for oxygen transfer from a gas bubble to a bacterial cell in an aqueous medium containing an oxygen vector. B) Profile of oxygen transfer in a cultivation medium containing a spreading oxygen vector. a_2 and a_3 represent the gas-vector and vector-water interfacial areas. Adapted from [146].

contacting an aqueous phase. The spreading coefficient (S_{VW}) is used to predict the behavior of liquid vectors in aqueous media [146, 147]:

$$S_{VW} = \sigma_{WG} - (\sigma_{VG} + \sigma_{VW}) \quad (2.1)$$

Where σ_{ij} is the interfacial tension between the (V)ector, (W)ater and (G)as phases. Positive values of S_{VW} indicate that a liquid vector will spread as a thin film over gas bubbles, while negative spreading coefficients ($S_{VW} < 0$) typically result in the formation of discrete droplets [148]. For spreading liquid vectors, the most likely pathway of oxygen transfer is parallel transfer (i.e. simultaneous gas-water and gas-vector oxygen transfer) [138, 146]. However, mass transfer in series (i.e. gas-vector-water or gas-water-vector oxygen transfer) was determined to be the most significant pathway in vector-water systems [147], and the significantly higher k_L values for gas-vector compared to gas-water oxygen transfer for spreading vectors (and highly similar k_L for vector-water and gas-water) indicate that mass transfer occurs in series by the gas-vector-water pathway (then taken up by the bacterial cells) [146]. In addition, the significantly reduced γ between gas and vector relative to gas and the aqueous phase favors gas-vector transfer by reducing the local free energy [149]. 'Coalescence' of gas bubbles and vector (*n*-dodecane or forane) droplets has been observed in a static aqueous system [146], confirming that gas-vector mass transfer is a likely scenario. Gas-vector coalescence has also been observed in dynamic experiments in which toluene, *n*-dodecane or refined petrol were injected into a water stream containing a fixed number of stationary gas bubbles [150]. The formation of gas-vector complexes can be addressed from the point of view of a change in surface energy (E_S):

$$\Delta E_S = 4\pi([\sigma_{GV} R_b^2 + \sigma_{VW} R_c^2] - \sigma_{VW} R_a^2 - \sigma_{GW} R_b^2) \quad (2.2)$$

Where R_b, R_c and R_d represent the radii of the gas bubble, gas-vector complex and vector droplet, respectively. If the vector droplet is much smaller than the gas bubble (which can be achieved mechanically), then $R_c \sim R_b$, and the following condition of the bubble-to-droplet size ratio favoring gas-vector coalescence (i.e. $\Delta E_S < 0$) can be derived from Equation 2.3:

$$\left(\frac{R_b}{R_d}\right)^2 < \frac{\sigma^*_{OW}}{\sigma^*_{OW}+\sigma^*_{OG}-\sigma^*_{WG}} = \frac{\sigma^*_{OW}}{-S^*} \qquad \text{(for } S^* < 0\text{)} \qquad (2.3)$$

Where * indicates properties of a mutually saturated system. For $S^* > 0$, gas-vector coalescence would be favorable for any size ratio [150]. One additional criterion must be met to attain vector film formation over droplet separation, in addition to Equation 2.3, which is the minimum vector film thickness (2-10 nm) [151].

2.5.2 Oxygen storage in hydrocarbons and perfluorocarbons

While hydrocarbons have been used extensively as oxygen vectors in bacterial cultivation (simulated or otherwise) [137-139, 146, 152-156], perfluorocarbons show considerable promise as next generation oxygen vectors due to substantially higher oxygen solubilities, lower γ and biocompatibility [157]. The enhanced solubility of oxygen in perfluorocarbons can be attributed to their intermolecular arrangement, rather than F-O electrostatic interactions, as confirmed by several studies of paramagnetic relaxation induced by the presence of oxygen in perfluorocarbons and hydrocarbons. The longitudinal relaxation time (T_1) corresponds to the process of establishing (or re-establishing) the normal Gaussian population distribution of α and β spin states in a magnetic field [158]. Nuclear relaxation arises from a dipolar interaction between the electron spins of oxygen and spins of the solvent nuclei (either F or C in this case)

modulated by molecular motion [159]. T_1 can be related to the mole fraction of solute (x_G) by Equation 2.4:

$$\frac{1}{T_1} - \frac{1}{T_1^0} = q_x x_G \tag{2.4}$$

Where T_1^0 is the relaxation time of the pure solvent and q_x is the relaxation coefficient [159, 160]. perfluorocarbons consistently present lower q_x values compared to their parent hydrocarbons (e.g., 60 and 40 s^{-1} for benzene and perfluorobenzene, respectively), such that an inverse (roughly linear) relationship between q_x and oxygen solubility exists [159, 161]. Relaxation rates (LHS of Equation 2.4) in hydrocarbon systems can be attributed to a continuous translational diffusion of oxygen through the network of hydrocarbon molecules. Conversely, a discontinuous diffusion model of oxygen molecules in perfluorocarbons has been proposed, in which a network of solvent molecules would enclose a cavity in which an oxygen molecule is temporarily trapped prior to migrating into an adjacent cavity [159, 161]. The relatively large size of fluorine atoms in perfluorocarbons (compared to hydrogen atoms in hydrocarbons) causing irregular molecular arrangements and, in turn, opening large cavities for oxygen entrapment, is a reasonable picture of the action of perfluorocarbons in dissolving large quantities of gaseous molecules given the lower boiling points and higher viscosities of perfluorocarbons versus hydrocarbons [161].

2.5.3 Solid vectors

Enhanced oxygen transfer rates (OTR) via solid vectors is thought to occur through 1) increased turbulence at the gas-water interface through particle-stagnant film collision (reduced gas bubble size via mechanical disruption will also occur), and/or 2) the shuttling effect which entails particles saturated with oxygen at the gas-water interface moving into the bulk liquid

where the oxygen is desorbed (regenerating the particle for subsequent transfer) [139, 162]. The effectiveness factor (*EF*) has been used to compare the performance of oxygen vectors [139]:

$$EF = \left(\frac{OTR_{VW}}{OTR_{W}} - 1\right) \times 100\% \tag{2.5}$$

While certain solid vectors possess high affinities for oxygen, they often provide lower values of *EF* than those with significantly lower (in some cases negligible) affinity. The equilibrium concentration of oxygen in the combined liquid phase (C^*_{mix}) was used to evaluate enhancements to the concentration gradient driving mass transfer:

$$C^*_{mix} = f_W \frac{C_G}{K_{GW}} + f_V \frac{C_G}{K_{GV}} \tag{2.6}$$

Where f_i is the volume fraction of respective phases, C_g is the concentration of gaseous oxygen and K_{ij} represents the partitioning coefficients between respective phases. Kraton™ and Desmopan™ provided increases of 220% and 175%, respectively, to the concentration gradient available for mass transfer (based on relative C^*_{mix} values), while respective *EF* values for Kraton™ and Desmopan™ were 23% and 171% [139]. Similarly, glass beads (D_{oxygen}<1x10^{-15} cm^2/s) and nylon 6,6 (D_{oxygen}=1.6x10^{-9} cm^2/s) provided significant enhancements to the k_La, while silicone rubber (D_{oxygen}=3.4x10^{-5} cm^2/s) and a styrene-butadiene copolymer (D_{oxygen}=1.4x10^{-6} cm^2/s) caused a reduction to the k_La in a STR [163]. The reduced k_La values were likely due to an increase in the time needed to reach oxygen saturation in the bulk liquid in the presence of silicone rubber (i.e. the vector was absorbing the oxygen), as the OTR in this dispersed system was significantly higher compared to that without vector. Accordingly, the work completed to date demonstrates that the selection of solid vectors is a complex process for

which the oxygen affinity of a given material is only one consideration (and will not guarantee a higher OTR as is evident from the performance of Kraton™).

2.5.4 Enhancements to oxygen transfer

The effect of oxygen vectors on a in gas-vector-water systems is poorly understood. It has been reported that small increases in a arise from the prevention of gas bubble coalescence for low f_V values (dispersed toluene), while a decreases as f_V increases further due to reduced turbulence [164, 165] (dispersed *n*-dodecane, *n*-heptane and 1-octanol decreased a as f_V increased without achieving a maxima in ref [37]). Conversely, a 15% decrease in the bubble Sauter mean diameter was observed for a *n*-dodecane dispersed system for $f_V = 0.23$ (also corresponding to the maximum k_La), representing a proportional increase in a [146]. Increasing f_V further resulted in a reduction in the k_La, suggesting that a similar reduction in a may have resulted from exceeding the optimal f_V value (which was not observed in ref [37]). Conversely, dispersed FC-40 (a perfluorocarbon) had no significant effect on a for f_V up to 0.15, although the OTR steadily increased with f_V up to a value of 0.4 [147]. It is, therefore, evident that no consensus exists on the effects of liquid vectors on a, and further investigation is required to understand this phenomena. The effect of solid vectors on a has not been studied in detail, however, an increase in a is expected due to direct mechanical bubble breakage [139].

As discussed for solid vectors, the k_La may not fully represent the utility of an oxygen vector for enhancing oxygen availability in bacterial cultivations, as the initial loading of the vector may extend the time required to reach saturation in the bulk liquid. Moreover, reports of the effect of the dispersed phase on the k_La are at times inconsistent, as is the case with estimation of a. For example, *n*-dodecane was reported to enhance k_La slightly up to $f_V \sim 0.01$

after which a decline was observed [165], while the k_La increased ~3-fold at $f_V = 0.23$ (a linear increase was observed up to $f_V = 0.23$, followed by a sharp decline) in an earlier study [146]. Furthermore, another study found that *n*-dodecane reduced the k_La in a f_V-independent manner, while dispersed *n*-hexadecane provided enhancements to the k_La [166]. The results of the latter study are particularly confusing given that for both hydrocarbons $S_{VW} < 0$, $S_{VW,hexadecane}$ is 3.6-fold lower than $S_{VW,dodecane}$, and that dispersed beading hydrocarbons typically provide a reduction or no changes in the k_La [148]. For hydrocarbons of $S_{VW} > 0$, the k_La initially decreases quickly for low f_V and then gradually approaches the baseline value (i.e. that observed without the vector) [165, 167, 168]. It was hypothesized that the initial decrease in the k_La resulted from increased liquid phase resistance due to accumulation of surface active contaminants at the gas-water interface, and that gas bubble size decreased with increasing vector concentration (γ is reduced which, in turn, increases a and the k_La) as the system approached the f_V at which phase inversion occurs [167, 168].

2.5.5 Application to bacterial cultivation

Oxygen vectors have been applied successfully to bacterial cultivations for the production of biopolymers, recombinant proteins and antibiotics. The HA titer and MW were increased by ~50% and 200%, respectively, in *S. zooepidemicus* cultures in which 0.5% v/v *n*-hexadecane was added at the time of inoculation [152]. In the same study, *n*-dodecane (1% v/v) led to increased biomass (relative to cultivation with *n*-hexadecane), but negligible improvements to titer (although MW increased by 100%). In an earlier study, the use of a perfluorocarbon (i.e. perfluorodecalin) in *S. zooepidemicus* cultures resulted in an improved HA titer (32%), although MW was not assessed [140]. Titers were slightly higher when using

dispersed perfluorodecalin compared to a three phase agitation strategy in which the agitation speed in a STR was increased from 200 to 600 rpm, and the MW may have been enhanced due to reduced shear stress. Dispersed *n*-heptane (0.3% v/v) provided an ~25% increase to titer and MW of poly(γ-glutamic acid) (PGA) produced in *B. subtilis* [153]. In the same study, the use of *n*-dodecane as vector decreased the PGA titer and MW substantially, and the significant difference in culture performance was attributed to a low NADH/NAD+ ratio and ATP levels when *n*-dodecane was applied. The application of *n*-hexane (1% v/v) and *n*-dodecane (0.5% v/v) as oxygen vectors resulted in respective 12% and 27% increases in the titer of ε-poly-lysine produced in cultures of *Streptomyces albulus*, while, surprisingly, oleic acid as dispersed phase (0.2% v/v) provided only a 7% increase in titer (*n*-hexane and oleic acid are spreading vectors, while *n*-dodecane beads) [154]. Finally, the actinorhodin (antibiotic and pigment) titer doubled in cultures of *Streptomyces coelicolor* when using dispersed perfluorodecalin (10% v/v), while biomass was reduced proportionally [142]. The increase in culture performance was attributed to the substantial improvements to the oxygen uptake rate (OUR) and k_La (3- to 4-fold for both) upon vector addition after oxygen-limited conditions developed.

Chapter 3

Development of a CRISPR-Cas9 toolkit for comprehensive engineering of *B. subtilis*

3.1 Introduction

Genetic engineering strategies aimed at converting common microbes to productive cell factories are becoming increasingly common [11]. Strain construction entails metabolic design of biosynthetic pathways and genetic manipulations. To enhance productivity, key genes for heightened expression are introduced via plasmid transformation or genomic integration (knock-in; KI), while divergent pathways are eliminated via gene disruption (i.e. KO) [169]. However, certain genes, particularly those associated with central metabolism or core aspects of physiology (e.g. membrane integrity, ATP generation, etc.), cannot be completely inactivated, otherwise host viability can be compromised. In such cases, reducing expression levels of the key genes (i.e. KD) may ultimately prove effective [98].

While engineering microbial genomes is challenging, recent application of CRISPRs and their Cas proteins has dramatically altered the course of genomic engineering across the spectrum of life. CRISPR arrays are part of an adaptive prokaryotic viral defense system, and contain target-specific protospacers that are expressed as crRNAs [170]. crRNAs direct Cas nucleases to DNA targets based on the presence of a PAM specific to the Cas protein [171, 172] and protospacer homology. In type II systems such as CRISPR-Cas9 from *S. pyogenes*, a tracrRNA is required for processing a pre-crRNA into a functional crRNA [78]. More recently, the synthetic gRNA, comprised of a protospacer, CBH, and transcriptional terminator, has been

used for targeting, further simplifying application of the CRISPR-Cas9 system [79]. The CRISPR-induced DSBs enable selection of mutants that evade DNA cleavage via recombination of exogenous editing templates. Accordingly, the CRISPR-Cas9 system has proven an indispensable tool for genome editing in bacteria [19, 20, 82, 86-89, 173-179], yeast [21, 22] and higher eukaryotes [84, 91-93].

In addition to genome editing, the CRISPR-Cas9 system can be applied to reversibly regulating gene transcription, known as CRISPRi for which a Cas9 variant (dead Cas9; dCas9), exhibiting loss of endonucleolytic activity while retaining DNA-binding capability, acts as a transcriptional repressor [23, 180]. While various RNA-mediated regulatory mechanisms, such as *cis*-acting riboswitches [95] and asRNAs with [96, 97] or without [98, 99] recruiting motifs for proteins promoting hybridization, have been developed for tailoring gene expression, inherent complexities exist in the application of these technologies. The use of *cis*-acting riboswitches requires upstream sequence modifications to the targeted gene [95], limiting their practical utility for metabolic engineering and genetic screening. Similarly, the design of recruiting scaffolds for synthetic asRNAs entails extensive screening of endogenous regulatory RNAs and evaluation of synthetic constructs [96, 97], while off target effects may also be a concern when applying asRNAs [98]. On the other hand, CRISPRi provides excellent transcriptional control and is simple to implement in many organisms. The CRISPR-dCas9 system has been applied to genome-scale transcriptional repression [101] and activation [101, 102] for interrogation of gene function in human cell lines as well as to genetic and metabolic engineering of *E. coli* [103, 181], *Corynebacterium glutamicum* [182], and mycobacterium [183].

B. subtilis is a model Gram-positive organism sought after for its capacity in high-level production of biopolymers [5], metabolites [184], and recombinant proteins [185]. In contrast to *E. coli*, *B. subtilis* has received a GRAS designation, readily secretes products into the extracellular medium, and can metabolize nearly any carbon source, making it an attractive biomanufacturing platform [185]. While *B. subtilis* is an ideal organism for industrial application, available genetic tools are lagging behind popular production hosts such as *E. coli* and *S. cerevisiae* [11, 12]. Because markerless genome engineering is essential for the development of commercial *B. subtilis* strains, a common approach has been the application of counter-selectable markers, such as *upp* [14, 186], *blaI* [67] and *mazF* [13], flanked by short direct repeats (DR) for auto-eviction of the selection cassettes by single-crossover recombination. While these methods are simple to use, the editing efficiencies are relatively low, conditional genetic backgrounds are required in some cases, and cloning of integration constructs (i.e. integration vectors or PCR-amplified integration cassettes) can be complicated and/or time consuming. Moreover, multiplexing is not practical as the number of available selection and counter-selection markers is limited, exposure to multiple antibiotics is not preferable (i.e. may compromise cell physiology), and counter-selection will become increasingly difficult (i.e. less efficient or more time consuming) as the number of simultaneous targets increases. On the other hand, site-specific recombination via the Cre/*loxP* [15] and FLP/*FRT* [16] systems has also been applied to markerless recombineering in *B. subtilis* with a generally higher efficiency than counter-selection methods. Additionally, ssDNA recombineering mediated by the λ-Red phage β-recombinase provides a high editing efficiency [70]. However, these systems are not particularly conducive to multiplexing either given the requirement for multiple selection (and potentially counter-selection) markers and subsequent tedious screening.

In this study, we developed a CRISPR-Cas9 toolkit for comprehensive engineering of *B. subtilis* to overcome major limitations associated with existing genome engineering technologies (e.g. low editing efficiency, tedious cloning, and limited multiplexing capability). While CRISPR-Cas9 offers potential solutions to these technical issues in *E. coli* and *S. cerevisiae* [21, 22, 82, 86], the protocols include multicopy plasmids which must be removed from the cell. In that regard, an ideal CRISPR-Cas9 system should facilitate multiple mutations, either in series or simultaneously, while imposing minimal physiological impact to the host. Our approach not only simplifies construction of genetic elements required for CRISPR-Cas9-mediated genome editing and transcriptional interference in *B. subtilis*, but also obviates reliance on potentially unstable multicopy plasmids and subsequent plasmid curing. We demonstrated high editing efficacy of our novel gRNA transcription and delivery system based on a simple counter-selection procedure with the capacity for successive genomic manipulations, including site-specific mutations for gene inactivation, and gene insertions. The effects of editing template characteristics and PAM site sensitivity were also investigated to increase editing efficiency. Finally, we expand our toolkit for transcriptional repression of gene expression using dCas9 with our gRNA delivery system. The developed toolkit will advance technologies in engineering of *B. subtilis* to achieve its full potential as a biomanufacturing platform.

3.2 Materials and methods

3.2.1 Bacterial strains, primers and plasmids

The *B. subtilis* strains used in this study are listed in Table S3.1. *E. coli* HI-Control™ 10G chemically competent cells (Lucigen; Wisconsin, USA) were prepared as electrocompetent cells as described previously [187] and used as host for plasmid construction. *B. subtilis* and *E.*

coli strains were maintained as glycerol stocks at -80 °C. Primers (Table S3.1) were synthesized by Integrated DNA Technologies (IDT; Iowa, USA). Plasmids pIEFBPR (ECE195), pDG1731 (ECE119) and pAX01 (ECE137) were obtained from the Bacillus Genetic Stock Center (BGSC; Columbus, Ohio). pCRISPR and pCas9 were gifts from Luciano Marraffini (Addgene plasmids # 42875 and 42876, respectively), and pgRNA-bacteria and pdCas9-bacteria were gifts from Stanley Qi (Addgene plasmid # 44251 and 44249, respectively).

3.2.2 Plasmid and editing template construction

DNA manipulation was performed using standard cloning techniques [187], and DNA sequencing was conducted by The Centre for Applied Genomics (TCAG; Ontario, Canada). We previously identified the *thrC* locus as a recombination 'hot spot' in the genome of *B. subtilis*, making it a potential site for integration of gRNA transcription cassettes. To construct the gRNA delivery vector, we began by amplifying the *thrC* 5'- and 3'- homology lengths (HLs) from plasmid pDG1731 [188] with primers P3.1/P3.2 and P3.3/P3.4, respectively, followed by insertion in place of the corresponding *bpr* HL-5' and HL-3' of pIEFBPR [13] using the respective SbfI/NheI and XmaI/SpeI restriction sites, yielding pAW001-2. Subsequently, the ampicillin resistance marker (Amp^R) in pAW001-2 was replaced with an erythromycin cassette (Erm^R). To do this, the ColE1 replicon was amplified from pIEFBPR with primers P3.5/P3.6, the Erm^R cassette was amplified from pAX01 [189] with primers P3.7/P3.8, and the two fragments were spliced via Splicing by Overlap Extension (SOE)-PCR (this process will be subsequently referred to as splicing), followed by insertion of the spliced fragment into pAW001-2 using the SacI/NgoMIV restriction sites, resulting in pAW002-2.

Potentially due to leaky transcription from the *spac* promoter (P_{spac}), the transformation efficiencies of pIEFBPR and pAW002-2 in *B. subtilis* were unacceptably low. Accordingly, the tightly regulated *xylA*/*R* promoter cassette from *Bacillus megaterium* ($P_{xylA,\ Bm}$) was amplified from pAX01 with primers P3.9/P3.10 (--/MfeI), *mazF* was amplified from pIEFBPR with primers P3.11/P3.12 (BamHI/--), and the two fragments were spliced. The resulting $P_{xylA,\ Bm}$::*mazF* cassette replaced the P_{spac}::*mazF* cassette in BamHI/EcoRI digested pAW002-2, yielding pAW003-2. Though transformation efficiency was improved in *B. subtilis*, propagation of pAW003-2 was difficult in *E. coli*, prompting us to identify another inducible promoter to drive *mazF*. The *araE/R* promoter system from *B. subtilis* (P_{araE}) was chosen as it is very tightly repressed in the presence of glucose due to the presence of the catabolite repression element (CRE) upstream of the *araE* open reading frame (ORF) [190]. The P_{araE} cassette was amplified with primers P3.13/P3.14 from 1A751 genomic DNA (gDNA) and was spliced with *mazF* as previously described. The resulting P_{araE}::*mazF* cassette was used to replace the P_{spac}::*mazF* cassette in pAW002-2 using the BamHI/EcoRI restriction sites, resulting in plasmid pAW004-2, a vector found to be stable in *E. coli* while providing significantly enhanced transformation efficiency in *B. subtilis* relative to pAW002-2.

The *xylA* promoter (P_{xylA}) from *B. subtilis* was used to drive transcription of gRNAs. To do this, P_{xylA} was amplified with primers P3.15/P3.16 from 1A751 gDNA, replacing the 6 base pairs (bp) between the -10 and +2 regions of P_{xylA} with a SphI restriction site. The resulting promoter, $P_{xylA.SphI+1}$ (Figure 3.1A), was inserted in place of the direct repeat (DR) adjacent to the *thrC* HL-5' of pAW004-2 using the NheI/BamHI restriction sites, yielding pAW005-2 (Figure 3.1B). The gRNA cassettes *ugtP*-gRNA.P395T, *amyE*-gRNA.P25NT, *amyE*-gRNA.P330T, *amyE*-gRNA.P636T, *amyE*-gRNA.P1344T, and *seHas*-gRNA.P394T, were amplified from

pgRNA-bacteria [23] with respective forward primers P3.17-P3.22 containing unique protospacers, and a common reverse primer P3.23. Each gRNA cassette was inserted downstream of $P_{xylA.SphI+1}$ in pAW005-2 using SphI/BamHI restriction sites to obtain single-gRNA delivery vectors (Figure 3.1B). To generate the native CRISPR array (CRISPRa) for *ugtP* disruption (*ugtP*-CRISPRa.P395T), the empty CRISPRa was amplified from pCRISPR [82] with primers P3.24/P3.25 and inserted in place of the DR adjacent to the *thrC* HL-5' of pAW004-2 using the NheI/BamHI restriction sites, yielding pAW012-2. Oligonucleotides P3.26/P3.27 were then annealed and ligated into BsaI digested pAW012-2 as previously described [82], resulting in pAW013-2. The *lacA* locus was chosen for genomic integration of *cas9*. To do this, pAW016-2 (Figure 3.1C) was constructed by removing the $P_{xylA,\ Bm}$ cassette from pAX01 by SacI digestion and self-ligation, and then inserting the *cas9*-tracrRNA cassette amplified from pCas9 [82] with primers P3.34/P3.35 using the XbaI restriction sites. The orientation of the *cas9*-tracrRNA cassette was confirmed by DNA sequencing.

To construct the multi-gRNA delivery vector, the BamHI restriction site downstream of *mazF* was replaced with a NcoI restriction site, and the BglII restriction site upstream of *mazF* was removed and a new BglII restriction site was inserted between the NheI restriction site and $P_{xylA.SphI+1}$ in pAW006-2 (Figure 3.2), to facilitate Biobrick cloning of gRNA transcription cassettes. This was accomplished by amplifying the $P_{xylA.SphI+1}$::*ugtP*-gRNA.P395T cassette and *mazF* from pAW006-2 with primers P3.28/P3.29 (NheI/--) and P3.30/P3.31 (--/BamHI), respectively, followed by splicing of the two fragments to generate a $P_{xylA.SphI+1}$::*ugtP*-gRNA.P395T-*mazF* cassette. The $P_{xylA.SphI+1}$::*ugtP*-gRNA.P395T-*mazF* cassette was subsequently inserted into NheI/BglII digested pAW005-2, yielding pAW014-2, and the modifications to pAW005-2 which resulted in pAW014-2 are summarized in Figure 3.2. In this

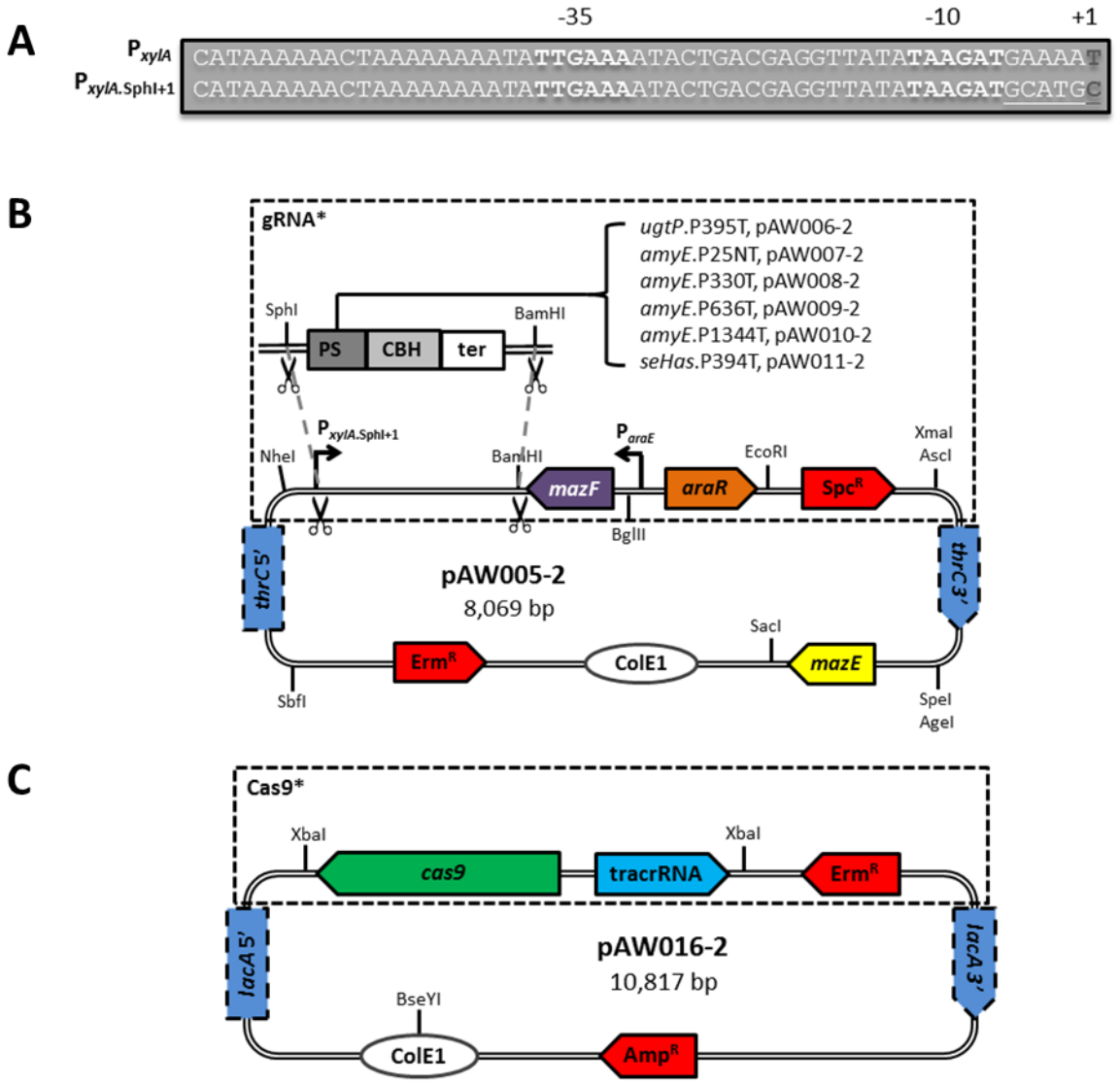

Figure 3.1. Schematic representation of the $P_{xylA.SphI+1}$ gRNA transcription cassette, and the single-gRNA and Cas9 delivery vectors. A) Sequences of the native promoter P_{xylA} of *B. subtilis* and $P_{xylA.SphI+1}$ are provided. The 6 bp between the -10 and +2 regions of P_{xylA} were replaced with a SphI restriction site enabling protospacer (represented as PS in the figure) exchange without the need for inverse PCR. A unique protospacer is introduced as an overhang in the forward primer amplifying the CBH and terminator (represented as ter in the figure) as a single fragment, and the resulting gRNA cassette is inserted downstream of $P_{xylA.SphI+1}$ in the single-gRNA delivery vector. The -35 and -10 regions are in bold font, the +1 is in dark bold font and the SphI restriction site is underlined. B) $P_{xylA.SphI+1}$ was inserted into pAW004-2 removing the DR adjacent to the *thrC* HL-5', yielding pAW005-2. gRNA cassettes were inserted between the SphI and BamHI restriction sites of pAW005-2, generating respective single-gRNA delivery vectors. Transformation of a linearized single-gRNA delivery vector results in integration of the combined $P_{xylA.SphI+1}$::gRNA-P_{araE}::*mazF*-Spc^R (gRNA*) cassette at the *thrC* locus. The gRNA* cassette is subsequently evicted by transformation of the *thrC* editing template, followed by arabinose selection to induce *mazF* expression, and screening for spectinomycin sensitivity. C)

The $P_{xylA,\ Bm}$ cassette was removed from pAX01 and the *cas9*-tracrRNA cassette inserted, yielding pAW016-2. Transformation of linearized pAW016-2 results in integration of the combined *cas9*-tracrRNA-Erm^R (Cas9*) cassette at the *lacA* locus.

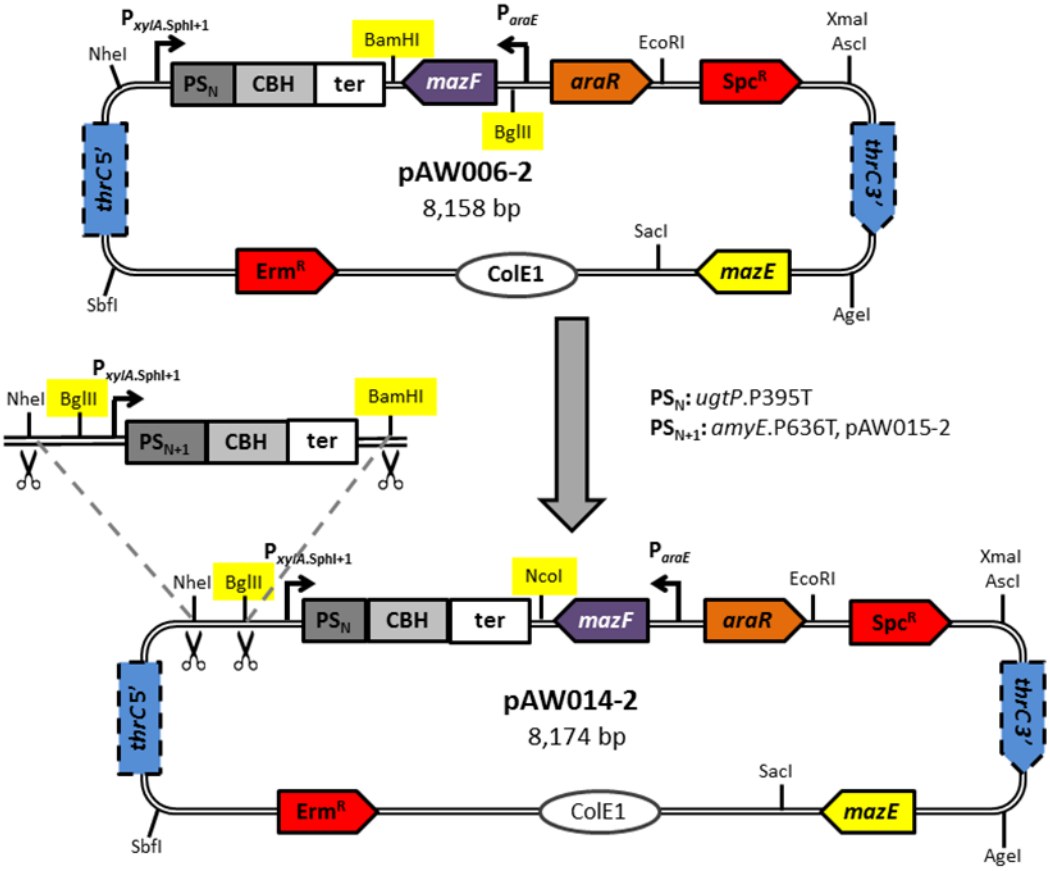

Figure 3.2. Schematic representation of the construction of the multi-gRNA delivery vector. The BamHI restriction site was replaced with a NcoI restriction site, and the BglII restriction site moved between the NheI restriction site and $P_{xylA.SphI+1}$ in pAW006-2 (top) to facilitate Biobrick cloning, yielding pAW014-2 (bottom). The $P_{xylA.SphI+1}$::*amyE*-gRNA.P636T cassette was inserted between the NheI/BglII restriction sites of pAW014-2, resulting in pAW015-2. In general, a single-gRNA delivery vector is generated from pAW005-2, and the gRNA transcription cassette is amplified, digested with NheI\BamHI and inserted into the NheI/BglII digested multi-gRNA delivery vector. If a single-gRNA delivery vector is not required, $P_{xylA.SphI+1}$ and the gRNA cassette can be spliced and cloned directly into the multi-gRNA delivery vector (protospacer is represented as PS and terminator as ter in the figure).

arrangement, the first gRNA cassette to be inserted into the multi-gRNA delivery vector is

amplified with a forward primer introducing the unique protospacer and reverse primer P3.32

from pgRNA-bacteria (or any plasmid containing a gRNA), and cloned into pAW014-2 using the SphI/NcoI restriction sites. Each additional gRNA is cloned into pAW005-2, generating single-gRNA delivery vectors from which the corresponding gRNA transcription cassettes are amplified with primers P3.28/P3.33 (NheI/BamHI) and sequentially inserted into the NheI/BglII digested multi-gRNA delivery vector. All gRNA delivery vectors were linearized via SacI digestion prior to transformation into *B. Subtilis*. To enable continuous genome editing (a procedure which is summarized in Figure 3.3), 1A751 was first transformed with BseYI-linearized pAW016-2, resulting in strain AW001-2, which constitutively expresses Cas9 from the *lacA* locus. Continuous editing is then performed by transforming AW001-2 (or its derivatives) with a single- or multi-gRNA delivery vector, integrating the combined $P_{xylA.SphI+1}$::gRNA-P_{araE}::*mazF*-Spc^R cassette (gRNA*) at the *thrC* locus, and an editing template(s) introducing the desired mutation(s). Cells containing the desired mutation(s) evade the CRISPR-Cas9-mediated chromosomal DSB(s) [as elimination of the PAM site(s) occurs in edited gDNA], and the mutation(s) is verified with genetic screening and sequencing. The gRNA* cassette is subsequently removed via transformation of the *thrC* editing template, restoring the integration site for the next round of editing.

To construct the gRNA delivery vector for dCas9 targeting, the *wprA* HL-5' was amplified with primers P3.36/P3.37, and $P_{xylA.SphI+1}$ with P3.38/P3.39 from 1A751 gDNA, and the two fragments were spliced, followed by insertion of the spliced fragment in place of the *thrC* HL-5' in pAW004-2 using the SbfI/NcoI restriction sites. The vector was completed by amplifying the *wprA* HL-3' with primers P3.40/P3.41 from 1A751 gDNA, followed by insertion in place of the *thrC* HL-3' using the AscI/AgeI restriction sites, resulting in pAW017-2. The *wprA* locus was chosen as the integration site for dCas9-targeting gRNA transcription cassettes

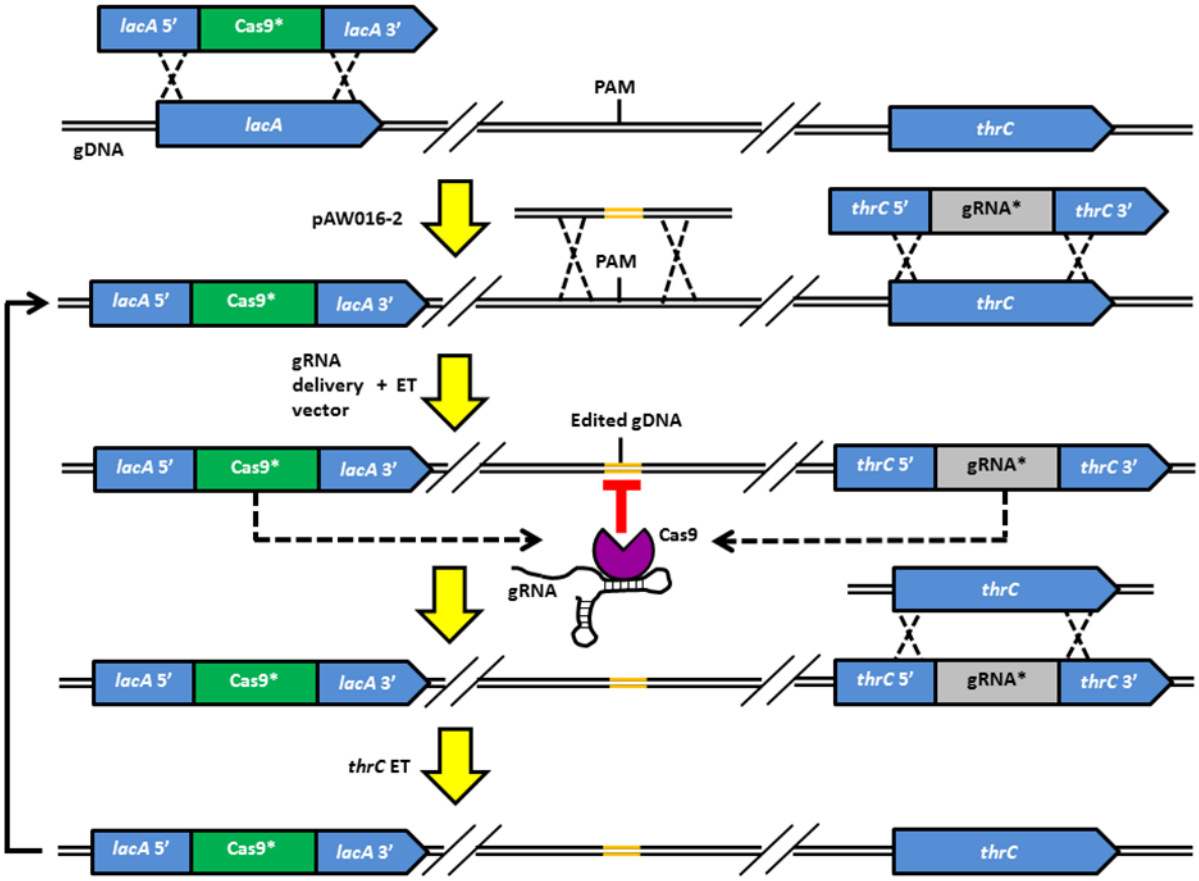

Figure 3.3. Continuous editing with the CRISPR-Cas9 toolkit. The combined *cas9*-tracrRNA-Erm^{R} (Cas9*) cassette was integrated into the *lacA* locus of 1A751 via transformation with pAW016-2, generating strain AW001-2, which constitutively expresses Cas9. A linearized single- or multi-gRNA delivery vector, and the editing template(s) [represented as ET in the figure], are transformed into AW001-2 (or one of its derivatives), resulting in integration of the combined $P_{xylA.SphI+1}$::gRNA-P_{araE}::*mazF*-Spc^{R} (gRNA*) cassette at the *thrC* locus, and introduction of the desired mutation(s) via integration of the editing template (s). Cells containing the desired mutation(s) evade the CRISPR-Cas9-mediated chromosomal DSB(s) due to the elimination of the PAM site(s) in the edited gDNA. The resulting mutant is resistant to spectinomycin and sensitive to arabinose induction of *mazF* expression. After the desired mutation(s) is verified, the gRNA* cassette is evicted by transformation of the *thrC* editing template to arabinose resistance and spectinomycin sensitivity, restoring the native *thrC* locus. The mutant is now ready for the next round of editing using the same procedure. Refer to Figures 3.1B and 3.1C for schematic representations of the gRNA* and Cas9* cassettes, respectively.

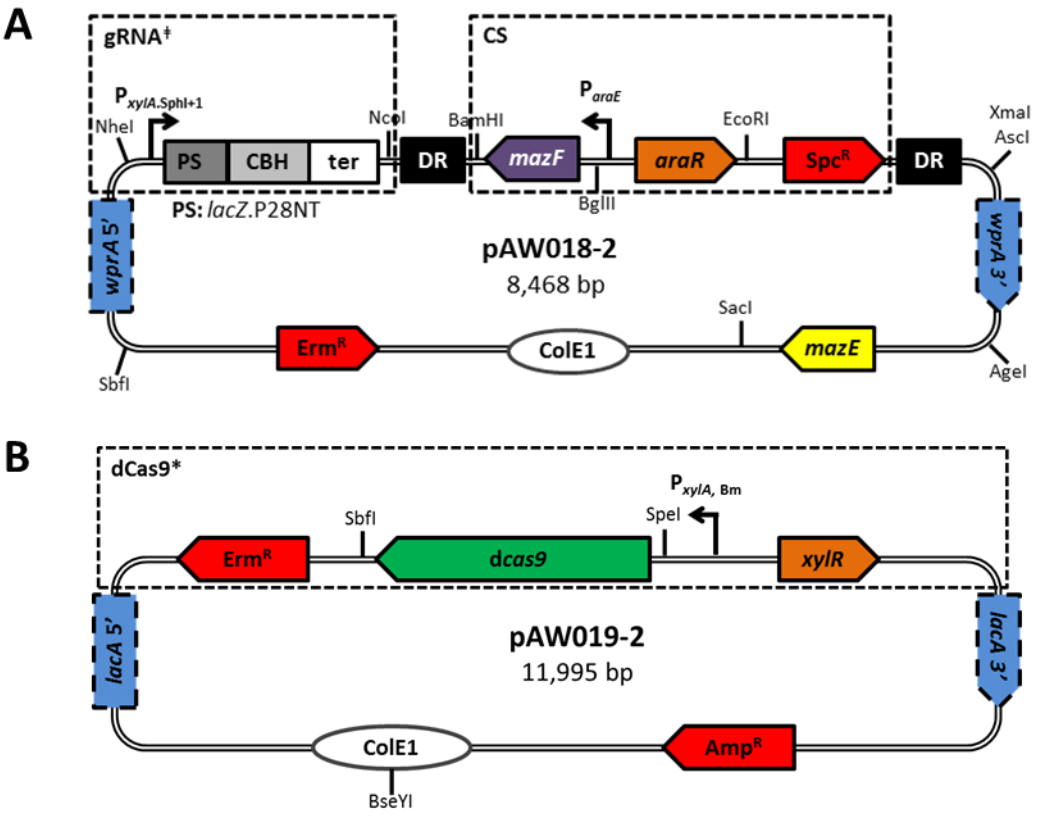

Figure 3.4. Schematic representation of the gRNA delivery vector for integration of dCas9-targeting gRNA transcription cassettes, and the dCas9 delivery vector. A) The *wprA* HL-5' and $P_{xylA.SphI+1}$ were spliced and inserted in place of the *thrC* HL-5' of pAW004-2 preserving the adjacent DR, and the *thrC* HL-3' was replaced with the *wprA* HL-3', generating pAW017-2. *lacZ*-gRNA.P28NT was inserted between the SphI and NcoI restriction sites of pAW017-2, yielding pAW018-2. Transformation of linearized pAW018-2 results in integration of the $P_{xylA.SphI+1}$::*lacZ*-gRNA.P28NT (gRNA‡) cassette, and the combined P_{araE}::*mazF*-Spc^R (CS) cassette at the *wprA* locus. The CS cassette is auto-evicted via single-crossover recombination between the flanking DRs. B) *dcas9* was inserted downstream of $P_{xylA, Bm}$ in pAX01 yielding pAW019-2. Transformation of linearized pAW019-2 results in integration of the combined $P_{xylA, Bm}$::*dcas9*-Erm^R (dCas9*) cassette at the *lacA* locus (protospacer is represented as PS and terminator as ter in the figure).

for compatibility purposes based on intended future applications for CRISPRi in other areas of research conducted by our group. The *lacZ*-gRNA.P28NT cassette was amplified from pgRNA-bacteria with primers P3.42/P3.32 and cloned into pAW017-2 using the SphI/NcoI restriction sites, yielding pAW018-2 (Figure 3.4A). pAW018-2 was linearized via SacI digestion prior to

transformation into *B. Subtilis*. Similar to *cas9*, the *lacA* locus was selected for genomic integration of the xylose-inducible dCas9 cassette. To do this, pAW019-2 (Figure 3.4B) wasconstructed by amplifying *dcas9* from pdCas9-bacteria [23] with primers P3.43/P3.44 (SpeI/BglII), followed by insertion into SpeI/BamHI digested pAX01. To enable transcriptional interference via dCas9 (a procedure which is summarized in Figure 3.5), AW009 was transformed with BseYI-linearized pAW019-2, yielding strain AW014-2, which expresses xylose-inducible dCas9 from the *lacA* locus. Note that the HA-producing strain AW009 was selected as the host for CRISPRi demonstration to accommodate our research in strain engineering for enhanced HA production in *B. subtilis,* and any strain possessing an intact *lacA* locus (e.g. 1A751) can be used in place of AW009. AW014-2 was then transformed with pAW018-2, resulting in integration of the $P_{xylA.SphI+1}$::*lacZ*-gRNA.P28NT cassette and the combined P_{araE}::*mazF*-Spc^R (CS) cassette at the *wprA* locus. The CS cassette was subsequently auto-evicted via single-crossover recombination between the flanking DRs [13], yielding strain AW015-2, which transcribes *lacZ*-gRNA.P28NT from the *wprA* locus. Subsequent genomic integration of an inducible copy of *lacZ* from *E. coli* at the *ugtP* locus was performed to assess CRISPRi. To do this, AW015-2 was transformed with pAW016, a vector previously constructed in our lab for genomic integration of isopropyl β-D-thiogalactopyranoside (IPTG)-inducible *lacZ* at the *ugtP* locus, yielding strain AW016-2 (note that this part is not shown in Figure 3.5). The gRNA directs dCas9 to the target (i.e. *lacZ*) based on the presence of a PAM site and adjacent seed region complementary to the protospacer, and the dCas9-gRNA complex remains bound to the target, blocking transcription by RNA polymerase (RNAP).

For the *ugtP* KO, PAM site *ugtP*.P395T was selected, where the number in the nomenclature corresponds to the position of the first bp of the PAM site (P) relative to the

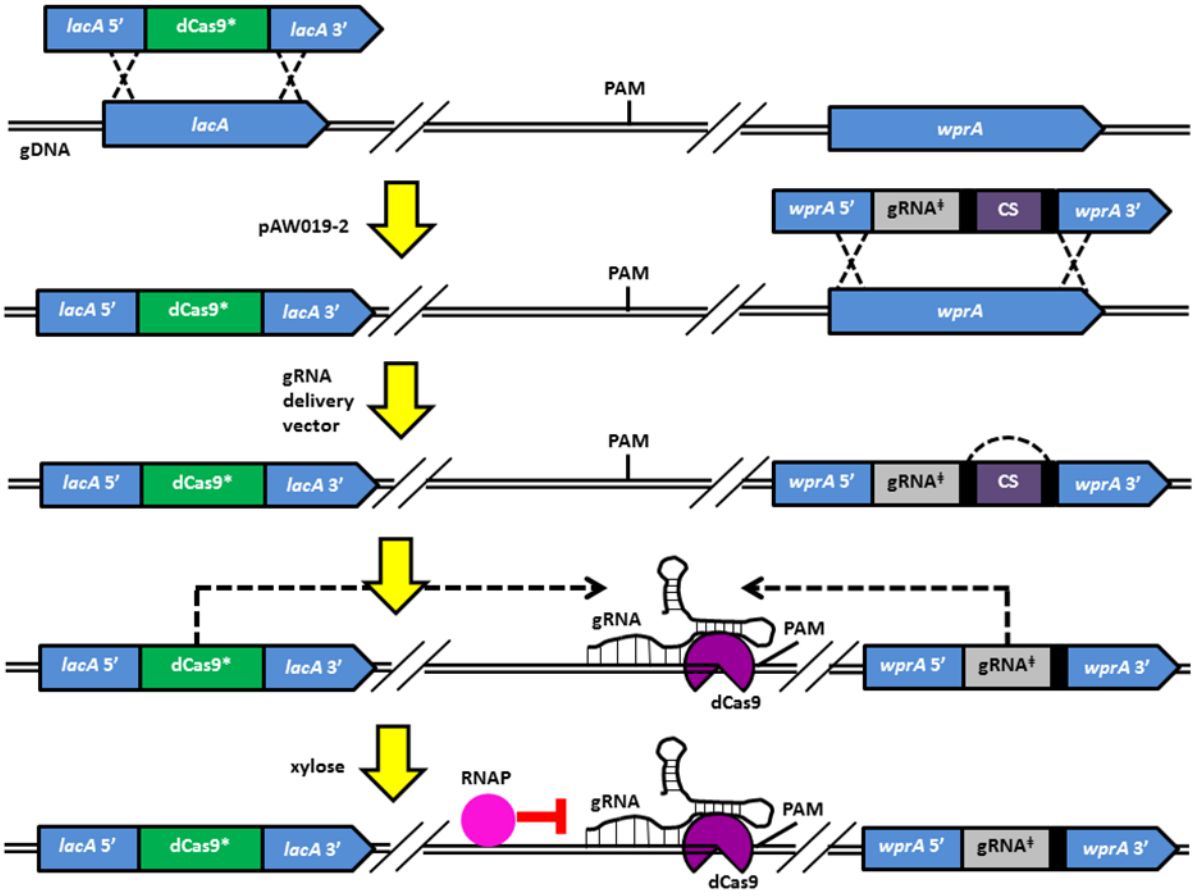

Figure 3.5. Implementing CRISPRi with the CRISPR-Cas9 toolkit. The combined $P_{xylA,Bm}$::*dcas9*-Erm^R (dCas9*) cassette was integrated into the *lacA* locus of strain AW009 via transformation with pAW019-2, yielding strain AW014-2, which expresses xylose-inducible dCas9 [note that any strain possessing an intact *lacA* locus (e.g. 1A751) can be used in place of AW009]. AW014-2 was then transformed with pAW018-2, resulting in integration of the $P_{xylA.SphI+1}$::*lacZ*-gRNA.P28NT (gRNA‡) cassette, and the combined P_{araE}::*mazF*-Spc^R (CS) cassette, at the *wprA* locus (the resulting mutant was spectinomycin resistant and arabinose sensitive). The CS cassette was subsequently auto-evicted via single-crossover recombination between the flanking DRs (black rectangles), yielding strain AW015-2 (spectinomycin sensitive and arabinose resistant), which transcribes *lacZ*-gRNA.P28NT from the *wprA* locus [subsequent integration of IPTG-inducible *lacZ* (*E. coli*) at the *ugtP* locus was performed to assess CRISPRi, and is not shown in Figure 3.5]. The gRNA directs dCas9 to the target based on the presence of a PAM site and adjacent seed region complementary to the protospacer, and the dCas9-gRNA complex remains bound to the target, blocking transcription by RNA polymerase (RNAP). Refer to Figures 3.4A and 3.4B for schematic representations of the gRNA‡ and dCas9* cassettes, respectively.

beginning of the *ugtP* ORF (i.e. CGG, where the cytosine is the 395th bp in the ORF), and base-pairing occurs with the template (T) strand (or the non-template (NT) strand for other PAM sites). The full length *ugtP* editing template was generated by splicing the two 1,337 bp and 1,332 bp HLs (flanking a 12 bp mutation region; Figure 3.6A) amplified with primers P3.45/P3.46 and P3.47/P3.48, respectively, from 1A751 gDNA. The *ugtP* editing templates of HLs 100, 300, 500, 750 and 1,000 bp (Figure 3.6A) were amplified with primers P3.49/P3.50, P3.51/P3.52, P3.53/P3.54, P3.55/P3.56 and P3.57/P3.58, respectively, from the full length *ugtP* editing template, and, therefore, preserved the original 12 bp mutation region. The full length *amyE* editing template (*amyE*.P636T) was constructed by splicing the two 1,368 bp and 1,335 bp HLs (flanking a 15 bp mutation region; Figure 3.6B) amplified with primers P3.67/P3.68 and P3.69/P3.70, respectively, from 1A751 gDNA. The full length *amyE* editing template was inserted into pJET1.2/blunt using the CloneJET PCR Cloning Kit (ThermoFisher Scientific; Massachusetts, USA) as per the manufacturer's instructions, yielding pAW022-2 which was linearized via BsaI digestion prior to transformation into *B. subtilis* as an editing template. The 1,000 bp HL *amyE* editing template (*amyE*.P636T) was amplified from the full length *amyE* editing template with primers P3.71/P3.72 preserving the original 15 bp mutation region. The *amyE* editing templates for PAM sites *amyE*.P25NT (primers P3.73/P3.74 and P3.75/P3.76), *amyE*.P330T (primers P3.77/P3.78 and P3.79/P3.80) and *amyE*.P1344T (primers P3.81/P3.82 and P3.83/P3.84) were constructed in the same way as the full length *amyE* editing template (*amyE*.P636T), except that only 1,000 bp HLs flanked 11 bp (*amyE*.P330T) or 12 bp (*amyE*.P25NT and *amyE*.P1344T) mutation regions (Figure 3.6B). Editing templates introduced premature stop codons and restriction sites in place of PAM sites and adjacent nucleotides. Alternatively, the HA operon (i.e. P_{grac}::*seHas*:*tuaD*) flanked by the *amyE* HL-5' and HL-3' was

also used as the editing template for evading the DSB associated with PAM site *amyE*.P636T, resulting in KI of the HA operon at the *amyE* locus. To construct this editing template, the partial HA operon KI cassette, containing the 759 bp *amyE* HL-3' and 2,909 bp P_{grac}::*seHas*:*tuaD* HA operon, was amplified from pAW008, a vector previously constructed in our lab, with primers P3.59/P3.60, and inserted into pJET1.2/blunt, yielding an intermediate vector. To complete the HA operon KI cassette, the 738 bp *amyE* HL-5' was amplified from 1A751 gDNA with primers P3.61/P3.62 and inserted into the intermediate vector using the NcoI/NheI restriction sites, yielding pAW020-2. pAW020-2 was linearized via ScaI digestion prior to transformation into *B. subtilis* as an editing template. The *seHas* editing template (*seHas*.P394T) was constructed by splicing the two 1,303 bp and 1,338 bp HLs (flanking a 15 bp mutation region; Figure 3.6C) amplified with primers P3.63/P3.64 and P3.65/P3.66, respectively, from pAW020-2. The *seHas* editing template was inserted into pJET1.2/blunt to enhance transformation efficiency of the poorly transformable HA-producing strain AW005-2, and the resulting plasmid was pAW021-2. pAW021-2 was linearized via ScaI digestion prior to transformation into *B. subtilis* as an editing template. The *thrC* editing template used to evict gRNA transcription cassettes was generated as a 2,876 bp PCR product (i.e. 1,452 bp and 1,306 bp fragments flanking the deleted 118 bp region of *thrC*) amplified with primers P3.85/P3.86 from 1A751 gDNA.

3.2.3 Competent cell preparation and transformation

Transformation of *B. subtilis* was performed using a standard protocol for natural competence [8]. SpC media contained the following: $(NH_4)_2SO_4$, 1.67 g/L; K_2HPO_4, 11.64 g/L; KH_2PO_4, 5.0 g/L; trisodium citrate dihydrate, 833 mg/L; glucose, 4.17 g/L; $MgSO_4 \cdot 7H_2O$, 151 mg/L; yeast extract, 1.67 g/L; casamino acids, 208 mg/L; Arg, 7.5 g/L; His, 383 mg/L; Trp, 48

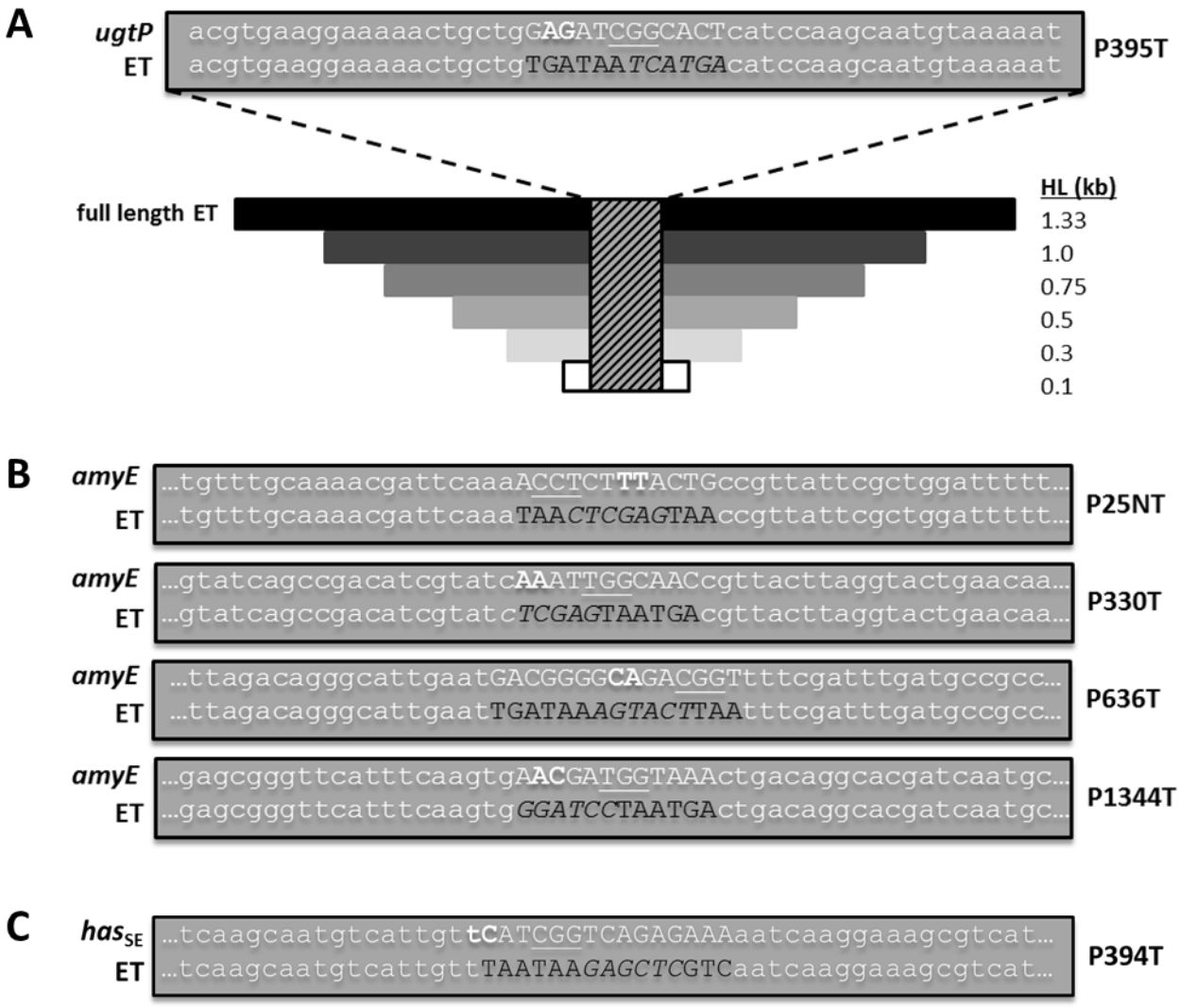

Figure 3.6. Unaltered sequences and mutation regions of editing templates for *ugtP*, *seHas* and *amyE* KOs, and schematic representation of the KI of the HA biosynthetic operon at the *amyE* locus. (A) The native (*ugtP*) and modified (editing template) sequences of the mutation region for *ugtP* KO at *ugtP*.P395T are capitalized, and the adjacent 20 bp of flanking homology are in lowercase font. In the native sequence, the PAM site is underlined and the two bp between which the DSB occurs are in bold font. The BspHI restriction site is italicized in the modified sequence, and a summary of HLs analyzed during editing template HL optimization are shown (editing template is represented as ET in the figure). (B) The native (*amyE*) and modified (editing template) sequences of the mutation regions for *amyE* KO at *amyE*.P25NT, *amyE*.P330T, *amyE*.P636T and *amyE*.P1344T are capitalized, and the adjacent 18-21 bp of flanking homology are in lowercase font. In the native sequences, PAM sites are underlined and the two bp between which the DSBs occur are in bold font. The XhoI (*amyE*.P25NT and *amyE*.P330T), ScaI (*amyE*.P636T) and BamHI (*amyE*.P1344T) restriction sites are italicized in the modified sequences. (C) The unaltered (*seHas*) and modified (editing template) sequences of the mutation region for *seHas* KO at *seHas*.P394T are capitalized, and the adjacent 18 bp of flanking

homology are in lowercase font. In the unaltered sequence, the PAM site is underlined and the two bp between which the chromosomal DSB occurs are in bold font.

mg/L. SpII media contained the following: $(NH_4)_2SO_4$, 1.67 g/L; K_2HPO_4, 11.64 g/L; KH_2PO_4, 5.0 g/L; trisodium citrate dihydrate, 833 mg/L; glucose, 4.17 g/L; $MgSO_4 \cdot 7H_2O$, 725 mg/L; yeast extract, 858 mg/L; casamino acids, 86 mg/L; Arg, 3.78 g/L; His, 189 mg/L; Trp, 24 mg/L; $CaCl_2$, 48 mg/L. To improve transformation efficiency, the following modifications were made to the cited protocol: i) yeast extract was increased by 30% in SpC (2.17 g/L) and SpII (1.12 g/L) media, ii) glycerol was removed from the resuspension media, and iii) cells were resuspended in 1/40 of the initial volume of SpII media (the cited protocol specifies 1/10 of the initial volume). *B. subtilis* strains were plated on non-select lysogeny broth (LB) containing 5 g/L NaCl, 5 g/L yeast extract and 10 g/L tryptone, and incubated overnight (O/N). Pre-warmed SpC media was inoculated by cell patches from the O/N plate to OD_{600} 0.5-0.7. Seventy five min after the logarithmic growth phase ended, cultured cells were then diluted 100-fold in pre-warmed SpII media, and incubated for 110 min before harvesting. Two µg of gRNA delivery vector and 2 µg of each editing template were used per transformation (400 µL total volume), and transformed cells were incubated for 80 min [260 revolutions per min (rpm)], and then plated on LB agar containing 12 g/L glucose (LBG) and 85 µg/mL spectinomycin to select recombinants. All cultivation steps were conducted at 37 °C and 300 rpm unless otherwise indicated, and all experiments were performed in triplicate. To remove the gRNA transcription cassettes by transformation of the *thrC* editing template, cells were transformed with 1.5 µg of the *thrC* editing template, plated on LB agar containing 20 g/L arabinose (LBA) to select recombinants, and screened for spectinomycin sensitivity. To facilitate auto-eviction of the combined

P_{araE}::*mazF*-Spc^R cassette after transformation of pAW018-2, cells were grown for ~20 h in non-select LB at 37 °C and 260 rpm, plated on LBA and screened for spectinomycin sensitivity.

3.2.4 HA production, purification and analysis

To assess HA production, AW005-2 was plated on non-select LB and grown O/N at 37 °C. A single colony was used to inoculate 25 mL non-select LB, and the culture was grown for ~14 h at 37 °C and 280 rpm. The culture was then used to inoculate 20 mL pre-warmed non-select cultivation media (4% v/v) of the following composition: $(NH_4)_2SO_4$, 1 g; $K_2HPO_4 \cdot 3H_2O$, 9.15 g; KH_2PO_4, 3 g; trisodium citrate· $2H_2O$, 1 g; yeast extract, 10 g; casamino acids, 2.5 g; $CaCl_2$, 5.5 mg; $FeCl_2 \cdot 6H_2O$, 13.5 mg; $MnCl_2 \cdot 4H_2O$, 1 mg; $ZnCl_2$, 1.7 mg; $CuCl_2 \cdot 2H_2O$, 0.43 mg; $CoCl_2 \cdot 6H_2O$, 0.6 mg; $Na_2MoO_4 \cdot 2H_2O$, 0.6 mg. Glucose or sucrose was used as primary carbon source (20 g/L), and the cultures were grown at 37 °C and 280 rpm in triplicate. Samples were diluted two-fold in phosphate buffered saline, and HA was purified with cetylpyridinium chloride as previously described [128]. HA titer was determined using the modified carbazole assay [191], and molecular weight (MW) was analyzed via agarose gel electrophoresis [192] with slight modifications. 2 µg of purified HA was loaded per well, and gels stained O/N in 0.005% Stains-All (50% v/v ethanol) were destained for ~8 h in 20% v/v ethanol, followed by destaining for ~16 h in 10% v/v ethanol. Gels were then photobleached for 20 min on a LED light box, and scanned with an Epson Perfection V600 Photo scanner (Epson; Nagano, Japan). Scanned images were analyzed using ImageJ [193], and data analysis was performed as previously described [192]. All samples were analyzed in duplicate.

3.2.5 Sample preparation and evaluation of β-galactosidase activity

To assess transcriptional interference of *lacZ*, a single colony was used to inoculate 25 mL LB (85 µg/mL spectinomycin) and the seed culture was incubated for ~14 h at 37 °C and 280 rpm. 0.5 mL of the seed culture was transferred into 50 mL LB containing 85 µg/mL spectinomycin, 1 mM IPTG for induction of *lacZ*, and 1.2 % (w/v) xylose for induction of dCas9, and grown to OD_{600} of ~1.6. To obtain cell extract, cells in the amount of 30 OD_{600}-units (defined as the product of cell density in OD_{600} and sample volume in mL) were centrifuged at 10,000g for 10 min at room temperature. The cell pellet was resuspended in 1.5 mL Z-buffer and sonicated intermittently (0.5/0.5 s on/off) for 4 min in an ice water environment with a Sonicator 3000 ultrasonic liquid processor and microtip (Misonix; New York, USA). The raw cell extract was then used to determine β-galactosidase activity as previously described [194]. All experiments were performed in triplicate.

3.2.6 Real-time quantitative reverse transcription PCR (qRT-PCR)

For RNA isolation, cells were grown as described in the preceding section. Total RNA was prepared using the High Pure RNA Isolation Kit (Roche Diagnostics; Basel, Switzerland) as per the manufacturer's instructions. cDNAs were synthesized using the High-Capacity cDNA Reverse Transcription Kit (ThermoFisher Scientific; Massachusetts, USA). Sequence specific primers were used for reverse transcription of the *lacZ* (P3.88) mRNA and internal control *rpsJ* (P3.90) mRNA, encoding the 30S ribosomal protein S10, at a final concentration of 1 µM. 100 ng of total RNA and 20 units of Murine RNase Inhibitor (New England Biolabs (NEB); Massachusetts, USA) were used per 20 µL reaction. Real-time qRT-PCR was carried out using the Power SYBR® Green PCR Master Mix (ThermoFisher Scientific; Massachusetts, USA) in an Applied Biosystems StepOnePlus™ System as per the manufacturers' instructions. Sequence

specific primers were used for amplification of *lacZ* (P3.87/P3.88) and *rpsJ* (P3.89/P3.90). Data analysis to quantify relative expression between cultures with or without induction of dCas9 was performed as previously described [195]. All experiments were performed in triplicate.

3.3 Results

3.3.1 Design and evaluation of the $P_{xylA.SphI+1}$ gRNA transcription cassette

Compared to the native pre-crRNA/tracrRNA duplex, the chimeric gRNA has been preferred for CRISPR-Cas9-mediated genome editing and transcriptional interference [19, 20, 23, 84, 101-103, 196] since its introduction. We first developed a gRNA transcription cassette facilitating simple replacement of the protospacer without the requirement for inverse PCR, which is a procedure often employed to replace the existing protospacer [23, 197]. Given the requirement for a precise 5' end to the protospacer [197], we chose the native promoter P_{xylA} for its considerable strength and annotated transcriptional start site [198]. To facilitate insertion of the gRNA transcription cassette, we introduced a SphI restriction site between the -10 and +2 regions of P_{xylA}, yielding $P_{xylA.SphI+1}$ (Figure 3.1A). This arrangement allowed the addition of a unique protospacer as an overhang in the forward primer amplifying the combined CBH-terminator fragment, generating a gRNA cassette that can be inserted downstream of $P_{xylA.SphI+1}$ using restriction/ligation cloning. To construct the base *B. subtilis* strain for evaluation of CRISPR-Cas9 toolkit components, we transformed pAW016-2 into 1A751, resulting in AW001-2, which constitutively expressed *cas9* and transcribed the tracrRNA from the *lacA* locus. On the other hand, the gRNA transcription cassette(s) was integrated into the *thrC* locus of the *B. subtilis* genome to ensure gRNA stability and to allow simple eviction of the cassette with a subsequent integration event using the *thrC* editing template once the CRISPR-Cas9-mediated

mutation was complete. Also, *mazF* was included in the gRNA delivery vectors for genomic co-integration with the gRNA transcription cassette as it is an effective counter-selectable marker in *B. subtilis* [13]. To assess the vector design, we chose to KO *ugtP* (encoding a UDP-glucose diacylglyceroltransferase) since the mutation causes a distinct morphological change. For comparison purposes, AW001-2 was transformed with either pAW006-2 (transcribing a gRNA targeting *ugtP*.P395T) or pAW013-2 (transcribing a CRISPR array targeting *ugtP*.P395T), and the full length *ugtP* editing template, generating AW002-2 and AW003-2, respectively. The editing efficiency was evaluated via phenotypical screening, followed by colony PCR, subsequent BspHI digestion (Figure 3.7A), and sequencing of selected colonies. Similar editing efficiencies were observed when transforming pAW006-2 (79%) and pAW013-2 (82%) (Figure 3.7B), suggesting functional promoter activity of $P_{xylA.\mathrm{SphI+1}}$. Nevertheless, the transformation efficiency remained low at less than 20 CFU μg^{-1} editing template. We then modified the competence protocol to increase transformation efficiency as described in M&M.

3.3.2 Continuous editing for gene KI and KOs

With the modified transformation protocol, we exploited the capacity of our toolkit for continuous editing. We first conducted genomic insertion of the HA operon (P_{grac}::*seHas*:*tuaD)* into the *amyE* locus (*amyE*.P636T). HA is a linear, unbranched polysaccharide composed of alternating GlcNAc and GlcUA residues, reaching up to 8 MDa in size [5]. The hyaluronan synthase (HasA) autonomously synthesizes HA from UDP-GlcNAc and UDP-GlcUA [115], which are precursors for cell wall synthesis in *B. subtilis*. As a result, HasA is the only heterologous enzyme required to produce HA in this organism [5]. UDP-GlcUA availability has been shown to limit HA production in *B. subtilis*, such that constitutive expression of the UDP-

glucose 6-dehydrogenase is required to achieve high-level production [5]. P_{grac} is a strong hybrid promoter developed for *B. subtilis* [39], whereas *seHas* and *tuaD* encode the HasA from *Streptococcus equisimilis* [108] and native UDP-glucose 6-dehydrogenase [TuaD] [5], respectively. HA was chosen for demonstration for the following reasons. First, it is a high-value therapeutic biopolymer and only two genes (i.e. *seHas* and *tuaD*, or equivalent homologues) need to be expressed in *B. subtilis* to achieve significant production. Additionally, HA-producing strains have a prominent and observable mucoid phenotype [5], facilitating evaluation of editing efficiency. AW001-2 was transformed with pAW009-2 (transcribing a gRNA targeting *amyE*.P636T) and pAW020-2 (as an editing template), resulting in a mucoid strain (AW004-2) upon successful KI. The high KI efficiency for the HA operon (69%; Figure 3.7C) was attributed to the enhanced transformation which led to a 5-fold increase in the number of successful mutants relative to the initial *ugtP* KO demonstration. To prepare for the next round of editing, AW004-2 was transformed to be arabinose-resistant with the *thrC* editing template (refer to Figure 3.3 for continuous editing procedure), producing AW005-2. Eviction of the combined $P_{xylA.SphI+1}$::*amyE*-gRNA.P636T-P_{araE}::*mazF*-Spc^R cassette was confirmed by screening for spectinomycin sensitivity. The efficiency of *mazF* counter-selection was, however, low (6%), compared to the initial demonstration [13], due to the significant reduction (~30-fold) in transformation efficiency observed for HA-encapsulated strains (data not shown). For the next round of editing, s*eHas* was mutated by transformation of AW005-2 with pAW011-2 (transcribing a gRNA targeting *seHas*.P394T) and pAW021-2 (as an editing template), abolishing HA production and the mucoid phenotype in the resulting strain (AW006-2). The *seHas* editing efficiency was also low (Figure 3.7C), owing to transformation interference from the HA capsule. To further challenge the toolkit, we removed the combined $P_{xylA.SphI+1}$::*seHas*-

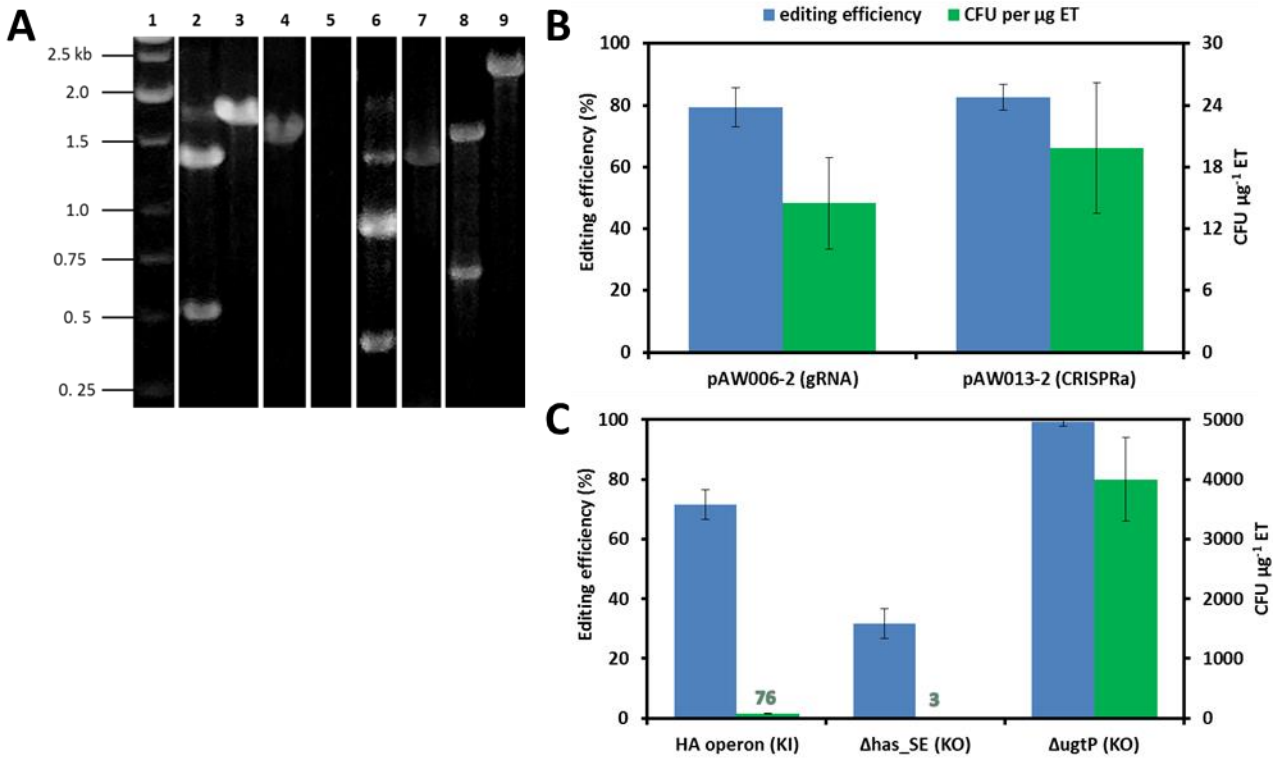

Figure 3.7. Assessment of the $P_{xylA.SphI+1}$ gRNA transcription cassette, and continuous editing with the CRISPR-Cas9 toolkit. A) Colony PCR screening of *ugtP*, *seHas* and *amyE* KOs, and KI of the HA operon. To screen for the *ugtP* KO (*ugtP*.P395T), primers P3.45/P3.138 amplified a 1,817 bp product, and successful recombination of the editing template generated products of 1,344 bp and 473 bp upon BspHI digestion. To screen for the *seHas* KO (*seHas*.P394T), primers P3.139/P3.140 amplified a 1,284 bp product, and successful recombination of the editing template generated products of 407 bp and 877 bp upon SacI digestion. To screen for the KI of the HA operon (*amyE*.P636T), primers P3.141/P3.143 amplified a 1,559 bp product upon successful recombination of the editing template (no product is observed in the absence of recombination). To screen for the *amyE* KO (*amyE*.P636T), primers P3.142/P3.143 amplified a 2,286 bp product, and successful recombination of the editing template generated products of 690 bp and 1,596 bp upon ScaI digestion. Lane 1: marker; lanes 2 and 3: modified (2) and unmodified (3) colonies screened for the *ugtP* KO; lanes 4 and 5: modified (4) and unmodified (5) colonies screened for the KI of the HA operon; lanes 6 and 7: modified (6) and unmodified (7) colonies screened for the *seHas* KO; lanes 8 and 9: modified (8) and unmodified (9) colonies screened for the *amyE* KO. Images of multiple agarose gels have been spliced together for the purpose of condensing the data presented. B) The $P_{xylA.SphI+1}$ gRNA transcription cassette was assessed in a parallel comparison with the native CRISPRa by transforming AW001-2 with either pAW006-2 (transcribing a gRNA targeting *ugtP*.P395T) or pAW013-2 (transcribing a CRISPRa targeting *ugtP*.P395T), and the full length *ugtP* editing template to KO *ugtP*. Editing efficiency was evaluated via phenotypical screening and colony PCR (and subsequent BspHI digestion). Transformation efficiency is defined as the total number of colony forming units (CFU) containing the desired mutation generated per µg of editing template DNA (represented as ET in the figure). Standard deviations (SD) of experiments performed in triplicate are shown. C)

The capacity of the toolkit for continuous editing was evaluated by introducing three successive mutations into the same background. First, the HA operon (P_{grac}::*seHas*:*tuaD*) was inserted into the *amyE* locus (*amyE*.P636T) of AW001-2 via transformation of pAW009-2 and pAW020-2, resulting in mucoid strain AW004-2. KI efficiency was evaluated via phenotypical screening followed by colony PCR. The combined $P_{xylA.SphI+1}$::*amyE*-gRNA.P636T-P_{araE}::*mazF*-Spc^R cassette was evicted from AW004-2 by transformation of the *thrC* editing template to arabinose resistance (and spectinomycin sensitivity), resulting in AW005-2. Next, *seHas* was mutated (at *seHas*.P394T) in AW005-2 via transformation of pAW011-2 and pAW021-2, resulting in AW006-2, a strain exhibiting the WT morphology. Editing efficiency was evaluated by phenotypical screening, followed by colony PCR (and subsequent SacI digestion). The combined $P_{xylA.SphI+1}$::*seHas*-gRNA.P394T-P_{araE}::*mazF*-Spc^R cassette was evicted from AW006-2 as previously described, yielding AW007-2. Finally, *ugtP* was mutated (at *ugtP*.P395T) in AW007-2 via transformation of pAW006-2 and the full length *ugtP* editing template. Editing efficiency was evaluated by phenotypical screening, followed by colony PCR (and subsequent BspHI digestion). SD of experiments performed in triplicate are shown.

gRNA.P394T-P_{araE}::*mazF*-Spc^R cassette using the same counter-selection procedure, yielding AW007-2, and subsequently mutated *ugtP* by transformation of AW007-2 with the full length *ugtP* editing template and pAW006-2 (transcribing a gRNA targeting *ugtP*.P395T), generating AW008-2. The *mazF* counter-selection efficiency was significantly higher when generating AW007-2 (31%) compared to AW005-2 (6%), supporting the conclusion that poor transformability led to low editing efficiency. The high editing efficiency for the *ugtP* KO (99%; Figure 3.7C) represented a substantial improvement over the initial *ugtP* KO demonstration (79%; Figure 3.7B) and this observation coincides with the 276-fold increase in transformation efficiency obtained with the enhanced competence protocol (4.0×10^3 CFU μg^{-1} editing template vs. 14.5 CFU μg^{-1} editing template). Note that the KI efficiency of the HA operon was comparable to that of single gene insertions reported in *E. coli* [20]. Also, the *ugtP* editing efficiency was in line with systems developed for *E. coli* [19, 20] and *S. cerevisiae* [21, 22], all of which rely on multicopy vectors to deliver CRISPR-Cas9 machinery.

We assessed the capacity of AW005-2 to produce high MW HA using glucose or sucrose as primary carbon source. Similar growth patterns were observed during cultivation on either

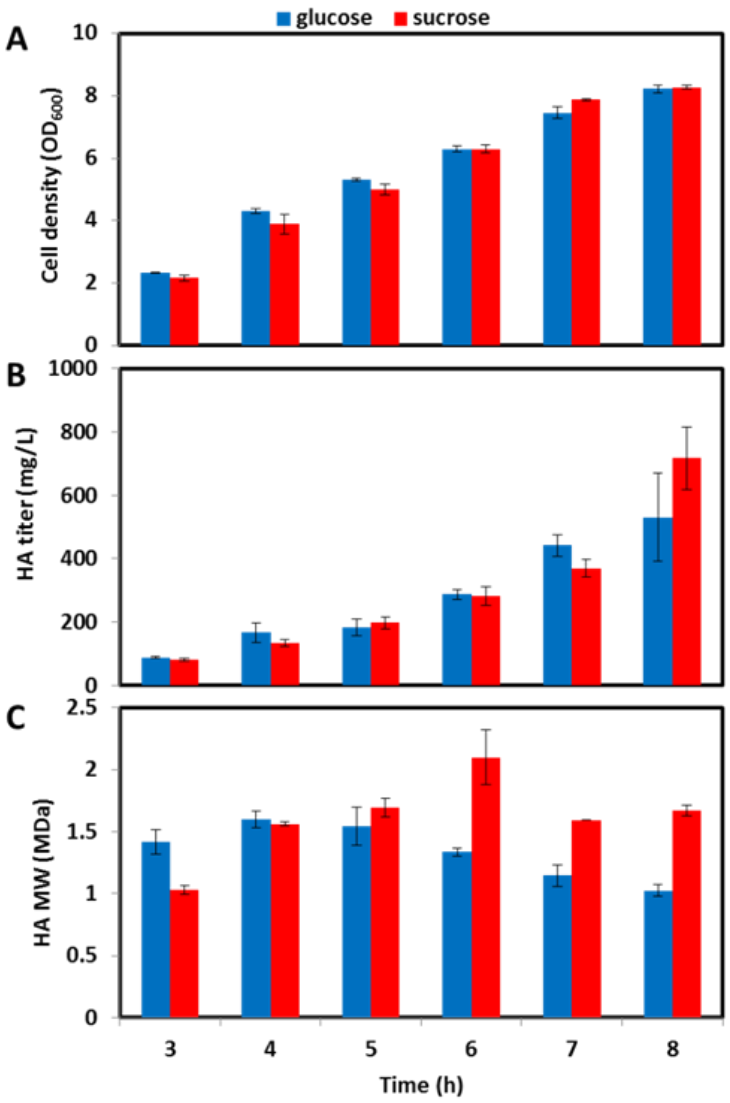

Figure 3.8. Cultivation of AW005-2 for HA production. A) Cell density, B) HA titer and C) HA MW. SD of experiments performed in triplicate are shown in Panels A and B, and SD of duplicate samples are shown in Panel C.

carbon source (OD_{600} ~8 after 8 h; Figure 3.8A), and were similar to those of our HA-producing strains constructed using traditional cloning techniques (data not shown). The HA titer was slightly higher for the 8 h cultivation sample with sucrose (717 ± 99 mg/L) as the carbon source, compared to glucose (530 ± 139 mg/L; Figure 3.8B), although sucrose metabolism generally led

to a significantly higher MW (1.67 ± 0.05 MDa and 1.15 ± 0.09 MDa for sucrose and glucose, respectively) (Figure 3.8C). Moreover, a higher maximum MW was obtained (2.1 ± 0.22 MDa and 1.60 ± 0.07 MDa for sucrose and glucose, respectively), and the MW peaked later (and declined to a lesser extent) for the sucrose cultivation. The MW observed during cultivation on either carbon source compares favorably to a previous report of HA production in *B. subtilis* [5], and both HA titer and MW were similar to those obtained with our HA-producing strains developed through conventional cloning. The titers obtained with AW005-2 also compared favorably to the titer reported for a similar strain of *B. subtilis* over the same cultivation period [128]. A significantly longer cultivation was required to achieve a similar titer, and MW was not assessed in the aforementioned study. In addition, the titer and MW of HA produced by AW005-2 was similar to those obtained with strains of *B. subtilis* overexpressing additional enzymes of the HA biosynthetic pathway (i.e. GtaB, GlmM, GlmS and GlmU), in combination with HasA and TuaD [130]. Accordingly, it appears that chromosomal expression of Cas9 does not hinder HA production, and this feature is critical for the toolkit to be applied to industrial strain development. Finally, the HA titer increased by extending the cultivation, although a concomitant decrease in MW was observed. Declining MW during extended cultures of HA-producing strains of *B. subtilis* has been reported [5, 129].

3.3.3 Application of the CRISPR-Cas9 toolkit to multiplexing

For simultaneous editing of *B. subtilis* genomic targets, we constructed a multi-gRNA delivery vector to accommodate multiple gRNAs using the Biobrick assembly approach [199]. Each gRNA transcription cassette can be transferred from its respective single-gRNA delivery vector to the multi-gRNA delivery vector or by direct cloning of the spliced $P_{xylA.SphI+1}$ and

gRNA cassette as described in M&M. To assess multiplexing capability, the $P_{xylA.SphI+1}$::*amyE*-gRNA.P636T cassette was inserted into pAW014-2 using NheI and BglII restriction sites, yielding pAW015-2, to enable simultaneous KO of *ugtP* and *amyE*. AW001-2 was transformed with pAW015-2 (transcribing two gRNAs targeting *ugtP*.P395T and *amyE*.P636T) and the full length *ugtP* and *amyE* editing templates which each contain ~1,330 bp HLs. Colonies were first assessed for the *ugtP* null phenotype, after which *ugtP* mutant and non- mutant colonies were screened for α-amylase (encoded by *amyE*) deficiency via iodine staining. Colonies from each of the phenotype subsets (i.e. $ugtP^+/amyE^+$, Δ*ugtP*/$amyE^+$, $ugtP^+$/Δ*amyE* and Δ*ugtP*/Δ*amyE*) were screened via colony PCR and subsequent BspHI (*ugtP*) or ScaI (*amyE*) digestion, and selected colonies were sequenced. While simultaneous KO of *ugtP* and *amyE* was successful, the multiplexing efficiency was only 36% (Figure 3.9A), owing to a much lower editing efficiency for *amyE* compared to *ugtP* (38 and 86%, respectively). Hence, several genome editing factors potentially limiting multiplexing efficiency, specifically editing template type (i.e. PCR product vs. linearized plasmid), HL size, and PAM site sensitivity, were investigated.

3.3.4 Effect of editing template type

Due to the distinctively low *amyE* editing efficiency and given that transformation efficiencies for PCR products are expectedly lower compared to linearized plasmids [186], the *amyE* single KO was evaluated by transforming AW001-2 with pAW009-2 (transcribing a gRNA targeting *amyE*.P636T), and the full length *amyE* editing template (as a PCR product editing template) or pAW022-2 (as a plasmid editing template). While the *amyE* editing efficiency was significantly higher as a single KO (93%; Figure 3.9B), the transformation efficiency (2.69×10^2 CFU μg^{-1} editing template) was low. On the other hand, the use of

pAW022-2 as an editing template increased transformation efficiency by nearly six-fold (1.55 $\times 10^3$ CFU μg^{-1} editing template) and, in turn, editing efficiency (100%; Figure 3.9B) compared to the full length *amyE* editing template.

3.3.5 Effect of HL size

The optimal HL was determined by targeting *ugtP* as it was perceived to be a recombination 'hot spot' based on generally high editing and transformation efficiencies. Editing templates containing 100, 300, 500, 750 and 1,000 bp HLs were constructed from the full length *ugtP* editing template such that the same mutation region was flanked by the specified HL (Figure 3.6A). Various editing templates were transformed with pAW006-2 (transcribing a gRNA targeting *ugtP*.P395T) into AW007-2. The editing efficiency remained high for HLs between 500 and 1,000 bp (>97%; Figure 3.9C), but decreased dramatically when HL was reduced to 300 bp. No transformants were obtained for 100 bp HL. Our results are consistent with earlier reports suggesting that 400-500 bp HLs are sufficient for acceptable transformation efficiency of linear DNA in *B. subtilis* [15]. The optimal HL was determined to be 1,000 bp, for which editing efficiency reached ~100%.

3.3.6 PAM site sensitivity

To further improve *amyE* editing efficiency, we assessed three PAM sites in the *amyE* ORF, in addition to the original PAM site (*amyE*.P636T). The PAM sites were selected based on the purine content of the last four bp of the 3' end of the protospacer [min. 75%] [196], and the location relative to the initial PAM site. P25NT was the first available site in the ORF; P330T was approximately half the distance from P25NT to P636T; P1344T was approximately half the

distance from P636T to the stop codon. Due to the moderate GC content of the *B. subtilis* genome (43.5%), all protospacers were 40-55% GC, and the targeting strand was not considered a priority due to a modest effect on gRNA efficacy [196]. AW001-2 was transformed with pAW007-2 (transcribing a gRNA targeting *amyE*.P25NT), pAW008-2 (transcribing a gRNA targeting *amyE*.P330T), pAW009-2 (transcribing a gRNA targeting *amyE*.P636T) or pAW010-2 (transcribing a gRNA targeting *amyE*.P1344T), using the optimized editing template HL of 1,000 bp. Editing efficiency was evaluated via iodine staining, followed by colony PCR and subsequent digestion with XhoI (*amyE*.P25NT and *amyE*.P330T), ScaI (*amyE*.P636T) or BamHI (*amyE*.P1344T) [Figure 3.9E]. The editing efficiencies for the first three PAM sites from the start codon were similar (87, 85 and 91%, respectively; Figure 3.9D) with *amyE*.P636T being targeted most effectively, suggesting minimal bias for the targeted strand. The observation of the low editing efficiency when targeting P1344T (23%) is consisent with the previous report that editing efficiency can vary dramatically between PAM sites in a single gene [22].

3.3.7 Enhanced multiplexing efficiency under optimized conditions

To enhance the multiplexing capacity of the toolkit, we re-explored the double KO of *amyE* and *ugtP* (by targeting *ugtP*.P395T and *amyE*.P636T) under the optimized conditions for editing template and *amyE* PAM site. Two editing template combinations were evaluated: 1) PCR products containing 1,000 bp HLs (*amyE* and *ugtP*), and 2) PCR product containing 1,000 bp HLs (*ugtP*) and pAW022-2 (*amyE*). AW001-2 was transformed with pAW015-2 (transcribing two gRNAs targeting *ugtP*.P395T and *amyE*.P636T) and either editing template combination 1 or 2. Relative to the initial multiplexing experiment (Figure 3.9A), using editing template

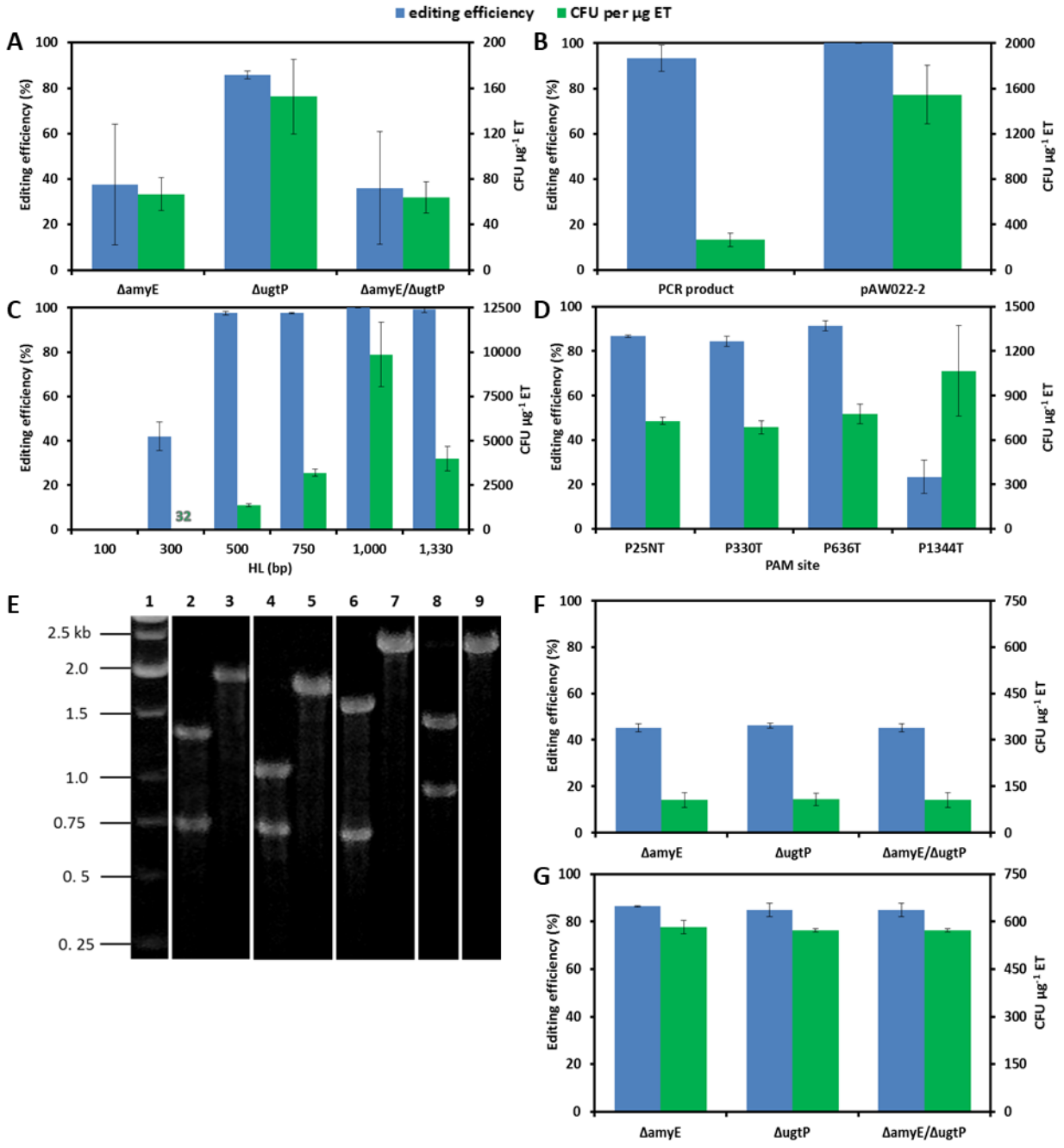

Figure 3.9. Application of the CRISPR-Cas9 toolkit to multiplexing. A) The preliminary evaluation of multiplexing efficiency was performed by simultaneously mutating *ugtP* and *amyE* via transformation of AW001-2 with pAW015-2, and the full length *ugtP* (*ugtP*.P395T) and *amyE* (*amyE*.P636T) editing templates. Mutants were first screened for the *ugtP* null phenotype, followed by iodine staining of mutant and WT colonies to evaluate *amyE* editing efficiency. Colonies from each of the phenotype subsets (i.e. $ugtP^{+}/amyE^{+}$, Δ*ugtP*/$amyE^{+}$, $ugtP^{+}$/Δ*amyE* and Δ*ugtP*/Δ*amyE*) were screened via colony PCR, and subsequent BspHI (*ugtP*) or ScaI (*amyE*) digestion. Transformation efficiency is defined as the total number of CFU containing the desired mutation generated per µg of editing template DNA (represented as ET in the figure). SD

of experiments performed in triplicate are shown. B) *amyE* was evaluated as a single KO (at *amyE*.P636T) by transforming AW001-2 with either the full length *amyE* editing template or linearized pAW022-2, and pAW009-2. Editing efficiency was evaluated via iodine staining, followed by colony PCR and subsequent ScaI digestion. SD of experiments performed in triplicate are shown. C) Editing template HL was optimized using *ugtP* as a KO target (*ugtP*.P395T). Editing templates containing HLs of 100, 300, 500, 750 and 1,000 bp (in addition to the full length *ugtP* editing template) were assessed by transforming AW007-2 with pAW006-2 and the corresponding editing templates. Editing efficiency was evaluated by phenotypical screening, followed by colony PCR (and subsequent BspHI digestion). SD of experiments performed in triplicate are shown. D) PAM site sensitivity analysis for *amyE*. Three PAM sites in the *amyE* ORF were evaluated (*amyE*.P25NT, *amyE*.P330T and *amyE*.P1344T), in addition to *amyE*.P636T, using the optimized editing template HL of 1,000 bp. AW001-2 was transformed with pAW007-2 (*amyE*.P25NT), pAW008-2 (*amyE*.P330T), pAW009-2 (*amyE*.P636T) or pAW010-2 (*amyE*.P1344T), and the corresponding editing templates. Editing efficiency was evaluated via iodine staining, followed by colony PCR and subsequent XhoI (*amyE*.P25NT and *amyE*.P330T), ScaI (*amyE*.P636T) or BamHI (*amyE*.P1344T) digestion. SD of experiments performed in triplicate are shown. E) Colony PCR screening of *amyE* KOs at *amyE*.P25NT, *amyE*.P330T, *amyE*.P636T or *amyE*.P1344T. To screen for the *amyE* KO at *amyE*.P25NT, primers P77/P80 amplified a 2,001 bp product, and successful recombination of the editing template generated products of 685 bp and 1,316 bp upon XhoI digestion. To screen for the *amyE* KO at *amyE*.P330T, primers P3.67/P3.76 amplified a 1,772 bp product, and successful recombination of the editing template generated products of 703 bp and 1,069 bp upon XhoI digestion. To screen for the *amyE* KO at *amyE*.P636T, primers P3.142/P3.143 amplified a 2,286 bp product, and successful recombination of the editing template generated products of 690 bp and 1,596 bp upon ScaI digestion. To screen for the *amyE* KO at *amyE*.P1344T, primers P3.142/P3.143 amplified a 2,286 bp product, and successful recombination of the editing template generated products of 1,396 bp and 890 bp upon BamHI digestion. Lane 1: marker; lanes 2 and 3: modified (2) and unmodified (3) colonies screened for the *amyE* KO at *amyE*.P25NT; lanes 4 and 5: modified (4) and unmodified (5) colonies screened for the *amyE* KO at *amyE*.P330T; lanes 6 and 7: modified (6) and unmodified (7) colonies screened for the *amyE* KO at *amyE*.P636T; lanes 8 and 9: modified (8) and unmodified (9) colonies screened for the *amyE* KO at *amyE*.P1344T. Images of multiple agarose gels have been spliced together for the purpose of condensing the data presented. F) Enhanced multiplexing using editing template combination 1. *ugtP* and *amyE* were simultaneously mutated by transforming AW001-2 with pAW015-2, and the 1,000 bp HL *ugtP* (*ugtP*.P395T) and *amyE* (*amyE*.P636T) editing templates. Editing efficiency was evaluated as described for Panel A, and SD of experiments performed in triplicate are shown. G) Enhanced multiplexing using editing template combination 2. *ugtP* and *amyE* were simultaneously mutated by transforming AW001-2 with pAW015-2, and the 1,000 bp HL *ugtP* (*ugtP*.P395T) editing template and pAW022-2 (*amyE*.P636T). Editing efficiency was evaluated in the same way as for editing template combination 1. SD of experiments performed in triplicate are shown.

combination 1 resulted in an improved editing efficiency for both the *amyE* KO (45%) and the double KO (45%), although a substantial reduction was observed for the *ugtP* KO (46%; Figure

3.9F). On the other hand, using editing template combination 2 led to drastic improvements in editing efficiency for both the *amyE* KO (86%) and the double KO (85%), with a similarly high efficiency for the *ugtP* KO (85%; Figure 3.9G). The high multiplexing efficiency observed for editing template combination 2 was similar to reports of the double editing efficiency with ssDNA as an editing template (83%) [19], but somewhat lower compared to the editing with a dsDNA editing template [97%] [20] in *E. coli*. These results suggest that our CRISPR-Cas9 toolkit can achieve high multiplexing efficiency in *B. subtilis*, even when challenging targets (such as *amyE*) are chosen.

3.3.8 Extension of the CRISPR-Cas9 toolkit to transcriptional interference

To exploit the full utility of the toolkit, we extended our existing CRISPR-Cas9 platform from genome editing to CRISPRi for transcriptional interference. The *lacZ* gene was used as a reporter to assess repression at the level of transcription and protein expression in AW016-2. To construct AW016-2, we began by transforming AW009 with pAW019-2, yielding strain AW014-2, which expresses xylose-inducible dCas9 from the *lacA* locus. AW014-2 was then transformed with pAW018-2, followed by auto-eviction of the CS cassette (Figure 3.4A), yielding strain AW015-2, in which a gRNA targeting *lacZ*.P28NT was transcribed from the *wprA* locus. Finally, IPTG-inducible *lacZ* was integrated into the *ugtP* locus of AW015-2 via transformation of pAW016, generating strain AW016-2. Cultures of AW016-2 in which dCas9 expression was induced with xylose were compared with uninduced cultures to assess CRISPRi efficiency. Nearly 8-fold reduction in both *lacZ* mRNA and β-galactosidase activity was observed in AW016-2 upon induction of dCas9 (Figure 3.10), demonstrating the efficacy of our toolkit for reducing gene expression.

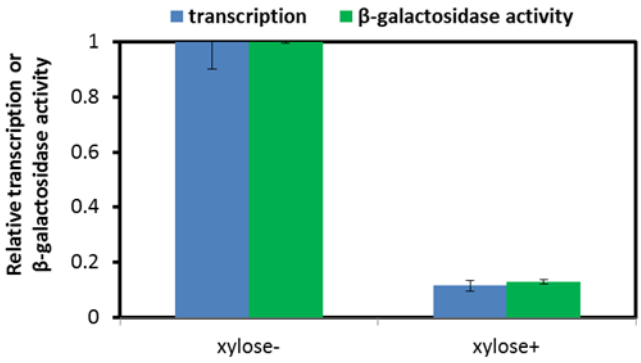

Figure 3.10. Evaluation of CRISPRi-mediated repression of *lacZ* expression at the level of transcription and protein expression. AW016-2 was grown in LB supplemented with 85 µg/mL spectinomycin, 1 mM IPTG to induce *lacZ* expression, and 1.2% (w/v) xylose to induce dCas9 expression (xylose+) or without xylose (xylose-). *rpsJ*, encoding the 30S ribosomal protein S10, served as an internal control for analysis of transcriptional repression via real-time qRT-PCR. β-galactosidase activity was evaluated using the Miller assay to assess repression at the level of protein expression. Relative transcription (i.e. relative to transcription of *rpsJ*) and protein expression were normalized to the values obtained from cultures in which dCas9 expression was not induced (xylose-). SD of experiments performed in triplicate are shown.

3.4 Discussion

Recent advent of the CRISPR-Cas9 system has significantly increased the capacity for genome editing and transcriptional modulation in a selection of organisms [19, 21, 84, 88, 92, 94]. *B. subtilis* shows considerable promise as an established industrial workhorse [24, 200], such that a CRISPR-Cas9 toolkit is essential to its progression towards full industrial utility. Traditional methods employed in *B. subtilis* such as auto-evicting counter-selectable markers and site-specific recombination suffer from low editing efficiency [13, 67] and/or limited capacity for multiplexing. Furthermore, existing technologies for transcriptional metering require extensive characterization or sequence modification prior to deployment, making their adoption cumbersome and time-consuming [95-99]. Here we propose an effective and scalable CRISPR-Cas9 toolkit for comprehensive engineering of *B. subtilis*, including targeted single gene KO and KI, continuous genome editing, multiplexing and targeted transcriptional repression. We

employed chromosomal maintenance of CRISPR-Cas9 machinery for several reasons: i) Multicopy plasmids are potentially unstable, an issue that is of particular concern in *B. subtilis* [30-32]; ii) Multicopy plasmids can impose a fitness burden on the host, particularly when selection is required to maintain them; iii) CRISPR-Cas systems naturally exist in many bacteria, and presumably do not impede cell viability in this context; iv) The transformation efficiency of monomeric plasmids obtained from traditional cloning procedures is typically low in *B. subtilis* [8, 201]; and v) Plasmids must be cured from the engineered cell.

For the development of the counter-selectable gRNA delivery vectors, we tested two promoters for inducible *mazF* expression, in addition to P_{spac}, whose leaky nature presumably resulted in low transformation efficiency in *B. subtilis*. The resulting vector (pAW003-2) based on the use of $P_{xylA,\ Bm}$, a stronger and more tightly controlled promoter [189], was difficult to maintain in *E. coli*. The reduced viability of the *E. coli* strain carrying pAW003-2 could not be resolved, even by replacing *mazF* with *mazE*, encoding the antitoxin of MazF (MazE). On the other hand, the use of P_{araE} resulted in a vector (pAW004-2) that was stable in *E. coli* and effectively transformed into *B. subtilis*. The presence of the native CRE between P_{araE} and the ribosome binding site (RBS) of *mazF* provides additional regulation of transcription in the presence of glucose, and this feature is desirable given the strong dependence of toolkit performance on transformation efficiency (as subsequently discussed). To exploit the simplicity of the CRISPR-Cas9 system, we developed a gRNA transcription cassette using a modified version of the native promoter P_{xylA}, i.e. $P_{xylA.SphI+1}$, facilitating the construction of gRNA delivery vectors. The transcriptional start site (+1) of P_{xylA} was determined to be 4-6 bp downstream of the -10 region [198], while that of the similar $P_{xylA,\ Bm}$ was found to be located 6 bp downstream of the -10 region [202]. Accordingly, a single mismatch at the 5' end of the gRNA (i.e. the 6th bp of

the SphI restriction site; Figure 3.1A) appears to have a negligible effect on Cas9 targeting given high editing efficiencies and transcriptional repression observed in general.

As the CRISPR-Cas9 mechanism involves at least two simultaneous recombination events [i.e. integration of gRNA(s) and editing template(s)], effective transformation becomes critical. Our enhanced competence protocol significantly improved DNA transformation into *B. subtilis*, leading to high editing efficiencies with our CRISPR-Cas9 toolkit. Using the improved protocol, the transformation efficiency for the *ugtP* KO with the 1,000 bp HL editing template (8.87×10^3 CFU μg^{-1} editing template; Figure 3.9C) exceeds that of a recent report of enhanced transformation efficiency of individual dsDNA PCR products (~4.0×10^3 CFU μg^{-1} dsDNA) and is similar to efficiency reported for linearized plasmid (~1.0×10^4 CFU μg^{-1} plasmid) via induction of the master competence regulator ComK [186]. Our toolkit also provided high editing efficiencies for both a multi-gene KI and a single-gene KO over sequential rounds of editing using the counter-selectable marker *mazF*. While our toolkit is not necessarily a convenient option to replace existing technologies for single KIs and KOs, it is more efficient for continuous genome engineering in *B. subtilis.* Using successive knock-outs as an example, this procedure would entail two rounds of restriction/ligation cloning to replace the HLs of an existing vector, or using an advanced cloning technique (e.g. Gibson assembly) to fuse various DNA fragments, (i.e. the plasmid backbone, the 5'-HL, the selection and counter-selection markers, and the 3'-HL). These methods are either time consuming or resulting in unwanted mutations. The situation becomes more complicated for conventional cloning when mutations are introduced into the targeted ORF. This will require that either 1) the DRs of the integration vector be redesigned such that the single-crossover event between them needed to excise the selection and counter-selection markers results in the introduction of the desired mutation, or 2)

an editing template be designed to replace the selection and counter-selection markers with the desired mutation. Another option would be to construct an integration cassette using multiple rounds of SOE-PCR, which can be unreliable due to large DNA sizes [203]. On the other hand, our toolkit requires only a single restriction/ligation step to insert the new gRNA (102 bp) into the gRNA delivery vector, and a single round of SOE-PCR to generate the editing template (which can be as small as 1 kb). Furthermore, our toolkit requires no additional effort to introduce specific mutations, beyond designing the mutation region of the editing template to introduce the desired mutation, and, if necessary, an additional silent mutation to remove the PAM site [94].

The improved editing efficiency observed for the *ugtP* KO compared to the KI of the HA operon (Figure 3.7C) was expected given that increasing insertion size has been shown to correlate with decreasing editing efficiency in CRISPR-Cas9 systems [19, 86]. Moreover, the reduced recombination frequency of the HA operon KI cassette could have been exacerbated by an excessive metabolic burden associated with HA synthesis, which is an energy and carbon intensive process directly competing with central metabolism and cell wall synthesis [5]. This conclusion was supported by our observation of a few transformants with the KI of the HA operon but showing no mucoid phenotype, implying that expression of functional *seHas* and/or *tuaD* can be inactivated. In addition to the expected reduction in recombination frequency associated with large insertions, recombination may occur less effectively at certain genomic loci. Considering that the number of escapers were similar between the KI of the HA operon (at *amyE*.P636T), the *ugtP* KO and the single *amyE* KOs (except at *amyE*.P1344T), discrepancies in transformation and editing efficiencies at the *amyE* and *ugtP* loci (Figures 3.7C, 3.8B and 3.8D) could have been influenced by different recombination frequencies at these sites. Interestingly,

our KI efficiency for the 2,909 bp HA operon (69%) exceeds that reported for a 3,000 bp CRISPR-Cas9-mediated insertion in *E. coli* [59%] [19]. This comparison corroborates the efficacy of our toolkit for large chromosomal insertions given the insertion location of *amyE* appears to be a difficult recombination site and the inserted operon imparts a significant metabolic burden on the host. Finally, chromosomal expression of Cas9 appeared to have a minimal effect on cell viability given that the specific growth rates and final cell densities were similar between 1A751 and AW001-2 (data not shown), and Cas9 was stably maintained in the chromosome across three sequential rounds of editing.

The low efficiency of the initial multiplexing trial (36%) suggests that *amyE* is a difficult recombination target. As previously discussed, the similar number of escapers observed when targeting *amyE* and *ugtP* suggests that CRISPR-Cas9-mediated cleavage was not the limiting factor for the low *amyE* editing efficiency. Various factors limiting the editing efficiency were systematically evaluated to enhance the performance of our toolkit when targeting difficult sites. Our results for the *ugtP* KO (Figure 3.9C) support the previous conclusion that 400-500 bp HLs are sufficient to achieve an acceptable transformation efficiency of linear DNA in *B. subtilis* [15]. Decline in transformation efficiency for increasing homology beyond an optimal length has been reported elsewhere [204], and was attributed to the reduced number of plasmids transformed at larger HLs (based on an equivalent quantity of DNA per transformation). A stark decline in CRISPR-Cas9 editing efficiency in *S. cerevisiae* was also observed upon increasing the editing template HL from 50 to 60 bp, and sequence-specific features of the longer editing template causing premature termination of the hybrid editing template-crRNA transcript were the proposed cause [22].

Targeting *amyE*.P25NT, *amyE*.P330T and *amyE*.P636T resulted in comparable transformation and editing efficiencies, with *amyE*.P636T being targeted most effectively (Figure 3.9D). Small discrepancies in the number of escapers were observed, suggesting that Cas9 accessibility to the *amyE* locus was not limiting the editing efficiency. On the other hand, it has been perceived that certain PAM sites are less susceptible to CRISPR-Cas9-mediated DSBs since the editing efficiency can vary substantially between PAM sites in a single gene [22]. The poor editing efficiency when targeting *amyE*.P1344T supports this theory, although gRNA sequence characteristics can also affect targeting efficacy [196]. With the critical design parameters (except targeting strand for which minimal bias appears to exist) in mind [196], the underlying problem in gRNA design may be associated with potential secondary structures formed *in vivo*. Several secondary structures are generally possible for each gRNA sequence such that unwanted secondary structures may form, reducing the binding capacity (or frequency of binding) of Cas9 to the gRNA.

The multiplexing efficiency of our toolkit reached 85% through optimization of various editing template parameters and PAM sites (Figure 3.9G). A high multiplexing efficiency (up to 97%) was reported for the double KO of *maeA* and *maeB* in *E. coli*, although the multiplexing capacity was limited by the inclusion of gRNA transcription cassettes and editing templates in a single plasmid [20]. A CRISPR-Cas9 system recently developed for *S. cerevisiae* provided a high multiplexing efficiency for three targets (up to 87%), however, a long period of cultivation after transformation was required, significantly increasing the duration of a single round of editing [22]. In contrast to these systems and other improved methods for use in *E. coli* [19] and *S. cerevisiae* [21], our toolkit provides comparably high multiplexing efficiencies via CRISPR-Cas9 elements maintained in the chromosome. Our approach is more similar to the chromosomal

arrangement of CRISPR-Cas systems in native hosts, and takes advantage of the simplicity of the gRNA for Cas9 targeting.

The extension of our toolkit to CRISPRi provides an effective strategy for transcriptional modulation in *B. subtilis*. We demonstrate that expressing dCas9 and transcribing gRNAs chromosomally is sufficient to achieve efficient transcriptional repression in *B. subtilis*, which is likely the case in *E. coli* and many other bacterial species [197]. This is an attractive aspect of our approach due to potential plasmid instability [30-32], which is a greater concern when applying CRISPRi as dCas9 and gRNA transcription cassettes must be stably maintained in the cell. The extent of repression achieved with our toolkit is comparable to that obtained with existing asRNA protocols. Repression levels as high as 90% were obtained using an asRNA targeting *buk* mRNA (encoding the butyrate kinase) in *Clostridium acetobutylicum* [98]. However, significant repression of the acetate kinase (encoded by *ack*) was observed in the same strain, owing to the large degree of homology between *buk* and *ack*, demonstrating the potential for off target effects when applying asRNA strategies. Similar repression of DsRed2 expression was observed in *E. coli* using an asRNA containing an Hfq-recruiting scaffold to enhance hybridization, although the assessment of multiple scaffold sequences from endogenous asRNAs was necessary to achieve maximum repression [96]. Higher repression levels (>98%) were obtained in *E. coli* with 5'-*cis* sequences inserted upstream of the RBS (to which the sequences were complementary) of a green fluorescent protein, blocking recognition of the RBS by the 30S ribosomal subunit via a stem-loop structure [95]. Repression could be deactivated with a trans-activating RNA, although application of this strategy requires upstream sequence modification of the target gene, making it tedious to apply, particularly for multiplexing. A significant level of repression of β-galactosidase expression via CRISPRi was reported in *E. coli*, in which dCas9

and a *lacZ*-targeting gRNA were maintained in plasmids [23]. In the same study, up to 300-fold repression of expression of a monomeric red fluorescent protein (mRFP) was observed, which is similar to the CRISPR-dCas9-mediated RFP repression levels achieved in *Corynebacterium glutamicum* [182]. The differences in repression efficiency observed between β-galactosidase and RFP suggests that certain targets may be more susceptible to CRISPRi. Varying degrees of repression between different targets has also been observed in mycobacteria when applying CRISPRi, although the differences were less dramatic [183]. To allow targeting of multiple genes for multiplexing or targeting multiple sites in the same gene for enhanced repression, a multi-gRNA delivery vector was also constructed to enable auto-eviction of the P_{araE}::*mazF*-Spc^R cassette, while the multi-gRNA array is retained in the chromosome, using the same approach as outlined for pAW014-2 (Figure 3.2). Finally, the repression level can be adjusted by tuning gRNA design parameters established previously [23], rather than adjusting xylose concentration for inducing dCas9 expression [197]. For example, mismatches introduced in bp 8-12 of the protospacer (relative to the 3' end) cause a dramatic reduction in repression, while mismatches in bp 13-20 have a less significant effect on repression efficiency [the first 7 bp of the protospacer should not be altered] [23]. Moreover, the repression level is inversely proportional to the distance of the targeted PAM site from the start codon of the target ORF [23].

Chapter 4

Engineering of cell membrane to enhance heterologous production of HA in *B. subtilis*

4.1 Introduction

HA is naturally synthesized by certain pathogenic strains of bacteria, such as Lancefield group A [107] and C [108] streptococci, and Type A *P. multocida* [109], as a means of evading the host immune response [111]. HAS autonomously synthesizes HA from UDP-GlcNAc and UDP-GlcUA, and is classified as either a Class I or II HAS based on topology (i.e. transmembrane and peripheral membrane proteins for Class I and II HAS, respectively) and the number of glycosyltransferase 2 family modules present (i.e. one and two modules for Class I and II HAS, respectively). The relatively small size and few transmembrane domains of streptococcal HAS suggest that they cannot facilitate pore formation for translocation of the growing HA chain [115]. This theory was supported by the observation that mutation of a component of an ABC transporter complex reduced HA capsule size in *S. pyogenes*, suggesting that additional proteins may assist translocation [116]. However, recent work showed that SeHAS could mediate the release of the small fluorescent dye Cascade Blue from inside liposomes, and that mutations, which decreased HAS activity and HA MW in an earlier study, in one of its transmembrane domains resulted in reduced Cascade Blue efflux [117, 205]. Similarly, purified SeHAS, reconstituted into *E. coli*-derived or synthetic proteoliposomes, synthesized and translocated high MW HA into the vesicle lumen, requiring only exogenous UDP-GlcUA and UDP-GlcNAc [118]. These observations, along with the demonstration of HA production in a variety of bacteria heterologously expressing HAS [5, 6, 131, 133], indicate that a single HAS

protein produces HA autonomously via a process requiring as many as seven different functions to initiate and elongate the HA chain, and extrude it across the membrane [115].

CL is the least abundant phospholipid present in the membrane of growing *B. subtilis* cells as a dimer of the essential and abundant anionic phospholipid phosphatidylglycerol (PG) [206, 207]. PG is synthesized from cytosine diphosphate (CDP)-diacylglycerol by phosphatidylglycerophosphate synthase (PgsA; encoded by *pgsA*), and CL is subsequently produced from PG by the major CL synthase (ClsA; encoded by *clsA*) [206]. ClsA localizes at the septal region of the *B. subtilis* membrane in a FtsZ-dependent manner (Note that FtsZ initiates cell division.), presumably to assist in the assembly of the cell division machinery [208]. FtsZ depletion potentially results in dispersion of ClsA along the lateral membrane and, in turn, spatially coupled dispersion of CL [209]. The dependence of Class I HAS activity on its orientation with CL was first observed when the activity of the solubilized HAS of *S. pyogenes* (SpHAS) was recovered upon treatment with CL [120]. Active SpHAS and SeHAS were observed to be ~23 kDa larger than the purified enzymes, both of which were inactive [119]. Furthermore, the activity of purified SpHAS was not significantly enhanced by other lipids *in vitro*, and although the *in vitro* activity of purified SeHAS was stimulated by phosphatidic acid (PA) and phosphatidylserine, CL provided the greatest enhancements to SeHAS activity [121]. Therefore, it was proposed that ~16 CL molecules interact with a single SpHAS or SeHAS protein, and that loss of even a single molecule can cause enzyme inactivation. Accordingly, CL may assist HAS in creating an internal pore-like passage for HA translocation [119], which is similar to the function of CL proposed for several mitochondrial membrane proteins that lack transport capability in its absence [210]. In addition, interactions between CL and HA may add to the net retention force that keeps the HA-UDP/HAS complex together during polymerization until a sufficient opposing [release] force exceeds the net retention force, resulting in the release (and cessation of growth) of the growing HA chain [121, 211].

While membrane engineering for enhanced biological production is a challenging strategy with increasing applications in bacteria [29, 212], the approach is unpopular for *B. subtilis*. A documented study focused on the alteration of the lipid composition of the *B. subtilis* membrane, leading to enhanced secretion of the industrially important enzyme α-amylase [213]. Mutation of *clsA* or *pssA*, encoding phosphatidylserine synthase (PssA), significantly increased extracellular amylase production, presumably through creating a more negative membrane charge density [213]. In this study, we engineered the cell membrane of an HA-producing strain of *B. subtilis* to increase the functional expression of heterologously expressed SeHAS and, in turn, improve HA production. The membrane CL content was increased by overexpressing *pgsA* and *clsA*, resulting in significant improvements to the HA titer and MW. To further enhance the functional expression of SeHAS, we then altered the distribution of CL in the membrane by reducing the expression of *ftsZ* via CRISPRi using our recently developed CRISPR-Cas9 toolkit for *B. subtilis* [214]. The reduced *ftsZ* expression led to partial redistribution of CL along the lateral membrane and, as a result, improved HA titers and MWs in shake flask cultures. We also assessed the efficacy of increasing dCas9 expression to modulate targeted gene expression. The results of this study have shed new light on the lipid dependence for functional expression of streptococcal Class I HAS in *B. subtilis*.

4.2 Materials and Methods

4.2.1 Bacterial strains, primers and plasmids

The *B. subtilis* strains used in this study are listed in Table S4.1. *E. coli* HI-Control™ 10G chemically competent cells were prepared to be electrocompetent as described previously [187] and used as host for molecular cloning and plasmid construction. *B. subtilis* and *E. coli* strains were maintained as glycerol stocks stored at -80 °C. Primers (Table S4.1) were synthesized by Integrated DNA Technologies.

4.2.2 Plasmid construction and transformation

DNA manipulation was performed using standard molecular cloning techniques [187], and DNA sequencing was conducted by The Centre for Applied Genomics. To construct an expression cassette in which *pgsA* and *clsA* were driven by the strong promoter P_{grac}, *pgsA* and *clsA* were amplified with respective primers P4.122/P4.123 and P4.124/P4.125 from 1A751 gDNA, and the two fragments were spliced. The spliced fragment was then inserted into BamHI/SpeI-digested pAW005, yielding pAW001-4. pAW005 is a pHT01 [215] derivative containing a multiple cloning site (MCS) comprised of BamHI-AatII-SbfI-AscI and SpeI-NgoMIV-NotI-AsiSI-AgeI-XmaI restriction sites flanking promoter $P_{grac.max}$, a modified version of P_{grac} (i.e. promoter P01) [40]. The MCS was synthesized by Bio Basic (Ontario, Canada) and the sequence is provided in Table S4.1. $P_{grac.max}$ contains the upstream promoter element (UP) of promoter P64, the -35 region of promoter P71, the -15 region of promoter P57, the native -10 region, and a T-C substitution at the +3 site [40]. pAW005 was constructed by amplifying the synthesized MCS with primers P4.126/P4.127, followed by insertion into BamHI/XmaI-digested pHT01. The P_{grac}::*pgsA*:*clsA* cassette, including the partial MCS and *trpA* terminator from *E. coli*, was amplified with primers P4.128/P4.129 from pAW001-4, and the *thrC* 5'- homology length (HL-5') was amplified with primers P4.130/P4.131 from 1A751 gDNA, and the two fragments were spliced, generating a *thrC* HL-5'-P_{grac}::*pgsA*:*clsA* cassette. This cassette was inserted into SbfI/NheI-digested pAW004-2 [214], yielding pAW002-4. Plasmid pAW003-4 is similar to pAW002-4 but contains promoter $P_{grac.UPmod}$, i.e. promoter P61 which is a weaker derivative of promoter P_{grac}, in place of promoter P_{grac}. It was constructed from pAW001-4 in the same way as pAW002-4, except that primers P4.132 and P4.133 were used in place of primers P4.128 and P4.131, respectively. The gRNA cassettes *ftsZ*-gRNA.P79NT, *ftsZ*-gRNA.P79NT(10A-G), *ftsZ*-gRNA.P79NT(15C-U), *ftsZ*-gRNA.P244NT, *ftsZ*-

gRNA.P244NT(15C-A), and *ftsZ*-gRNA.P533NT were amplified with respective forward primers P4.134-P4.139 and a common reverse primer P4.32 from pgRNA-bacteria [23], and inserted into SphI/NcoI-digested pAW017-2 [214] to obtain respective gRNA delivery vectors pAW004-4, pAW005-4, pAW006-4, pAW007-4, pAW008-4, and pAW009-4. All gRNA delivery vectors were linearized with SacI prior to transformation. To construct the integration vector for mutation of *pssA*, the *pssA* HL-5' and HL-3' were amplified from 1A751 gDNA with respective primers P4.140/P4.141 and P4.142/P4.143, followed by sequential insertion in place of the corresponding *thrC* HL-5' and HL-3' of pAW004-2 using the respective SbfI/NheI and AscI/AgeI restriction sites, yielding pAW010-4. pAW011-4, an integration vector for mutation of *ugtP*, was constructed in the same way as pAW010-4, except the *ugtP* HL-5' and HL-3' were amplified with primers P4.144/P4.145 and P4.146/P4.147. Competent cell preparation and transformation, and eviction of the P_{araE}::*mazF*-Spc^R cassette after transformation of counter-selectable integration vectors were performed as previously described [214].

4.2.3 HA production, purification and analysis

HA production medium and seed culture preparation have been described previously (see section 3.2.4) [214], with some modifications. An overnight culture was used to inoculate flasks containing 25 mL prewarmed nonselect cultivation medium (20 g/L glucose) to an initial cell density of ~ 0.1 OD_{600}. Purification of HA and analysis of HA titer and MW were also performed as previously outlined (see section 3.2.4) [214].

4.2.4 Fluorescence microscopy

B. subtilis strains were grown to mid-exponential growth phase prior to the addition of 10-*N*-nonyl-acridine orange (NAO; ThermoFisher Scientific; Massachusetts, USA) in semi-defined medium with the following composition: $(NH_4)_2SO_4$, 0.83 g/L; K_2HPO_4, 5.82 g/L;

KH_2PO_4, 2.5 g/L; trisodium citrate dihydrate, 417 mg/L; glucose, 4.17 g/L; $MgSO_4 \cdot 7H_2O$, 151 mg/L; yeast extract, 1.67 g/L; casamino acids, 208 mg/L; Arg, 7.5 g/L; His, 383 mg/L; Trp, 48 mg/L. *B. subtilis* strains were plated on non-select lysogeny broth (LB) agar containing 5 g/L NaCl, 5 g/L yeast extract, 10 g/L tryptone, and 15 g/L agar, and incubated overnight at 37 °C. Pre-warmed medium (24 mL) was inoculated with cell patches from the overnight plate to OD_{600} 0.1-0.2, and cultured cells were grown to OD_{600} 0.3-0.5, at which time NAO was added to a final concentration of 1 µM. Cultures containing NAO were incubated in the dark at room temperature and 260 rpm for 25 min. The stained cells were then washed once in phosphate buffered saline (PBS; NaCl, 8 g/L; KCl, 0.2 g/L; Na_2HPO_4, 1.44 g/L; KH_2PO_4, 0.24 g/L) and resuspended in ProLong™ Live Antifade Reagent (ThermoFisher Scientific; Massachusetts, USA) diluted 25-fold from the stock concentration. The stained cells were then mounted on object slides covered with agarose pads (1% wt/v in PBS). Fluorescence images were viewed using an Axio Imager D1 microscope and an AxioCam MRm camera (Carl Zeiss; Oberkochen, Germany). Green and red fluorescence from NAO was detected using standard filters, and exposure times were automatically set to less than 0.8 s. Captured images were processed using ImageJ [193].

4.3 Results

4.3.1 Derivation of HA-producing strains of B. subtilis

Significant HA production can be achieved in strains of *B. subtilis* coexpressing only HAS and TuaD [5, 128, 216], for which the expression is repressed in the presence of excess phosphate [127]. Accordingly, an HA-producing control strain was constructed by transforming *B. subtilis* 168 with NdeI-linearized pAW008 [214], a vector previously constructed for the integration of a P_{grac}::*seHas*:*tuaD* cassette at the *amyE* locus (Figure 4.1), yielding strain AW006 with a prominent mucoid phenotype characteristic of HA production in *B. subtilis* [5]. However, for unknown reasons, AW006 formed a segregated population with the majority of cells being

reverted to the wild-type phenotype upon strain revival. Such genetic instability was also an issue for AW007, an HA-producing 1A786 derivative constructed in the same manner as AW006. Consequently, 1A751 was selected as the production host due to its superior genetic stability based on the persistence of the mucoid phenotype of the HA-producing strain AW008, i.e. 1A751 transformed with NdeI-linearized pAW008. We then assessed HA production in shake flask cultures of AW008 as the control for comparison with other mutants. The cell density and HA titer reached OD_{600} 4.2 (Figure 4.2A) and 0.48 g/L (Figure 4.2B), respectively, after 10 h, while the MW peaked at 1.95 MDa at 8 h (Figure 4.2C). Decreasing MW with prolonged cultivation time has been reported for HA-producing strains of *B. subtilis* [5, 214], and, therefore, the cultivations were terminated at 10 h in light of declining MW. The HA titer compared favorably to a previous report of a similar HA-producing strain of *B. subtilis* [128], as did the peak MW [5, 216]. In each case, *B. subtilis* 168 or its derivatives were used to coexpress SeHAS or SzHAS, and TuaD [5, 128, 216]. The improved culture performance of AW008 relative to similar HA-producing *B. subtilis* mutants may result, in part, from the promoter driving expression of SeHAS and TuaD. Specifically, the *grac* promoter (P_{grac}) was reported to be 30 times stronger than the commonly employed promoter $P_{xylA,\,Bm}$ [40], which was used to drive the expression of SzHAS in the aforementioned study [216]. Medium composition may also be related to culture performance as minimal medium was used for HA production in some studies [5, 128], resulting in lower MWs compared to cultivation in complex medium based on our observations (data not published).

4.3.2 Increased membrane CL content enhances HA production

Given the dependence of HAS activity on its orientation with CL in the membrane, we sought to assess the effects of increased membrane CL content on HA production. Accordingly, an HA-producing strain which produced more CL than the wild-type background was

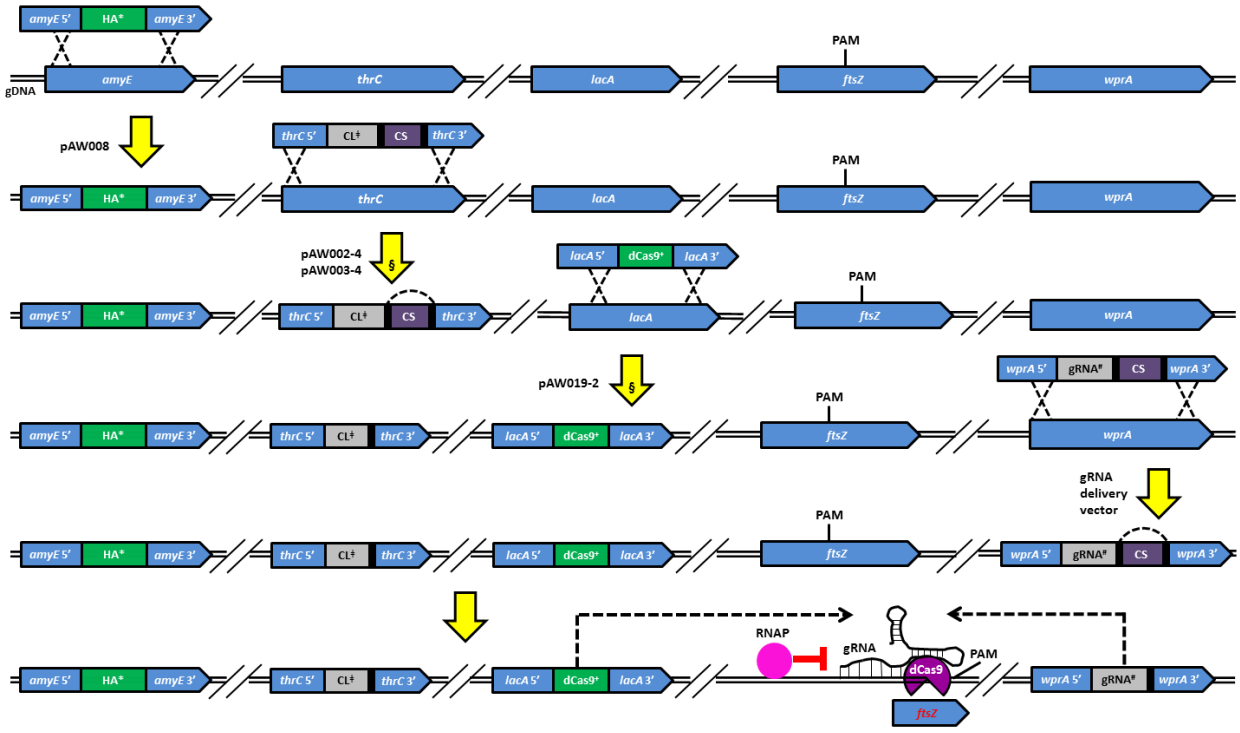

Figure 4.1. Genomic engineering strategies to enhance HA production in *B. subtilis*. The combined P_{grac}::*seHas*:*tuaD*-Neo^R (HA*) cassette was integrated into the *amyE* locus of 1A751 via transformation with pAW008, yielding strain AW008, which synthesizes HA. AW008 was then transformed with pAW002-4, resulting in integration of the P_{grac}::*pgsA*:*clsA* ($CL^‡$) cassette, and the combined P_{araE}::*mazF*-Spc^R (CS) cassette, at the *thrC* locus (the resulting mutant was spectinomycin resistant and arabinose sensitive). The CS cassette was subsequently auto-evicted via single-crossover recombination between the flanking direct repeats (black rectangles), yielding strain AW001-4 (spectinomycin sensitive and arabinose resistant), which overproduces CL. To generate strains in which expression of *ftsZ* was repressed, AW008 was first transformed with pAW019-2, resulting in integration of the combined $P_{xylA,\ Bm}$::*dcas9*-Erm^R ($dCas9^+$) cassette at the *lacA* locus, yielding strain AW002-4, which expresses xylose-inducible dCas9. AW002-4 was then transformed with either pAW002-4 or pAW003-4, resulting in integration of the P_{grac}::*pgsA*:*clsA* and $P_{grac.UPmod}$::*pgsA*:*clsA* ($CL^‡$) cassettes, respectively, and the CS cassette, at the *thrC* locus. The CS cassettes were subsequently auto-evicted, yielding respective strains AW003-4 and AW007-4, which both overproduce CL (AW003-4 produces more CL than AW007-4). AW003-4 was then transformed with pAW006-4, resulting in integration of the $P_{xylA.SphI+1}$::*ftsZ*-gRNA.P79NT(15C-U) ($gRNA^‡$) cassette, and the CS cassette, at the *wprA* locus. The CS cassette was subsequently auto-evicted, yielding strain AW004-4, which transcribes *ftsZ*-gRNA.P79NT(15C-U). AW007-4 was transformed with either pAW006-4, pAW007-4, pAW008-4, or pAW009-4, resulting in integration of the $P_{xylA.SphI+1}$::*ftsZ*-gRNA.P79NT(15C-U), $P_{xylA.SphI+1}$::*ftsZ*-gRNA.P244NT, $P_{xylA.SphI+1}$::*ftsZ*-gRNA.P244NT(15C-A), and $P_{xylA.SphI+1}$::*ftsZ*-gRNA.P533NT ($gRNA^‡$) cassettes, respectively, and the CS cassette, at the *wprA* locus. The CS cassettes were subsequently auto-evicted, yielding respective strains AW008-4, AW009-4, AW010-4, and AW011-4, which transcribe *ftsZ*-gRNA.P79NT(15C-U), *ftsZ*-gRNA.P244NT, *ftsZ*-gRNA.P244NT(15C-A), and *ftsZ*-gRNA.P533NT, respectively. The gRNAs direct dCas9 to

the target (i.e. *ftsZ*) based on the presence of a PAM site and adjacent seed region complementary to the protospacer, and the dCas9-gRNA complex remains bound to the target, partially blocking transcription of *ftsZ* by RNA polymerase (RNAP). [§]The $dCas9^{+}$ cassette was chromosomally integrated prior to the $CL^{\ddagger}$ cassette in strains in which *ftsZ* expression was repressed.

constructed by transforming AW008 with SacI-linearized pAW002-4, resulting in strain AW001-4, which constitutively expressed *pgsA* and *clsA* (regulated by promoter P_{grac}) from the *thrC* locus (Figure 4.1). Compared to the control strain AW008, the HA titer increased by 32% (0.63 g/L) for strain AW001-4 after 10 h of cultivation (Figure 4.2B). Moreover, the peak MW was higher (2.06 MDa) and declined to a lesser extent between 8 and 10 h of cultivation (Figure 4.2C), such that the MW of HA produced in cultures of AW001-4 after 10 h was comparable to the peak MW in cultures of AW008. An 83% increase in the final cell density, i.e. OD_{600} 7.7 for AW001-4 vs. 4.2 for AW008 (Figure 4.2A), was also observed, and the improved cell growth may partially explain the increased HA titer in cultures of AW001-4. We qualitatively assessed the CL levels in the membranes of our engineered strains using the CL-specific fluorescent dye NAO [208, 209]. Binding of NAO to CL results in the dimerization of NAO monomers, causing a shift in the emitted fluorescence peak of the monomer from green (at 525 nm) to red (at 640 nm) due to the metachromatic effect [208]. Red fluorescence was observed to co-localize with green fluorescence at the poles and septa of all strains analyzed, as exemplified in Figures 4.3A-C, in which green (Figure 4.3A) and red (Figure 4.3B) fluorescence emitted from NAO-stained AW008 co-localized in Figure 4.3C (i.e. an image generated by merging Figures 4.3A and 4.3B). The increased amount of CL in the membrane of AW001-4 was clearly visible (Figure 4.3D) based on the significantly higher fluorescence observed at the poles and septa of the cells, compared with AW008 (Figure 4.3C).

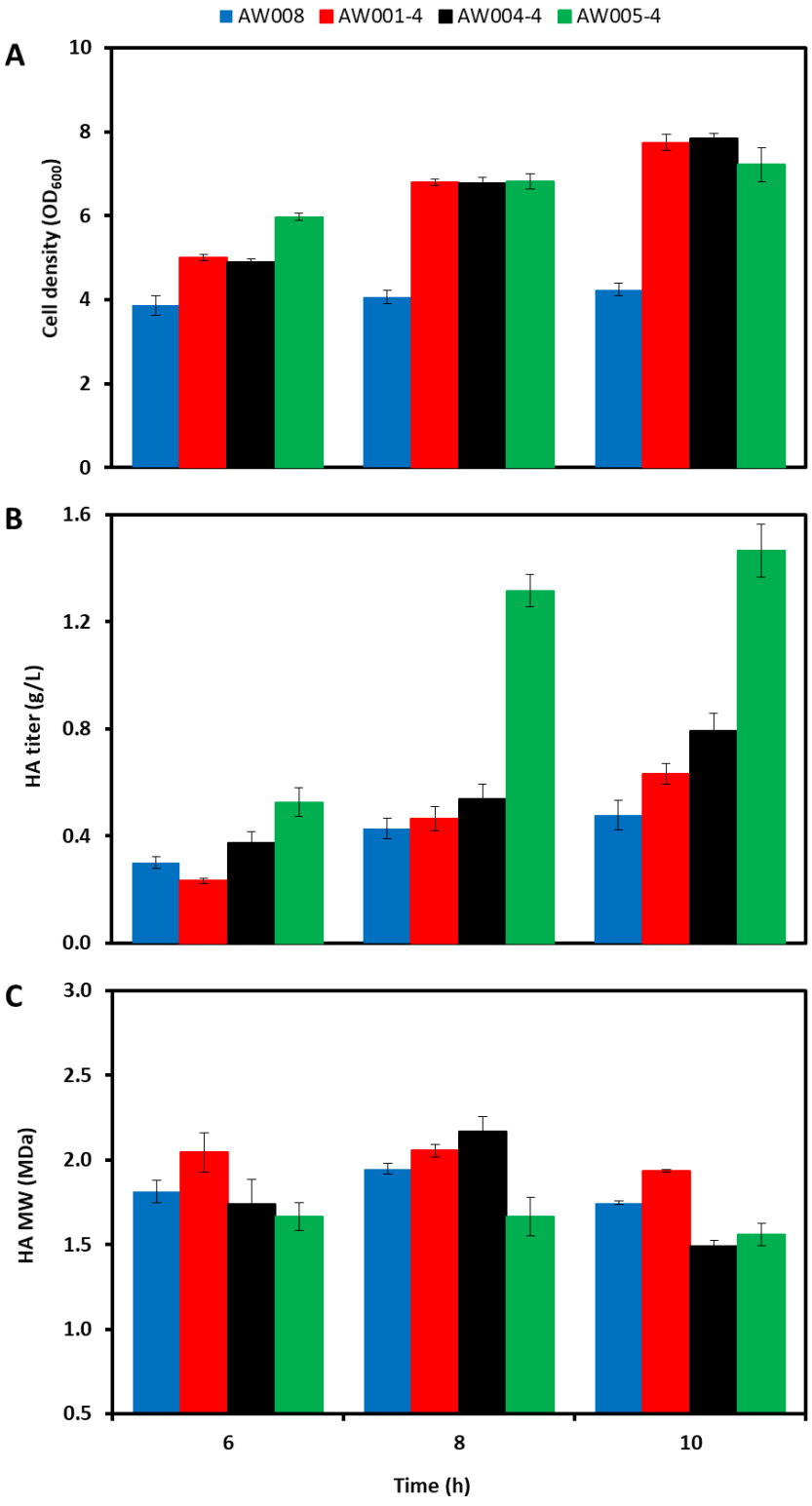

Figure 4.2. Time profiles of A) cell density, B) HA titer, and C) HA MW in cultures of AW008, AW001-4, AW004-4, and AW005-4. SD of experiments performed in triplicate are shown in Panels A and B, and SD of duplicate samples are shown in Panel C.

4.3.3 Redistributing CL in the membrane further enhances HA production

The localization of CL at the poles and septal regions of the *B. subtilis* cell membrane during exponential growth presumably facilitates cell division through the formation of non-bilayer structures in the presence of divalent cations, such as Ca^{2+} or Mg^{2+} [208, 210]. Given that SeHAS is a foreign protein to *B. subtilis* with no known homologue, it should not interact with other cellular machinery that may restrict its localization and distribution in the membrane. Also, as the intended function of Class I HAS in streptococci is to encapsulate the entire cell to prevent recognition by the host immune response [122], SeHAS may be distributed throughout the membrane of *B. subtilis*. We hypothesized that a narrow distribution of CL in the *B. subtilis* cell membrane could reduce its interaction with SeHAS, such that altering the distribution of CL may increase its availability to SeHAS, thereby enhancing the functional expression of the enzyme. Accordingly, we sought to tune the expression of *ftsZ* to redistribute CL along the lateral membrane in AW001-4. Recently, we developed a CRISPR-Cas9 toolkit enabling both genome editing and transcriptional interference in *B. subtilis* [214]. To apply CRISPRi for the purpose of modulating *ftsZ* expression, AW008 was transformed with BseYI-linearized pAW019-2 [214], yielding strain AW002-4 in which xylose-inducible dCas9 was expressed from the *lacA* locus (Figure 4.1). AW002-4 was subsequently transformed with SacI-linearized pAW002-4, generating strain AW003-4 which is a CL-overproducing strain suitable for evaluation of various gRNAs targeting *ftsZ*. Six *ftsZ*-targeting gRNAs were designed to cover the range of relative repression efficiency by manipulating gRNA design parameters previously described [23, 197]. Mismatches introduced in base pairs (bp) 8-12 of the protospacer (relative to the 3'-end) cause a dramatic reduction in repression efficiency, while mismatches in bp 13-20 have a reduced effect on repression efficiency (Note that the first 7 bp should not be altered.) [23, 197]. Moreover, repression levels are roughly inversely proportional to the distance between the selected PAM site and the start codon of the target ORF [23, 197]. We chose PAM sites P79NT, P244NT, and

P533NT, which correspond to relative distances of 0.06, 0.21, and 0.46, respectively, from the start codon (Note that the first bp of the start codon and last bp of the stop codon correspond to relative distances of 0 and 1, respectively.). Based on proximity to the start codon alone, the relative repression efficiency afforded by targeting PAM sites P79NT, P244NT, and P533NT were estimated to be 1, 0.8, and 0.4, respectively [23]. Mismatches were introduced in the protospacer at position 10 and 15 to further reduce the relative repression efficiency by ~75% and ~30%, respectively. We assumed that the effects of PAM site selection and mismatches introduced in the protospacer were multiplicative when estimating the overall relative repression efficiency. For example, the relative repression efficiency of *ftsZ* expression resulting from transcription of *ftsZ*-gRNA.P244NT(15C-A) was estimated to be 0.8 × 0.7 = 0.56. Table 4.1 summarizes various *ftsZ*-targeting gRNAs with their corresponding protospacer sequence and estimated relative repression efficiency.

Table 4.1. *ftsZ*-targeting gRNAs and their respective protospacer sequence and estimated relative repression efficiency

gRNA	protospacer sequence^	Relative repression efficiency
ftsZ-gRNA.P79NT	ATTTTCAATCATTCGGTTAA	1
ftsZ-gRNA.P79NT(10A-G)	ATTTTCAATC<u>G</u>TTCGGTTAA	0.25
ftsZ-gRNA.P79NT(15C-U)	ATTTT<u>T</u>AATCATTCGGTTAA	0.7
ftsZ-gRNA.P244NT	CTGCTCTTTGCTTTCTTCAG	0.8
ftsZ-gRNA.P244NT(15C-A)	CTGCT<u>A</u>TTTGCTTTCTTCAG	0.56
ftsZ-gRNA.P533NT	TCGCGGAATGCTTCAAGCAT	0.4

^mismatches are underlined

Of the six gRNA delivery vectors constructed, only pAW006-4, containing *ftsZ*-gRNA.P79NT(15C-U), could be stably transformed into AW003-4 as the resulting strain AW004-4 maintained the mucoid phenotype upon revival from a glycerol stock. Interestingly,

AW004-4 produced 65% and 25% more HA than AW008 and AW001-4, respectively, after 10 h cultivation (0.79 g/L; Figure 4.2B), while the peak MW of 2.17 MDa obtained at 8 h was a moderate improvement relative to either strain (Figure 4.2C). However, the MW decreased substantially to 1.49 MDa after 10 h, resulting in a lower overall MW than AW008 or AW001-4. Note that the growth profile of AW004-4 was nearly identical to that of AW001-4, with the final cell density reaching OD_{600} 7.8 (Figure 4.2A). Fluorescence microscopy revealed a moderate reduction in the fluorescence intensity of CL domains in the membrane of AW004-4 (Figure 4.3E), compared to AW001-4 (Figure 4.3D), indicating that partial redistribution of CL along the lateral membrane of AW004-4 had occurred, presumably due to reduced *ftsZ* expression. Furthermore, a moderate degree of filamentation was observed for AW004-4 (Figure 4.3E).

We then examined the effect of dCas9 expression on HA production using cultures of AW004-4 induced with xylose under different concentrations. No significant change in the HA titer, MW or cell growth was observed except at the highest xylose concentration of 1% wt/v, which resulted in decreases to the titer and cell density after 10 h (Figure 4.4). These observations may be explained by a visible increase in filamentation in cultures induced with 1% wt/v xylose, resulting in large aggregate formation in the flasks, skewing cell density measurements, and potentially disrupting the extracellular release of HA. The results suggest that tailoring transcriptional repression via CRISPRi by adjusting dCas9 expression may be ineffective [197], while manipulating the protospacer sequence and PAM site selection may provide more control over repression efficiency.

4.3.4 Targeting ftsZ for CL redistribution is sensitive to CL or ClsA levels in the membrane

To separate the effects of reduced *ftsZ* expression and increased membrane CL content on HA production as well as to determine if the poor transformability of gRNA delivery vectors bearing *ftsZ*-targeting gRNAs was related to elevated CL levels in AW003-4, AW002-4 was

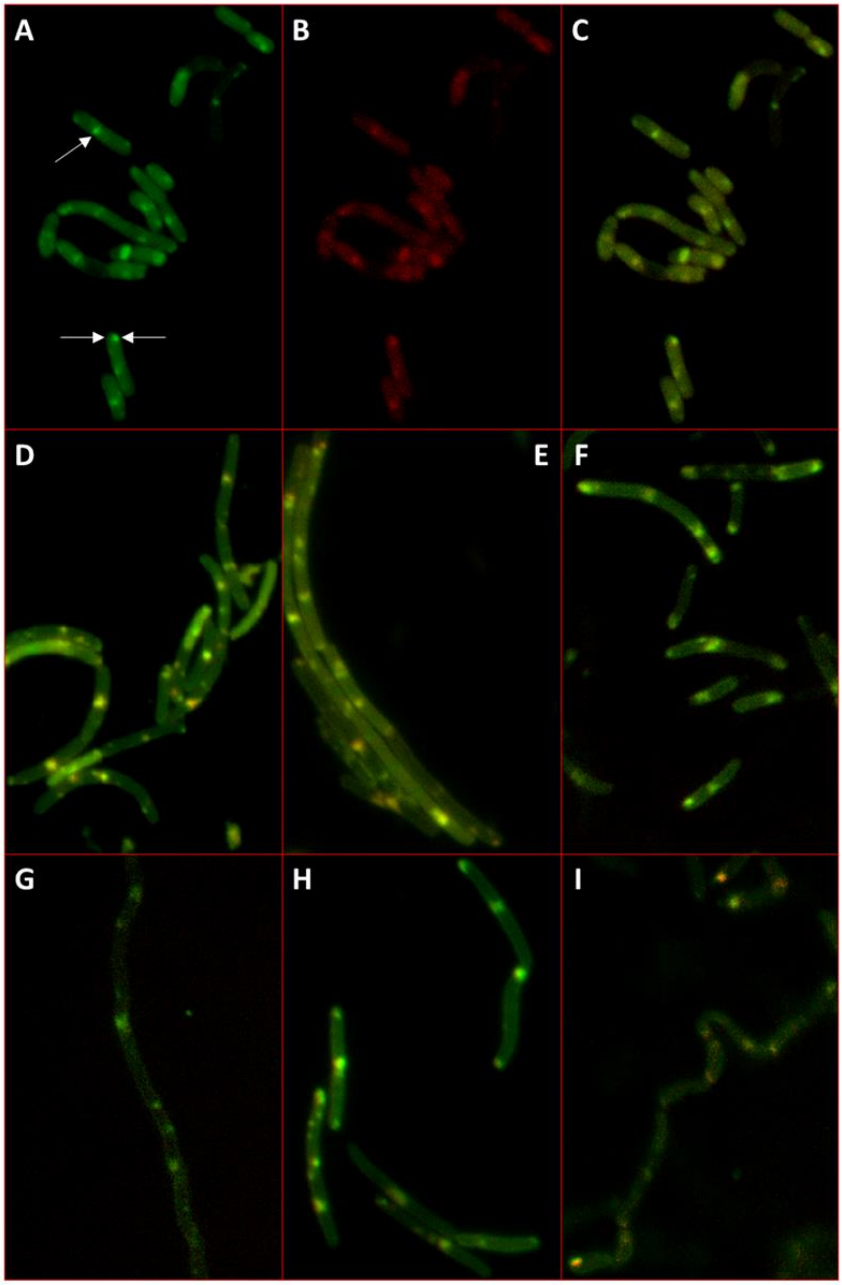

Figure 4.3. Representative images of strains of *B. subtilis* stained with NAO obtained with fluorescence microscopy. Panels A and B display green and red fluorescence emitted by AW008, respectively, and Panels C (AW008), D (AW001-4), E (AW004-4), F (AW007-4), G (AW009-4), H (AW010-4), and I (AW011-4) are merged images of green and red fluorescence emitted by respective strains. The single arrow indicates localization of CL at the septal region of the cell membrane, and the double arrows indicate localization of CL at the pole in Panel A. NAO was added to cultures during mid-exponential growth phase to a final concentration of 1 µM, followed by incubation in the dark at room temperature and 260 rpm for 25 min. Stained cells were then washed once in PBS and resuspended in ProLong™ Live Antifade Reagent diluted 25-fold from the stock concentration, prior to mounting on object slides (see section 4.2.4). 100X magnification.

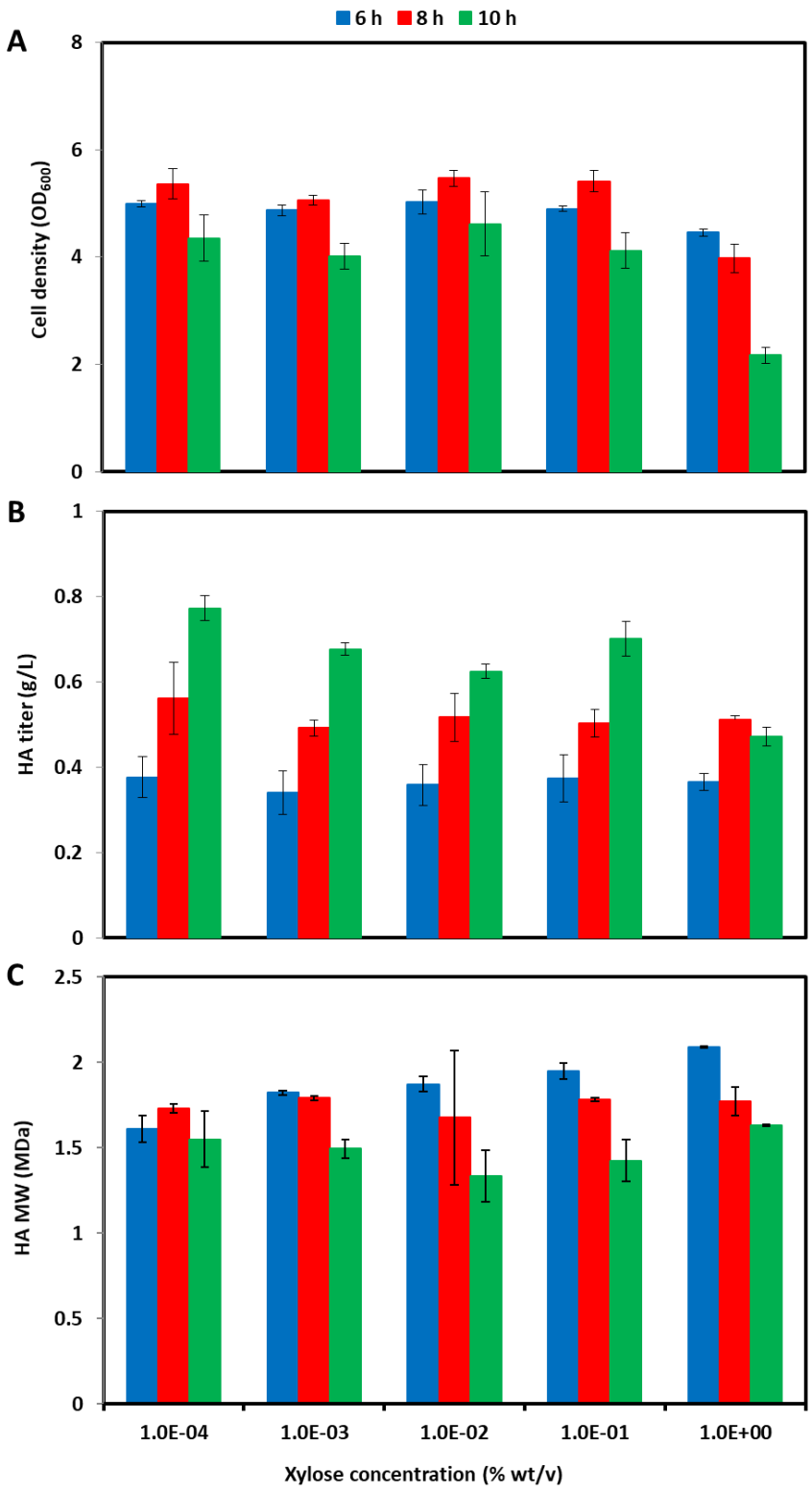

Figure 4.4. Time profiles of A) cell density, B) HA titer, and C) HA MW in cultures of AW004-4 induced with xylose 2 h after inoculation. SD of experiments performed in duplicate are shown.

transformed with pAW006-4 and pAW007-4, which could not be transformed into AW003-4, yielding genetically stable strains AW005-4 and AW006-4, respectively. The observation that AW002-4, but not AW003-4, could be transformed with pAW007-4 suggests that the impact of reduced *ftsZ* expression on cell physiology was related with the level of CL (or ClsA) in the membrane. Accordingly, AW002-4 was transformed with SacI-linearized pAW003-4, generating strain AW007-4 containing a $P_{grac.UPmod}$::*pgsA*:*clsA* cassette at the *thrC* locus (Figure 4.1). Promoter $P_{grac.UPmod}$ is a weaker derivative of promoter P_{grac} with the relative promoter strength of ~0.5 [40], and fluorescence microscopy confirmed the reduced CL levels in the membrane of AW007-4 (Figure 4.3F), compared to AW001-4 (Figure 4.3D). AW007-4 was subsequently transformed with pAW006-4, pAW007-4, pAW008-4, and pAW009-4, yielding genetically stable strains AW008-4, AW009-4, AW010-4, and AW011-4, respectively, with the mucoid phenotype upon revival from glycerol stocks (Note that pAW004-4 and pAW005-4 could not be transformed into AW007-4.). The enhanced transformability of AW007-4 associated with gRNA delivery vectors containing *ftsZ*-targeting gRNAs confirmed that the sensitivity of strains of *B. subtilis* to reduced *ftsZ* expression was dependent on membrane CL (or ClsA) levels. Our results are consistent with the previous observation that the distribution of ClsA in the membrane is dependent on FtsZ or some other component(s) of the cell division machinery [209].

Upon transformation of AW003-4 and AW007-4 with pAW006-4, distinct changes in morphology were observed for the resulting strains AW004-4 and AW008-4. AW004-4 formed small colonies surrounded by a clear HA capsule for which the thickness could be visually distinguished from the edge of the colony. As expected, the colonies had a stringy texture associated with cell filamentation resulting from reduced *ftsZ* expression [209]. On the other hand, AW008-4, with a lower CL level than AW004-4, formed large colonies and more resembled the parent strain, suggesting that the effects of repression of *ftsZ* expression on cell physiology are related to CL levels in the membrane. In addition, AW010-4 formed relatively

large colonies (though not as large as AW004-4) with a less stringy texture (but more stringy than AW008-4) compared to AW004-4. AW009-4 and AW011-4 formed very small translucent colonies for which the HA capsule could not be distinguished from the colony, as was the case for AW004-4, and the colonies had a more stringy texture than AW004-4. Fluorescence microscopy revealed a significant degree of CL redistribution along the lateral membrane of AW009-4 (Figure 4.3G) and AW011-4 (Figure 4.3I), while the membrane CL distribution in AW010-4 (Figure 4.3H) was less drastically altered. Similarly, extensive filamentation of AW009-4 (Figure 4.3G) and AW011-4 (Figure 4.3I) occurred, while AW010-4 (Figure 4.3H) retained a morphology similar to that of AW007-4 (Figure 4.3F). Based on the results of fluorescence microscopy, cell morphology, and the transformation efficiencies associated with various gRNA delivery vectors, the highest relative repression efficiency of *ftsZ* expression resulted from transcription of *ftsZ*-gRNA.P244NT, followed by *ftsZ*-gRNA.P533NT, *ftsZ*-gRNA.P244NT(15C-A), and *ftsZ*-gRNA.P79NT(15C-U), in the order of declining repression efficiency.

Mutants transcribing *ftsZ*-targeting gRNAs derived from AW002-4 (i.e. AW005-4) and AW007-4 (i.e. AW008-4, AW009-4, AW010-4, and AW011-4) were further evaluated for HA production in shake flask cultures. AW005-4 produced 204% and 85% more HA than AW008 and AW004-4, respectively, with the titer reaching 1.46 g/L after 10 h (Figure 4.2B). While the peak MW was only 1.67 MDa after 8 h in cultures of AW005-4 (Figure 4.2C), the MW did not decline substantially afterwards, and was slightly higher than the MW of HA produced in cultures of AW004-4 after 10 h (Figure 4.2C). The culture performance of AW004-4 (Figures 4.2A-C) and AW008-4 (Figures 4.5A-C) was similar, with the MW of HA and cell density of AW008-4 being slightly lower. Notably, AW011-4 produced 1.25 g/L of HA after only 8 h (Figure 4.5B), while the MW reached 2.10 MDa and declined slightly by 10 h (Figure 4.5C).

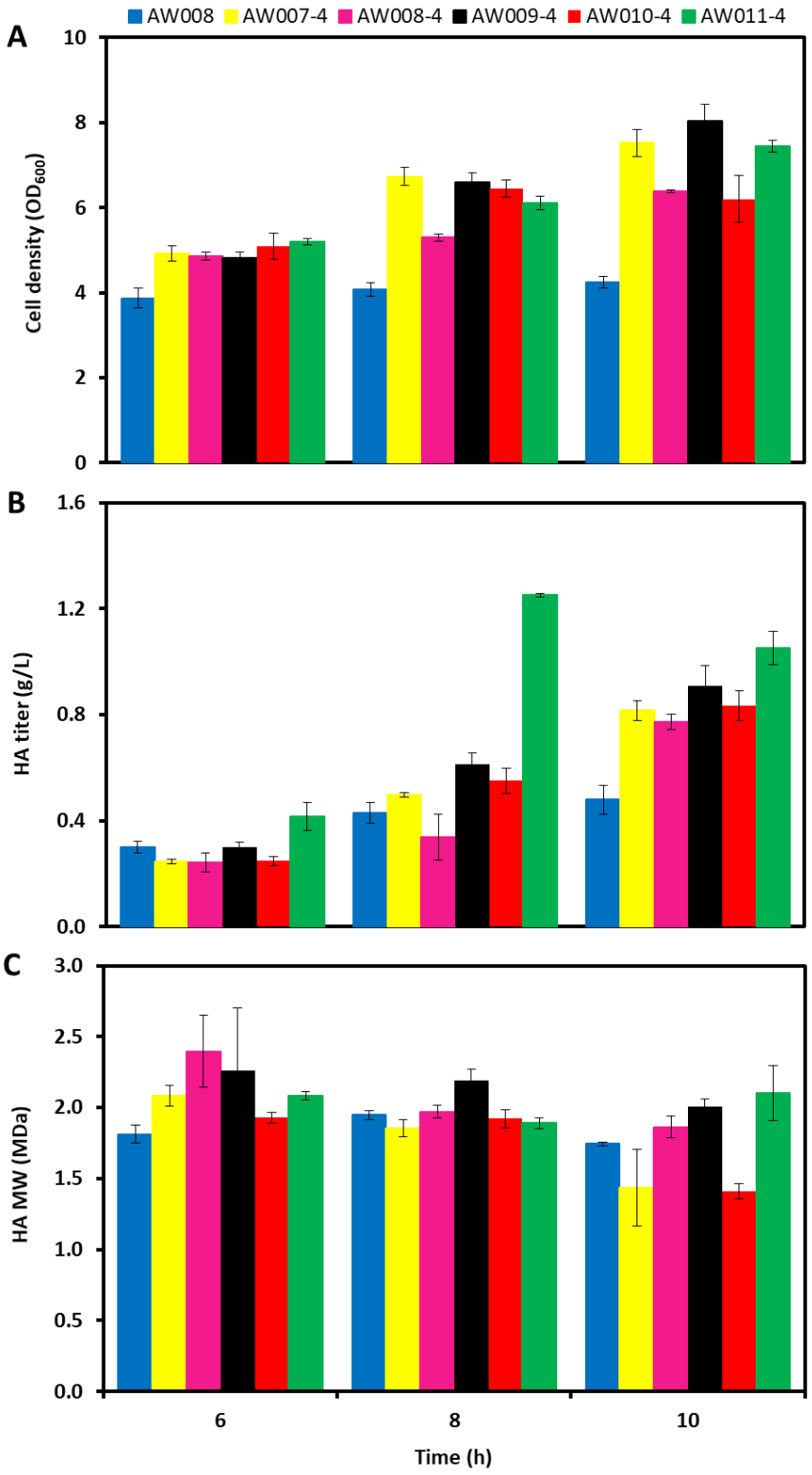

Figure 4.5. Time profiles of A) cell density, B) HA titer, and C) HA MW in cultures of AW008, AW007-4, AW008-4, and AW009-4, AW010-4, and AW011-4. SD of experiments performed in triplicate are shown in Panels A and B, and SD of duplicate samples are shown in Panel C.

4.4 Discussion

HA synthesis is an intricate process performed by Class I or II HAS, with the former being a relatively small integral membrane protein which requires precisely coordinated lipid molecules to autonomously polymerize and extrude the growing HA chain. Here, we have shown that engineering of the cell membrane can enhance heterologous HA production in *B. subtilis* expressing SeHAS. Given that the activity of streptococcal Class I HAS is restored upon reconstitution of the purified enzyme with CL *in vitro* [120, 121], it is plausible that the presence and distribution of CL in the cell membrane can critically affect HA synthesis and even secretion. However, the results of a prior study in *S. pyogenes* [217] and ours suggest that the lipid dependence of streptococcal Class I HAS *in vitro* may be less flexible than its lipid dependence *in vivo*.

Microbial cultivation has become the dominant method of industrial HA production in recent years [105]. Group C streptococci (e.g. *S. zooepidemicus*) are the most commonly employed production hosts, due to their capability to produce HA of MWs up to 5.9 MDa, with titers reaching 7 g/L [124, 218]. However, the production of exotoxins, poor growth characteristics and extensive nutritional requirements, and lack of genetic tractability [5, 219] prompted exploration of alternate microbial HA production platforms. *L. lactis* is a promising candidate for industrial HA production as it has been granted GRAS status, tools are available for its genetic manipulation, and it has produced HA titers of up to 1.8 g/L in batch cultivations [132]. While the nutritional requirements of *L. lactis* are simple, its slow growth rate can potentially result in higher biomanufacturing costs. High-level heterologous HA production has also been achieved in *S. albulus*, which can generate significant quantities of ATP required for the natural production of ε-poly-L-lysine [133]. As a result, an HA titer of 6.2 g/L was obtained in a fed-batch cultivation, which is comparable to that obtained in streptococcal cultivations. However, the application of *S. albulus* to biomanufacturing may be limited by slow growth,

relatively difficult genetic manipulation, problems expressing HAS, and lack of GRAS status [133]. Heterologous HA production has also been achieved with some success in the yeast *Pichia pastoris* [220]. While highly amenable to genetic manipulation and commonly employed for recombinant protein expression [221], *P. pastoris* grows slowly and its HA production capacity is poor compared to bacteria (up to 1.7 g/L HA produced after 48 h fed-batch cultivation) [220]. *E. coli* has also been used as a host for heterologous HA production, generating titers of up to 3.8 g/L with GlcNAc supplementation [6]. While *E. coli* is the preferred industrial bacterium for biomanufacturing for well-known reasons, its use is still hampered by endotoxin contamination of its products [222]. Of all the non-native hosts used for heterologous HA production to date, *B. subtilis* may show the most promise. We have obtained a HA titer of 3.5 g/L in a 10 h batch cultivation of AW008 (data not shown), and fed-batch cultivation has led to titers exceeding 7 g/L [5]. High production capacity coupled with easy genetic manipulation, excellent growth on simple media, and GRAS status, make *B. subtilis* an ideal choice for industrial HA production. However, *B. subtilis*, like all other heterologous producers of HA investigated to date, produce lower MW HA than group C streptococci. Accordingly, improving the MW of heterologously produced HA is currently the major challenge to be addressed with advanced strain engineering strategies.

The significant increase in the amount of CL in AW001-4 (Figure 4.3D), compared with AW008 (Figure 4.3C), was associated with the increased levels of *pgsA* and *clsA*. The relative membrane CL levels between AW001-4 (Figure 4.3D) and AW007-4 (Figure 4.3F) appeared to be less significant given that the strength of promoter P_{grac} is only twice that of promoter $P_{grac.UPmod}$ [40]. On the other hand, the enhanced transformability of gRNA delivery vectors containing *ftsZ*-targeting gRNAs in AW007-4, compared to AW003-4, suggests that membrane CL levels may be significantly different between the two strains. Comparison of the culture performance of both AW001-4 and AW007-4 to AW008 shows that moderation of the

membrane CL content (based on the use of different promoters driving the expression of *pgsA* and *clsA*) may provide similar improvements to cell density, while resulting in a higher titer and lower MW of HA for AW007-4. This suggests that a higher amount of CL in the membrane may have increased the functional expression of SeHAS, although the increased CL synthesis may have simultaneously diminished the carbon flux available for HA production. The addition of CL to purified SeHAS or SpHAS resulted in the highest enzyme activity *in vitro*, compared to the addition of other lipids [120, 121], and exogenous CL was shown to enhance the activity of both enzymes in the membrane fractions of *E. coli* cells, suggesting that the ratio of CL to HAS was not high enough to maximize the activity of heterologously expressed HAS [119]. It was revealed that controlling chain length and polymerizing activity are independent functions of SeHAS that are not coupled to one another [211], although CL may play dual roles in chain elongation. CL may assist HAS in the formation of pores in the cell membrane through which the growing HA chain is translocated [119], and its interaction with HA may contribute to the net force required to retain the chain as it is extended . Accordingly, increased CL availability in the cell membrane of HA-producing *B. subtilis* could enable more of the total expressed enzyme per cell to achieve higher activity (i.e. higher polymerization rate) and improved functionality with regard to the retention and translocation of the growing HA chain, resulting in the improved functional expression of SeHAS. This may partially explain the improved culture performance of AW001-4, compared to AW008, although the lower specific HA titer (Figure 4.6) indicates that overproduction of CL competed with HA synthesis for glucose. This point is supported by the nearly identical specific HA titers in cultures of AW007-4 and AW008 (Figure 4.6), and the similar final cell densities observed in cultures of AW001-4 (Figure 4.2A) and AW007-4 (Figure 4.5A), such that further increasing CL production in AW001-4, compared to AW007-4, reduced the HA titer without affecting biomass accumulation. Accordingly, optimizing the expression of *pgsA* and *clsA* may be necessary to balance the MW and HA titer in HA-producing strains of *B.*

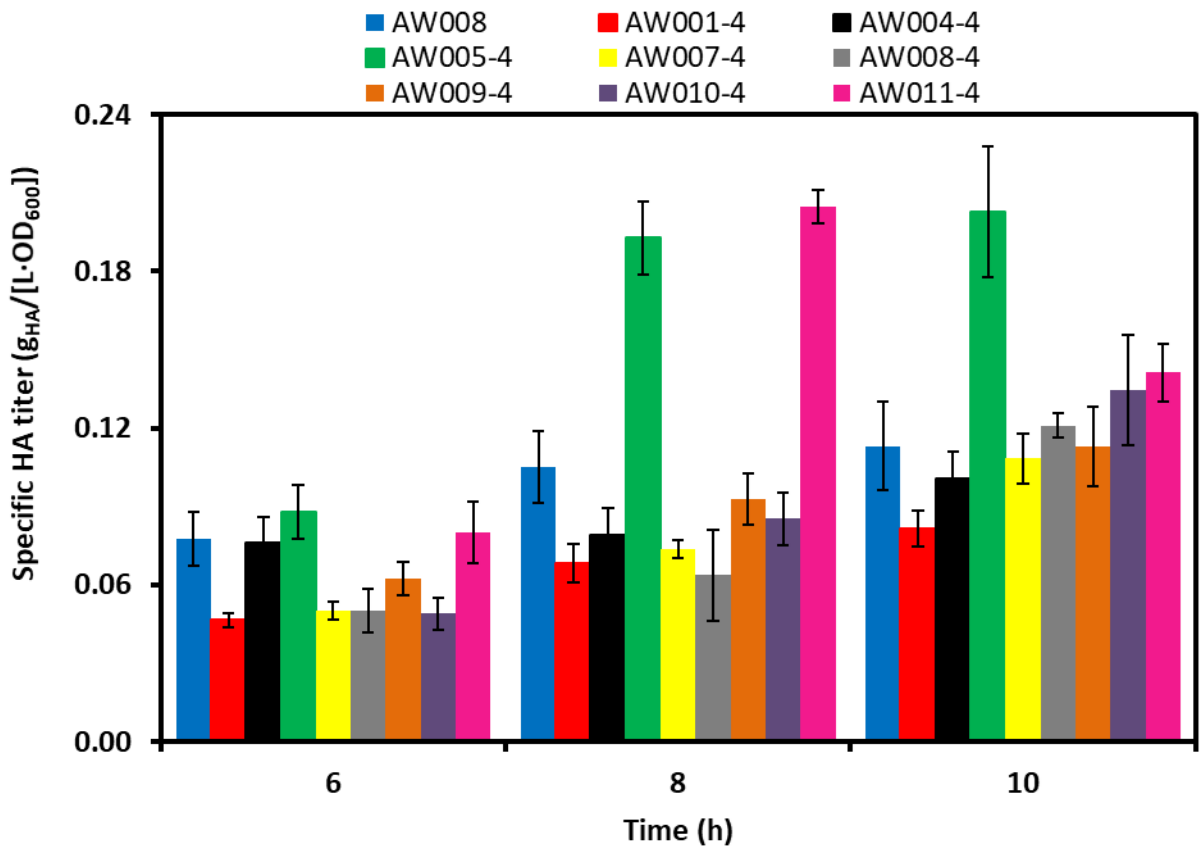

Figure 4.6. Time profiles of the specific HA titer in cultures of AW008, AW001-4, AW004-4, AW005-4, AW007-4, AW008-4, and AW009-4, AW010-4, and AW011-4. SD of experiments performed in triplicate are shown.

subtilis. Deletion of *cls*, encoding the sole CL synthase, in *Streptococcus mutans* significantly increased the doubling time and reduced the final cell density in acidic medium, relative to the parent strain, while growth characteristics were identical between both strains in neutral medium [223]. CL has also been implicated in the adaptive response of *B. subtilis* to conditions of high salinity [224]. The poor oxygen mass transfer and lack of pH control in shake flask cultures can result in their acidification as the culture progresses, such that the initial pH in our cultivations (i.e. pH 7) would have declined by the end of the cultivation. The enhanced cell growth in cultures of AW001-4, compared to AW008, suggests that increasing the amount of CL in the *B. subtilis* membrane may improve the acid-adaptive response. However, we observed that the

exponential growth rates of both AW008 and AW001-4 declined by ~30%, while the respective final cell densities increased and decreased by 10% and 24% in medium titrated to pH 6 (data not shown). Furthermore, AW001-4 did not grow, while the logarithmic growth rate and final cell density of AW008 did not change (although the length of the lag phase increased by 60%) as the initial pH of the medium was further reduced to 5.7. Accordingly, the improved growth of AW001-4, compared to AW008, does not appear to be related to an improved acid-adaptive response. Further investigation is required to elucidate the mechanism(s) through which cell physiology was improved upon increasing the membrane CL level. As HA is a growth-associated product [225], the increased HA titers in cultures of CL-overproducing strains can be explained, in part, by their improved growth, which is evident from the similar specific HA titers observed in cultures of AW007-4 and AW008 (Figure 4.6).

While higher cell densities were achieved in cultivation medium with strains in which expression of *ftsZ* was repressed, relative to AW008, the opposite behavior was observed for cultures with LB medium, i.e. the final cell density of overnight LB cultures of AW008 were higher in each case (data not shown). The improved growth of these strains in cultivation medium may have resulted from the presence of divalent metals, which have been shown to enhance self-assembly of high MW FtsZ oligomers *in vitro* [226]. Moreover, Z-ring formation is coupled to pyruvate levels via the E1α subunit of pyruvate dehydrogenase [227], such that cultivation medium containing glucose may enhance FtsZ polymerization relative to LB which lacks a preferred carbon source. The relatively small amount and narrow spatial distribution of CL in the cell membrane of *B. subtilis* may result in CL levels which are not sufficient to maximize the functional expression of SeHAS, which was observed in *E. coli* heterologously expressing streptococcal Class I HAS [119]. Note that CL localizes at the poles and septal regions of the cell membrane in both *E. coli* and *B. subtilis* [208, 228]. Thus, the functional expression of SeHAS may be improved by redistributing CL along the lateral membrane, which

may partially explain the increased MW and HA titers observed in cultures of certain strains in which expression of *ftsZ* is repressed. The redistribution of natural CL without carbon being siphoned away from HA production to accommodate CL overproduction, may partially explain the significantly improved HA titer obtained in cultures of AW005-4, relative to all other strains. However, the reduced peak MW of HA produced in cultures of AW005-4, compared to AW008, was unexpected, given that AW004-4 and strains derived from AW007-4 in which *ftsZ* expression was repressed, produced HA of an equivalent or higher peak MW compared to their respective parent strains. Moreover, the significantly increased specific HA titer in cultures of AW005-4, compared to AW008 (Figure 4.6), may indicate that more glucose was available for HA synthesis due to the reduced expression of FtsZ. Taken together, the increased specific HA titer and reduction in MW in cultures of AW005-4, compared to AW008, suggest that improved carbon flux through the HA biosynthetic pathway, rather than the enhanced functional expression of SeHAS, had a greater impact on the culture performance of AW005-4. In general, an increase in the specific HA titer was observed in cultures of strains in which expression of *ftsZ* was repressed, compared to their respective parent strains, which could be partially attributed to increased carbon availability for HA synthesis due to reduced FtsZ expression, and/or reduced biomass accumulation in the case of AW008-4 and AW010-4. The improved HA titer in cultures of AW011-4, compared to AW008-4 and AW010-4 (Figure 4.5B), suggests that the repression of *ftsZ* expression was conducive to HA production in *B. subtilis*. On the other hand, a further increase in repression efficiency may reduce the HA titer, as observed in cultures of AW009-4 (Figure 4.5B), without significantly affecting the MW. The results suggest that a delicate balance between the CL level and distribution in the cell membrane of *B. subtilis* appears to be critical for optimization of culture performance for heterologous HA production.

The improvements to the MW of HA produced by most engineered *B. subtilis* strains possessing CL-enriched membranes in this study was modest. This is not entirely surprising

given that a *cls* (encoding CL synthase) deficient *S. pyogenes* mutant retained the full ability to produce the HA capsule, relative to the parent strain which constitutively produced HA due to a mutation of the transcriptional regulator CovR [217]. Moreover, the titer and MW of HA produced by strains of *B. subtilis* expressing only SeHAS and TuaD were comparable to those based on streptococcal cultivations [5], in spite of the relatively small amount of CL naturally present in the *B. subtilis* membrane. Similarly, heterologous HA production was achieved in a variety of bacterial hosts expressing Class I HAS from group C streptococci without alterations to the host membrane [131, 133, 134]. Accordingly, it appears that alternate lipids may suffice to assist bacterial Class I HAS in HA synthesis. The *B. subtilis* membrane is composed mainly of PG (the only essential lipid) and phosphatidylethanolamine (PE), in addition to a large amount of neutral glycolipids (GL) [206]. The dependence of SeHAS activity on PG could not be assessed *in vivo* in *B. subtilis* as *pgsA* mutants are not viable [229]. However, PG was observed to have no stimulatory effect on the activity of purified SeHAS *in vitro* [121]. To determine if either of the other major lipids present in the *B. subtilis* membrane, i.e. PE and GL, were critical in maintaining the activity of SeHAS, we respectively mutated *pssA* (encoding PssA, an enzyme for synthesizing phosphatidylserine, which is subsequently converted to PE) and *ugtP* (encoding UDP-glucose diacylglyceroltransferase; UgtP, an enzyme involved in the conversion of PA to GL [206]) in AW008 via transformation of respective plasmids pAW010-4 and pAW011-4, generating respective mutant strains AW012-4 and AW013-4. The HA titers obtained in cultures of AW012-4 and AW013-4 were not significantly different from that obtained in cultures of AW008 (data not shown). The fact that PE deficiency did not significantly alter HA production in *B. subtilis* was not surprising, given that PE marginally enhanced the activity of purified SeHAS *in vitro* [121], and that, like CL, PE localizes at the septal regions of the membrane in *B. subtilis* [209]. On the other hand, UgtP is involved in the synthesis of diglucosyldiacylglycerol, the membrane anchor for lipoteichoic acids [206, 230], and in the coupling of nutrient

availability to cell division by potentially inhibiting Z ring formation in nutrient rich conditions [231], such that its mutation results in pronounced growth defects [206, 230]. Regardless of the physiological defects arising from UgtP deficiency, AW013-4 reached a similar cell density to AW008 with a comparable HA titer, suggesting that SeHAS might not preferentially coordinate with GL. Based on our results and the previous observation of HA synthesis in *cls*-deficient *S. pyogenes* whose membrane is composed primarily of CL, PG, and GL [217], PG may satisfy the lipid requirements of streptococcal Class I HAS *in vivo*. Our results also suggest that HA synthesis in *B. subtilis* is a robust process potentially insensitive to major physiological perturbations in the host.

The estimated relative repression efficiencies of *ftsZ*-targeting gRNAs did not agree well with our experimental observations, particularly in terms of transformability, morphology, and microscopy analysis. For example, *ftsZ*-gRNA.P79NT(10A-G) was expected to provide the lowest degree of repression of *ftsZ* expression, but it appeared to show a high level of repression relative to four of the other five gRNAs tested, and the nature of the substitution may be associated with the observed high level of repression. On the other hand, *ftsZ*-gRNA.P79NT(15C-U) resulted in the lowest level of repression of *ftsZ* expression while it was anticipated to provide a high repression level of 0.7. A recent investigation of the kinetics of dCas9 binding to off-target sequences indicated that the apparent association rates for targets in which A-G mismatches had been introduced outside of the seed region (Note that the seed region includes the first seven bp adjacent to the PAM site.) were typically high [232]. Substitution of an A with a G residue could potentially result in a G-T wobble base pair (in which hydrogen bonds link N1 of G with O2 of T and O6 of G with N3 of T) which can be accommodated in biologically active dsDNA [233]. A poly(T) signal and/or more stable hairpin structure in the protospacer of *ftsZ*-gRNA.P79NT(15C-U) may have led to low repression of *ftsZ* expression in AW004-4 and AW008-4. The protospacer of *ftsZ*-gRNA.P79NT is expected to form a minimally

stable hairpin structure (ΔG = -2.46 kcal/mole), although substitution of the C with a U residue at position 15 for *ftsZ*-gRNA.P79NT(15C-U) may result in the formation of a more stable hairpin structure (ΔG = -4.07 kcal/mole). While the poly(T) signal is a distinguishing characteristic of rho-independent terminators in bacteria, its presence alone is typically not sufficient to achieve efficient transcription termination [234, 235], as is the case in eukaryotes [236]. Accordingly, it is likely that hairpin formation in the protospacer may disrupt base pairing between the gRNA and the DNA target. Evidently, tuning repression efficiency by introducing mismatches in the protospacer of gRNAs when applying CRISPRi is a complicated and trial-and-error process, given the availability of a meticulous gRNA design protocol. On the other hand, the selection of PAM sites based on their proximity to the beginning of the target ORF may provide more control over relative repression efficiency without enabling precise adjustment to target gene expression.

Chapter 5

Metabolic engineering to enhance heterologous production of HA in *B. subtilis*

5.1 Introduction

In light of significant advances in the areas of synthetic biology, metabolic engineering, and molecular biology, strain engineering to enhance target metabolite production has become increasingly common [11]. The standard approach begins with the rational design of a biosynthetic pathway to generate the desired product. Heightened expression of key genes, in parallel with inactivation of genes in competing pathways, aims to direct carbon flux toward target metabolite formation [237]. However, complete inactivation of certain essential genes associated with central metabolism or core aspects of physiology (e.g. ATP generation, cell division, etc.) may not be feasible, such that reducing expression levels of these genes, while maintaining cell physiology, may ultimately prove more effective [98]. Prior efforts to produce HA in *B. subtilis* have primarily involved overexpressing genes comprising the HA biosynthetic pathway (Figure 5.1). Initially, it was shown that UDP-GlcUA is limiting for HA biosynthesis, such that coexpression of *tuaD* and *seHas* was critical for high-level HA production [5]. Coexpression of additional native enzymes involved in cell wall biosynthesis, i.e. GtaB and GcaD, moderately improved HA production. On the other hand, coexpression of *szHas*, *tuaD*, and *vhb*, significantly improved HA production, presumably due to increased ATP production resulting from *vhb* expression [128]. Recently, the coexpression of *szHas*, *tuaD*, *gtaB*, *glmS*, *glmM*, and *gcaD* improved the HA titer by ~30%, compared to the coexpression of only *szHas* and *tuaD*, or *szHas* and *gcaD*, without improving the MW, while simply downregulating the expression of *pfkA*, via replacement of the native ATG start codon with TTG, moderately

improved HA production [130]. Moreover, the carbon source used to produce HA in *B. subtilis* can affect the MW [238], and modifying the CL content and distribution in the cell membrane can improve both the titer and MW [239]. Collectively, the results from prior studies of HA production in *B. subtilis* suggest that coexpressing key genes from the HA biosynthetic pathway results in diminishing returns on the titer and MW, while metabolic engineering strategies, such as enhancing ATP generation or reducing glycolytic flux, have a greater impact on culture performance by reducing the burden on cellular resources.

Heterologous HA production directly competes with central metabolism and cell wall synthesis, making it particularly challenging to manipulate with metabolic engineering strategies. In *B. subtilis*, glucose-6-P enters the branch point between the PPP, glycolysis, and the synthesis of cell wall components (Figure 5.1). Glucose-6-phosphate 1-dehydrogenase (Zwf; encoded by *zwf*) converts glucose-6-P to 6-phosphogluconolactone to initiate the oxidative branch of the PPP. In opposing directions, phosphoglucomutase (PgcA; encoded by *pgcA*) and Glucose-6-P isomerase (Pgi; encoded by *pgi*) convert glucose-6-P to glucose-1-P and fructose-6-P, respectively. Glucose-1-P feeds into the synthesis of cell wall components (e.g. teichoic and teichuronic acids), and fructose-6-P will enter glycolysis upon conversion to fructose-1,6-bisphosphate by PfkA, or be converted to glucosamine-6-P, an intermediate in the synthesis of peptidoglycan and other cell wall constituents, by GlmS. Streptococcal Class I HAS alternately adds UDP-GlcNAc and UDP-GlcUA, intermediates in the synthesis of cell wall components respectively derived from glucosamine-6-P and glucose-1-P, to the reducing end of the growing HA chain [110]. Presumably, shifting carbon flux from central metabolism toward cell wall synthesis may improve HA production though cell physiology may be affected. In fact, inactivation of *pfkA* was lethal to *B. subtilis* [229, 240], and inactivation of *zwf* led to significant

carbon flux rerouting into glycolysis [240]. Accordingly, repression of *pfkA* and/or *zwf* expression may be an effective approach to redirect carbon flux from glycolysis and the PPP, respectively, toward cell wall biosynthesis and, ultimately, HA biosynthesis with minimum impact to cell physiology.

In this study, we engineered the metabolism of a HA-producing strain of *B. subtilis* to redirect more carbon flux from the PPP and glycolysis into HA biosynthesis. An improved base strain AW002-3 was first developed for more effective HA production than our previous engineered strain AW008 [239]. The base strain was also less sensitive to catabolite repression when expressing genes from a xylose-inducible promoter due to the genomic integration of constitutively expressed *araE*, encoding the broad specificity transporter of L-arabinose and D-xylose (AraE). Microbial strain engineering has recently advanced at an unprecedented rate due to the widespread adoption of the CRISPR-Cas9 system, an effective biotool for genome editing and transcriptional interference [241, 242]. To redirect carbon flux from the PPP and glycolysis into HA biosynthesis, we repressed the expression of *zwf* and *pfkA*, respectively, via CRISPRi using our recently developed CRISPR-Cas9 toolkit for *B. subtilis* [238]. While, compared to the control strain, lower cell densities were obtained potentially due to a reduced carbon flux into the PPP or glycolysis, the volumetric HA titers generally maintained significantly higher or, at least, similar levels, resulting in substantial improvements to the specific HA titers. However, in most cases, the MW of HA was negatively affected. On the other hand, multiplexed repression of both *pfkA* and *zwf* expression resulted in substantial improvements to both the HA titer and MW. Moreover, the addition of exogenous GlcUA and GlcNAc markedly increased the MW but decreased the titer of HA, providing further evidence that chain elongation and polymerizing activity are independent functions of the heterologously expressed streptococcal HAS. Overall,

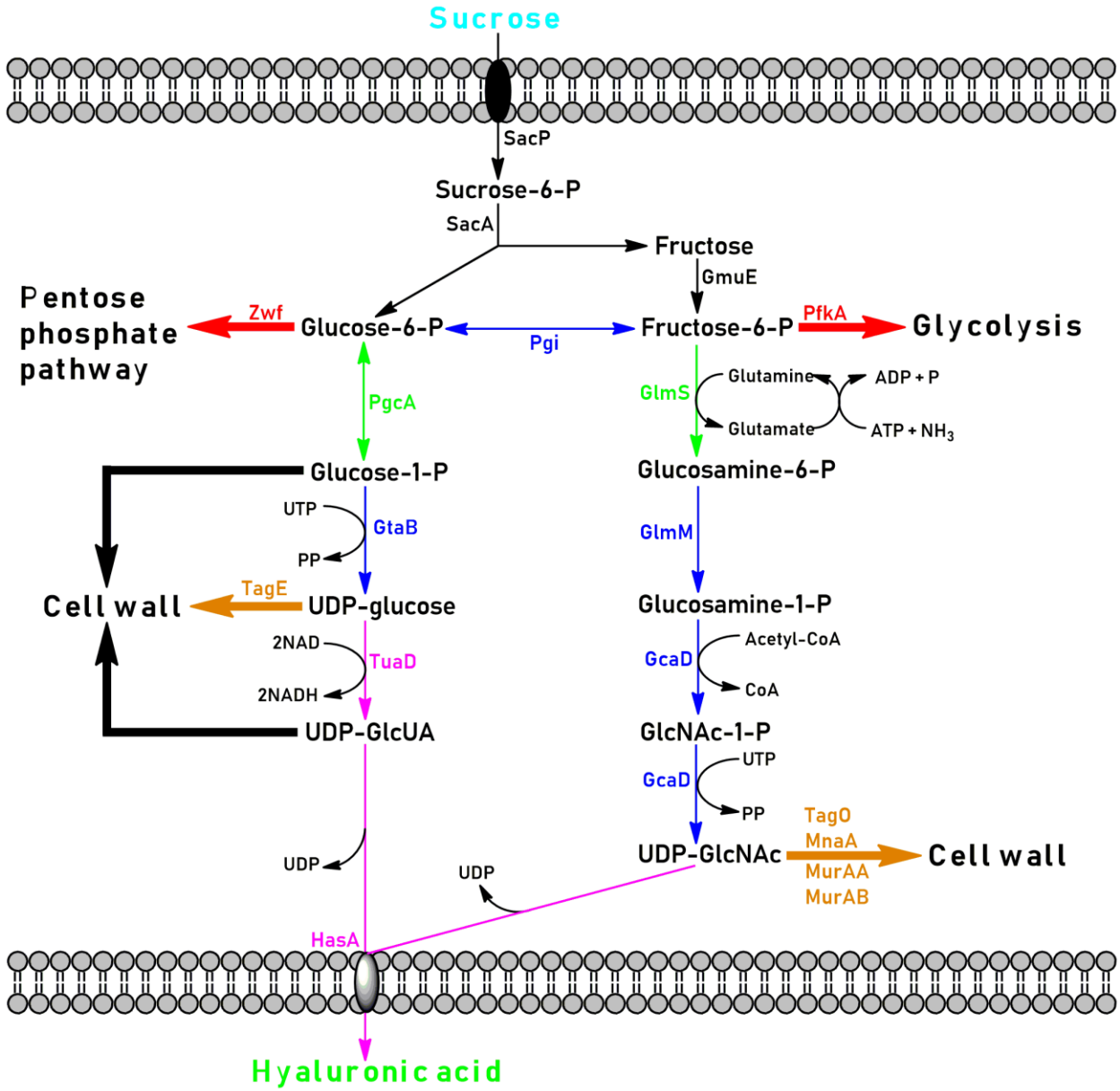

Figure 5.1. The HA biosynthetic pathway in *B. subtilis.* Pink arrows: upregulated in all strains. Green arrows: upregulated in certain strains. Blue arrows: potential targets for upregulation. Red arrows: downregulated in certain strains. Orange arrows: potential targets for downregulation. Enzymes listed by category: TuaD, UDP-glucose 6-dehydrogenase; HasA, hyaluronan synthase; PgcA, phosphoglucomutase; GlmS, glutamine-fructose-6-P amidotransferase; Pgi, glucose-6-P isomerase; GtaB, UTP-glucose-1-P uridylyltransferase; GlmM, phosphoglucosamine mutase; GcaD, UDP-GlcNAc pyrophosphorylase; Zwf, glucose-6-P 1-dehydrogenase; PfkA, 6-phosphofructokinase; TagE, UDP-glucose:polyglycerol phosphate glucosyltransferase; TagO, UDP-GlcNAc:undecaprenyl-P N-acetylglucosaminyl-1-P transferase; MnaA, UDP-N-acetylmannosamine (ManNAc) 2-epimerase; MurAA, UDP-GlcNAc 1-carboxyvinyltransferase; MurAB, UDP-GlcNAc 1-carboxyvinyltransferase; SacP, phosphotransferase system sucrose-specific transporter; SacA, Sucrose-6-P hydrolase; GmuE, fructokinase.

our study clearly demonstrates that simultaneously maximizing the titer and MW of HA produced in *B. subtilis* is a challenging task.

5.2 Materials and Methods

5.2.1 Bacterial strains, primers and plasmids

The *B. subtilis* strains used in this study are listed in Table S5.1. *E. coli* HI-Control™ 10G chemically competent cells were prepared as electrocompetent cells as described previously [187] and used as host for plasmid construction. *B. subtilis* and *E. coli* strains were maintained as glycerol stocks at -80 °C. Primers (Table S5.1) were synthesized by Integrated DNA Technologies.

5.2.2 Plasmid construction

DNA manipulation was performed using standard cloning techniques [187], and DNA sequencing was conducted by The Centre for Applied Genomics. To construct pAW009, promoter $P_{grac.UPmod}$ (i.e. promoter P61), a weaker derivative of promoter P_{grac} (i.e. promoter P01) for which the relative promoter strength is ~0.5 [40], was amplified from pHT01 [215] with primers P5.97/P5.98, and inserted into SalI/BamHI digested pAW008 [238]. Transformation of pAW009 into *B. subtilis* results in the integration of a $P_{grac.UPmod}$::*seHas*:*tuaD* cassette at the *amyE* locus (Figure 5.2). To construct the expression cassette in which *araE*, encoding the broad specificity transporter of L-arabinose and D-xylose (AraE) [243], was driven by promoter $P_{grac.UPmod}$ from the *vpr* locus, $P_{grac.UPmod}$ was amplified with primers P5.114/P5.115 from pHT01, *araE* was amplified with primers P5.116/P5.117 from 1A751 gDNA, and the two fragments were spliced, generating a $P_{grac.UPmod}$::*araE* cassette. The *vpr* homology length (HL)-5' was then

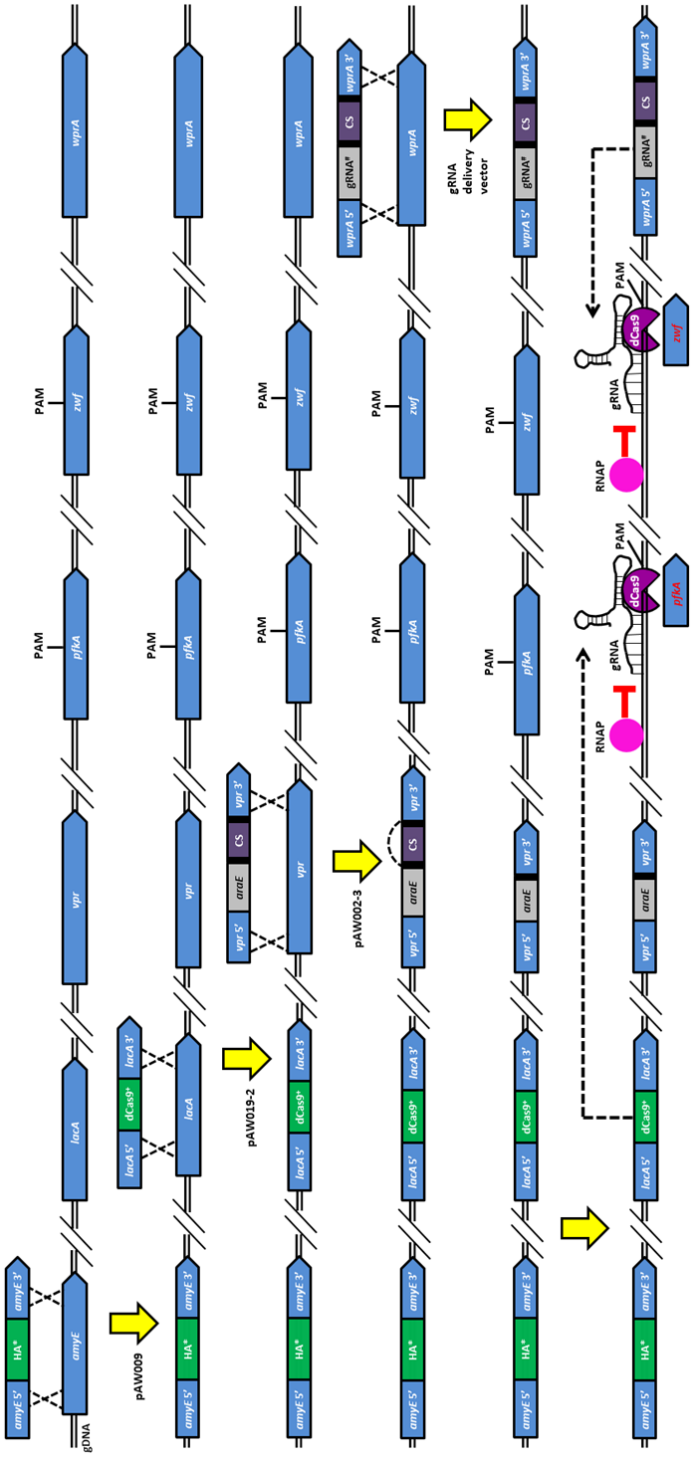

Figure 5.2. Genomic engineering strategies to enhance HA production in *B. subtilis*. *B. subtilis* 1A751 was transformed with pAW009, yielding strain AW009, which synthesizes HA.AW009 was subsequently transformed with pAW019-2, yielding strain AW014-2, which expresses xylose-inducible dCas9. AW014-2 was then transformed with pAW002-3, and the combined P_{araE}::*mazF*-Spc^{R} (CS) cassette was subsequently auto-evicted via single-crossover recombination between the flanking direct repeats (black rectangles), yielding strain AW002-3,

which constitutively expresses *araE* to enhance xylose uptake. To generate strains in which expression of *pfkA* was repressed, AW002-3 was transformed with various gRNA delivery vectors containing *pfkA*-targeting gRNAs. Similarly, to generate strains in which expression of *zwf* was repressed, AW002-3 was transformed with various gRNA delivery vectors containing *zwf*-targeting gRNAs. To generate strains in which expression of both *pfkA* and *zwf* were repressed, AW002-3 was transformed with pAW017-3 or pAW018-3, resulting in respective strains AW018-3 and AW019-3 that transcribe both *pfkA*- and *zwf*-targeting gRNAs. The gRNAs direct dCas9 to *pfkA* and/or *zwf* based on the presence of a PAM site and adjacent seed region complementary to the protospacer, and the dCas9-gRNA complex remains bound to the target, partially blocking transcription of *pfkA* and/or *zwf* by RNA polymerase (RNAP).

amplified with primers P5.118/P5.119 and spliced with the $P_{grac.UPmod}$::*araE* cassette, yielding a *vpr* HL-5'-$P_{grac.UPmod}$::*araE* cassette, which was subsequently inserted into SbfI/AsiSI-digested pAW002-4 [239]. To complete the vector, the *vpr* HL-3' was amplified with primers P5.120/P5.121 from 1A751 gDNA and inserted in place of the *thrC* HL-3', yielding pAW001-3. To construct pAW002-3, promoter $P_{grac.\Delta UP}$ was amplified with primers P5.150/P5.151 from pAW009 and inserted into AvrII/SphI-digested pAW001-3. $P_{grac.\Delta UP}$ (i.e. promoter P70) is a weaker derivative of P_{grac} for which the relative promoter strength is ~0.1 [40].

The gRNA cassettes *pfkA*-gRNA.P41NT, *pfkA*-gRNA.P41NT(10C-A), *pfkA*-gRNA.P41NT(15U-C), *pfkA*-gRNA.P315NT(10G-A), *pfkA*-gRNA.P315NT(15U-G), *pfkA*-gRNA.P610NT(10G-A), and *pfkA*-gRNA.P610NT(15U-C) were amplified with respective forward primers P5.107-P5.113 and common reverse primer P5.32 from pgRNA-bacteria [23], and inserted into SphI/NcoI-digested pAW017-2 [238] to obtain respective gRNA delivery vectors pAW003-3, pAW004-3, pAW005-3, pAW006-3, pAW007-3, pAW008-3, and pAW009-3. The gRNA cassettes *zwf*-gRNA.P92NT, *zwf*-gRNA.P92NT(10U-G), *zwf*-gRNA.P92NT(15C-A), *zwf*-gRNA.P603NT, *zwf*-gRNA.P603NT(10U-C), and *zwf*-gRNA.P603NT(15G-U) were amplified with respective forward primers P5.152-P5.157 and common reverse primer P5.32 from pgRNA-bacteria, and inserted into SphI/NcoI-digested pAW017-2 to obtain respective

gRNA delivery vectors pAW010-3, pAW011-3, pAW012-3, pAW013-3, pAW014-3, and pAW015-3. To construct the multi-gRNA delivery vector, the BglII and BamHI restriction sites upstream and downstream of *mazF*, respectively, were removed, and a new BglII restriction site was inserted between the NheI restriction site and promoter $P_{xylA.SphI+1}$ in pAW017-2 to facilitate Biobrick cloning of gRNA transcription cassettes as previously described [238]. This was accomplished by amplifying the $P_{xylA.SphI+1}$-DR cassette and *mazF* from pAW017-2 with primers P5.28/P5.158 (NheI/--) and P5.159/P5.31 (--/BamHI), respectively, followed by splicing of the two fragments to generate a $P_{xylA.SphI+1}$-DR-*mazF* cassette, which was subsequently inserted into NheI/BglII digested pAW017-2, generating pAW016-3. The previously amplified *zwf*-gRNA.P603NT(10U-C) cassette was then inserted into SphI/NcoI-digested pAW016-3. To complete the respective dual gRNA delivery vectors pAW017-3 and pAW018-3, the $P_{xylA.SphI+1}$::*pfkA*-gRNA.P41NT and $P_{xylA.SphI+1}$::*pfkA*-gRNA.P41NT(10C-A) cassettes were amplified with primers P5.28/P5.33 (NheI/BamHI), and inserted into the NheI/BglII-digested derivative of pAW016-3 containing *zwf*-gRNA.P603NT(10U-C). All gRNA delivery vectors were linearized with SacI prior to transformation into *B. subtilis*.

To construct an expression cassette in which *pgcA* was driven by promoter P_{grac} from the *thrC* locus, the *thrC* HL-5'-P_{grac} cassette was amplified with primers P5.160/P5.161 from pAW002-4, *pgcA* was amplified with primers P5.162/P5.163 from 1A751 gDNA, and the two fragments were spliced, generating a *thrC* HL-5'-P_{grac}::*pgcA* cassette, which was subsequently inserted into SbfI/AsiSI digested pAW002-4, yielding pAW019-3. Similarly, to construct an expression cassette in which *glmS* was driven by promoter P_{grac} from the *thrC* locus, the *thrC* HL-5'-P_{grac} cassette was amplified with primers P5.160/P5.164 from pAW002-4, *glmS* was amplified with primers P5.165/P5.166 from 1A751 gDNA, and the two fragments were spliced,

generating a *thrC* HL-5'-P_{grac}::*glmS* cassette, which was subsequently inserted into SbfI/AsiSI digested pAW002-4, yielding pAW020-3. Finally, to construct an expression cassette in which *pgcA* and *glmS* were driven by promoter P_{grac} from the *thrC* locus, *glmS* was amplified with primers P5.167/P5.166 from 1A751 gDNA, and was subsequently inserted into ClaI/AsiSI digested pAW019-3, yielding pAW021-3.

5.2.3 Competent cell preparation and transformation

Transformation of *B. subtilis* was performed using a standard protocol for natural competence [8]. SpC medium contained the following (per L): $(NH_4)_2SO_4$, 1.67 g; K_2HPO_4, 11.64 g; KH_2PO_4, 5.0 g; trisodium citrate dihydrate, 833 mg; glucose, 4.17 g; $MgSO_4 \cdot 7H_2O$, 151 mg; yeast extract, 1.67 g; casamino acids, 208 mg; Arg, 7.5 g; His, 383 mg; Trp, 48 mg. SpII medium contained the following (per L): $(NH_4)_2SO_4$, 1.67 g; K_2HPO_4, 11.64 g; KH_2PO_4, 5.0 g; trisodium citrate dihydrate, 833 mg; glucose, 4.17 g; $MgSO_4 \cdot 7H_2O$, 725 mg; yeast extract, 858 mg; casamino acids, 86 mg; Arg, 3.78 g; His, 189 mg; Trp, 24 mg; $CaCl_2$, 48 mg. *B. subtilis* strains were plated on non-select lysogeny broth (LB) agar containing 5 g/L NaCl, 5 g/L yeast extract, 10 g/L tryptone, and 15 g/L agar, and incubated overnight. Pre-warmed SpC medium was inoculated by cell patches from the overnight plate to OD_{600} 0.5-0.7. Seventy five min after the logarithmic growth phase ended, cultured cells were then diluted 100-fold in pre-warmed SpII medium, and incubated for 110 min before harvesting. Transformed cells were incubated for 80 min at 260 rpm, and then plated on LBG containing 85 µg/mL spectinomycin to select recombinants. To facilitate auto-eviction of the P_{araE}::*mazF*-Spc^R cassette after transformation of counter-selectable integration vectors, cells were grown for ~20 h in non-select LB at 37 °C and 260 rpm, plated on LB agar containing 20 g/L arabinose (LBA), and screened for spectinomycin

sensitivity. All cultivation steps were conducted at 37 °C and 300 rpm unless otherwise indicated.

5.2.4 HA production, purification and analysis

HA production was assessed as previously described [238] with minor modifications. *B. subtilis* strains were plated on non-select LB and grown overnight at 37 °C. A single colony was used to inoculate 25 mL non-select LB, and the culture was grown for ~13 h at 37 °C and 280 rpm. The culture was then used to inoculate 20 mL pre-warmed non-select cultivation medium (4% v/v) of the following composition (per L): sucrose, 20 g; $(NH_4)_2SO_4$, 1 g; $K_2HPO_4 \cdot 3H_2O$, 9.15 g; KH_2PO_4, 3 g; trisodium citrate$\cdot$ $2H_2O$, 1 g; yeast extract, 10 g; casamino acids, 2.5 g; $CaCl_2$, 5.5 mg; $FeCl_2 \cdot 6H_2O$, 13.5 mg; $MnCl_2 \cdot 4H_2O$, 1 mg; $ZnCl_2$, 1.7 mg; $CuCl_2 \cdot 2H_2O$, 0.43 mg; $CoCl_2 \cdot 6H_2O$, 0.6 mg; $Na_2MoO_4 \cdot 2H_2O$, 0.6 mg. Cultures were grown at 37 °C and 280 rpm, and were induced with xylose (0.75% wt/v) 1.5 h after inoculation. Samples were diluted appropriately in PBS (NaCl, 8 g/L; KCl, 0.2 g/L; Na_2HPO_4, 1.44 g/L; KH_2PO_4, 0.24 g/L), and HA was purified with cetylpyridinium chloride as previously described [128]. HA titers were determined using the modified carbazole assay [191], and MW was analyzed via agarose gel electrophoresis [192] with slight modifications. 2 µg of purified HA was loaded per well, and gels stained O/N in 0.005% Stains-All (50% v/v ethanol) were destained for ~8 h in 20% v/v ethanol, followed by destaining for ~16 h in 10% v/v ethanol. Gels were then photobleached for 20 min on a LED light box, and scanned with an Epson Perfection V600 Photo scanner (Nagano, Japan). Scanned images were analyzed using ImageJ [244], and data analysis was performed as previously described [192]. All samples were analyzed in duplicate.

5.3 Results

5.3.1 Strain engineering of B. subtilis as a base strain for improved HA production

We previously constructed a *B. subtilis* strain capable of high-level production of high MW HA, i.e. AW008, in which coexpression of *seHas* and *tuaD* was driven by the strong promoter P_{grac} [239]. We also observed that reducing the strength of the promoter driving CL overproduction in an AW008 derivative, in which the membrane CL content was artificially enhanced, improved the HA titer by 30% with a slight reduction in the MW [239]. This prompted us to examine the effects of *seHas* and *tuaD* expression on HA production via construction of strain AW009, in which coexpression of both genes was driven by the promoter $P_{grac.UPmod}$, a derivative of P_{grac} with a relative promoter strength of ~0.5 [40]. AW009 was constructed via transformation of *B. subtilis* 1A751 with NdeI-linearized pAW009 (Figure 5.2). Similar to AW008, AW009 presented a mucoid phenotype, a characteristic for HA production in *B. subtilis* [5], and was genetically stable based on the persistence of the mucoid phenotype upon repetitive revival. AW009 produced approximately twice as much HA as AW008 (0.97 g/L vs. 0.48 g/L; Figure 5.3A) after 10 h of shake flask cultivation, while the MW slightly declined by 12% (Figure 5.3B). Moreover, the cell density of the AW009 culture at 10 h was 45% higher than that of AW008 (Figure 5.3C). The improved cell growth of AW009, compared to AW008, may have contributed to the enhanced HA production as HA is a growth-associated product [225]. UDP-GlcNAc is the limiting substrate for HA biosynthesis in *S. zooepidemicus*, such that expression of *hasD* (a *gcaD* homologue) and/or *hasE* (a *pgi* homologue) improved the MW of HA, relative to the wild-type strain [245]. Accordingly, the slight MW reduction in AW009 may have resulted from reduced expression of *tuaD*, which subsequently reduced the level of UDP-

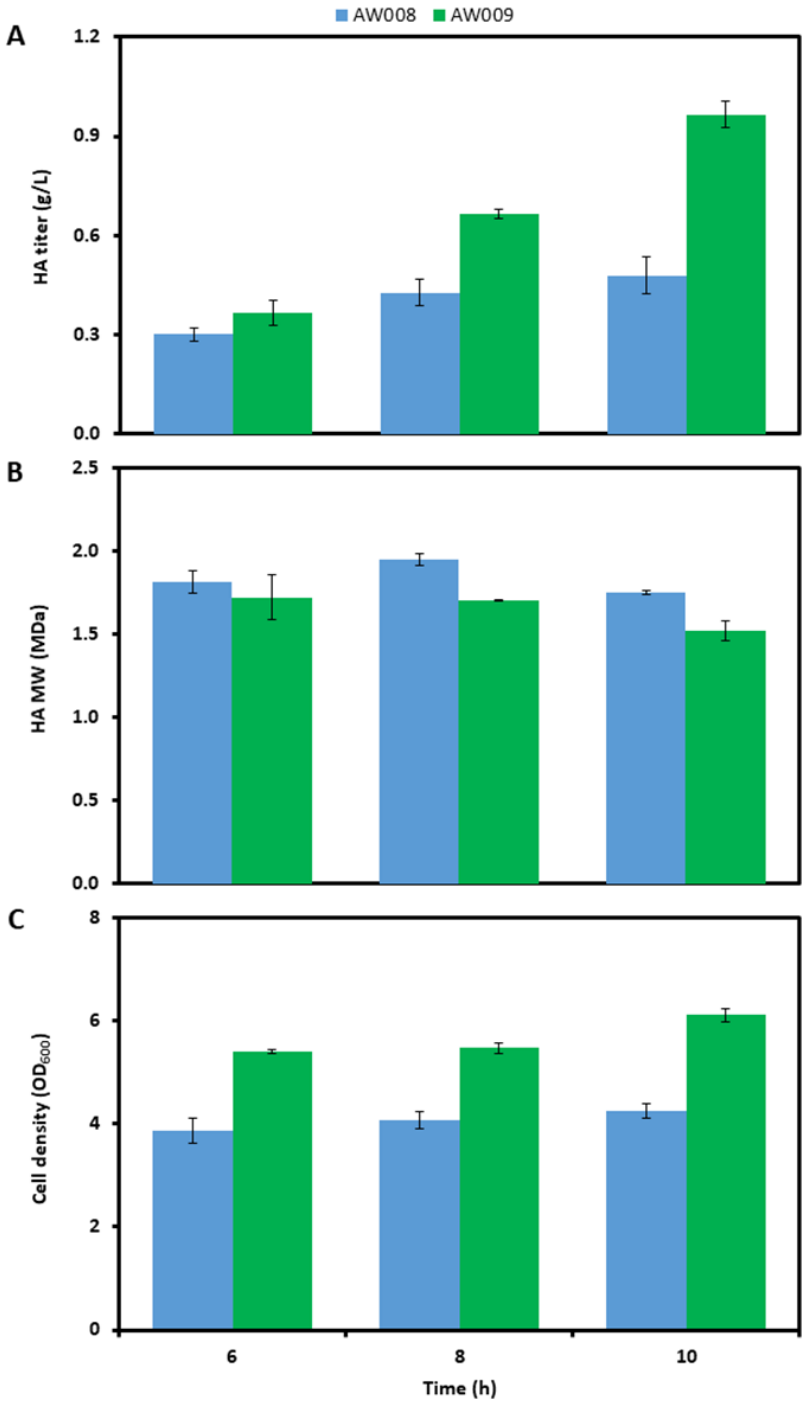

Figure 5.3. Time profiles of A) HA titer, B) HA MW, and C) cell density in cultures of AW008 and AW009. AW008 and AW009 each coexpress *seHas* and *tuaD*, under control of the constitutive promoters P_{grac} and $P_{grac.UPmod}$, respectively, from the *amyE* locus. Cultivation conditions were the same as those described in M&M, except that glucose was the primary carbon source (20 g/L), the culture volume was 25 mL, and the inoculum size was 2% v/v. SD of experiments performed in triplicate are shown in Panels A and C, and SD of duplicate samples are shown in Panel B.

GlcUA as the limiting substrate in *B. subtilis*. With a better overall culture performance, AW009 was selected as the host for metabolic engineering via CRISPRi to enhance HA production. To conduct CRISPRi, AW009 was transformed with pAW019-2, generating AW014-2 which expressed xylose-inducible dCas9 from the *lacA* locus (Figure 5.2) [238].

The *araE* gene encodes a broad specificity transporter of L-arabinose, D-xylose and other sugars [243]. Expression of *araE* is not induced by xylose and is subject to CcpA-mediated catabolite repression via a CRE upstream of the ORF of *araE* [190, 246]. Given that the major carbon source for HA cultivation was sucrose (which can catabolically repress *araE* expression) and dCas9 expression was driven by the xylose-inducible promoter $P_{xylA,\,Bm}$ [238], we opted to integrate constitutively expressed CRE-free *araE* into the *vpr* locus of AW014-2 to enhance xylose uptake for induction of dCas9 expression. To achieve this, AW014-2 was transformed with SacI-linearized pAW001-3, generating AW001-3. However, AW001-3 had a specific growth rate of approximately half that of the parent strain, indicating that expression of *araE* from $P_{grac.UPmod}$ significantly impacted cell growth. We hypothesized that such physiological burden was associated with the promoter strength and, therefore, replaced $P_{grac.UPmod}$ (with a relative promoter strength of ~0.5) with $P_{grac.\Delta UP}$ (with a relative promoter strength of ~0.1). To do this, we transformed AW014-2 with SacI-linearized pAW002-3, yielding AW002-3 (Figure 5.2), a strain with a specific growth rate similar to that of the parent strain.

To evaluate this approach for enhancing xylose uptake, we transformed AW002-3 with pAW018-2 [238], generating AW003-3, a strain that transcribed *lacZ*-gRNA.P28NT (a gRNA targeting the *lacZ* ORF of *E. coli*) from the *wprA* locus. After counter-selection to evict the P_{araE}::*mazF*-Spc^R cassette, AW003-3 was subsequently transformed with pAW016 [238], generating AW004-3, a strain that expressed IPTG-inducible *lacZ* from the *ugtP* locus. AW004-

3 and AW016-2 [238], an equivalent strain to AW004-3 but without constitutively expressed *araE*, were assessed for the repression efficiency of *lacZ* expression in cultivation medium containing 2% wt/v sucrose and IPTG, in the presence or absence of xylose, as previously described [238]. The specific β-galactosidase activities of uninduced cultures of AW004-3 and AW016-2 were 8.1-fold and 6.5-fold, respectively, that of the xylose-induced cultures of the corresponding strains (data not shown), implying less catabolite repression in AW004-3. Moreover, the 8.1-fold difference in the specific β-galactosidase activity between uninduced and xylose-induced AW004-3 grown in sucrose-containing medium compared favorably to the 7.7-fold difference in the specific β-galactosidase activity between uninduced and xylose-induced AW016-2 grown in LB (containing no sucrose) [238], suggesting that catabolite repression effect was insignificant in both cultures.

5.3.2 Repression of pfkA expression increases the HA titer but decreases the MW

Overexpressing genes in the HA biosynthetic pathway has been extensively explored for heterologous HA production in *B. subtilis*. As UDP-GlcUA is the limiting substrate in phosphate-rich medium, coexpression of *hasA* and *tuaD* is necessary to enhance HA production [5]. However, the expression of additional genes in the HA biosynthetic pathway resulted in modest gains in the HA titer, while having essentially no effect on the MW [5, 130]. Accordingly, we imposed a more dramatic shift in carbon flux away from central metabolism toward HA biosynthesis. We engineered *B. subtilis* by reducing *pfkA* expression to siphon fructose-6-P directly from glycolysis using our recently developed CRISPR-Cas9 toolkit [238]. We previously showed that introducing mismatches in the protospacer sequence (i.e. gRNA base-pairing region) of dCas9-targeting gRNAs and/or PAM site selection based on the relative

distance from the start codon could effectively alter repression efficiency when applying CRISPRi in *B. subtilis* [239]. Thus, this strategy was applied in the design of seven *pfkA*-targeting gRNAs covering a range of relative repression efficiency. Single mismatches in base pairs (bp) 8-12 of the protospacer sequence (relative to the 3'-end) of gRNAs cause a dramatic (~75%) reduction in repression efficiency, while single mismatches in bp 13-20 cause a slight (~30%) reduction in repression efficiency (Note that the first 7 bp should not be altered as single mismatches in this region almost eliminate the repression efficiency.) [23, 197]. Moreover, repression levels are roughly inversely proportional to the distance between the selected PAM site and the start codon of the target ORF [23, 197]. We chose PAM sites P41NT, P315NT, and P610NT, which correspond to relative distances of 0.04, 0.33, and 0.64, respectively, from the start codon (Note that the first bp of the start codon and last bp of the stop codon correspond to relative distances of 0 and 1, respectively.). Based on proximity to the start codon alone, the relative repression efficiency afforded by targeting PAM sites P41NT, P315NT, and P610NT were estimated to be 1.0, 0.5, and 0.3, respectively [23]. Single mismatches were introduced in the protospacer sequence of gRNAs at position 10 and 15 to further reduce the relative repression efficiency by ~75% and ~30%, respectively. We assumed that the effects of PAM site selection and mismatches introduced in the protospacer sequence of gRNAs were multiplicative when estimating the overall relative repression efficiency. For example, the relative repression efficiency of *pfkA* expression resulting from transcription of *pfkA*-gRNA.P41NT(10C-A) was estimated to be $1.0 \times 0.25 = 0.25$. Table 5.1 summarizes various *pfkA*-targeting gRNAs with their corresponding protospacer sequence and estimated relative repression efficiency.

Table 5.1. *pfkA- and zwf*-targeting gRNAs and their respective protospacer sequence and estimated relative repression efficiency

gRNA	Protospacer sequence[^]	Relative repression efficiency
pfkA		
pfkA-gRNA.P41NT	CGAACTGCTGCGTTCATTCC	1.0
pfkA-gRNA.P41NT(10C-A)	CGAACTGCTG<u>A</u>GTTCATTCC	0.25
pfkA-gRNA.P41NT(15U-C)	CGAAC<u>C</u>GCTGCGTTCATTCC	0.7
pfkA-gRNA.P315NT(10G-A)	TAATTTTTTC<u>A</u>CACCCATAT	0.13
pfkA-gRNA.P315NT(15U-G)	TAATT<u>G</u>TTTCGCACCCATAT	0.35
pfkA-gRNA.P610NT(10G-A)	GTTCGTGGCC<u>A</u>CGTTTTAAG	0.08
pfkA-gRNA.P610NT(15U-C)	GTTCG<u>C</u>GGCCGCGTTTTAAG	0.21
zwf		
zwf-gRNA.P92NT	TTTGTCCGTTTTGATATAAA	1.0
zwf-gRNA.P92NT(10U-G)	TTTGTCCGTT<u>G</u>TGATATAAA	0.25
zwf-gRNA.P92NT(15C-A)	TTTGT<u>A</u>CGTTTTGATATAAA	0.7
zwf-gRNA.P603NT	ATGTAGCGGTTTGTCCAAAG	0.55
zwf-gRNA.P603NT(10U-C)	ATGTAGCGGT<u>C</u>TGTCCAAAG	0.14
zwf-gRNA.P603NT(15G-U)	ATGTA<u>T</u>CGGTTTGTCCAAAG	0.39

[^]mismatches are underlined

To reduce *pfkA* expression with various repression efficiencies in HA-producing *B. subtilis*, AW002-3 was respectively transformed with SacI-linearized pAW003-3, pAW004-3, pAW005-3, pAW006-3, pAW007-3, pAW008-3, and pAW009-3, generating corresponding strains AW005-3, AW006-3, AW007-3, AW008-3, AW009-3, AW010-3, and AW011-3. All *pfkA*-repressed strains produced more HA than the control strain AW009 under shake flask cultivation (Figure 5.4A). In particular, AW005-3, AW006-3, and AW007-3, which all transcribe gRNAs targeting P41NT, had HA titers ~50% higher than that of AW009 after 10 h. However, the peak and final MWs of HA produced by all *pfkA*-repressed strains were somewhat lower compared to

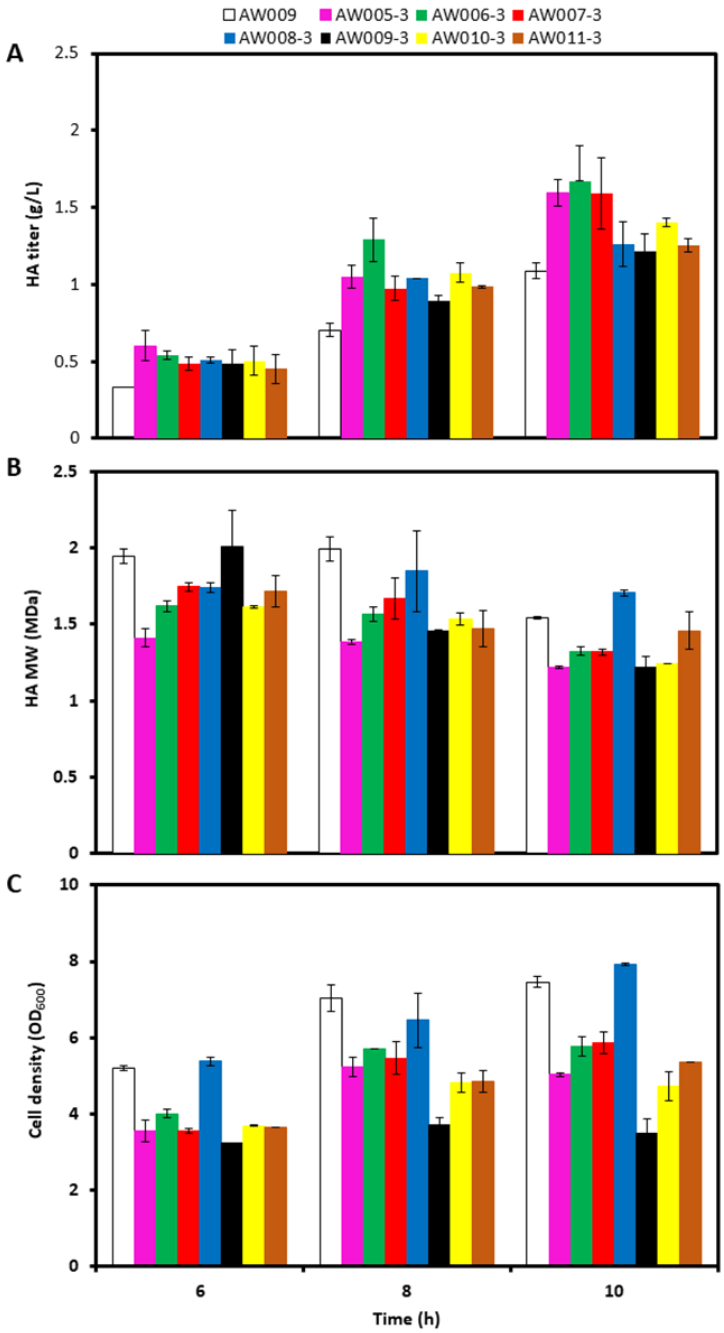

Figure 5.4. Time profiles of A) HA titer, B) HA MW, and C) cell density in cultures of AW009, AW005-3 (transcribing *pfkA*-gRNA.P41NT), AW006-3 (transcribing *pfkA*-gRNA.P41NT(10C-A)), AW007-3 (transcribing *pfkA*-gRNA.P41NT(15U-C)), AW008-3 (transcribing *pfkA*-gRNA.P315NT(10G-A)), AW009-3 (transcribing *pfkA*-gRNA.P315NT(15U-G)), AW010-3 (transcribing *pfkA*-gRNA.P610NT(10G-A)), and AW011-3 (transcribing *pfkA*-gRNA.P610NT(15U-C)). All strains transcribing *pfkA*-targeting gRNAs are derivatives of AW002-3, which expresses xylose-inducible dCas9 with constitutively expressed *araE* to enhance xylose uptake. SD of experiments performed in duplicate are shown in Panels A, B, and C.

AW009 (Figure 5.4B), with the exception of AW008-3, for which the final MW was slightly higher (1.71 MDa vs. 1.54 MDa; Figure 5.4B). As expected, the final cell density of *pfkA*-repressed strains was significantly lower than AW009 (Figure 5.4C), with the exception of AW008-3, for which the final cell density was slightly higher (7.9 OD_{600} vs. 7.45 OD_{600}; Figure 5.4C). As a result, the specific HA titers in cultures of AW005-3, AW006-3, and AW007-3 were 116%, 98%, and 86% respectively higher than that of AW009 (0.146 g/L/OD_{600}), suggesting that the dissimilated carbon flux was redirected from biomass accumulation to HA biosynthesis upon *pfkA* repression.

5.3.3 Repression of zwf expression can affect HA production

As the PPP is another central metabolic pathway potentially competing with the HA biosynthetic pathway for the dissimilated carbon flux, we extended our metabolic engineering strategy for carbon flux redirection by reducing *zwf* expression. We chose two PAM sites P92NT and P603NT, which correspond to relative distances of 0.06 and 0.41, respectively, from the start codon of the *zwf* ORF. Based on proximity to the start codon alone, the relative repression efficiency afforded by targeting PAM sites P92NT and P603NT were estimated to be 1.0 and 0.55, respectively. Single mismatches were introduced in the protospacer sequence of gRNAs at position 10 and 15 to further reduce the relative repression efficiency. Table 5.1 summarizes various *zwf*-targeting gRNAs with their corresponding protospacer sequences and estimated relative repression efficiencies.

To reduce *zwf* expression with various repression efficiencies in HA-producing *B. subtilis*, AW002-3 was respectively transformed with SacI-linearized pAW010-3, pAW011-3, pAW012-3, pAW013-3, pAW014-3, and pAW015-3, generating corresponding strains AW012-

3, AW013-3, AW014-3, AW015-3, AW016-3, and AW017-3. Culture performance for HA production for these *zwf*-repressed strains varied considerably, with the HA titers of AW012-3, AW014-3, AW015-3, and AW016-3 being 33%, 44%, 26%, and 74% respectively higher than that of AW009 after 8 h, while those of AW013-3 and AW017-3 were lower (Figure 5.5A). However, HA production for AW012-3, AW014-3, AW015-3, and AW016-3 did not persist much between 8 h and 10 h, such that the final HA titers of these strains were similar to that of AW009. Moreover, the peak MW of HA produced by all *zwf*-repressed strains was somewhat lower compared to AW009, although the final MW of HA produced by AW014-3 (1.64 MDa) and AW017-3 (1.77 MDa) was higher (Figure 5.5B). Also, the growth of *zwf*-repressed strains varied considerably. Cultures of AW012-3, AW013-3, and AW016-3 reached substantially lower final cell densities compared to AW009, while the final cell density in cultures of AW014-3 was a bit higher (Figure 5.5C). Accordingly, the specific HA titers in cultures of AW014-3 and AW016-3 were respectively equal to and 131% higher than that of AW009.

5.3.4 Multiplexed repression of pfkA and zwf expression further improves the HA titer and restores the MW

We next evaluated the effect of multiplexed repression of *pfkA* and *zwf* expression on HA production. Given the significant improvements to the volumetric HA titer and, in particular, the specific HA titer in cultures of AW005-3, AW006-3, and AW016-3 compared to AW009, we selected *pfkA*-gRNA.P41NT or *pfkA*-gRNA.P41NT(10C-A) to be co-transcribed with *zwf*-gRNA.P603NT(10U-C) for gene repression in the newly derived strains. Accordingly, AW002-3 was respectively transformed with SacI-linearized pAW017-3 and pAW018-3, generating corresponding strains AW018-3 and AW019-3. The HA titer in cultures of AW018-3 and

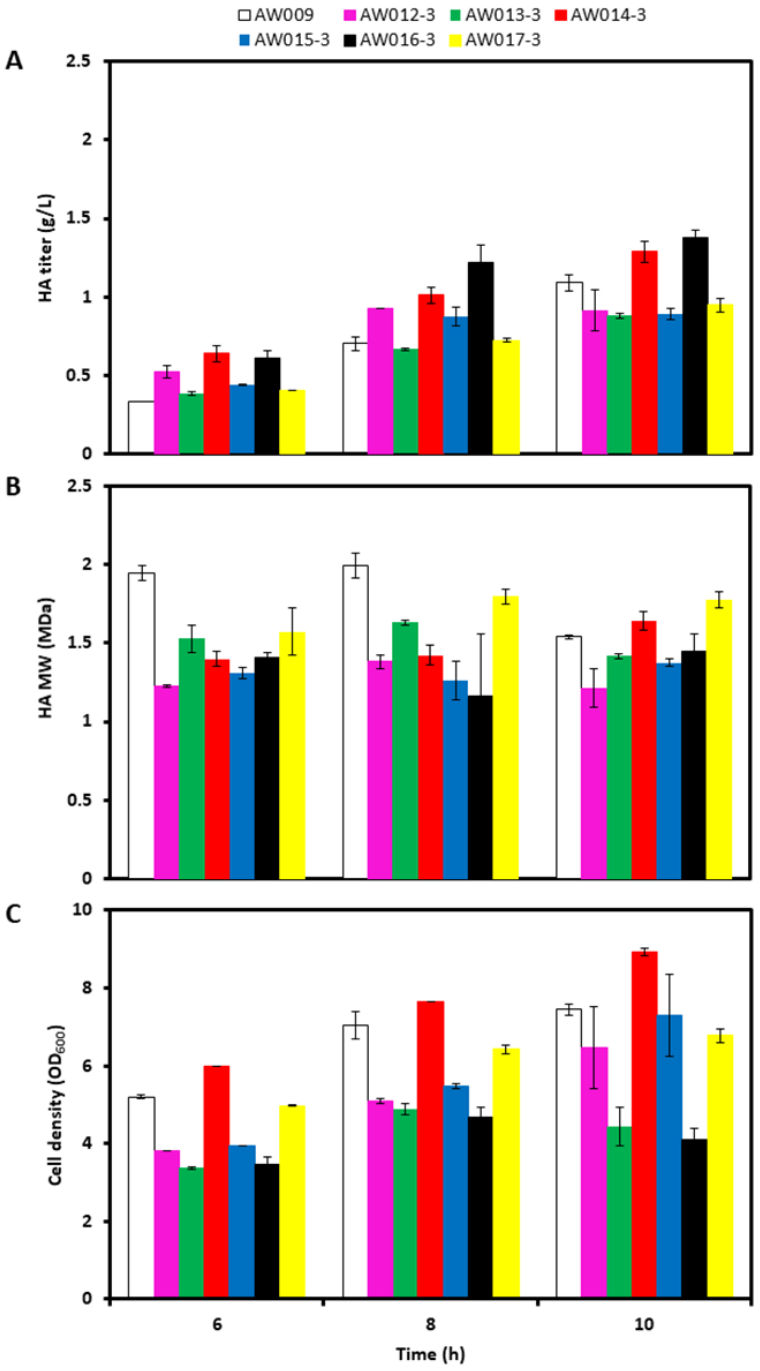

Figure 5.5. Time profiles of A) HA titer, B) HA MW, and C) cell density in cultures of AW009, AW012-3 (transcribing *zwf*-gRNA.P92NT), AW013-3 (transcribing *zwf*-gRNA.P92NT(10U-G)), AW014-3 (transcribing *zwf*-gRNA.P92NT(15C-A)), AW015-3 (transcribing *zwf*-gRNA.P603NT), AW016-3 (transcribing *zwf*-gRNA.P603NT(10U-C)), and AW017-3 (transcribing *zwf*-gRNA.P603NT(15G-U)). All strains transcribing *zwf*-targeting gRNAs are derivatives of AW002-3, which expresses xylose-inducible dCas9 with constitutively expressed *araE* to enhance xylose uptake. SD of experiments performed in duplicate are shown in Panels A, B, and C.

AW019-3 reached 2.16 g/L and 2.26 g/L after 10 h (Figure 5.6A), respectively, representing 98% and 108% increases compared to AW009. Importantly, the peak MW of HA produced by either strain was slightly higher, while the final MW in cultures of AW018-3 and AW019-3 was equal to and 14% higher, respectively, compared to AW009 (Figure 5.6B). Surprisingly, the final cell density in cultures of AW018-3 (i.e. a strain with multiplexed repression of *pfkA* and *zwf*) was 53% and 88% higher, compared to AW005-3 and AW016-3 (i.e. strains with single repression of *pfkA* or *zwf*), respectively, and was slightly higher compared to AW009 (Figure 5.6C). Similarly, the final cell density in cultures of AW019-3 (i.e. a strain with multiplexed repression of *pfkA* and *zwf*) was 16% and 63% higher compared to AW006-3 and AW016-3 (i.e. strains with single repression of *pfkA* or *zwf*), respectively, although was slightly lower compared to AW009. Accordingly, the specific HA titers in cultures of AW018-3 and AW019-3 were 92% and 131% higher after 10 h cultivation, compared to AW009. The results suggest that proper modulation of repression of *pfkA* and *zwf* expression could significantly enhance HA production without negatively affecting the MW of produced HA.

5.4 Discussion

HA biosynthesis is a metabolically demanding process, requiring 2 mol glucose, 3 mol ATP, 2 mol UTP, and 1 mol acetyl-CoA to generate 1 mol of the HA disaccharide. The major substrates for HA biosynthesis, i.e. nucleotide sugars UDP-GlcUA and UDP-GlcNAc, are also required for cell wall biosynthesis. Hence, HA biosynthesis directly competes with the PPP and glycolysis for glucose-6-P and fructose-6-P, respectively. However, heterologous HA production in *B. subtilis* often does not significantly alter the cell growth profile based on our observations (unpublished data) and others [5], suggesting that an autonomously balanced substrate allocation

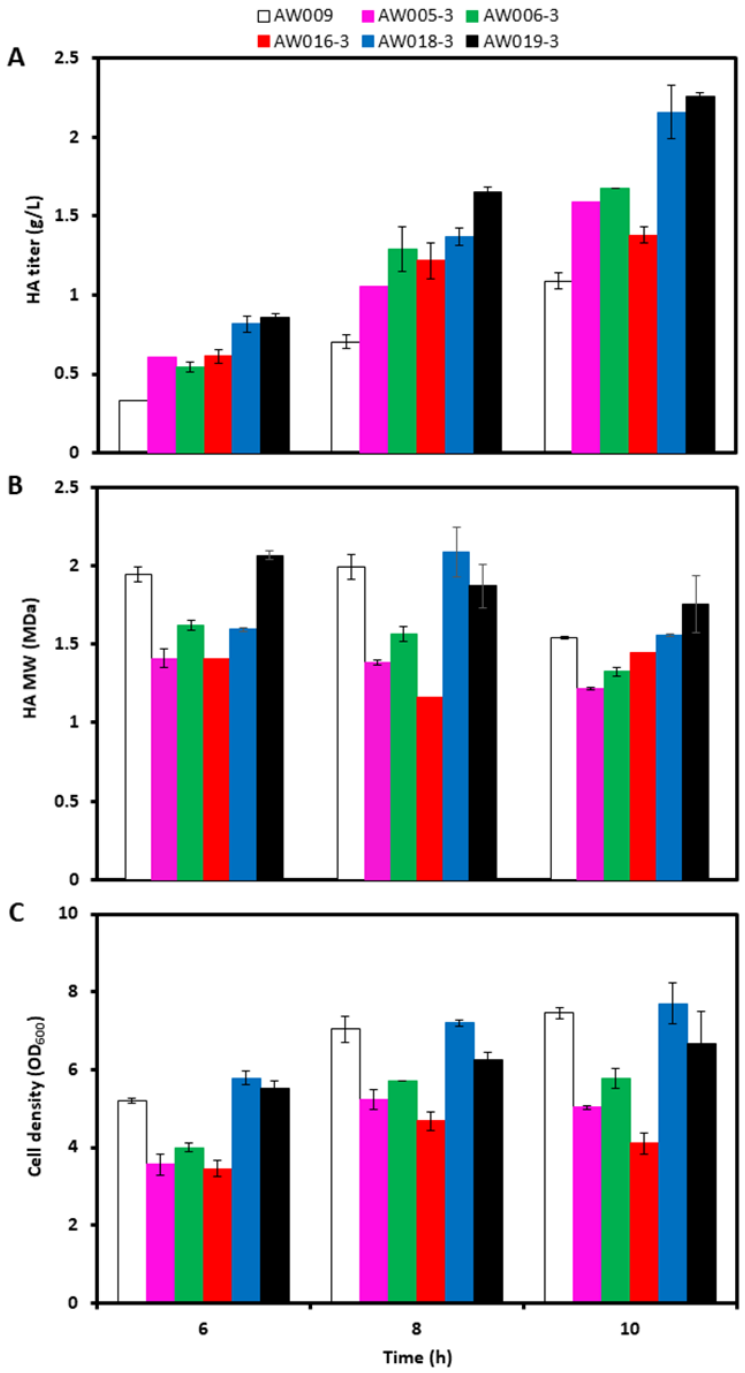

Figure 5.6. Time profiles of A) HA titer, B) HA MW, and C) cell density in cultures of AW009, AW005-3 (transcribing *pfkA*-gRNA.P41NT), AW006-3 (transcribing *pfkA*-gRNA.P41NT(10C-A)), AW016-3 (transcribing *zwf*-gRNA.P603NT(10U-C)), AW018-3 (transcribing *pfkA*-gRNA.P41NT and *zwf*-gRNA.P603NT(10U-C)), and AW019-3 (transcribing *pfkA*-gRNA.P41NT(10C-A) and *zwf*-gRNA.P603NT(10U-C)). All strains transcribing *pfkA*- and/or *zwf*-targeting gRNAs are derivatives of AW002-3, which expresses xylose-inducible dCas9 with constitutively expressed *araE* to enhance xylose uptake.SD of experiments performed in triplicate are shown in Panels A and C, and SD of duplicate samples are shown in Panel B.

can exist between central metabolism and biosynthesis of HA and cell wall. Accordingly, overexpressing enzymes involved in HA biosynthesis may be futile, particularly if substrate availability is the limiting factor due to strict carbon flux partitioning in the HA-producing host.

In this study, we redirected carbon flux from central metabolism, i.e. the PPP and glycolysis, toward HA biosynthesis by repressing expression of *zwf* and/or *pfkA*, which encode branch point enzymes driving dissimilated carbon into the respective pathways. Significant improvements to the HA titer were obtained in cultures of all seven AW002-3 derivatives transcribing *pfkA*-targeting gRNAs covering a range of relative repression efficiency (Figure 5.4A). Note that *pfkA* is an essential gene in *B. subtilis* [229, 240] that cannot be knocked out, and repression of *pfkA* expression should reduce glycolytic carbon flux. Our results are consistent with a previous study in which attenuated *pfkA* expression via start codon replacement improved the HA titer in *B. subtilis* [130]. However, the increase in the HA titer was accompanied by a decrease in the MW (Figure 5.4B). HA biosynthesis is limited by insufficient UDP-GlcNAc levels in *S. zooepidemicus* [245], such that overexpression of *hasE* and *hasD* (i.e. respective homologues of *pgi* and *gcaD* encoding enzymes involved in UDP-GlcNAc synthesis) [245], or addition of exogenous GlcNAc [247] dramatically improved the MW. A similar substrate imbalance could exist with UDP-GlcUA being the limiting substrate for HA biosynthesis in *B. subtilis* under our cultivation conditions (i.e. using a medium with a high phosphate content), potentially causing premature termination of the growing HA polymer [245]. Theoretically, overexpression of *tuaD* should at least partially resolve the natural imbalance between UDP-GlcUA and UDP-GlcNAc. However, we suspected that the reduced expression of *pfkA* might have increased the conversion of fructose-6-P to glucosamine-6-P via GlmS and,

therefore, increased the carbon flux through the UDP-GlcNAc branch of the HA biosynthetic pathway, resulting in an imbalance between substrate levels and a reduction in the MW.

To test this hypothesis, we supplemented cultures of AW006-3 with either GlcUA or GlcNAc at a concentration of 0.4 g/L or 0.8 g/L. Interestingly, the addition of GlcUA and GlcNAc to 0.4 g/L reduced the final HA titer by 31% and 55%, respectively, compared to cultures without exogenous GlcUA and GlcNAc, while increasing the concentration of each substrate to 0.8 g/L led to respective 18% and 24% increases in the final HA titer, compared to the corresponding cultures with a concentration of 0.4 g/L (Figure 5.7A). Moreover, the addition of 0.4 g/L GlcUA resulted in a 35% increase in the peak MW (2.19 MDa; at 8 h), compared to the peak MW (1.62 MDa; at 6 h) of the control culture lacking exogenous supplementation (Figure 5.7B). The effect on MW was even more pronounced in the culture supplemented with 0.4 g/L GlcNAc, and the peak MW reached 2.62 MDa at 10 h, representing a 62% increase compared to the control culture (Figure 5.7B). A further increase in the concentration of either substrate to 0.8 g/L had a marginal effect on the MW, compared to the corresponding culture with a concentration of 0.4 g/L (Figure 5.7B). The decrease in the HA titer without cell growth being negatively affected upon the addition of exogenous GlcUA or GlcNAc may suggest that imbalanced substrate levels occurred even at the lowest concentration of 0.4 g/L. The activity of membrane-bound SeHAS was observed to decrease with increasing UDP-GlcUA concentration, particularly when the ratio of UDP-GlcUA to UDP-GlcNAc was significantly higher than 1:1 [248]. While a proposed decline in the activity of SeHAS may seem counterintuitive given the large increase in the MW observed upon the addition of either GlcUA or GlcNAc, note that the polymerizing activity (affecting HA titer) and control of chain length (affecting HA MW) are independent functions of SeHAS that are not necessarily coupled to each other [211]. On the

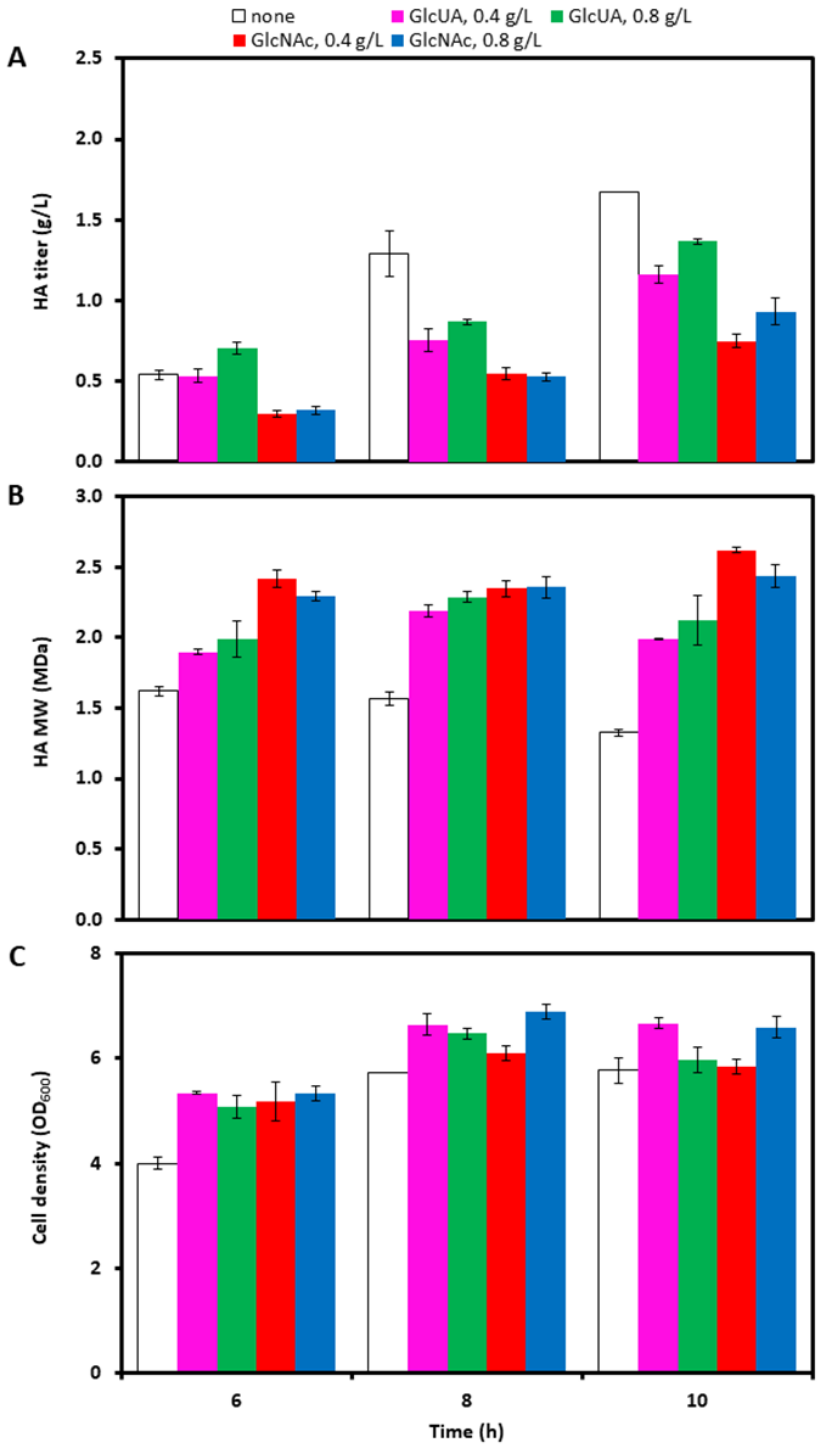

Figure 5.7. Time profiles of A) HA titer, B) HA MW, and C) cell density in cultures of AW006-3, an AW002-3 derivative transcribing *pfkA*-gRNA.P41NT(10C-A), supplemented with GlcUA or GlcNAc at a concentration of 0.4 g/L or 0.8 g/L. SD of experiments performed in triplicate are shown in Panels A and C, and SD of duplicate samples are shown in Panel B.

other hand, in the presence of excess UDP-GlcUA or UDP-GlcNAc, chain elongation might stall temporarily as the excess substrate transiently occupies the binding site of the other substrate as a competitive inhibitor [248], but the chain is retained until the appropriate substrate is available for synthesis and chain elongation to commence. An alternate explanation might be that supplementing cultures with GlcNAc altered the rate of synthesis of UDP-GlcNAc. GlcNAc is simultaneously transported into the cell and phosphorylated to yield GlcNAc-6-P by the GlcNAc specific phosphotransferase system transporter NagP, and GlcNAc-6-P is subsequently converted to glucosamine-6-P by GlcNAc-6-P deacetylase (i.e. NagA) [249]. Glucosamine-6-P inhibits expression of *glmS* by associating with its 5'-untranslated region (UTR), resulting in self-cleavage of the 5'-UTR by the *glmS* ribozyme, and subsequent targeting of the *glmS* mRNA for degradation [250]. Accordingly, the addition of exogenous GlcNAc in cultures of AW006-3 may disrupt the dissimilated carbon flux into the UDP-GlcNAc branch of the HA biosynthetic pathway and, therefore, increase the ratio of UDP-GlcUA to UDP-GlcNAc, resulting in decreased HA titers and increased MWs. We have previously observed that increased HA titers in cultures of *B. subtilis* are often accompanied by a decrease in the MW [239], and the yield on glucose and MW of HA produced in *S. zooepidemicus* were not correlated [245]. In any case, further investigation is required to elucidate the effects of overall carbon flux into the HA biosynthetic pathway and the UDP-GlcNAc/UDP-GlcUA ratio on the titer and MW of HA produced in *B. subtilis*.

The culture performance of *zwf*-repressed strains varied considerably. Mutation of *zwf* resulted in increased glycolytic flux in *B. subtilis* grown on glucose, albeit with a lower biomass yield [240]. This is consistent with our results as the final cell density of all *zwf*-repressed strains except AW014-3 was lower compared to AW009 (Figure 5.5C). Clearly, the majority of carbon

diverted from the PPP either entered glycolysis or another pathway other than HA biosynthesis given that the HA titers were not necessarily increased in these *zwf*-repressed strains (Figure 5.5A). In this context, improving HA production may not be possible without reducing *pfkA* expression, particularly when the primary carbon source is sucrose with half of the dissimilated carbon naturally bypassing Zwf. By simultaneously repressing the expression of both *pfkA* and *zwf* in AW018-3 and AW019-3, we obtained significant increases in the HA titer (Figure 5.6A) and modest enhancements to the MW relative to AW009 (Figure 5.6B), indicating a significantly higher and more balanced carbon flux through the UDP-GlcUA and UDP-GlcNAc branches for HA biosynthesis. Note that the high degree of reversibility for the interconversion of glucose-6-P and fructose-6-P by Pgi is well documented [251, 252], potentially leading to more balanced flux distribution at these two nodes toward UDP-GlcUA and UDP-GlcNAc, respectively, in AW018-3 and AW019-3.

A common approach to improve microbial HA production has been to overexpress genes in either branch of the HA biosynthetic pathway to upregulate the level of the limiting substrate (i.e. UDP-GlcUA or UDP-GlcNAc), but this strategy often yields modest returns on the HA titer and MW [5, 130]. To this end, we also evaluated the effects of overexpressing *pgcA*, *glmS*, or both genes on HA biosynthesis by transforming AW009 respectively with pAW019-3, pAW020-3, and pAW021-3, generating corresponding strains AW020-3, AW021-3, and AW022-3. The titers and MWs of HA produced in cultures of AW020-3, AW021-3, and AW022-3 were highly similar to those obtained in cultures of AW009 (data not shown), confirming the deficiency of this metabolic approach.

In addition to *pfkA* and *zwf*, we also targeted additional essential genes of interest for transcriptional interference, i.e. *tagO*, encoding UDP-GlcNAc-undecaprenyl-phosphate *N*-

acetylglucosaminephosphotransferase (TagO) that converts UDP-GlcNAc to *N*-acetyl-glucosaminyldiphospho-*ditrans,octacis*-undecaprenol during teichoic acid synthesis, and *murAA*, encoding UDP-GlcNAc 1-carboxyvinyltransferase (MurAA) that converts UDP-GlcNAc to UDP-GlcNAc-enolpyruvate during UDP-N-acetylmuramoyl-pentapeptide (i.e. cell wall) synthesis (Figure 5.1) [229]. However, preliminary attempts to reduce the expression of *tagO* and *murAA* via CRISPRi in AW002-3 resulted in poor growth and genetic instability, as certain derived *B. subtilis* strains lost the mucoid phenotype for HA-production (data not shown). Accordingly, future attempts to repress expression of these genes may employ very low levels of repression.

While the feasibility of repressing the expression levels of *pfkA* and *zwf* for enhanced HA production has been demonstrated, there appears to be no correlation between the repression efficiencies and culture performance. For example, the HA titer, MW, and cell density profiles in cultures of AW005-3, AW006-3, and AW007-3 were quite similar, even though the respective gRNAs in AW006-3 and AW007-3, i.e. *pfkA*-gRNA.P41NT(10C-A) and *pfkA*-gRNA.P41NT(15U-C), contained single mismatches in their protospacers and, thus, should have significantly lowered repression efficiency compared to *pfkA*-gRNA.P41NT in AW005-3 for which the protospacer was unaltered. Moreover, AW009-3 achieved a significantly lower cell density compared to AW005-3, although the gRNA in AW009-3, i.e. *pfkA*-gRNA.P315NT(15U-G), targeted dCas9 to a PAM site significantly further from the start codon of the *pfkA* ORF, compared to *pfkA*-gRNA.P41NT, and contained a single mismatch in the protospacer. Similarly, the HA titers and MWs were similar in cultures of AW012-3 and AW013-3 while transcription of *zwf*-gRNA.P92NT(10U-G) in AW013-3 should reduce the repression efficiency of *zwf* expression by ~75%, relative to the transcription of *zwf*-gRNA.P92NT in AW012-3.

Accordingly, anticipating the effects of altered repression efficiency for the expression of genes in the central metabolic pathways may not be practical, such that the design of multiple gRNAs for a single target is deemed necessary to realize the true impact of its repression on target metabolite production. Nevertheless, our results stress the importance of balancing intracellular substrate levels of UDP-GlcUA and UDP-GlcNAc for high-level production of high-MW HA in engineered *B. subtilis*.

Chapter 6

Application of hydrocarbon and perfluorocarbon oxygen vectors to enhance heterologous production of HA in engineered *B. subtilis*

6.1 Introduction

Industrial bioprocesses based on microbial platforms are typically aerobic and utilize aqueous growth medium containing salts and other nutrients [253]. Oxygen is sparingly soluble in aqueous solutions, a limitation that is exacerbated by factors such as salinity and culture viscosity [254, 255]. High-cell-density cultures are highly viscous, and, therefore, the diffusivity of oxygen becomes limited, causing a steep decline in dissolved oxygen (DO) levels [253, 255]. The increase in culture viscosity is more severe in bioprocesses in which high molecular weight (MW) biopolymers are secreted into the extracellular environment. For example, a substantial increase in viscosity (up to 500-fold) is observed as HA titers exceed 5 g/L in microbial cultivations [5]. The DO concentration is an intrinsic factor influencing HA synthesis due to a high demand of ATP for HA-producing cells [5, 225]. Oxygen transfer in microbial cultivations can be improved by increasing agitation and aeration rates, and, if necessary, pure oxygen supplementation. However, shearing due to high agitation and aeration rates may reduce the quality (i.e. MW) of HA [136, 152, 256], and supplementing pure oxygen can be detrimental to microorganisms as exposure to reactive oxygen species such as H_2O_2, O_2^-, and OH• can result in DNA instability, and protein and lipid denaturation [257]. Moreover, recombinant protein expression may be hampered by excessive DO levels due to misfolding, loss of activity, and protease degradation [258, 259]. Consequently, alternate methods to improve oxygen transfer in microbial cultivations for HA production are of significant interest, and using oxygen vectors is one of them.

Oxygen vectors are water-immiscible compounds possessing a greater capacity to dissolve oxygen compared to water. Hydrocarbons [136-139], perfluorocarbons [140-142], vegetable oil

[143], and silicone oil [139, 144] can enhance oxygen transfer in microbial cultivations, while insoluble polymers such as silicone rubber [139, 145], nylon [145], glass beads [145], Hytrel [139], Kraton [139], Desmopan [139, 144], and Elvax [144] have also been investigated as oxygen vectors. Oxygen vectors can enhance oxygen transfer by 1) creating large local concentration gradients in the bulk aqueous phase by shuttling oxygen-rich vector droplets from the gas-liquid interface to the bulk liquid; 2) reducing surface tension at the air-water interface, resulting in reduced bubble coalescence and, in turn, smaller bubble diameter and increased interfacial area for oxygen transfer; and 3) colliding with and breaking air bubbles, in turn, reducing bubble diameter [144, 260]. Oxygen vectors are categorized based on their propensity to form discrete droplets (i.e. non-spreading) or films which spread over gas bubbles (i.e. spreading) in an aqueous phase, and the means by which they affect oxygen transfer may be dictated by their tendency to spread or lack thereof [148]. The selection of an appropriate oxygen vector can potentially reduce operating costs associated with power consumption from high agitation rates, compressed air delivery, and supplemental oxygen, and can reduce oxidative damage to the producing cell and target metabolite or protein, while also minimizing foaming during high-cell-density cultivations [139, 257, 261].

The application of hydrocarbon and perfluorocarbon oxygen vectors to microbial cultivations for HA production has been investigated, albeit to a limited extent. The addition of *n*-dodecane [262] and *n*-hexadecane [152] to *S. zooepidemicus* cultivations resulted in improvements to both the HA titer and MW, while perfluorodecalin also increased the HA titer in *S. zooepidemicus* cultivations relative to a three-stage agitation operation in which the agitation speed was increased in a step-wise manner [140]. However, these studies investigated only a few compounds as potential oxygen vectors, and no data is currently available on the application of oxygen vectors to heterologous HA production in common microbial hosts. In this study, we evaluated three hydrocarbons (i.e. *n*-heptane, *n*-hexadecane, and 2,2,4-trimethylpentane) and four perfluorocarbons (i.e. *n*-perfluorooctane, perfluorodecalin, perfluoromethyldecalin, and perfluoro-1,3-dimethylcyclohexane) as potential oxygen vectors to enhance heterologous HA production in an engineered strain of *B. subtilis* with a significantly higher HA producing capacity than our previously reported strain [239].

Significant improvements to the HA titer and/or cell density were observed in cultures containing *n*-heptane, *n*-hexadecane, perfluoromethyldecalin, and perfluoro-1,3-dimethylcyclohexane, although the MW was marginally affected. We then manipulated the vector concentration and timing of addition, resulting in further improvements to the culture performance. Assessment of oxygen transfer via measuring the overall oxygen mass transfer coefficient k_La revealed that, regardless of spreading characteristics, hydrocarbon vectors slightly reduced k_La over the low vector concentrations employed in this study, while perfluoromethyldecalin enhanced oxygen transfer. We also investigated culture performance at higher agitation rates, and observed that the addition of *n*-hexadecane or perfluoromethyldecalin further enhanced the HA titer and cell density, although the MW was somewhat reduced when *n*-hexadecane was present, suggesting that functional expression of hyaluronan synthase (HAS) may be affected by *n*-hexadecane exposure in *B. subtilis*. Moreover, our results indicate that higher shear rates may somehow drive more carbon flux through the HA biosynthetic pathway without negatively affecting the MW.

6.2 Materials and methods

6.2.1 Bacterial Strains and plasmid construction

E. coli HI-Control™ 10G chemically competent cells were prepared as electrocompetent cells as described previously [187] and used as host for plasmid construction. Strain 1A751 is a derivative of *B. subtilis* 168 (i.e. *B. subtilis* 168 *his npr*R2 *npr*E18 Δ*aprA*3 Δ*eglS*102 Δ*bglT bgl*SRV) that has proven to be an effective host for heterologous HA production [128, 239, 263]. *B. subtilis* and *E. coli* strains were maintained as glycerol stocks at -80 °C. To construct the genomic integration vector pAW009, promoter $P_{grac.UPmod}$ was amplified from pHT01 [215] with primers Pgrac.UPmod,SalI.f (5'-cagattgagtcgac**ggatcactag**aaaatttttatcttatcacttgaaattgg-3') and Pgrac.UPmod.BamHI.r (5'-gcacttgaggatcctttcctcctttaattggg-3'), followed by insertion into SalI/BamHI-digested pAW008 [263] as shown in Figure S6.1 (restriction sites are underlined in the primer sequences). $P_{grac.UPmod}$ (i.e. promoter P61) is a weaker derivative of promoter P_{grac} (i.e. promoter P01) that contains a modified upstream promoter element (UP) that reduces the relative

promoter strength by approximately half [40] [Note that the modified UP was introduced with primer Pgrac.UPmod,SalI.f and the modified sequence is in bold font.]. Transformation of pAW009 into *B. subtilis* results in the integration of a $P_{grac.UPmod}$::*seHas*:*tuaD* expression cassette at the *amyE* locus as shown in Figure S6.1 [*tuaD* encodes native UDP-glucose-6 dehydrogenase (TuaD) and *seHas* encodes hyaluronan synthase from *S. equisimilis* (SeHAS)]. Competent cell preparation and transformation of pAW009 was performed as previously described [263].

6.2.2 Cultivation medium and conditions

B. subtilis strains were plated on non-select LB agar (NaCl, 5 g/L; yeast extract, 5 g/L; tryptone, 10 g/L; agar, 15 g/L), and grown overnight at 37 °C. Shake flask cultures to compare HA production in AW008 and AW009 were performed as previously described (see section 4.2.3) [239]. To prepare the seed cultures for bioreactor cultivations, a single colony was used to inoculate 25 mL prewarmed non-select LB, and grown for ~8 h at 37 °C and 280 rpm to generate the starter culture. The starter culture was subsequently diluted 100-fold into 100 mL prewarmed non-select LB, and grown for ~13 h at 37 °C and 280 rpm to generate the seed culture. Cultivations were performed in a New Brunswick™ BioFlo® 115 bioreactor (Hamburg, Germany) under the following conditions: 0.7 L working volume (1.3 L vessel), 2 volume per volume per minute (vvm) [i.e. 1.4 L/min] air, 300 rpm, 37 °C, pH 7 (3 M NH_4OH). The non-select cultivation medium was of the following composition (per L): sucrose, 30 g; $(NH_4)_2SO_4$, 1 g; $K_2HPO_4 \cdot 3H_2O$, 9.15 g; KH_2PO_4, 3 g; trisodium citrate$\cdot$ $2H_2O$, 1 g; yeast extract, 10 g; $CaCl_2$, 5.5 mg; $FeCl_2 \cdot 6H_2O$, 13.5 mg; $MnCl_2 \cdot 4H_2O$, 1 mg; $ZnCl_2$, 1.7 mg; $CuCl_2 \cdot 2H_2O$, 0.43 mg; $CoCl_2 \cdot 6H_2O$, 0.6 mg; $Na_2MoO_4 \cdot 2H_2O$, 0.6 mg. The bioreactor was inoculated with 10% volume per volume (v/v) of the seed culture. HA purification and analysis was performed as previously described [263].

6.2.3 Determination of k_La

Experiments to determine k_La were performed under the same cultivation conditions described above without the inoculum. Measurements of k_La were performed using the dynamic "gas out-gas in" method, and the probe response time was neglected due to the relatively low k_La values obtained under our experimental conditions [264]. k_La values were obtained from the mass balance equation:

$$ln\left(\frac{DO^*-DO(t)}{DO^*-DO(t_0)}\right) = -k_La(t-t_0) \quad (6.1)$$

where DO^* is the saturation reading of the probe. ANOVA was performed to determine the significance between k_La measurements, and the results of the analysis are presented in Table S6.1.

6.2.4 Oxygen vectors

n-heptane (>99%), *n*-hexadecane (>99%), *n*-perfluorooctane (98%), perfluorodecalin (95%), and perfluoro-1,3-dimethylcyclohexane (80%) were obtained from MilliporeSigma (MO). Perfluoromethyldecalin (80%), a mixture of perfluoro-1-methyldecalin and perfluoro-2-methyldecalin, was also obtained from MilliporeSigma. *n*-Heptane (>99%) was obtained from J.T. Baker (NJ). The physical properties of oxygen vectors used in this study are provided in Table 6.1.

6.2.5 Side metabolite analysis

The titers of the side metabolites lactate, acetate, and 2,3-butanediol (2,3-BDO) were analyzed via high-performance liquid chromatography (HPLC). The system consists of a Shimadzu (Kyoto, Japan) LC-10AT solvent delivery unit, Shimadzu RID-10A refractive index detector, Shimadzu CTO-20A column oven, and an Aminex HPX-87H chromatographic column (Bio-Rad Laboratories, CA). The column temperature was maintained at 65°C, and the flow rate of the mobile phase (i.e. 5 mM H_2SO_4) was 0.6 mL/min. Signal acquisition and data processing was performed with Clarity Lite (DataApex, Prague, Czech Republic).

Table 6.1. Physical properties of oxygen vectors used in Chapter 6 measured at 25 °C and atmospheric pressure unless otherwise indicated.

Compound	Molecular formula / structure	Dynamic viscosity (mPa·s)	Density (g/mL)	Boiling point (°C)	Relative oxygen solubility*	References
n-hexadecane	$C_{16}H_{34}$ (linear)	3.0	0.77	287	8.2	[265, 266]
n-heptane	C_7H_{16} (linear)	0.39	0.68	98.4	10.8	[267, 268]
2,2,4-trimethylpentane	C_8H_{18} (branched)	3.19	0.77	99	14.0	[269, 270]
perfluoro-1,3-dimethylcyclohexane	C_8F_{16} (cyclic, branched)	1.92	1.83	102	16.1[a]	[271, 272]
perfluoromethyldecalin	$C_{11}F_{20}$ (bicyclic, branched)	6.47	1.95	137-160	12.7	[273, 274]
perfluorodecalin	$C_{10}F_{18}$ (bicyclic)	5.41	1.91	142	13.9[b]	[271, 275]
n-perfluorooctane	C_8F_{18} (linear)	1.26	1.77	103	14.0[c]	[275, 276]

*Expressed as the fold increase in oxygen solubility relative to water. Measured at 16 °C[a], 38 °C[b], and 36 °C[c]

6.3 Results

6.3.1 Preliminary evaluation of potential oxygen vectors

Three hydrocarbons and four perfluorocarbons were evaluated for their effects on HA production in batch cultivations of strain AW009 in a bench-scale STR. Potential oxygen vectors were selected based on their volatility (i.e. a minimum normal boiling point of ~100 °C) and relative oxygen solubility (i.e. at least 8-fold higher than water). Compounds such as *n*-heptane, *n*-hexadecane, and perfluorodecalin were preferred as they had been successfully applied to either microbial HA production [140, 152] or biopolymer production in *B. subtilis* [153]. In the preliminary evaluation, each compound was added to the cultivation medium at a concentration of 1% v/v 2 h

after inoculation. A relatively low agitation rate at 300 rpm was used to minimize potential HA degradation resulting from polymer shearing [136].

AW009 produced 992 mg/L of HA after 12 h (Figure 6.1A) with a peak MW of 1.2 MDa at 8 h, (Figure 6.1B), and final cell density of OD_{600} 12.8 (Figure 6.1C). The DO fell below 5% saturation after 4 h where it remained for the rest of the cultivation (Figure 6.1D). The addition of *n*-hexadecane resulted in a 34% increase to the final HA titer (1327 mg/L; Figure 6.1A), although the MW was not significantly affected (Figure 6.1B). Note that ANOVA was performed on all measurements of the HA titer, MW, and cell density for all data sets presented herein, and a summary of the results of the analysis is presented in Table S6.1 of the Supplementary Materials. Moreover, the cell growth rate was improved such that the final cell density (OD_{600} 13.3) was obtained at 10 h, compared to 12 h with no vector (Figure 6.1C). Notably, *n*-hexadecane was the only compound tested that provided a substantial increase in DO levels, which remained above 10% saturation throughout the cultivation (Figure 6.1D). While the addition of *n*-heptane did not markedly affect the volumetric HA titer, it did improve the specific HA titer by 26%, i.e. 97.6 mg/(L·OD_{600}) for *n*-heptane compared to 77.5 mg/(L·OD_{600}) with no vector. Moreover, the addition of *n*-heptane prolonged the oxygen limitation by 1 h compared to the cultivation with no vector (Figure 6.1D).

Two of the four perfluorocarbons tested, i.e. perfluoro-1,3-dimethylcyclohexane and perfluoromethyldecalin, significantly improved culture performance. The addition of perfluoro-1,3-dimethylcyclohexane and perfluoromethyldecalin resulted in 50% (1490 mg/L) and 49% (1481 mg/L) increases to the final HA titer (Figure 6.1A), respectively, although the MW was not significantly affected (Figure 6.1B). Moreover, the respective final cell densities increased by 16% (OD_{600} 14.8) and 11% (OD_{600} 14.2) relative to the cultivation with no vector (Figure 6.1C) although DO levels were marginally improved (Figure 6.1D). Conversely, the addition of *n*-perfluorooctane resulted in a 23% decrease to the HA titer (761 mg/L; Figure 6.1A), and an 11% decrease in the final cell density (OD_{600} 11.4; Figure 6.1C). The specific HA titer was highest for the cultivation with perfluoromethyldecalin (104.7 mg/(L·OD_{600})), compared to all other vectors, and was 35% higher relative to the cultivation with no vector. For initial experiments with *n*-hexadecane and perfluoro-

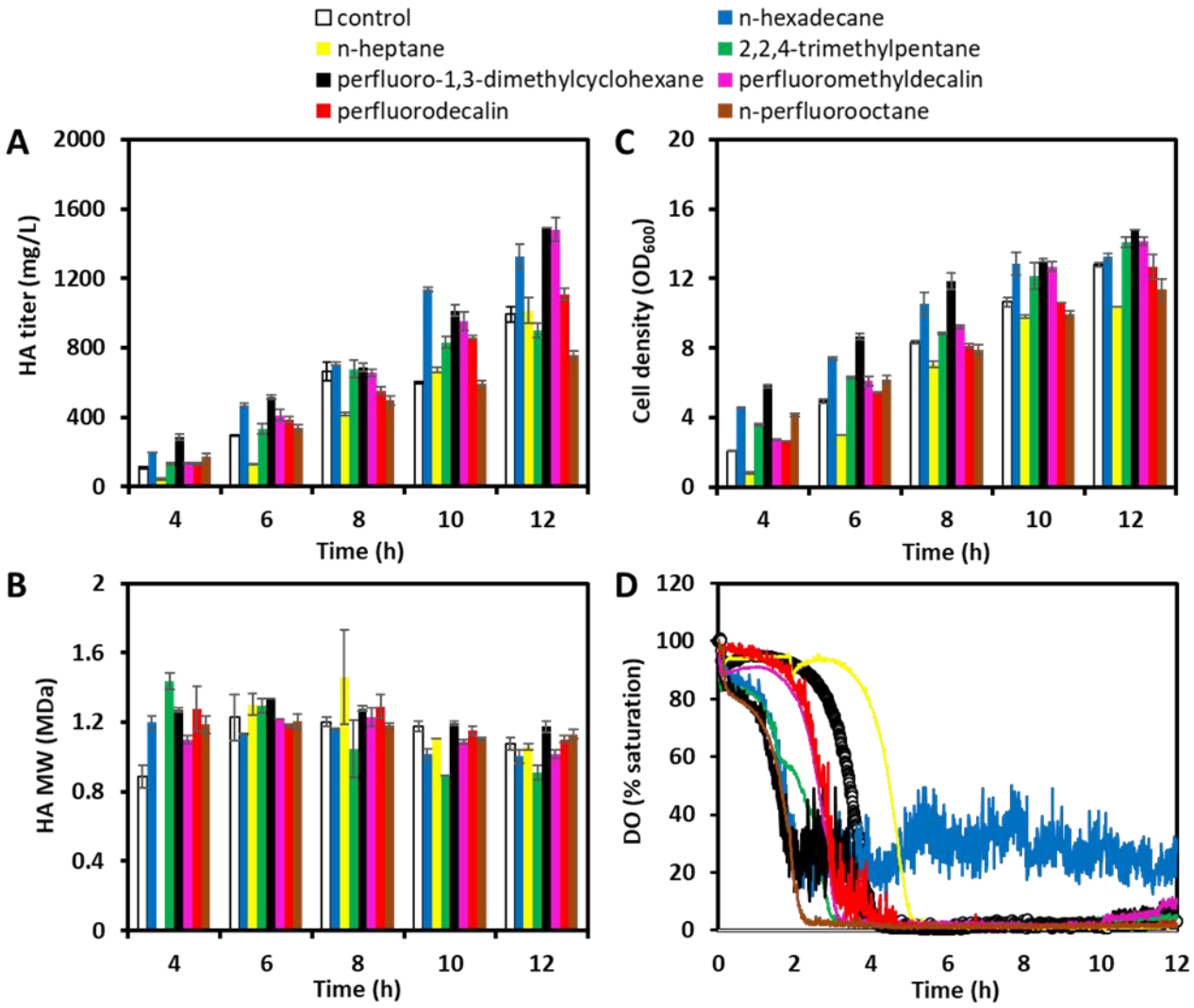

Figure 6.1. Time profiles of A) HA titer, B) HA MW, C) cell density, and D) DO in cultures of AW009 with no vector, or in which *n*-hexadecane, *n*-heptane, 2,2,4-trimethylpentane, perfluoro-1,3-dimethylcyclohexane, perfluoromethyldecalin, perfluorodecalin, or *n*-perfluorooctane was added 2 h after inoculation at a final concentration of 1% v/v. SD of duplicate samples shown in Panels A, B, and C.

1,3-dimethylcyclohexane, the oxygen vectors were added at the time of seed culture inoculation. However, the addition of 2,2,4-trimethylpentane and perfluoromethyldecalin at the time of inoculation completely inhibited growth, such that in subsequent experiments all vectors were added 2 h after inoculation when the exponential growth phase was reached. This bioprocessing strategy was developed based on the prior observation that 2,2,4-trimethylpentane is toxic to *E. coli* in the

stationary phase, but is not during exponential growth [277]. Adding *n*-hexadecane at the time of inoculation resulted in a 30% increase in the final HA titer (1731 mg/L; Figure 6.2A), a 14% increase in the final MW (1.14 MDa; Figure 6.2B), and a 22% increase in the final cell density (OD_{600} 16.1; Figure 6.2C), although DO levels were lower between 5 h and 8 h (Figure 6.2D), compared to the addition of *n*-hexadecane at 2 h. The addition of perfluoro-1,3-dimethylcyclohexane at the time of inoculation did not significantly increase the final HA titer or MW, although the titer after 10 h was similar to the final titer when the vector was added at 2 h (Figure 6.2A). Moreover, the final cell density increased by 15% (OD_{600} 17; Figure 6.2C), although the DO profiles were not significantly different (Figure 6.2D).

6.3.2 Vector concentration affects HA production

Based on the results from the preliminary evaluation, *n*-hexadecane provided the greatest enhancements to DO levels and HA production. Accordingly, we attempted to further improve culture performance by manipulating the *n*-hexadecane concentration. Reducing the *n*-hexadecane concentration to 0.5% v/v increased the final HA titer by 20% (1596 mg/L; Figure 6.3A), without significantly affecting the MW (Figure 6.3B). The final cell density also increased by 22% (OD_{600} 17.4; Figure 6.3C), which may be attributed, in part, to the increase in DO levels after 6 h (Figure 6.3D). Our results are similar to an earlier report of enhanced HA production in batch cultures of *S. zooepidemicus* upon the addition of *n*-hexadecane to 0.5% v/v, which maximized k_La [152]. In contrast, adding *n*-hexadecane to 1% v/v was found to be optimal for PGA production in *B. subtilis* [153]. The application of *n*-heptane as an oxygen vector to enhance PGA production in cultures of *B. subtilis* resulted in greater improvements to both the titer and MW, compared to cultures supplemented with *n*-hexadecane, and the optimal concentration of *n*-heptane (0.3% v/v) was significantly lower compared to *n*-hexadecane (1% v/v) [153]. On the other hand, we obtained significantly higher HA titers with *n*-hexadecane compared to *n*-heptane (Figure 6.1A), albeit with a slight reduction in MW (Figure 6.1B). Given that our preliminary evaluation was conducted with a vector concentration of 1% v/v, we considered that reducing the *n*-heptane

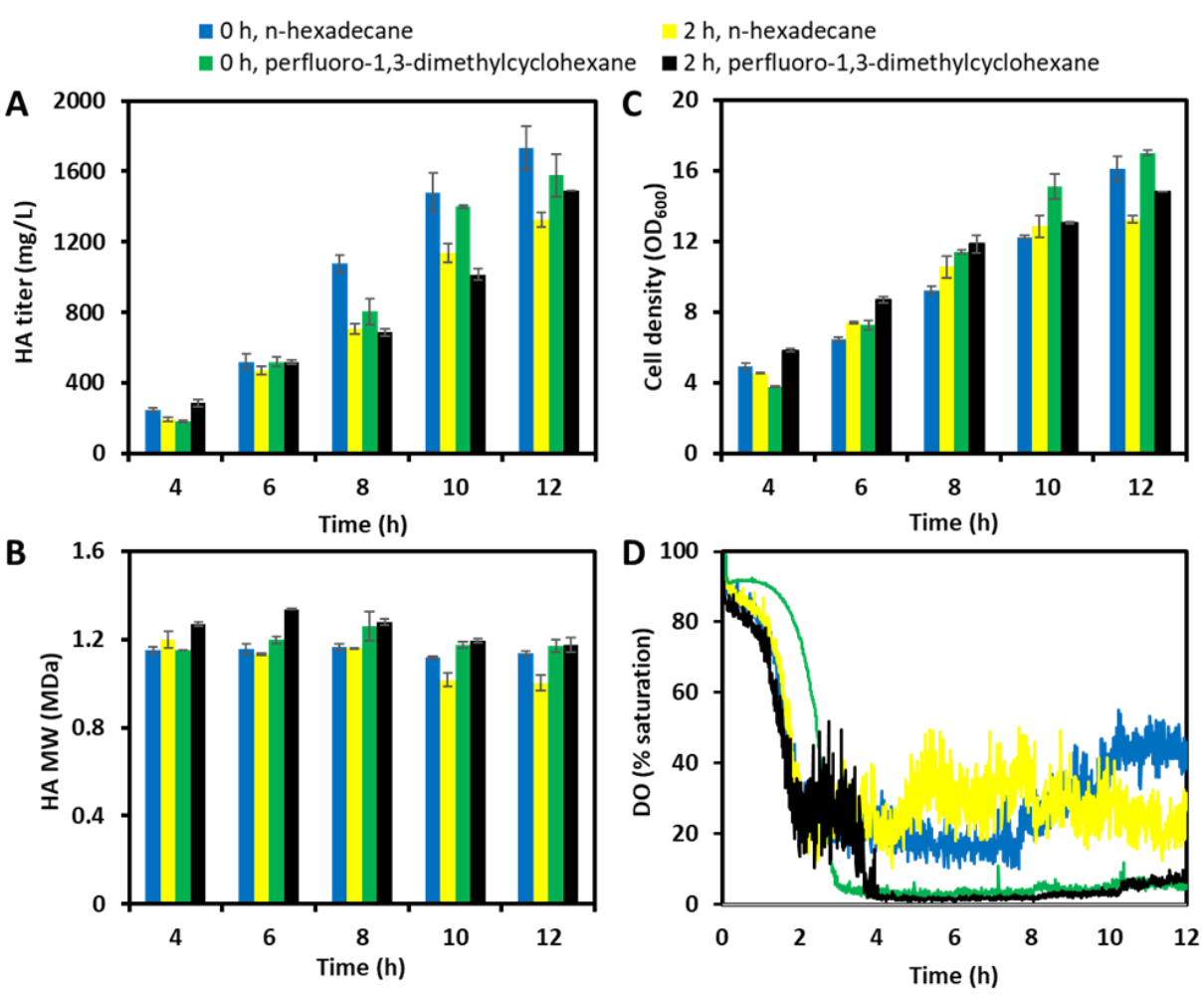

Figure 6.2. Time profiles of A) HA titer, B) HA MW, C) cell density, and D) DO in cultures of AW009 in which *n*-hexadecane or perfluoro-1,3-dimethylcyclohexane was added at the time of inoculation (0 h) or 2 h after inoculation at a final concentration of 1% v/v. SD of duplicate samples shown in Panels A, B, and C.

concentration might improve culture performance. Reducing the *n*-heptane concentration to 0.4% v/v resulted in a substantially higher HA titer after 10 h cultivation (1123 mg/L), compared to the cultivations containing either 1% v/v *n*-heptane (672 mg/L) or no vector (599 mg/L; Figure 6.4A). However, the final HA titer (Figure 6.4A) and MW profile (Figure 6.4B) were not significantly improved by reducing the *n*-heptane concentration. The DO levels declined quickly prior to the addition of 0.2% *n*-heptane, compared to the cultivation with no vector, and were only temporarily

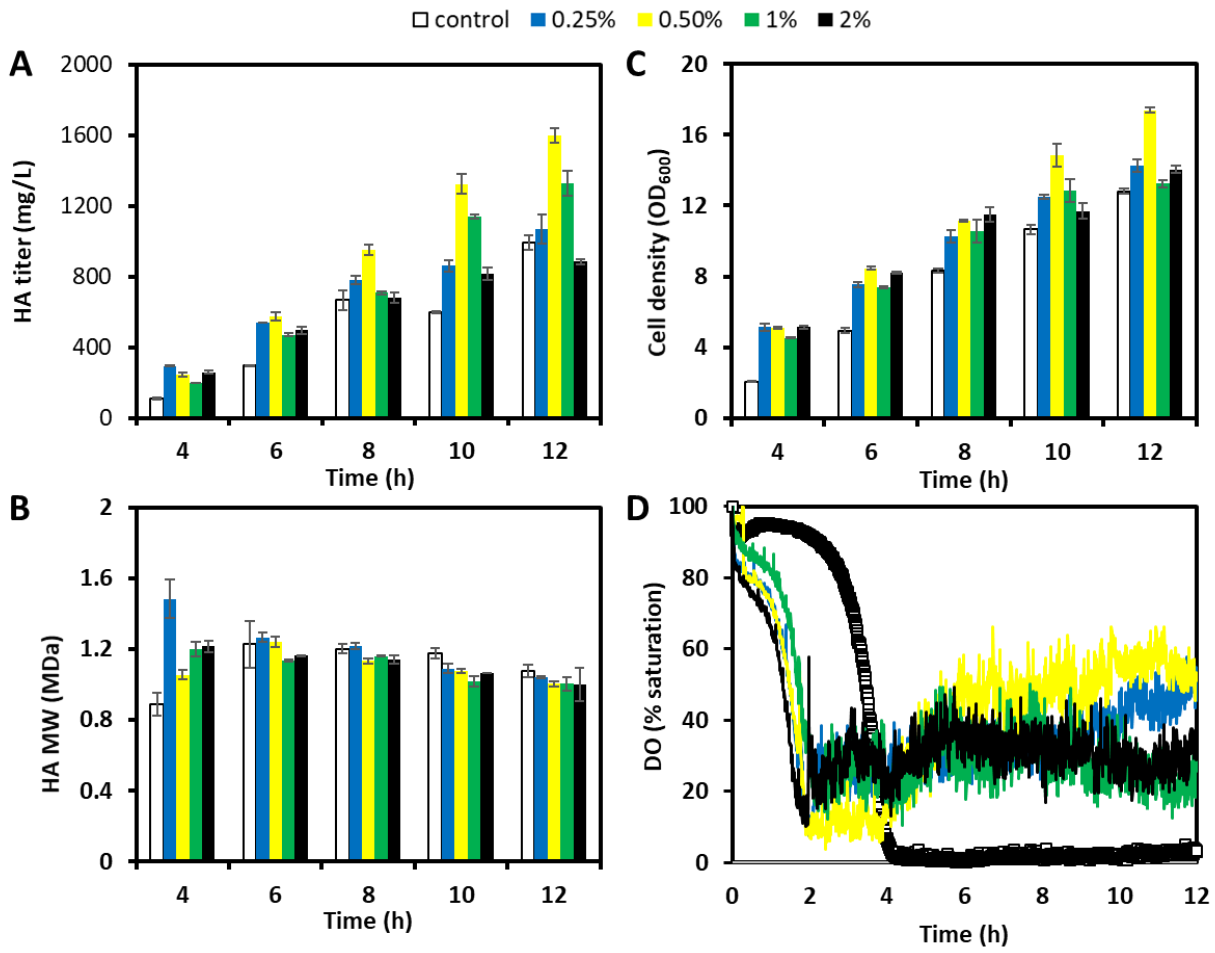

Figure 6.3. Time profiles of A) HA titer, B) HA MW, C) cell density, and D) DO in cultures of AW009 with no vector, or in which *n*-hexadecane was added 2 h after inoculation at a final concentration of 0.25%, 0.5%, 1%, or 2% v/v. SD of duplicate samples shown in Panels A, B, and C.

rescued upon adding *n*-heptane, before dropping to approximately 0% saturation at around 3 h (Figure 6.4D). Similarly, the addition of 0.4% v/v *n*-heptane did not delay oxygen limitation, compared to the cultivation with no vector, such that in both cultivations the DO level fell below 5% saturation after approximately 4 h (Figure 6.4D). This is in contrast to the cultivation containing 1% v/v *n*-heptane in which oxygen limitation was postponed by approximately 1 h.

Due to the high specific HA titer observed in the cultivation containing perfluoromethyldecalin, and its lower cost compared to perfluoro-1,3-dimethylcyclohexane, we

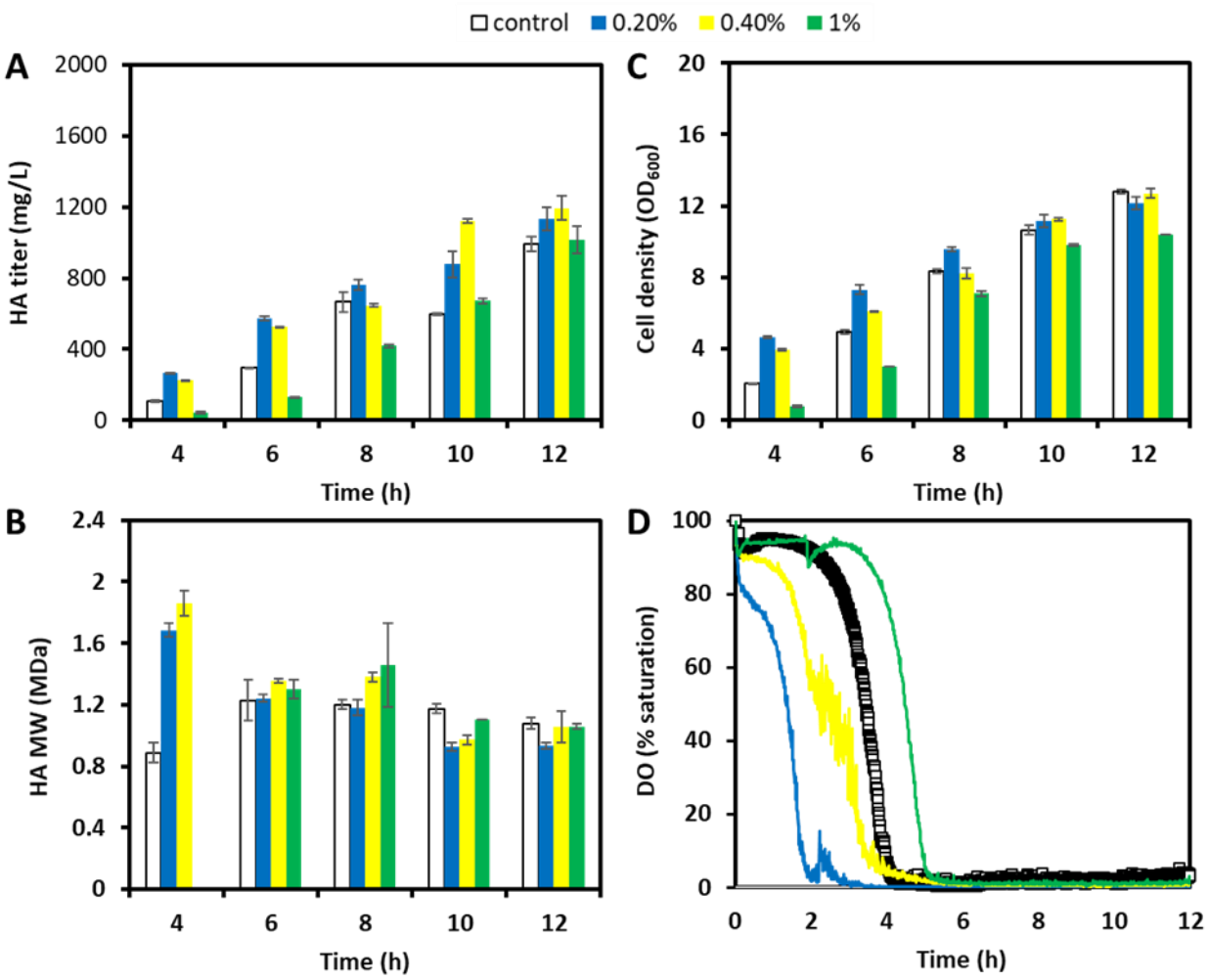

Figure 6.4. Time profiles of A) HA titer, B) HA MW, C) cell density, and D) DO in cultures of AW009 with no vector, or in which *n*-heptane was added 2 h after inoculation at a final concentration of 0.2%, 0.4%, or 1% v/v. SD of duplicate samples shown in Panels A, B, and C.

further evaluated the effect of perfluoromethyldecalin concentration on HA production. Reducing the perfluoromethyldecalin concentration to 0.5% v/v resulted in culture performance similar to the cultivation with no vector (Figure 6.5). Moreover, further increasing the perfluoromethyldecalin concentration to 2% v/v did not significantly improve the culture performance compared to 1% v/v (Figure 6.5). In spite of the delay in reaching oxygen limitation by 2 h upon adding perfluoromethyldecalin to 3% v/v, the final HA titer and cell density were not improved, compared to 2% v/v, and the MW declined potentially due to an increase in viscosity with increasing perfluoromethyldecalin concentration [122].

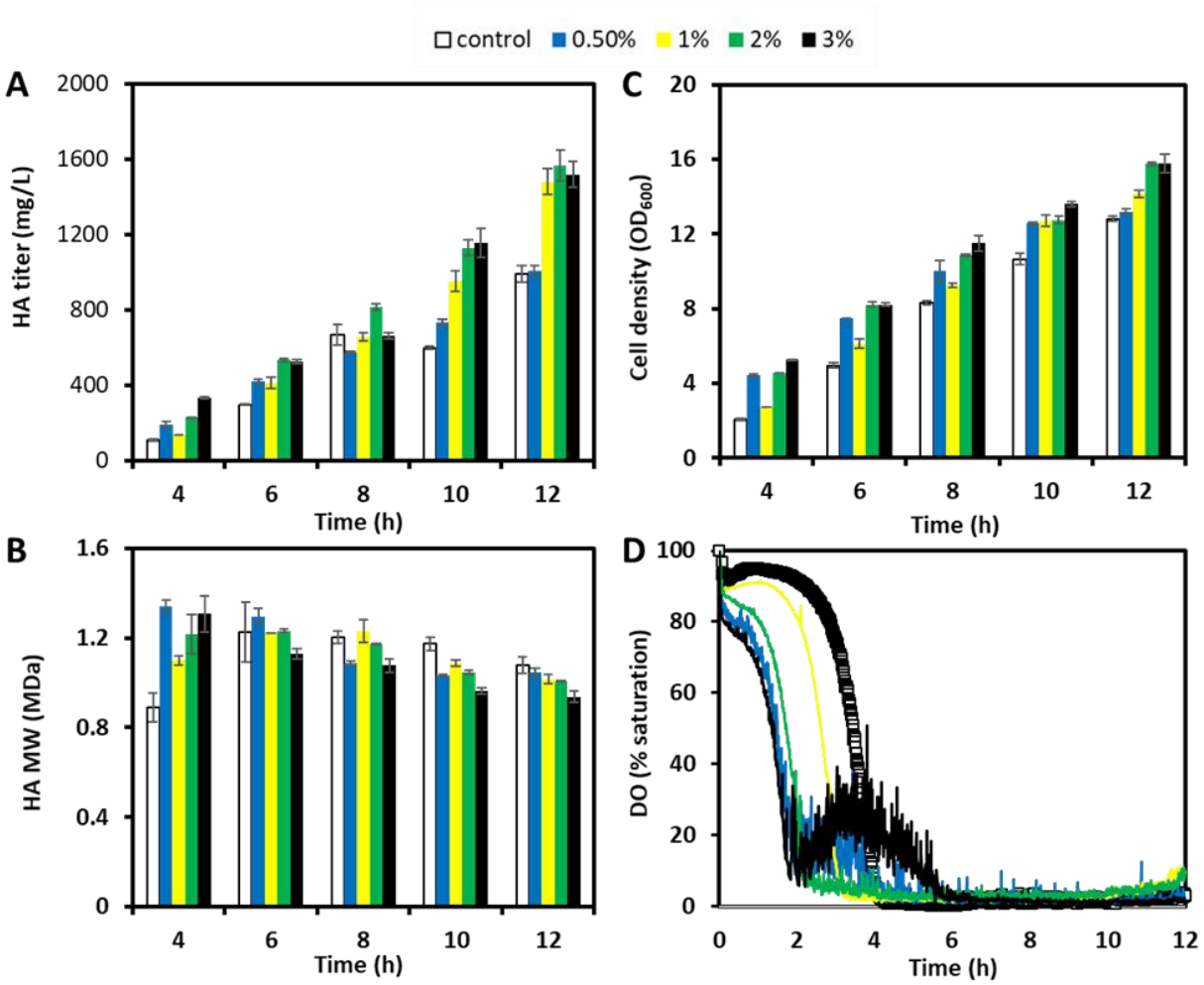

Figure 6.5. Time profiles of A) HA titer, B) HA MW, C) cell density, and D) DO in cultures of AW009 with no vector, or in which perfluoromethyldecalin was added 2 h after inoculation at a final concentration of 0.5%, 1%, 2%, or 3% v/v. SD of duplicate samples shown in Panels A, B, and C.

6.3.3 The effect of oxygen vectors on oxygen mass transfer

In an attempt to understand how oxygen vectors can enhance HA production in *B. subtilis*, we assessed oxygen mass transfer in our cultivation system. The addition of 0.25% v/v *n*-hexadecane resulted in a modest decrease in k_La, although increasing the concentration to 2% v/v had essentially no further effect on k_La (Figure 6.6A). The magnitude and trend of our k_La estimates with increasing

n-hexadecane concentration are consistent with previous work in which k_La decreased modestly for concentrations up to 2.5% v/v during the operation at 288 rpm and 1 vvm air-purging [152]. In contrast to our results, an initial increase in k_La was observed at low *n*-hexadecane concentrations (i.e. < 2.5% v/v), followed by a decline in k_La at higher *n*-hexadecane concentrations until phase inversion occurred (i.e. the culture becomes a continuous phase when the vector concentration is high enough) [278]. However, the latter study employed surface aeration in a STR operated at 1000 rpm such that direct comparison of results is difficult. As was the case for *n*-hexadecane, the addition of *n*-heptane at 0.2% v/v resulted in a modest decrease to k_La, and increasing the concentration to 1% v/v did not appreciably affect k_La (Figure 6.6B). In contrast to our results, the addition of *n*-heptane at 0.1% v/v in a STR operated at 300 rpm and 0.5 vvm resulted in a 15% increase in k_La, and increasing the *n*-heptane concentration to 5% v/v increased k_La by 175% [279]. On the other hand, simultaneously increasing the agitation and aeration rates to 400 rpm and 1 vvm, respectively, resulted in an initial 50% reduction in k_La for *n*-heptane concentrations up to 1% v/v, followed by a gradual increase in k_La with a further increase in the *n*-heptane concentration [279]. Accordingly, the effect of *n*-heptane on k_La in aerated STRs appears to vary considerably with agitation and aeration rates, such that our observation of a slight reduction in k_La was considered reasonable. Finally, *n*-heptane can dramatically increase k_La in bubble column reactors as both vector concentration and superficial gas velocity are increased [280]. In general, non-spreading hydrocarbons (e.g. *n*-hexadecane) negatively or hardly affect k_La [148], although at lower vector concentrations k_La may increase due to the shuttling effect, through which vector droplets briefly contact the air bubble surface and subsequently transfer oxygen to the bulk aqueous phase [139, 279]. Alternatively, spreading hydrocarbons (e.g. *n*-heptane) generally induce an initial decrease in k_La at low concentrations, followed by a gradual increase in k_La with increasing concentration [165, 167, 168, 279]. It was hypothesized that the initial decrease in k_La resulted from increased liquid phase resistance due to the accumulation of surface active contaminants at the gas-water interface, and that the gas bubble size decreased with an increasing vector concentration as the system approached

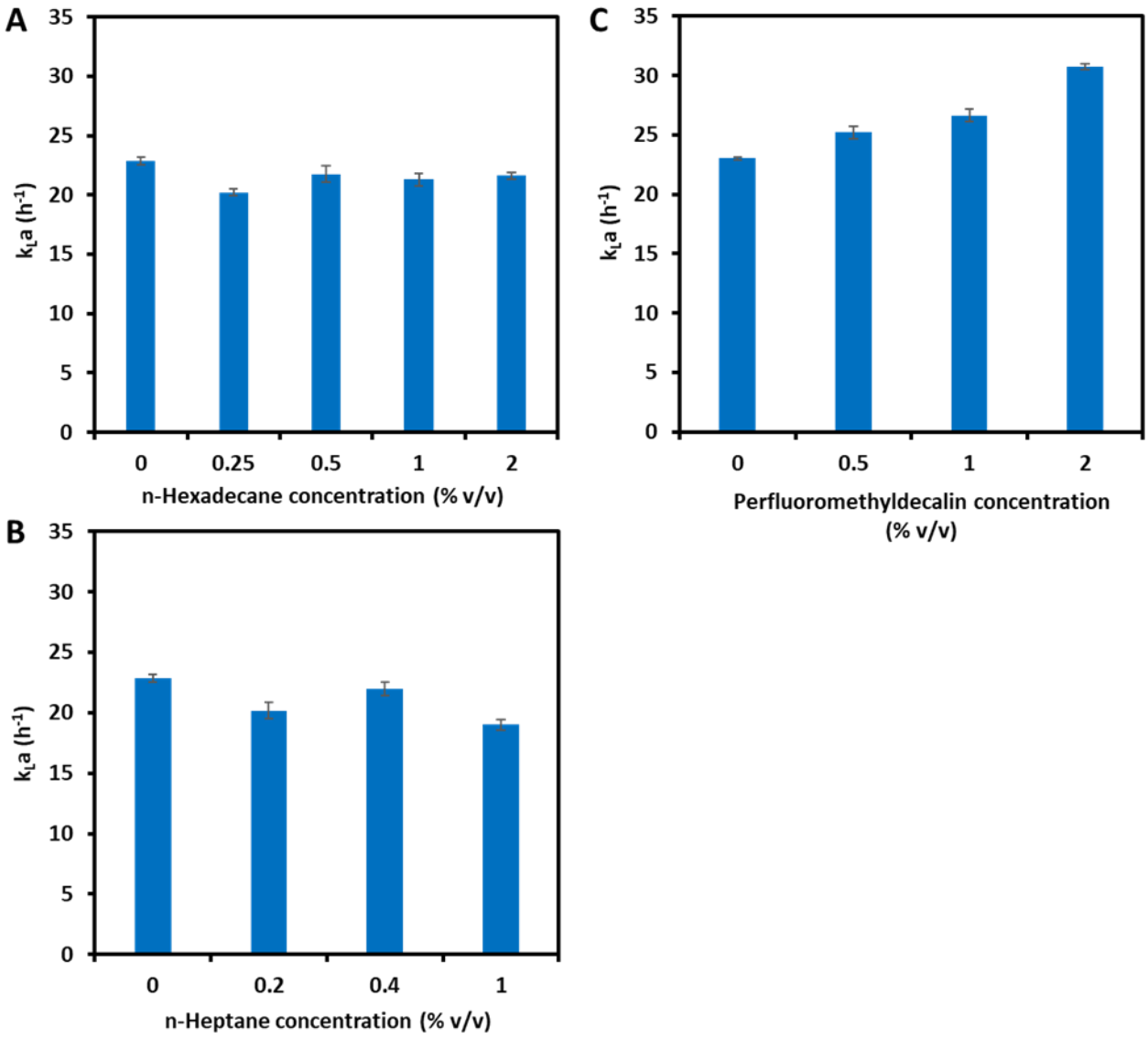

Figure 6.6. k_La determined for different concentrations of A) *n*-hexadecane, B) *n*-heptane, and C) perfluoromethyldecalin. Experimental conditions described in M&M. SD of three experiments shown.

phase inversion [167, 168]. An alternate/complementary explanation is that the vector film forming around air bubbles becomes unstable with increasing thickness as the vector concentration increases, resulting in the release of oxygen-rich droplets into the bulk aqueous phase [279].

While *n*-hexadecane and *n*-heptane slightly reduced k_La, perfluoromethyldecalin had the opposite effect such that k_La increased with increasing concentration up to 2% v/v, resulting in a

maximum increase of 35% in k_La compared to the control with no vector (Figure 6.6C). While k_La measurements for perfluoromethyldecalin are not available in the literature, perfluorodecalin, a structurally similar vector, was observed to increase k_La in a STR at concentrations up to 20% v/v, using the same agitation rate and lower aeration (1.1 vvm) compared to our study, resulting in a maximum increase of ~70% in k_La [281]. Similarly, the addition of perfluorodecalin to 5% v/v provided a slight increase in k_La in a STR operated at 300 rpm and 0.5 vvm air-purging, while increasing the concentration to 10% v/v resulted in a 40% increase in k_La [282]. The addition of forane F66E, an unsaturated perfluorocarbon, to *Aerobacter aerogenes* cultures operated at 400 rpm and 0.21 vvm air-purging, increased k_La for concentrations up to 23% v/v, resulting in a maximum increase of ~250% in k_La [141]. Accordingly, a consensus seems to exist regarding the positive influence of perfluorocarbons on oxygen transfer in biological cultivation systems, and this is in line with our observations.

6.4 Discussion

Simultaneously achieving a high MW and titer in cultivations for HA production is a challenging task. Generally, it requires a high carbon flux through both branches of the HA biosynthetic pathway to ensure a sufficient and balanced monomer supply of UDP-GlcNAc and UDP-GlcUA [245]. Moreover, an adequate supply of oxygen is essential to generate the substantial amount of ATP consumed during HA biosynthesis, and this is particularly challenging due to the rapid increase in culture viscosity with increasing HA titer [5, 140]. To further complicate matters, the functional expression of HAS to maximize HA production is dependent on its specific orientation with certain lipids in the cell membrane [123, 239]. Here we have shown that hydrocarbon and perfluorocarbon oxygen vectors can significantly increase the HA titer in *B. subtilis* cultures. However, certain vectors may reduce the efficacy with which streptococcal Class I HAS can extend the growing HA chain, compromising the MW of the produced HA in *B. subtilis*.

Maintaining the DO above a critical level of ~5% saturation was essential to maximize the HA yield in *S. zooepidemicus* cultivations [225], and this is expected given that three mol ATP are

required to produce one mol HA disaccharide [5]. While evidence exists to suggest that *B. subtilis* is a facultative anaerobe which uses nitrate as an electron acceptor [283, 284], our attempts to grow 1A751 anaerobically were unsuccessful (unpublished data), indicating that this strain may require a more oxygenic condition to achieve optimal growth. In our study, only supplementation of *n*-hexadecane resulted in DO levels that exceeded 5% saturation throughout the cultivation. Nonetheless, supplementation of *n*-hexadecane, *n*-heptane, perfluoro-1,3,-dimethylcyclohexane, and perfluoromethyldecalin resulted in improvements to the HA titer. To gain further insight into the improved culture performance upon the addition of *n*-hexadecane, we analyzed the side metabolite distribution in cultures with no vector or 0.5% v/v *n*-hexadecane. No ethanol or succinate was detected in cultures with or without *n*-hexadecane, and lactate (Figure 6.7A) and acetate (Figure 6.7B) accumulation were not significantly different between cultures as determined by ANOVA (Table S6.1). Conversely, the 2,3-BDO titer was 2-fold higher in cultures with no vector compared to those with *n*-hexadecane, i.e. 5385 mg/L with no vector compared to 2694 mg/L for *n*-hexadecane (Figure 6.7C). Exogenous supplementation of 2,3-BDO at a concentration of 10 g/L significantly reduced the PGA titer in *B. subtilis* cultures [285], such that 2,3-BDO accumulation in cultures with no vector may have negatively affected HA production in our study. Moreover, reduced carbon flux toward 2,3-BDO production due to improved aerobicity may, in part, explain the improved HA titers in cultures containing *n*-hexadecane compared to those with no vector. Interestingly, the HA titer was lower in cultures containing 1% v/v *n*-hexadecane, compared to 1% v/v perfluoro-1,3,-dimethylcyclohexane or perfluoromethyldecalin, in spite of significantly higher DO levels when *n*-hexadecane was present. Manipulation of the *n*-hexadecane concentration led to further increases to the DO level, particularly between 6 and 12 h, although the final HA titer was not significantly higher than that obtained in cultivations containing perfluoro-1,3-dimethylcyclohexane or perfluoromethyldecalin. As a result, we cultivated AW009 under a higher agitation rate of 600 rpm with or without *n*-hexadecane to investigate the individual effects of increased DO levels and *n*-hexadecane addition. The HA titer increased by 245% (3423 mg/L; Figure 6.8A) after 10 h and the peak MW at 6 h increased by 58% (1.94 MDa; Figure 6.8B) upon increasing the agitation rate from

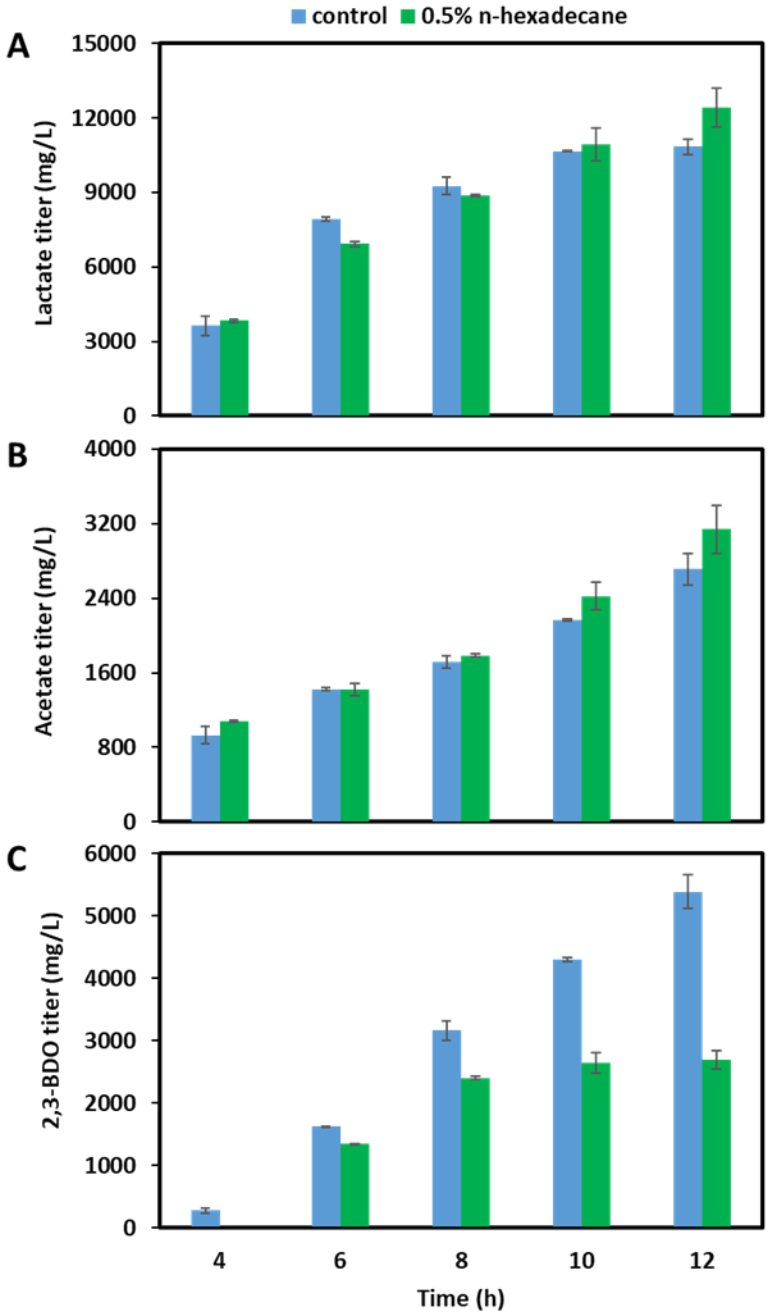

Figure 6.7. Time profiles of A) lactate titer, B) acetate titer, and C) 2,3-BDO titer in cultures of AW009 with no vector, or in which *n*-hexadecane was added 2 h after inoculation at a final concentration of 0.5% v/v. SD of duplicate samples shown in Panels A, B, and C.

300 to 600 rpm with no vector. Cultivation with 0.5% v/v *n*-hexadecane at 600 rpm further increased the HA titer by 30% (4,462 mg/L; Figure 6.8A), although the MW was 12% lower (1.71 MDa; Figure 6.8B), compared to the cultivation at 600 rpm with no vector. As was the case at 300 rpm, the

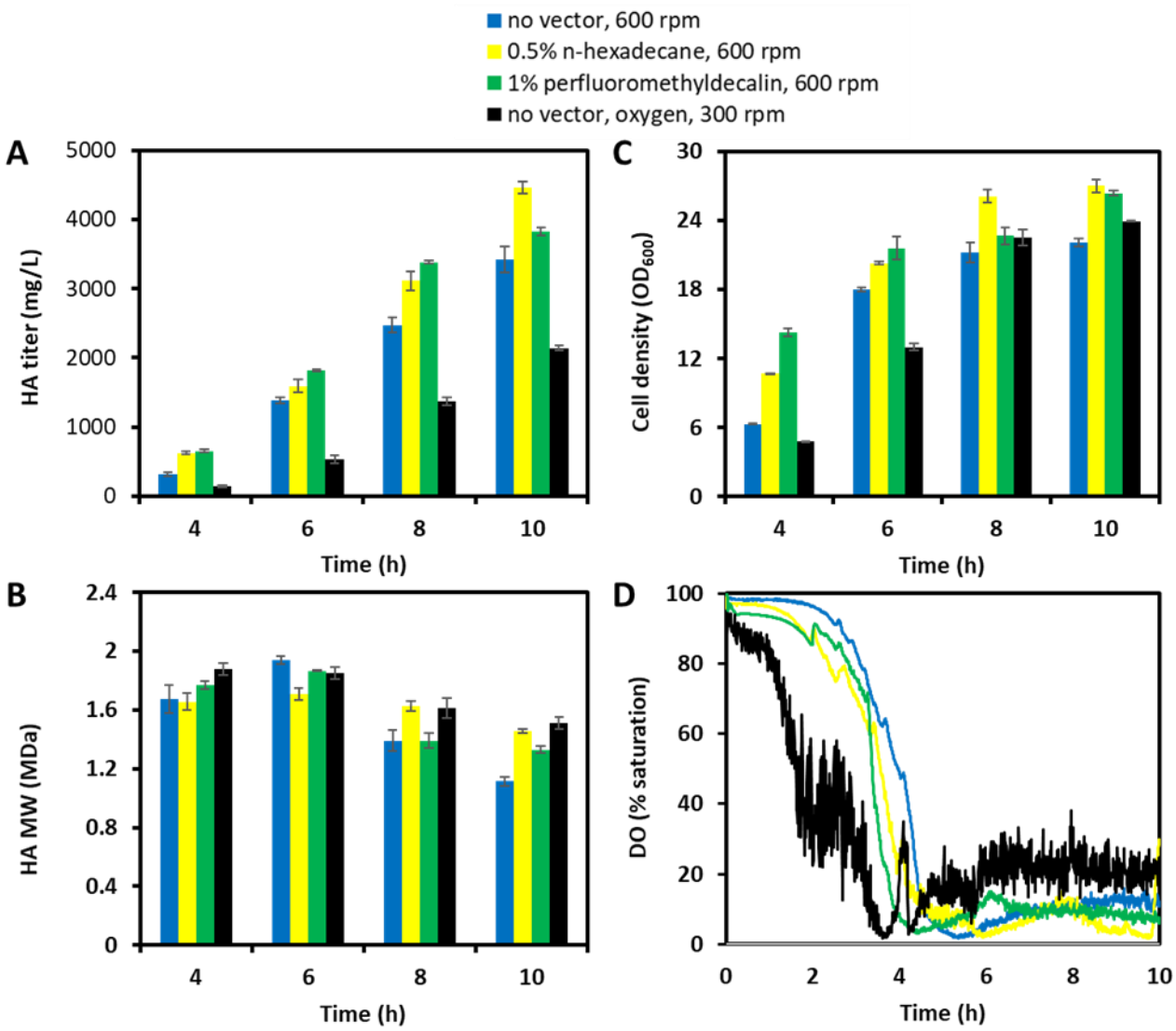

Figure 6.8. Time profiles of A) HA titer, B) HA MW, C) cell density, and D) DO in cultures of AW009. Experimental conditions: no vector and 600 rpm; 0.5% v/v *n*-hexadecane and 600 rpm; 1% v/v perfluoromethyldecalin and 600 rpm; or no vector, 300 rpm, and supplemental oxygen to maintain the DO concentration at 20 ± 5% saturation. Oxygen vectors were added 2 h after inoculation. SD of duplicate samples shown in Panels A, B, and C.

final cell density was improved upon the addition of *n*-hexadecane, i.e. OD_{600} 27 for 0.5% v/v *n*-hexadecane vs. OD_{600} 22.1 for the control with no vector (Figure 6.8C), although the DO profiles were not much different (Figure 6.8D). Moreover, increasing the *n*-hexadecane concentration to 1%

v/v during cultivation at 600 rpm reduced the MW by an additional 30%, compared to 0.5% v/v *n*-hexadecane, although DO levels were markedly increased and the final cell density was slightly higher (data not shown).

While our results show that *n*-hexadecane does not impede cell growth in the concentration range up to 2% v/v, the effects of *n*-hexadecane on HA production may be somewhat polar in nature. Streptococcal HAS is an integral membrane protein for autonomous HA synthesis, which is a process requiring as many as seven different functions for initiation, elongation, and secretion of the HA chain [115]. The relatively small size and few transmembrane domains of streptococcal HAS suggest that they cannot facilitate pore formation for translocation of the growing HA chain [115], and CL or other lipids may assist HAS in creating an internal pore for HA translocation [119, 239]. Moreover, interactions between CL and HA may add to the net retention force that keeps the HA-UDP/HAS complex together during polymerization until a sufficient opposing force exceeds the net retention force, resulting in the release of the growing HA chain [121, 211]. The use of *n*-hexadecane as an oxygen vector resulted in significant increases to the HA titer in this work, and in a prior study in which HA was produced in the native production host *S. zooepidemicus* [152]. Accordingly, the enhanced HA production upon supplementation of *n*-hexadecane may not be associated with the catalytic activities of HAS, but the increased ATP generation resulting from increased oxygen transfer [133]. On the other hand, the lower MW of HA produced in cultures containing *n*-hexadecane suggests premature release of the HA chain. Longer alkanes such as *n*- hexadecane can align parallel to the acyl chains in the lipid bilayer, and, therefore, affect acyl chain packing and tilt, resulting in a reduction in the projected area occupied per lipid molecule and an overall increase in the degree of ordering of the lipid bilayer [286, 287]. In our study, penetration of *n*-hexadecane through the cell membrane may result in the reordering of lipid acyl chains in the lipid bilayer, in turn, altering their interaction with SeHAS. As a result, the HA-binding regions that retain and coordinate translocation of the growing HA chain, and the pore-like structure through which the chain is extruded may be altered, resulting in lower MW HA.

In addition to the reordering of lipids in the bilayer, exposure to organic solvents can alter the fatty acid and lipid composition of the cell membrane. For example, insertion of long chain alcohols (>C5) into a lipid bilayer can increase membrane fluidity [288, 289], and an increase in the abundance of saturated fatty acids has been observed in the cell membrane of *E. coli* upon exposure to C5-C8 alcohols [290]. Conversely, exposure to ethanol resulted in an increase in unsaturated fatty acids, presumably to compensate for a reduction in membrane fluidity in *E. coli* [290]. Moreover, an increase in either saturated or unsaturated fatty acids has been reported for *E. coli* exposed to a number of other organic solvents [291]. In some cases, the shift in cellular fatty acid composition coincided with changes in the ratio of the major lipids PG and phosphatidylethanolamine, while certain solvents caused a dramatic increase in the CL content [291]. Considering that the functional expression of HAS is dependent on its orientation with certain lipids in the cell membrane (i.e. a strong preference for CL has been observed *in vitro*) [121], it is possible that alterations to the lipid content of the cell membrane of AW009 via exposure to various oxygen vectors could modulate the functional expression of SeHAS. Furthermore, the composition of CL acyl chains affected SeHAS activity *in vitro* [122, 123], such that a shift in acyl chain composition of lipids in the cell membrane may also affect the functional expression of SeHAS and, in turn, HA production.

The spreading coefficient (S_{vw}) is an indicator of the spreading characteristics of a given compound, and spreading behavior is anticipated when $S_{vw} > 0$ [141]. While measurements of S_{vw} tend to vary, there is agreement that S_{vw} decreases with increasing size and branching or methylation of the molecule [292-294]. *n*-Heptane is reportedly a spreading vector [278, 292], while *n*-hexadecane may be a spreading [278] or non-spreading [293] vector. Given the significant molecular size difference between the two vectors, *n*-heptane is more prone to spreading than *n*-hexadecane, such that oxygen transfer was more likely to improve upon the addition of *n*-hexadecane at the low concentrations employed in our study. However, our estimates of k_La suggest that the specific rate of oxygen transfer was nearly identical at the respective optimal concentration of each vector, i.e. 21.8 h^{-1} for 0.5% v/v *n*-hexadecane (Figure 6.6A) vs. 22 h^{-1} for 0.4% v/v *n*-heptane (Figure 6.6B), both of which are slightly lower than k_La with no vector (22.9 h^{-1}; Figure 6.6). The reduced k_La in the

presence of *n*-hexadecane could be due to an increased time needed to reach oxygen saturation in the bulk liquid, and this was observed during the application of silicone rubber, a compound with a high affinity for oxygen, as a solid oxygen vector [145]. In any case, the specific rate of oxygen transfer is not the sole determinant of culture performance for HA production, given that the HA titers and cell densities were higher in cultures containing the optimal concentration of *n*-hexadecane, compared to perfluoromethyldecalin, at both 300 rpm and 600 rpm. Furthermore, the relative affinities for oxygen between vectors do not correspond to culture performance, as the respective oxygen solubilities of *n*-heptane and perfluoromethyldecalin are ~80% and 100% higher than *n*-hexadecane [268, 274]. Consequently, alternate factors specific to cell physiology may contribute to the net effects of oxygen vectors on culture performance, and this is underlined by the observation that adding *n*-hexadecane to cultures in different growth phases, i.e. stationary at 0 h and exponential at 2 h, has a dramatic effect on culture performance (Figure 6.2). As previously mentioned, longer alkanes such as *n*-hexadecane can align parallel to the acyl chains in the lipid bilayer, affecting acyl chain packing and tilt for an overall increase in the ordering of the lipid bilayer [286, 287]. On the other hand, the interactions between smaller alkanes (e.g. *n*-heptane) and acyl chains disturb the interactions between acyl chains and, in turn, reduce the ordering of the lipid bilayer [286]. The net effect on the structure of the lipid bilayer of AW009 may partially explain the difference in culture performance, which seems to be largely dependent on cell growth, based on the highly similar specific HA titers of 91.7 mg/(L·OD_{600}) and 93.9 mg/(L·OD_{600}) obtained in cultivations containing optimal concentrations of *n*-hexadecane and *n*-heptane, respectively. In the case of perfluorocarbons, membrane uptake of them is slow compared to hydrocarbons due to their relatively high lipophobicity [295], such that partitioning of perfluoromethyldecalin into the lipid bilayer may be less extensive compared to hydrocarbon vectors. Accordingly, increased oxygen transfer may be the most significant factor enhancing culture performance with the presence of perfluoromethyldecalin and perfluoro-1,3-dimethylcyclohexane.

Evidence suggests that excessive shear stress due to high agitation rates can be detrimental to the MW of HA produced in *S. zooepidemicus* cultures [136, 152, 256]. The MW increased from 1.69 MDa to 2.01 MDa as the agitation rate increased from 150 rpm to 450 rpm, while at 700 rpm the

MW declined to 1.84 MDa [136]. However, the DO was not held constant during respective experiments at different agitation rates, and it was hypothesized that the lower OTR at 150 rpm negatively affected the MW [136]. Similarly, we observed a 58% increase in the MW of HA produced by AW009 as the agitation rate increased from 300 rpm to 600 rpm. To distinguish between the effects of shear stress and enhanced oxygen transfer, AW009 was cultivated at 300 rpm with supplemental oxygen to maintain the DO concentration at 20 ± 5% saturation (with no vector) to ensure operation above the critical DO level. The peak MW was within 3% (1.88 MDa; Figure 6.8B) and the final cell density was 9% higher (OD_{600} 24; Figure 6.8C), although the titer was 37% lower (2141 mg/L; Figure 6.8A) compared to the cultivation at 600 rpm with no vector. Based on these observations, it appears that a higher shear rate is not detrimental to the MW of HA produced by *B. subtilis* in batch cultivations operated up to 600 rpm and, in fact, may be beneficial in maximizing the HA titer. Maximum growth rates corresponding to optimal agitation rates have been observed in cultures of various microorganisms [296, 297], although the maximum growth rate also corresponded to a maximum OUR in *Brevibacterium flavum* [297]. In our study, oxygen uptake is not limiting in cultivations operated at 300 rpm with supplemental oxygen, suggesting that either a higher shear rate improved flux through the HA biosynthetic pathway, or excess DO levels were detrimental to the functional expression of SeHAS or carbon flux for HA production. An increase in the specific growth rate, cell density, and expression of certain extracellular enzymes was observed with increasing shear rates in *B. subtilis* cultures [298], indicating that a higher agitation rate could contribute to the higher growth rate and increased HA synthesis observed during operation at 600 rpm with no vector. On the other hand, excess DO can reduce the yields of certain recombinant proteins via oxidation of Met and Cys residues [257], resulting in misfolding, loss of activity, and protease degradation [258, 259]. Throughout much of the cultivation in our study, pure oxygen was needed to maintain the desired DO level. However, the peak MW of HA did not decrease when operating at 300 rpm with supplemental oxygen. While the functional expression of SeHAS could still be affected by pure oxygen feeding, the control of chain length and polymerizing activity are independent functions of SeHAS that are not coupled to one another [211]. Accordingly, further

investigation is required to elucidate the effects of shear stress and DO levels in cultivations of HA-producing *B. subtilis.* In addition, our results suggest that operating at agitation rates in excess of 300 rpm can enhance the MW and HA titer, and that oxygen vectors can further enhance culture performance under these conditions.

Few reports exist on the application of oxygen vectors to microbial HA production or biopolymer production in *B. subtilis.* The application of 0.5% v/v *n*-hexadecane to cultivations of *S. zooepidemicus* for HA production resulted in a similar increase to the HA titer as observed in our work [152]. However, the highest reported MW of 15.4 MDa in the cited study is far in excess of any reported MWs to date, such that comparison of MW data may be not be reasonable. *n*-Dodecane has also been applied to cultivations of *S. zooepidemicus* for enhanced HA production [262]. The addition of 5% v/v *n*-dodecane resulted in a 25% increase in the HA titer, although the maximum increase in MW of 46% was obtained at a concentration of 3% v/v *n*-dodecane, with the peak MW reaching 1.9 MDa [262]. Perfluorodecalin has also been used to enhance HA production in cultures of *S. zooepidemicus*, although the MW was not assessed [140]. The addition of perfluorodecalin to 3% v/v resulted in a 32% improvement to the HA titer, compared to a three phase agitation strategy in which the agitation speed was increased from 200 rpm to 600 rpm, and a further increase in the perfluorodecalin concentration reduced DO levels presumably due to an increase in culture viscosity [140]. While the application of oxygen vectors to cultivations of *S. zooepidemicus* result in relative increases in the HA titer similar to our cultivations with *B. subtilis*, the improvements to the MW suggest that the functional expression of native HAS may be less sensitive to perturbations that may affect cell membrane ordering and fluidity. *n*-Heptane and *n*-hexadecane have also been applied as oxygen vectors to PGA production in cultures of *B. subtilis* [153], resulting in respective increases in the titer of 25% and 20%, as well as respective increases in the MWs of 25% and 20%. PgsB and PgsC, which are the capsular PGA synthetase and capsular PGA amide ligase/translocase subunit, respectively, polymerize PGA, which is presumably translocated out of the cell by CapA and PgsE (whose respective functions have not been formally elucidated) with assistance from PgsC [299]. Accordingly, at least four proteins are involved in the synthesis and translocation of PGA in *B.*

subtilis, and this is in contrast to HA production for which a single enzyme (i.e. HAS) is responsible [115]. Due to the autonomous functionality of SeHAS, which is dependent on its orientation with lipids in the cell membrane [119, 239], reordering or alteration of lipids in the cell membrane may have a more pronounced impact on the functional expression of SeHAS, but not the elaborate PGA-producing enzyme complex. This potentially results in markedly different effects on the MW of different biopolymers.

Chapter 7

Metabolic engineering of *B. subtilis* for L-valine overproduction

7.1 Introduction

As one of the three branched-chain amino acids (BCAAs), L-valine is an essential nutrient for humans and animals, and is used in infusion solutions and human dietary supplements [300], commercial feed in the swine and poultry industries [301], and as a precursor for herbicide and antibiotic synthesis [301]. The extraction of L-valine, and most other amino acids, from protein hydrolysate has been replaced by microbial production and/or enzymatic synthesis [302]. To date, *E. coli* [303-305] and *C. glutamicum* [306-310] have been extensively engineered for microbial L-valine overproduction. *E. coli* is an endotoxin-producing bacterium [2] and, thus, is not an ideal production host for use in the pharmaceutical and food industries. On the other hand, *C. glutamicum* has been granted GRAS status and has been used for the large-scale production of a selection of amino acids [311]. However, genetic manipulation of *C. glutamicum* remains cumbersome due to the absence of an efficient recombination system [312], and engineered strains typically contain replicating plasmids that require antibiotic selection and may be unstable in the host cell. While *C. glutamicum* is currently the preferred workhorse for industrial amino acid production, other microorganisms may be promising candidates in this arena. *B. subtilis* is a genetically tractable model Gram-positive bacterium, grows rapidly in simple medium, has been granted GRAS status [1], and, therefore, can be an ideal host for L-valine production. Moreover, a comprehensive CRISPR-Cas9 toolkit was recently developed for *B. subtilis*, enabling efficient multiplexing of gene mutations and transcriptional repression [263], such that scalable strain construction can now be achieved in this organism. *B. subtilis*

serves as a biomanufacturing platform for the commercial production of enzymes [2], HA [105], and surfactants [313], and is capable of high-level isobutanol production [314], with which the L-valine biosynthetic pathway shares the common precursor 2-ketoisovalerate.

Like many important biomolecules, BCAAs are derived from pyruvate and their biosynthesis is controlled at the transcriptional level through a complex regulatory cascade in *B. subtilis*. Pyruvate is first converted to 2-acetolactate by an acetohydroxy-acid synthase (AHAS) composed of regulatory (i.e. IlvH, encoded by *ilvH*) and catalytic (i.e. IlvB, encoded by *ilvB*) subunits, or by acetolactate synthase (ALS) encoded by *alsS* (AlsS), as an intermediate of L-valine biosynthesis (Figure 7.1). In parallel, IlvBH can convert 2-ketobutyrate (derived from L-threonine) and pyruvate to 2-aceto-2-hydroxybutyrate as an intermediate of L-isoleucine biosynthesis (Figure 7.1). On the other hand, AlsS appears to be a dedicated ALS as it presumably cannot facilitate L-isoleucine synthesis [315], which is a common characteristic of several such bacterial enzymes that convert pyruvate to 2-acetolactate as a precursor to acetoin production [315, 316]. 2-acetolactate and 2-aceto-2-hydroxybutyrate are respectively converted to 2,3-dihydroxyisovalerate and 2,3-dihydroxy-3-methylpentanoate by acetohydroxy-acid isomeroreductase (i.e. IlvC, encoded by *ilvC*), followed by their conversion to 2-ketoisovalerate and 3-methyl-2-oxopentanoate, respectively, by dihydroxy-acid dehydratase (i.e. IlvD, encoded by *ilvD*) (Note that 2-ketoisovalerate is also an intermediate of L-leucine and pantothenate synthesis.). Finally, 2-ketoisovalerate and 3-methyl-2-oxopentanoate are converted to L-valine and L-isoleucine, respectively, by one of two BCAA aminotransferases, i.e. YbgE (encoded by *ybgE*) and YwaA (encoded by *ywaA*), either of which can also convert 4-methyl-2-oxopentanoate to L-leucine (Figure 7.1).

The genes comprising the biosynthetic pathways of BCAAs are organized into five

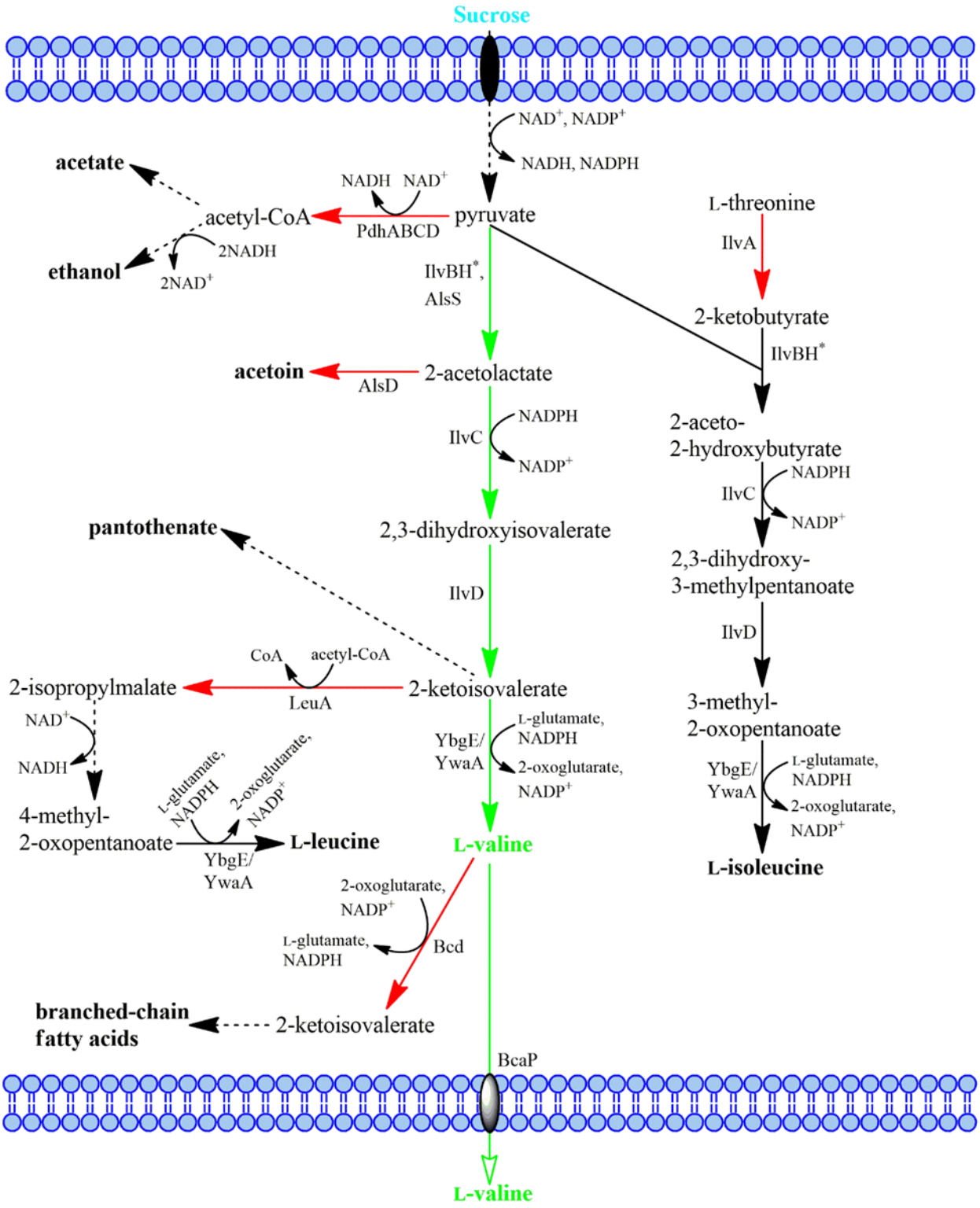

Figure 7.1. The L-valine biosynthetic pathway in B. subtilis. Green arrows represent reactions catalyzed by enzymes whose expression was upregulated, and red arrows represent reactions catalyzed by enzymes that were inactivated. AlsS, acetolactate synthase; BcaP, BCAA permease; Bcd, BCAA dehydrogenase; IlvA, L-threonine dehydratase; IlvB, acetohydroxy-acid synthase

catalytic subunit; IlvC, acetohydroxy-acid isomeroreductase; IlvD, dihydroxy-acid dehydratase; IlvH*, engineered acetohydroxy-acid synthase regulatory subunit; LeuA, 2-isopropylmalate synthase; PdhABCD, pyruvate dehydrogenase complex; YbgE, BCAA aminotransferase; YwaA; BCAA aminotransferase.

operons: 1) *ilvBHC-leuABCD* (*leuABCD* encodes 2-isopropylmalate synthase, 3-isopropylmalate dehydrogenase, and 2-isopropylmalate dehydratase large and small subunits, respectively); 2) *ilvA* (encoding L-threonine dehydratase); 3) *ilvD*; 4) *ybgE*; and 5) *ywaA* [317]. Operons 1-5 are repressed under amino acid-rich conditions by the activity of the transcriptional regulator CodY in *B. subtilis* [318-320], and L-valine and L-isoleucine are positive effectors of CodY such that BCAA biosynthesis is negatively autoregulated at relatively low BCAA concentrations [319]. Specifically, expression of the *ilvBHC-leuABCD* (*ilv-leu*) operon is repressed through the interaction of CodY with two high-affinity (i.e. CodY-I and CodY-II) and two low-affinity (i.e. CodY-III and CodY-IV) binding sites, while the CodY binding sites regulating the expression of *ilvA, ilvD, ybgE,* and *ywaA* have not been formally elucidated [318]. CodY-I, CodY-II, CodY-III, and CodY-IV are located at base pairs (bp) -42/-32, -84/-52, -154/-107, and -168/-185, respectively, relative to the transcriptional start site of promoter $P_{ilv\text{-}leu}$ [321, 322]. CodY-II partially overlaps a CRE (located at bp -96/-82) that, in combination with an upstream CRE site (located at bp -128/-110) that overlaps CodY-III, can facilitate catabolite activation of $P_{ilv\text{-}leu}$ by the transcriptional regulator carbon catabolite protein A (CcpA) complexed with P-Ser-histidine-containing phosphocarrier (HPr) protein [321]. CodY outcompetes the CcpA-P-Ser-HPr complex under amino acid-rich conditions, nearly abolishing catabolite activation of $P_{ilv\text{-}leu}$. Moreover, catabolite activation of $P_{ilv\text{-}leu}$ by the CcpA-P-Ser-HPr complex is also negatively regulated by the nitrogen sensing transcriptional regulator TnrA, which binds to the TnrA box located at bp -209/-193, presumably inducing DNA bending to enable interaction between TnrA

and the CcpA-P-Ser-HPr complex [321, 323]. Finally, a T-box located at bp +115/+361 serves as a transcription termination signal unless it is bound by uncharged $tRNA^{Leu}$, providing additional transcriptional regulation of the *ilv-leu* operon in the presence of excess L-leucine [324]. The *alsSD* operon is expressed during anaerobic fermentative growth, or under aerobic conditions as cells enter the stationary phase or during exponential growth under high glucose concentrations [315, 325]. The transcriptional regulator AlsR, encoded by *alsR*, activates transcription of *alsSD* from promoter P_{als} in response to the accumulation of its presumed inducer, acetate, via binding of AlsR tetramers to the regulatory and activator binding sites located at bp -78/-58 and -41/-26, respectively, relative to the transcriptional start site of P_{als}, and *alsR* is transcribed divergently from *alsSD* from the promoter adjacent to P_{als}, i.e. P_{alsR} [325]. In addition, the transcriptional repressor Rex may repress transcription from P_{als} in response to low NADH levels via a putative Rex binding site that has not been formally identified [326].

Once L-valine has been synthesized in *B. subtilis*, it can be utilized for protein synthesis, secreted from the cell, or converted back to 2-ketoisovalerate as an intermediate in the synthesis of branched-chain fatty acids, the major acyl constituents of the cell membrane [327]. The contribution of permeases BcaP, BraB, and BrnQ to BCAA uptake have been investigated, and BcaP, encoded by *bcaP*, appears to be the most efficient permease for the uptake of L-valine and L-isoleucine [328], such that it may be the most effective transporter of excess L-valine out of *B. subtilis*. The expression of *bcaP* is strongly repressed by CodY in amino acid-rich medium via binding sites CodY-I, located at bp -61/-31, and CodY-II, located at bp +65/+93, relative to the transcriptional start site of P_{bcaP} [329]. The conversion of L-valine to 2-ketoisovalerate as the first step of the L-valine degradation pathway is potentially catalyzed by YbgE, YwaA, or Bcd (i.e. BCAA dehydrogenase, encoded by *bcd*). Relatively small decreases in CodY activity can

significantly increase the expression of *bcd* and *ywaA*, compared to the expression of *ybgE*, which occurs when CodY is almost completely inactive [320]. Speculation has been made that the coexpression of YwaA and Bcd when CodY is largely active may indicate that both enzymes primarily convert BCAAs to their corresponding branched-chain keto acids (BCKAs), while YbgE converts BCKAs to BCAAs upon nutrient limitation [320]. However, the mutation of *bcd* completely abolished the growth of *B. subtilis* when L-valine and L-isoleucine were supplied as the sole nitrogen source [327], suggesting that YwaA does not naturally play a role in BCAA catabolism.

While *B. subtilis* has been employed extensively in biomanufacturing as previously outlined, it is not commonly used as a host for amino acid production. In this study, we engineered the metabolism of *B. subtilis* for L-valine overproduction using our recently developed CRISPR-Cas9 toolkit [263]. The L-valine titer was increased by >14-fold, compared to the wild-type strain, by replacing the $P_{ilv\text{-}leu}$ promoter and its regulatory elements, engineering IlvH to reduce L-valine feedback inhibition, chromosomally overexpressing *ilvD*, *ybgE*, and *ywaA*, and mutating *bcd*. Further investigation revealed that pyruvate availability was severely limiting L-valine overproduction in our engineered strains, which was overcome by mutating *pdhA*, encoding the E1α subunit (PdhA) of the pyruvate dehydrogenase complex (PdhABCD), resulting in a significant increase in the L-valine titer. Moreover, inactivation of the L-leucine and L-isoleucine biosynthetic pathways via mutation of *leuA* and *ilvA*, respectively, in the Δ*pdhA* background further improved L-valine overproduction, resulting in a titer of 4.61 g/L after 24 h in shake flask cultures. Interestingly, the L-valine titer reached 3.6 g/L after 24 h in shake flask cultures of a Δ*pdhA* Δ*leuA* Δ*ilvA* mutant expressing native *ilvH*, indicating that L-valine feedback inhibition of IlvBH is minimal in *B. subtilis*.

7.2 Materials and Methods

7.2.1 Bacterial strains, primers, and plasmids

The *B. subtilis* strains used in this study are listed in Table S7.1. *E. coli* HI-Control™ 10G chemically competent cells were prepared as electrocompetent cells as described previously [187] and used as host for plasmid construction. *B. subtilis* and *E. coli* strains were maintained as glycerol stocks at -80 °C. Primers (Table S7.1) were synthesized by Integrated DNA Technologies. Plasmid pAX01 (ECE137) was obtained from the Bacillus Genetic Stock Center, and pgRNA-bacteria was a gift from Stanley Qi (Addgene plasmid # 44251).

7.2.2 Plasmid and editing template construction

DNA manipulation was performed using standard cloning techniques [187], and DNA sequencing was conducted by The Centre for Applied Genomics. To construct a genomic integration vector for the xylose-inducible expression of *comK* and *comS* from the *bpr* locus, $P_{xylA,\ Bm}$ was amplified from pAX01 [330] with primers P7.1/P7.2, *comK* was amplified from 1A751 gDNA with primers P7.3/P7.4, and the two fragments were spliced. The *bpr* 5'-homology length (HL) was then amplified from 1A751 gDNA with primers P7.5/P7.6, and was spliced with the $P_{xylA,\ Bm}$::*comK* cassette, and the resulting *bpr* HL-5'- $P_{xylA,\ Bm}$::*comK* cassette was inserted into SbfI/NheI-digested pAW004-2 [263]. To complete the vector, the *bpr* HL-3' was amplified with primers P7.7/P7.8 from 1A751 gDNA and inserted in place of the *thrC* HL-3', yielding pAW001-5. *comS* was subsequently amplified from 1A751 gDNA with primers P7.9/P7.10 and inserted into NheI/NotI-digested pAW001-5, resulting in plasmid pAW002-5.

To construct a triple gRNA delivery vector for the simultaneous replacement of promoter $P_{ilv\text{-}leu}$, and mutation of *bcd* and *leuA*, the P_{grac}::*ilvBHC*-gRNA cassette was first amplified from

pgRNA-bacteria [23] with primers P7.11/P7.12, and inserted into SphI/NcoI-digested pAW014-2 [263], resulting in plasmid pAW003-5. The $P_{xylA.SphI+1}$ cassette was subsequently amplified from pAW014-2 with primers P7.13/P7.14 (NheI/--), the *bcd*-gRNA.P585T cassette was amplified from pgRNA-bacteria with primers P7.15/P7.16 (--/BamHI), and the two fragments were spliced. The resulting $P_{xylA.SphI+1}$::*bcd*-gRNA.P585T cassette was inserted into NheI/BglII-digested pAW003-5, yielding the dual gRNA delivery vector pAW004-5. Finally, the $P_{xylA.SphI+1}$ cassette was amplified from pAW014-2 with primers P7.13/P7.17 (NheI/--), the *leuA*-gRNA.P764NT cassette was amplified from pgRNA-bacteria with primers P7.18/P7.16 (--/BamHI), and the two fragments were spliced. The resulting $P_{xylA.SphI+1}$::*leuA*-gRNA.P764NT cassette was inserted into NheI/BglII-digested pAW004-5, yielding plasmid pAW005-5. To construct a dual gRNA delivery vector for the simultaneous insertion of P_{grac}::*ybgE*:*ywaA* and P_{grac}::*ilvD* cassettes at the *amyE* and *wprA* loci, respectively, *amyE*-gRNA.P636T was amplified from pgRNA-bacteria with primers P7.19/P7.12 and inserted into SphI/NcoI-digested pAW014-2, resulting in plasmid pAW006-5. The $P_{xylA.SphI+1}$ cassette was subsequently amplified from pAW014-2 with primers P7.13/P7.20 (NheI/--), the *wprA*-gRNA.P1419T cassette was amplified from pgRNA-bacteria with primers P7.21/P7.16 (--/BamHI), and the two fragments were spliced. The resulting $P_{xylA.SphI+1}$::*wprA*-gRNA.P1419T cassette was inserted into NheI/BglII-digested pAW006-5, yielding plasmid pAW007-5. To construct a dual gRNA delivery vector for the simultaneous mutation of *ilvB* and replacement of P_{als}, the $P_{xylA.SphI+1}$ cassette was amplified from pAW014-2 with primers P7.13/P7.22 (NheI/--), the $P_{grac.UPmod}$::*als*-gRNA cassette was amplified from pgRNA-bacteria with primers P7.23/P7.12 (--/NcoI), and the two fragments were spliced. The resulting $P_{xylA.SphI+1}$::$P_{grac.UPmod}$::*als*-gRNA cassette was inserted into NheI/NcoI-digested pAW014-2, yielding plasmid pAW008-5. The $P_{xylA.SphI+1}$ cassette was subsequently

amplified from pAW014-2 with primers P7.13/P7.24 (NheI/--), the *ilvB*-gRNA.P1101NT cassette was amplified from pgRNA-bacteria with primers P7.25/P7.16 (--/BamHI), and the two fragments were spliced. The resulting $P_{xylA.SphI+1}$::*ilvB*-gRNA.P1101NT cassette was inserted into NheI/BglII-digested pAW008-5, yielding plasmid pAW009-5. To construct a dual gRNA delivery vector for simultaneous mutation of *leuA* and *ilvA*, the $P_{xylA.SphI+1}$ cassette was amplified from pAW014-2 with primers P7.13/P7.26 (NheI/--), the *ilvA*-gRNA.P581NT cassette was amplified from pgRNA-bacteria with primers P7.27/P7.16 (--/BamHI), and the two fragments were spliced. The resulting $P_{xylA.SphI+1}$::*ilvA*-gRNA.P581NT cassette was inserted into NheI/BglII-digested pAW005-5, yielding plasmid pAW010-5. To construct a dual gRNA delivery vector for the simultaneous replacement of promoter P_{bcaP} and mutation of *sigF*, the $P_{xylA.SphI+1}$ cassette was amplified from pAW014-2 with primers P7.13/P7.28 (NheI/--), the $P_{grac.UPmod}$::*bcaP*-gRNA cassette was amplified from pgRNA-bacteria with primers P7.29/P7.12 (--/NcoI), and the two fragments were spliced. The resulting $P_{xylA.SphI+1}$::$P_{grac.UPmod}$::*bcaP*-gRNA cassette was inserted into NheI/NcoI-digested pAW014-2, yielding plasmid pAW011-5. The $P_{xylA.SphI+1}$ cassette was subsequently amplified from pAW014-2 with primers P7.13/P7.30 (NheI/--), the *sigF*-gRNA.P371T cassette was amplified from pgRNA-bacteria with primers P7.31/P7.16 (--/BamHI), and the two fragments were spliced. The resulting $P_{xylA.SphI+1}$::*sigF*-gRNA.P371T cassette was inserted into NheI/BglII-digested pAW011-5, yielding plasmid pAW012-5. To construct the single gRNA delivery vector pAW013-5, the *ilvH*-gRNA.P40T cassette was amplified from pgRNA-bacteria with primers P7.32/P7.12 and inserted into SphI/NcoI-digested pAW014-2. Similarly, the $P_{xylA.SphI+1}$ cassette was amplified from pAW014-2 with primers P7.13/P7.33 (NheI/--), the *alsD*-gRNA.P99T cassette was amplified from pgRNA-bacteria with primers P7.34/P7.12 (--/NcoI), and the two fragments were spliced. The resulting

$P_{xylA.SphI+1}$::*alsD*-gRNA.P99T cassette was inserted into NheI/NcoI-digested pAW014-2, yielding plasmid pAW014-5. Plasmids pAW015-5 and pAW016-5 were constructed in the same manner as pAW014-5, except that primers P7.35 and P7.36, and P7.30 and P7.31 were used in place of primers P7.33 and P7.34 to generate the respective $P_{xylA.SphI+1}$::*pdhA*-gRNA.P116T and $P_{xylA.SphI+1}$::*sigF*-gRNA.P371T cassettes.

The P_{grac}::*ilvBHC* editing template for replacement of $P_{ilv\text{-}leu}$ with promoter P_{grac}, i.e. plasmid pAW017-5, was constructed by amplifying the 808 bp and 765 bp HLs from 1A751 gDNA with respective primers P7.37/P7.38 and P7.39/P7.40, promoter P_{grac} (with an upstream SphI restriction site) from pAW008 [263] with primers P7.41/P7.42, and the plasmid backbone from pAW020-2 [263] with primers P7.43/P7.44, followed by assembly of the four fragments via the NEBuilder® HiFi DNA Assembly Master Mix (New England Biolabs; MA) as per the manufacturer's instructions. The mut.*bcd*.P585T editing template for mutation of *bcd*, i.e. plasmid pAW018-5, was constructed by amplifying the 782 bp and 764 bp HLs (flanking an in-frame BssHII restriction site followed by two stop codons) from 1A751 gDNA with respective primers P7.45/P7.46 and P7.47/P7.48, and the plasmid backbone from pAW020-2 with primers P7.49/P7.50, followed by assembly of the three fragments. The mut.*leuA*.P764NT editing template for mutation of *leuA*, i.e. plasmid pAW019-5, was constructed by amplifying the 762 bp and 739 bp HLs (flanking an in-frame BssHII restriction site followed by two stop codons) from 1A751 gDNA with respective primers P7.51/P7.52 and P7.53/P7.54, and the plasmid backbone from pAW020-2 with primers P7.55/P7.56, followed by assembly of the three fragments. The P_{grac}::*ybgE*:*ywaA* Δ*amyE* editing template for insertion of the P_{grac}::*ybgE*:*ywaA* expression cassette at the *amyE* locus, i.e. plasmid pAW020-5, was constructed by amplifying the combined *amyE* HL-5'-backbone-*amyE* HL-3'-P_{grac} fragment from pAW020-2 with primers P7.57/P7.58,

ybgE and *ywaA* from 1A751 gDNA with respective primers P7.59/P7.60 and P7.61/P7.62, followed by assembly of the three fragments. The P_{grac}::*ilvD* Δ*wprA* editing template for insertion of the P_{grac}::*ilvD* expression cassette at the *wprA* locus, i.e. plasmid pAW021-5, was constructed by amplifying the *wprA* HL-5' and HL-3' from 1A751 gDNA with respective primers P7.63/P7.64 and P7.65/P7.66, P_{grac} from pAW008 with primers P7.67/P7.68, *ilvD* from 1A751 gDNA with primers P7.69/P7.70, and the plasmid backbone from pAW020-2 with primers P7.71/P7.72, followed by assembly of the five fragments. The IlvH(N11A,G14D,N17F,N29H) editing template for engineering of IlvH to relieve L-valine feedback inhibition, i.e. plasmid pAW022-5, was constructed by amplifying the 808 bp and 774 bp HLs from 1A751 gDNA with respective primers P7.73/P7.74 and P7.75/P7.76, followed by splicing of the two fragments and subsequent insertion into pJET1.2/blunt using the CloneJET PCR Cloning Kit (ThermoFisher Scientific; MA) as per the manufacturer's instructions. The specified point mutations were introduced using primers P7.74 and P7.75, and a BssHII restriction site was introduced into the *ilvH* ORF as a result of the N11A mutation. The $P_{grac.UPmod}$::*als* editing template for replacement of the *als* promoter with promoter $P_{grac.UPmod}$, i.e. plasmid pAW023-5, was constructed by amplifying the 775 bp and 798 bp HLs from 1A751 gDNA with respective primers P7.77/P7.78 and P7.79/P7.80, $P_{grac.UPmod}$ (with an upstream XhoI restriction site) from pAW003-4 [239] with primers P7.81/P7.82, and the plasmid backbone from pAW020-2 with primers P7.83/P7.84, followed by assembly of the four fragments. The P_{mtlA}::*als* editing template for replacement of the *als* promoter with promoter P_{mtlA}, i.e. plasmid pAW024-5, was constructed by amplifying the combined HL-3'-backbone-HL-5' fragment from pAW023-5 with primers P7.85/P7.86, P_{mtlA} from 1A751 gDNA with primers P7.87/P7.88, followed by assembly of the two fragments. The mut.*ilvB*.P1101NT editing template for

mutation of *ilvB*, i.e. plasmid pAW025-5, was constructed by amplifying the 769 bp and 773 bp HLs (flanking an in-frame NheI restriction site preceded by two stop codons) from 1A751 gDNA with respective primers P7.89/P7.90 and P7.91/P7.92, and the plasmid backbone from pAW020-2 with primers P7.93/P7.94, followed by assembly of the three fragments. The mut.*ilvA*.P581NT editing template for mutation of *ilvA*, i.e. plasmid pAW026-5, was constructed by amplifying the 740 bp and 787 bp HLs (flanking an in-frame BssHII restriction site preceded by two stop codons) from 1A751 gDNA with respective primers P7.95/P7.96 and P7.97/P7.98, and the plasmid backbone from pAW020-2 with primers P7.99/P7.100, followed by assembly of the three fragments. The mut.*alsD*.P99T editing template for mutation of *alsD*, i.e. plasmid pAW027-5, was constructed by amplifying the 771 bp and 764 bp HLs (flanking an in-frame BseYI restriction site between two stop codons) from 1A751 gDNA with respective primers P7.101/P7.102 and P7.103/P7.104, and the plasmid backbone from pAW020-2 with primers P7.105/P7.106, followed by assembly of the three fragments. The $P_{grac.UPmod}$::*bcaP* editing template for replacement of the *bcaP* promoter with $P_{grac.UPmod}$, i.e. plasmid pAW028-5, was constructed by amplifying the 763 bp and 776 bp HLs from 1A751 gDNA with respective primers P7.107/P7.108 and P7.109/P7.110, $P_{grac.UPmod}$ (with an upstream XhoI restriction site) from pAW003-4 with primers P7.111/P7.112, and the plasmid backbone from pAW020-2 with primers P7.113/P7.114, followed by assembly of the four fragments. The mut.*sigF*.P371T editing template for mutation of *sigF*, i.e. plasmid pAW029-5, was constructed by amplifying the 773 bp and 763 bp HLs (flanking an in-frame AvrII restriction site between two stop codons) from 1A751 gDNA with respective primers P7.115/P7.116 and P7.117/P7.118, and the plasmid backbone from pAW020-2 with primers P7.119/P7.120, followed by assembly of the three fragments. The mut.*pdhA*.P116T editing template for mutation of *pdhA*, i.e. plasmid pAW030-5,

was constructed by amplifying the 806 bp and 795 bp HLs (flanking an in-frame XbaI restriction site followed by two stop codons) from 1A751 gDNA with respective primers P7.121/P7.122 and P7.123/P7.124, and the plasmid backbone from pAW020-2 with primers P7.125/P7.126, followed by assembly of the three fragments. Finally, the *thrC* editing template for removal of gRNA transcription cassettes from the *thrC* locus, i.e. pAW031-5, was constructed by amplifying a 2876 bp fragment consisting of 1452 bp and 1306 bp HLs flanking the deleted 118 bp region of the *thrC* ORF from 1A751 gDNA with primers P7.127/P7.128, followed by insertion into pJET1.2/blunt.

7.2.3 Competent cell preparation and transformation

Preparation and transformation of naturally competent *B. subtilis* was performed as previously described [263]. To prepare artificially supercompetent strains, cells were plated on non-select LB agar containing (per L) 5 g NaCl, 5 g yeast extract, 10 g tryptone, and 15 g agar, and incubated overnight at 37 °C. Pre-warmed LB medium (20 mL) containing 5 mM $MgSO_4$ was inoculated by cell patches from the overnight plate to OD_{600} 0.4-0.6, and the cultures were grown at 37 °C and 280 rpm. Once the cell density reached OD_{600} 0.8-1, xylose was added to the cultures at a final concentration of 10 g/L to induce the expression of *comK* and *comS*, and the induced cultures were incubated for 1.5 h to develop the artificially supercompetent state. 1.5 µg of gRNA delivery vector and 1.5 µg of each editing template were used per transformation, and transformed cells were incubated for 80 min at 280 rpm and 37 °C, and plated on LBG containing 85 µg/mL spectinomycin to select recombinants. The same procedure was used to evict gRNA transcription cassettes from the *thrC* locus after each round of CRISPR-Cas9 genome editing, except that 1 µg of ScaI-linearized pAW031-5 was used per transformation, and

cells were plated on LBA and subsequently tested for spectinomycin sensitivity [263]. Media was supplemented with 3 g/L sodium acetate when culturing Δ*pdhA* mutants.

7.2.4 Cultivation medium and conditions

B. subtilis strains were plated on non-select LB agar and grown overnight at 37 °C. A single colony was used to inoculate 25 mL non-select LB, and the culture was grown for ~12 h at 37 °C and 280 rpm. The culture was then used to inoculate 20 mL pre-warmed non-select cultivation medium (4% v/v) of the following composition (per L): sucrose, 30 g; mannitol, 10 g; $(NH_4)_2SO_4$, 17 g; $K_2HPO_4 \cdot 3H_2O$, 18.3 g; KH_2PO_4, 6 g; trisodium citrate· $2H_2O$, 1 g; yeast extract, 5 g; leucine, 250 mg; isoleucine, 250 mg; $MgSO_4$, 120 mg; $CaCl_2$, 5.5 mg; $FeCl_2 \cdot 6H_2O$, 13.5 mg; $MnCl_2 \cdot 4H_2O$, 1 mg; $ZnCl_2$, 1.7 mg; $CuCl_2 \cdot 2H_2O$, 0.43 mg; $CoCl_2 \cdot 6H_2O$, 0.6 mg; $Na_2MoO_4 \cdot 2H_2O$, 0.6 mg. Cultures were grown at 37 °C and 280 rpm, and the medium was supplemented with 3 g/L sodium acetate when culturing Δ*pdhA* mutants. To assess cell growth in the presence of L-valine, cells were grown in a minimal medium of the following composition (per L): sucrose, 10 g; $(NH_4)_2SO_4$, 12 g; $K_2HPO_4 \cdot 3H_2O$, 18.3 g; KH_2PO_4, 6 g; trisodium citrate· $2H_2O$, 1 g; $MgSO_4$, 120 mg; $CaCl_2$, 5.5 mg; $FeCl_2 \cdot 6H_2O$, 13.5 mg; $MnCl_2 \cdot 4H_2O$, 1 mg; $ZnCl_2$, 1.7 mg; $CuCl_2 \cdot 2H_2O$, 0.43 mg; $CoCl_2 \cdot 6H_2O$, 0.6 mg; $Na_2MoO_4 \cdot 2H_2O$, 0.6 mg. L-valine was supplemented at a concentration of 3 g/L, 8 g/L, or 20 g/L as indicated.

7.2.5 L-valine quantification

L-valine was first converted to its α-hydroxy acid, i.e. 2-hydroxy-3-methylbutyric acid, via nitrosation prior to quantification via HPLC as previously described [331] with minor modifications. Culture samples were centrifuged at 13000 rpm for 10 min, and the cell-free

supernatant was diluted as required. 500 µL of cell-free supernatant was mixed with 100 µL of 1 M KNO_2, and the nitrosation reaction was initiated by adding 20 µL of 3 M HCl. The reaction was conducted at 45 °C for 40 min, and was stopped by adding 100 µL of 2 M NaOH. The nitrosated samples were then degassed in an ultrasonic water bath at 50 °C for 30 min, and filter-sterilized prior to HPLC analysis. The HPLC system consists of a Shimadzu LC-10AT solvent delivery unit, Shimadzu RID-10A refractive index detector, Shimadzu CTO-20A column oven, and an Aminex HPX-87H chromatographic column. The column and detector temperatures were maintained at 27 °C and 30 °C, respectively, and the flow rate of the mobile phase (i.e. 5 mM H_2SO_4) was 0.4 mL/min. Signal acquisition and data processing were performed with Clarity Lite.

7.3 Results

7.3.1 Derivation of L-valine-overproducing strains of B. subtilis

To derive L-valine-overproducing strains of *B. subtilis*, we employed our recently developed CRISPR-Cas9 toolkit [263]. Overexpression of *comK*, encoding the competence transcription factor ComK, and *comS*, encoding competence protein S (ComS), during exponential growth can significantly improve the transformation efficiency of *B. subtilis* strains, compared to transformation via natural competence [65]. Accordingly, we transformed AW001-2 [263] with SacI-linearized pAW002-5, followed by auto-eviction of the P_{araE}::*mazF*-Spc^R cassette as previously described [263], resulting in the artificially supercompetent strain AW001-5 that coexpressed xylose-inducible *comK* and *comS* from the *bpr* locus (Figure 7.2). Given that *ilvBHC* are expressed as part of a single operon and the regulatory elements controlling its expression are spatially defined, we chose to replace the 677 bp region upstream of the *ilvB* RBS,

including the TnrA box, all four CodY binding sites, the CRE, the $tRNA^{Leu}$ T-box, and $P_{ilv\text{-}leu}$, with the strong constitutive promoter P_{grac}. We also sought to mutate *bcd* to prevent the conversion of L-valine to 2-ketoisovalerate. To simultaneously replace $P_{ilv\text{-}leu}$ and its regulatory elements with P_{grac}, and mutate *bcd*, AW001-5 was transformed with SacI-linearized pAW004-5 (transcribing gRNAs targeting bp +276 of $P_{ilv\text{-}leu}$ and *bcd*.P585T), and AhdI-linearized pAW017-5 (the P_{grac}::*ilvBHC* editing template) and pAW018-5 (the mut.*bcd*.P585T editing template). The resulting strain was subsequently transformed with ScaI-linearized pAW031-5 for gRNA eviction from the *thrC* locus, yielding strain AW002-5 (Figure 7.2). AW002-5 was then transformed with SacI-linearized pAW006-5 (transcribing a gRNA targeting *amyE*.P636T) and AhdI-linearized pAW020-5 (the P_{grac}::*ybgE*:*ywaA* Δ*amyE* editing template), resulting in integration of a P_{grac}::*ybgE*:*ywaA* expression cassette at the *amyE* locus in strain AW003-5 upon gRNA eviction (Figure 7.2). Similarly, AW003-5 was transformed with SacI-linearized pAW007-5 (transcribing a gRNA targeting *wprA*.P1419T) and ScaI-linearized pAW021-5 (the P_{grac}::*ilvD* Δ*wprA* editing template), resulting in integration of a P_{grac}::*ilvD* expression cassette at the *wprA* locus in strain AW004-5 upon gRNA eviction (Figure 7.2).

The inhibition of AHAS by BCAAs is well documented and is a common feature of most of them [316, 332]. IlvH of *B. subtilis* is a reportedly valine-sensitive AHAS that is similar in structure to AHAS III of *E. coli* (i.e. $IlvH^{Ec}$), and both enzymes possess several conserved amino acid residues that have been replaced to abolish or reduce the valine sensitivity of $IlvH^{Ec}$ [332-334]. Based on the results of cited mutational studies and patents based on $IlvH^{Ec}$, we introduced three point mutations to conserved amino acid residues in IlvH, i.e. N11A, G14D, and N29H. A fourth point mutation, i.e. N17F, was also introduced as the point mutation S17F reduced the valine sensitivity of $IlvH^{Ec}$ [333], and N and S are both polar amino acids. The specified point

mutations were introduced into native IlvH in AW004-5 via transformation of SacI-linearized pAW013-5 (transcribing a gRNA targeting *ilvH*.P40T) and AhdI-linearized pAW022-5 (the IlvH(N11A,G14D,N17F,N29H) editing template), resulting in the expression of engineered IlvH, i.e. IlvH*, in strain AW005-5 upon gRNA eviction (Figure 7.2). To compare the performance of strains expressing either IlvH, IlvH*, or AlsS for L-valine overproduction, we initially attempted to construct an editing template for the genomic integration of a P_{grac}::*ilvD*:*alsS* expression cassette at the *wprA* locus of AW003-5, in parallel with the mutation of *ilvB*. However, this plasmid was not stable in *E. coli* due to the presence of *alsS*, prompting us to replace the 186 bp region between bp 29 of the *alsR* ORF and bp 2 of the *alsS* ORF, including promoters P_{alsR} and P_{als}, and the AlsR regulatory and activator binding sites, with the relatively strong constitutive promoter $P_{grac.UPmod}$ (Note that a consensus RBS, 8 bp spacer region, and T-A substitution in bp 1 of the *alsS* ORF was inserted with $P_{grac.UPmod}$). The simultaneous engineering of the *als* promoter and mutation of *ilvB* was achieved by transforming AW004-5 with SacI-linearized pAW009-5 (transcribing gRNAs targeting bp +49 of P_{als} and *ilvB*.P1101NT), and AhdI-linearized pAW023-5 (the $P_{grac.UPmod}$::*als* editing template) and pAW025-5 (the mut.*ilvB*.P1101NT editing template), resulting in strain AW006-5 upon gRNA eviction.

1A751 (i.e. the wild-type strain), AW004-5, AW005-5, and AW006-5 were evaluated for L-valine overproduction in shake flask cultures. The cell density peaked at OD_{600} 4.6 after 12 h Figure 7.3A) and the L-valine titer was below the detectable limit of ~0.1 g/L in cultures of 1A751 (Figure 7.3B). On the other hand, the cell density reached OD_{600} 8.1 after 12 h (Figure 7.3A) and the final L-valine titer was 1.24 g/L in cultures of AW004-5 (Figure 7.3B), representing a >12-fold increase in L-valine production compared to 1A751. A slightly lower peak cell density of OD_{600} 7.7 after 12 h (Figure 7.3A) and higher final L-valine titer of 1.44 g/L

was observed in cultures of AW005-5, compared to AW004-5, suggesting that L-valine feedback inhibition of native IlvH in *B. subtilis* is modest at this level of L-valine overproduction. Interestingly, cell growth and L-valine overproduction were severely delayed in cultures of AW006-5, although the cell density was markedly higher (OD_{600} 12.3; Figure 7.3A) and the L-valine titer was comparable (1.5 g/L; Figure 7.3B) after 24 h, compared to cultures of AW005-5.

7.3.2 Pyruvate availability limits L-valine overproduction in B. subtilis

We next sought to identify potential bottlenecks limiting L-valine overproduction in *B. subtilis* to improve culture performance. L-leucine and L-valine biosynthesis are in direct competition for the intermediate 2-ketoisovalerate (Figure 7.1), while L-isoleucine is also derived from pyruvate by the same enzymes that synthesize L-valine (i.e. IlvBHCD, YbgE, and YwaA; Figure 7.1). Accordingly, we simultaneously mutated *leuA* and *ilvA* in AW005-5 via transformation of SacI-linearized pAW010-5 (transcribing gRNAs targeting *leuA*.P764NT and AW007-5 with SacI-linearized pAW008-5 and AhdI-linearized pAW023-5, resulting in strain AW008-5 upon gRNA eviction. However, a severe growth defect was observed for AW008-5, prompting us to insert a somewhat weaker inducible promoter upstream of *alsS*, i.e. the mannitol-inducible promoter P_{mtlA} [335], via transformation of AW007-5 with SacI-linearized pAW008-5 and AhdI-linearized pAW024-5 (the P_{mtlA}::*als* editing template), resulting in strain AW009-5 upon gRNA eviction (Figure 7.2). The peak cell density and final L-valine titer decreased to OD_{600} 3.6 after 8 h (Figure 7.4A) and 1.27 g/L (Figure 7.4B), respectively, in cultures of AW009-5 compared to AW007-5. We postulated that the enhanced conversion of2-acetolactate to acetoin due to the increased expression of *alsD* may have hindered the culture performance of AW009-5, and, thus, mutated *alsD* in AW009-5 via transformation of SacI-

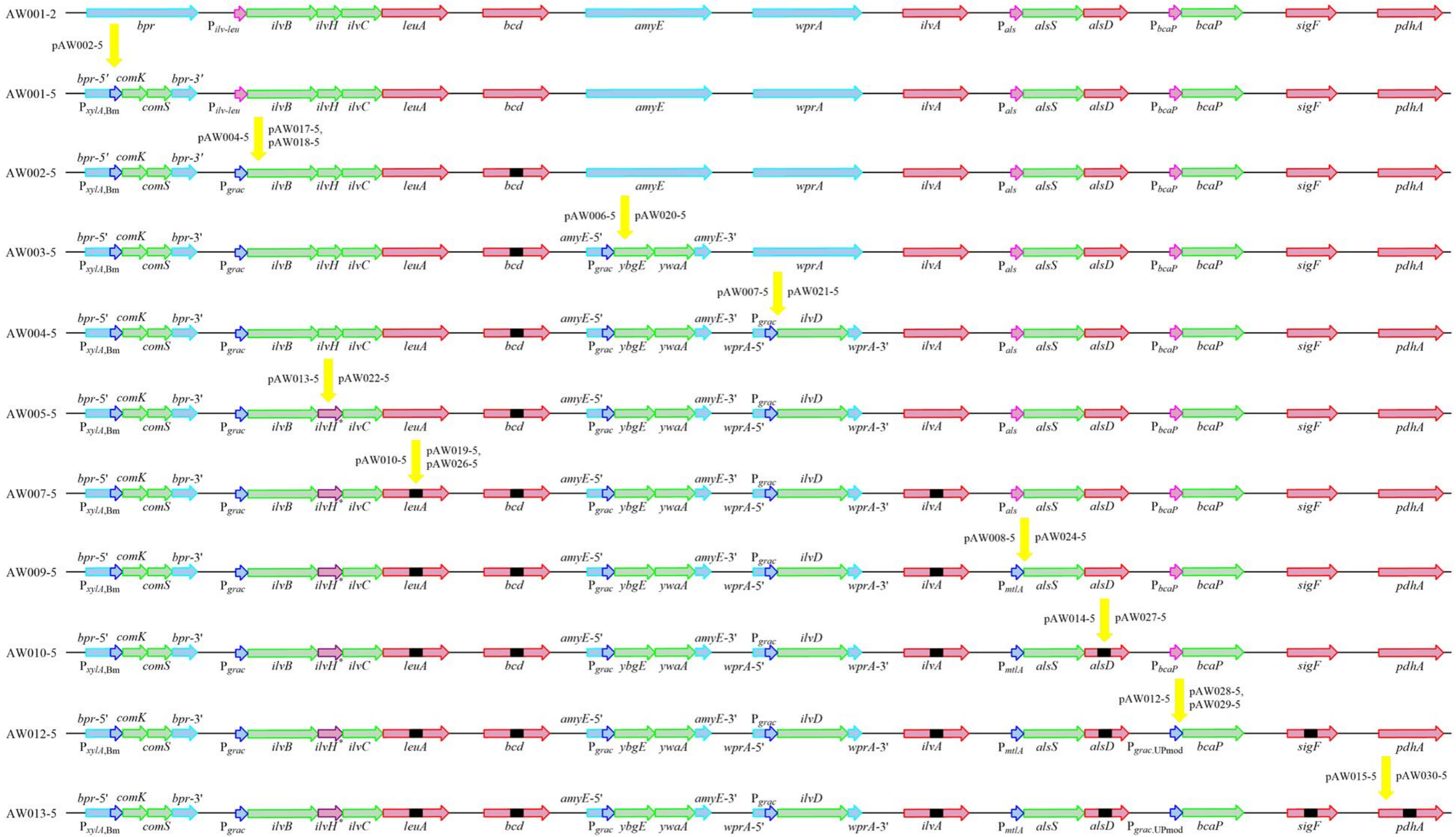
AW001-2
bpr
P ilv-leu
ilvB
ilvH
ilvC
leuA
bcd
amyE
wprA
ilvA
P als
alsS
alsD
P bcaP
bcaP
sigF
pdhA
pAW002-5
AW001-5
bpr-5'
comK
bpr-3'
P xylA,Bm
comS
pAW004-5
pAW017-5,
pAW018-5
AW002-5
P grac
pAW006-5
pAW020-5
AW003-5
amyE-5'
amyE-3'
ybgE
ywaA
pAW007-5
pAW021-5
AW004-5
ilvD
wprA-5'
wprA-3'
pAW013-5
pAW022-5
AW005-5
ilvH*
pAW010-5
pAW019-5,
pAW026-5
AW007-5
pAW008-5
pAW024-5
AW009-5
P mtlA
pAW014-5
pAW027-5
AW010-5
pAW012-5
pAW028-5,
pAW029-5
AW012-5
P grac.UPmod
pAW015-5
pAW030-5
AW013-5

Figure 7.2. Genome engineering strategies for L-valine overproduction in *B. subtilis*. Color legend for genes and promoters: light blue, genes serving as integration sites; green, genes to be overexpressed from engineered promoters (dark blue); red, genes that are mutation targets (black segment indicates mutation); pink, native promoters and corresponding regulatory elements. *alsD*, acetolactate decarboxylase; *alsS*, acetolactate synthase; *amyE*, α-amylase; *bcaP*, BCAA permease; *bcd*, BCAA dehydrogenase; *bpr*, bacillopeptidase F; *comK*, competence transcription factor; *comS*, competence protein S; *ilvA*, L-threonine dehydratase; *ilvB*, acetohydroxy-acid synthase catalytic subunit; *ilvC*, acetohydroxy-acid isomeroreductase; *ilvD*, dihydroxy-acid dehydratase; *ilvH*, native acetohydroxy-acid synthase regulatory subunit, *ilvH**, engineered acetohydroxy-acid synthase regulatory subunit; *leuA*, 2-isopropylmalate synthase; *pdhA*, E1α subunit of the pyruvate dehydrogenase complex; *sigF*, sporulation-specific transcription factor σ^F; *wprA*, cell wall-associated protease; *ybgE*, BCAA aminotransferase; *ywaA*; BCAA aminotransferase; $P_{ilv\text{-}leu}$, *ilvBHC-leuABCD* promoter and corresponding regulatory elements; P_{als}, *alsSD* promoter and corresponding regulatory elements; P_{bcaP}, *bcaP* promoter and corresponding regulatory elements; $P_{xylA,Bm}$, xylose-inducible *xylA* promoter (*Bacillus megaterium*); P_{grac}, constitutive promoter; P_{mtlA}, mannitol-inducible *mtlA* promoter; $P_{grac.UPmod}$, constitutive promoter.

linearized pAW014-5 (transcribing a gRNA targeting *alsD*.P99T) and AhdI-linearized pAW027-5 (the mut.*alsD*.P99T editing template), resulting in strain AW010-5 upon gRNA eviction (Figure 7.2). However, the peak cell density and final L-valine titer marginally increased to OD_{600} 4 after 24 h (Figure 7.4A), and 1.35 g/L (Figure 7.4B), respectively, in cultures of AW010-5, compared to AW009-5, suggesting that 2-acetolactate availability was not limiting L-valine overproduction in our strains.

L-valine overproduction was enhanced by overexpressing the BCAA exporters YgaZH in *E. coli* [305] and BrnFE in *C. glutamicum* [310], such that L-valine secretion could be a factor limiting overproduction in *B. subtilis* cultures. Accordingly, we replaced the 214 bp region upstream of the *bcaP* start codon, including CodY-I, CodY-II, and P_{bcaP}, with $P_{grac.UPmod}$ (Note that a consensus RBS and 8 bp spacer region were inserted with $P_{grac.UPmod}$.). Moreover, sporogenesis occurs in *B. subtilis* cultures in response to nutrient depletion and high cell densities [336], potentially hampering culture performance and preventing its application in the food industry [216]. Hence, we also selected *sigF*, encoding transcription factor σ^F that controls

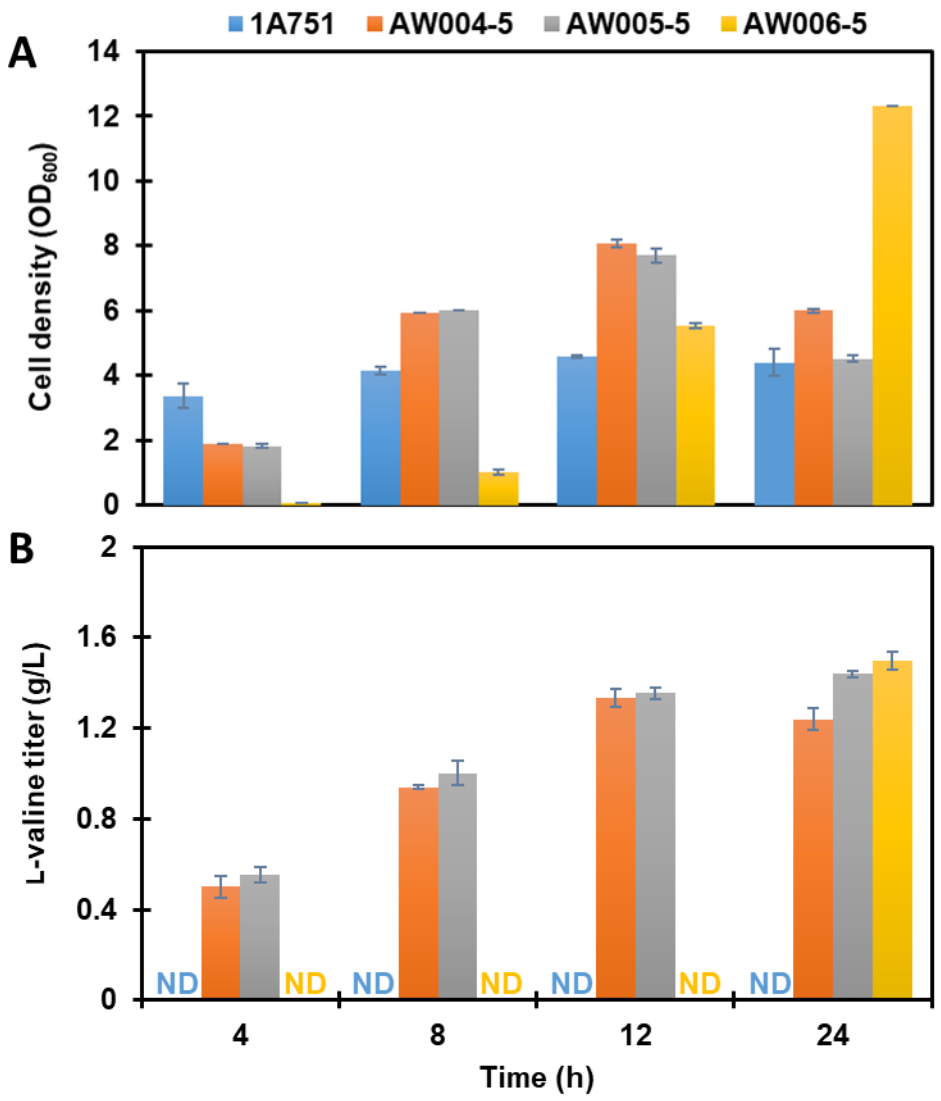

Figure 7.3. Time profiles of A) cell density and B) L-valine titer in cultures of 1A751, AW004-5, AW005-5, and AW006-5. SD of experiments performed in duplicate are shown in Panels A and B. ND indicates that the L-valine titer was below the detectable limit of ~0.1 g/L.

the expression of genes that initiate prespore development [336], as a mutation target to potentially improve culture performance and the utility of our strains for industrial application. To replace P_{bcaP} with $P_{grac.UPmod}$ with or without simultaneously mutating *sigF*, AW010-5 was transformed with SacI-linearized pAW011-5 (transcribing a gRNA targeting bp +7 of P_{bcaP}) and

AhdI-linearized pAW028-5 (the $P_{grac.UPmod}$::*bcaP* editing template), or SacI-linearized pAW012-5 (transcribing gRNAs targeting bp +7 of P_{bcaP} and *sigF*.P371T) with AhdI-linearized pAW028-5 and pAW029-5 (the mut.*sigF*.P371T editing template), resulting in respective strains AW011-5 and AW012-5 upon gRNA eviction (Figure 7.2). The peak cell density (OD_{600} 3.5 after 8 h; Figure 7.4A) and final L-valine titer (1.24 g/L; Figure 7.4B) declined slightly in cultures of AW011-5, compared to AW010-5, suggesting that L-valine secretion was not limiting overproduction in our strains. Similarly, the peak cell density (OD_{600} 3.2 after 8 h; Figure 7.4A) and final L-valine titer (1.09 g/L; Figure 7.4B) further declined in cultures of AW012-5, compared to AW011-5.

Finally, we attempted to increase pyruvate levels by mutating *pdhA* via transformation of AW012-5 with SacI-linearized pAW015-5 (transcribing a gRNA targeting *pdhA*.P116T) and AhdI-linearized pAW030-5 (the mut.*pdhA*.P116T editing template), resulting in strain AW013-5 upon gRNA eviction (Figure 7.2). The peak cell density and final L-valine titer increased by 128% (OD_{600} 7.3 after 12 h; Figure 7.4A) and 171% (2.95 g/L; Figure 7.4B) in cultures of AW013-5, compared to AW012-5. These results suggest that pyruvate availability limits L-valine overproduction in *B. subtilis*, which is true, in general, of L-valine overproducing strains of *C. glutamicum* [301].

7.3.3 Inactivating the L-leucine and L-isoleucine pathways significantly enhances L-valine overproduction in the ΔpdhA background

Upon identifying pyruvate availability as the major bottleneck limiting L-valine overproduction in *B. subtilis*, we reexamined previous strain engineering strategies in the Δ*pdhA* background. AW004-5, AW005-5, AW007-5, AW009-5, AW010-5, and AW011-5 were

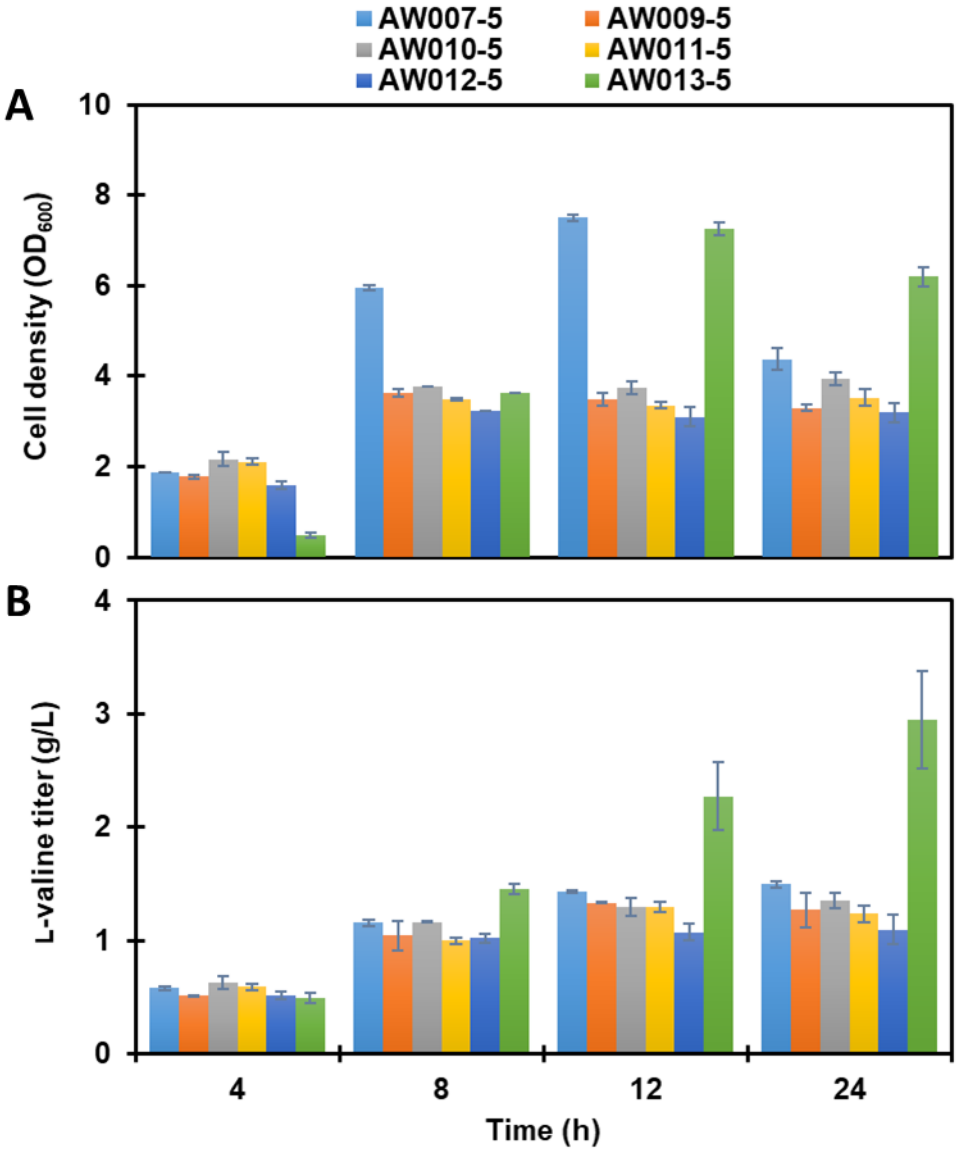

Figure 7.4. Time profiles of A) cell density and B) L-valine titer in cultures of AW007-5, AW009-5, AW010-5, AW011-5, AW012-5, and AW013-5. SD of experiments performed in duplicate are shown in Panels A and B.

transformed with SacI-linearized pAW015-5 and AhdI-linearized pAW030-5, resulting in respective strains AW014-5, AW015-5, AW016-5, AW017-5, AW018-5, and AW019-5 upon gRNA eviction. As expected, the mutation of *pdhA* resulted in significant improvements to L-valine overproduction in all previously derived strains (Figure 7.5). The final L-valine titers in

cultures of AW014-5 (2.2 g/L; Figure 7.5B) and AW015-5 (2.4 g/L; Figure 7.5B), i.e. respective Δ*pdhA* mutants that express native *ilvH* and *ilvH**, were similar, further suggesting that L-valine feedback inhibition of IlvBH is minimal in *B. subtilis*. Notably, the L-valine titer reached 4.61 g/L in cultures of AW016-5 (Figure 7.5B), representing a 92% increase compared to AW015-5. These observations suggest that a competition for cellular resources exists between the pathways for BCAA biosynthesis, such that *leuA* and *ilvA* are critical targets for mutation to significantly enhance L-valine overproduction in *B. subtilis* in spite of the resulting auxotrophy. On other hand, the L-valine titer declined to 3.01 g/L in cultures of AW017-5 (Figure 7.5B), suggesting, once again, that upregulating the expression of *alsS* in parallel with *ilvBH* impedes L-valine biosynthesis. In contrast to the *alsD* mutant AW010-5 that produced a similar L-valine titer to its parent strain AW009-5, AW018-5 produced even less L-valine than AW017-5 (i.e. 2.14 g/L compared with 3.01 g/L; Figure 7.5B), indicating that *alsD* is not an appropriate target for mutation to enhance L-valine overproduction. Similarly, the L-valine titer reached only 1.86 g/L in cultures of AW019-5 (Figure 7.5B), supporting the prior suggestion that increasing the expression of *bcaP* does not improve L-valine overproduction. Finally, the final L-valine titer was significantly higher in cultures of AW013-5 (2.95 g/L; Figure 7.4B), compared to AW019-5 (1.86 g/L; Figure 7.5B), indicating that the prevention of sporogenesis via mutation of *sigF* in AW013-5 improved culture performance. Accordingly, we mutated *sigF* in AW016-5 via transformation of SacI-linearized pAW016-5 (transcribing a gRNA targeting *sigF*.P371T) and AhdI-linearized pAW029-5, resulting in strain AW020-5 upon gRNA eviction. While the cell density profiles (Figure 7.6A) and L-valine titers (Figure 7.6B) were quite similar in cultures of AW016-5 and AW020-5, the absence of sporulation is a desirable trait for industrial production strains.

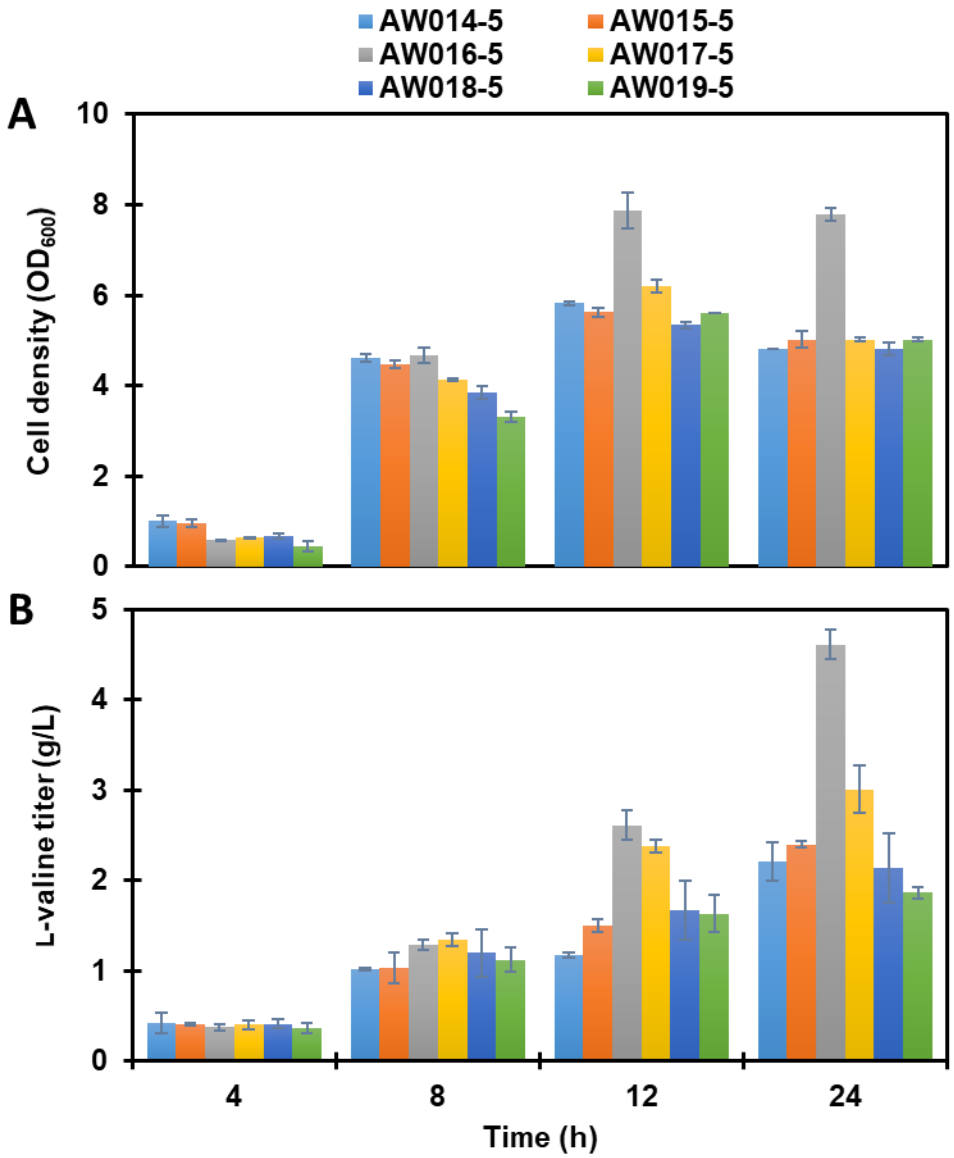

Figure 7.5. Time profiles of A) cell density and B) L-valine titer in cultures of AW014-5, AW015-5, AW016-5, AW017-5, AW018-5, and AW019-5. SD of experiments performed in duplicate are shown in Panels A and B.

7.4 Discussion

Due to its well characterized genetic profile and ease of manipulation, robust growth characteristics in simple media, and proven track record as a GRAS biomanufacturing platform, *B. subtilis* is a logical choice as a production host for amino acids. Here, we have demonstrated

high-level L-valine overproduction in engineered *B. subtilis* as a first step toward its development into an industrially relevant production host for amino acids. Importantly, our engineered strains contain no replicating plasmids and, therefore, do not require antibiotic selection and are inherently more stable than previously developed L-valine-overproducing strains of *E. coli* and *C. glutamicum*. It is anticipated that further strain and bioprocess development can lead to improved L-valine overproduction in our engineered strains, and that *B. subtilis* can be of industrial utility for the production of L-valine and potentially other amino acids.

The feedback inhibition of bacterial AHAS is a conserved feature among many, but not all, such enzymes [316]. Presumably due to the presence of the regulatory subunit (i.e. IlvH) that bears similarity to valine-sensitive $IlvH^{Ec}$, IlvBH has been identified as a valine-sensitive homologue of AHAS III from *E. coli* [332]. The half maximal inhibitory concentration (IC_{50}) of L-valine for the IlvBH homologue of *C. glutamicum*, i.e. $IlvBN^{Cg}$, is as low as 105 mg/L [337], and the minimum inhibitory concentration (MIC) of L-valine in *E. coli* K-12 and its derivatives, which lack functional L-valine-insensitive AHAS II, is as low as 2 mg/L [338]. On other hand, *B. subtilis* 168 can grow in medium containing at least 2.3 g/L L-valine as the sole nitrogen source [327], indicating that IlvBH is significantly less sensitive to L-valine compared to $IlvBH^{Ec}$. Our data is in agreement with this observation, as the L-valine titer reached 2.2 g/L in cultures of AW014-5, and the peak cell density exceeded that observed in cultures of 1A751, i.e. OD_{600} 5.8 and OD_{600} 4.6 for AW014-5 and 1A751, respectively. We further investigated potential L-valine feedback inhibition of IlvBH by simultaneously mutating *leuA* and *ilvA* in AW014-5 via transformation of SacI-linearized pAW010-5 with AhdI-linearized pAW019-5 and pAW026-5, resulting in strain AW021-5 upon gRNA eviction. The peak cell density and final L-valine titer reached OD_{600} 8 after 24 h (Figure 7.6A) and 3.6 g/L (Figure 7.6B), respectively, in cultures of

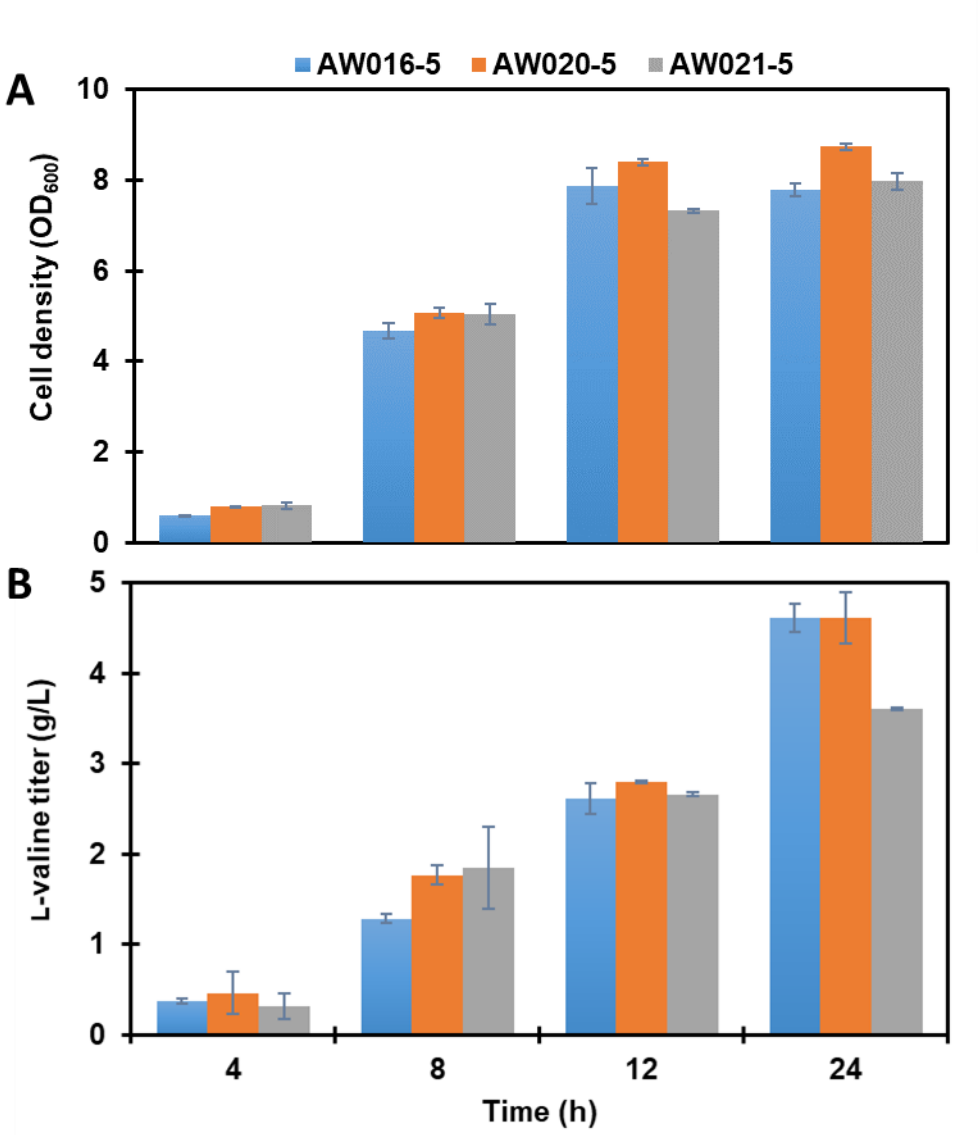

Figure 7.6. Time profiles of A) cell density and B) L-valine titer in cultures of AW016-5, AW020-5, and AW021-5. SD of experiments performed in duplicate are shown in Panels A and B.

AW021-5, representing no significant difference in cell growth and a 22% decrease in the L-valine titer compared to cultures of AW016-5 (4.61 g/L; Figure 7.6B), i.e. a strain expressing *ilvH** that is otherwise identical. We also performed growth experiments with AW004-5 and AW005-5 in minimal medium containing various concentrations of L-valine to establish if

growth inhibition occurred in the presence of excess L-valine. The growth profiles were nearly identical in cultures of AW004-5 and AW005-5 for L-valine concentrations up to 20 g/L (Figure 7.7), indicating that feedback inhibition of IlvBH by L-valine is not significant enough to affect cell growth. In fact, the respective final cell densities increased by 37% and 43% in cultures of AW004-5 and AW005-5 containing 20 g/L L-valine, compared to the respective controls without supplemental L-valine, suggesting that YbgE and/or YwaA could convert L-valine to 2-ketoisovalerate to initiate L-valine catabolism. These observations are in contrast to those of a prior study in which a Δ*bcd* mutant could not grow in minimal medium containing L-valine as the sole nitrogen source [327]. However, the expression of native *ybgE* and *ywaA* were presumably repressed by L-valine-activated CodY in the cited study. The improved L-valine overproduction in cultures of AW016-5, compared to AW021-5, may have resulted from a mild degree of feedback inhibition of IlvBH that is not sufficient to repress growth. Another possibility is that IlvH* modulated the activity of the IlvBH* holoenzyme, resulting in increased flux through the L-valine biosynthetic pathway, however, further investigation is required to establish the cause of the modest improvements to culture performance in strains expressing *ilvH**.

Given that AlsS is a dedicated ALS, one might expect its overexpression to be beneficial to L-valine overproduction, compared to IlvBH, which converts pyruvate to 2-acetolactate, and pyruvate and 2-ketobutyrate to 2-aceto-2-hydroxybutyrate during L-valine and L-isoleucine biosynthesis, respectively. Upregulating the expression of the *als* operon in the Δ*ilvB* background in AW006-5 resulted in severely delayed growth and L-valine overproduction in our production medium, while the overnight growth of AW006-5 in LB medium prior to inoculation was markedly poorer compared to all other strains evaluated in this work (data not shown). This

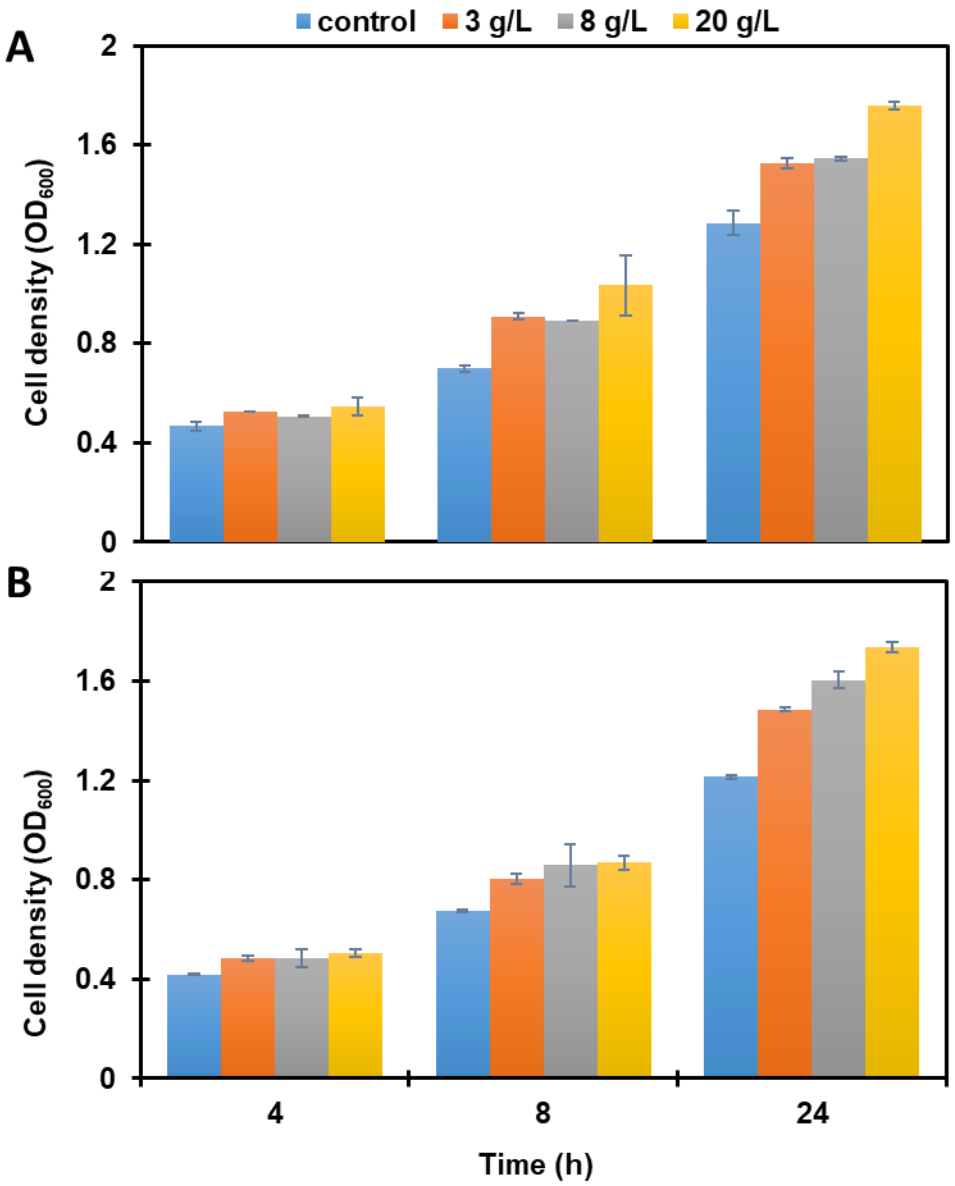

Figure 7.7. Time profiles of the cell density in cultures of A) AW004-5 and B) AW005-5 containing no supplemental L-valine (control), or 3 g/L, 8 g/L, or 20 g/L L-valine. SD of experiments performed in duplicate are shown in Panels A and B.

may be explained by the fact that the activity of dedicated ALS from acetoin-producing bacteria is optimal under low pH (~pH 6) [316], and that the expression of *alsSD* is induced in the presence of acetate and a low pH in *B. subtilis* [325]. In other words, cell growth and L-valine

overproduction are initially poor in our production medium that contains excess sucrose, until acetate begins to accumulate with a concomitant decrease in the pH of the culture, in turn, increasing the activity of AlsS. On the other hand, cell growth, and presumably L-valine overproduction, remain low in LB medium, which lacks a dedicated carbon source and can cause ammonification due to amino acid metabolism, in turn, increasing the pH of the culture. The compromised culture performance of AW018-5, i.e. a strain in which the expression of *alsS* was upregulated and *alsD* was mutated, suggests that 2-acetolactate levels are sufficient in our engineered strains, and that acetoin produced during carbon overflow metabolism in strains with intact *alsD* may serve as a carbon source in the later stages of the culture when sucrose is depleted [315].

BCAA exporters have been overexpressed in *E. coli*, i.e. YgaZH [305], and *C. glutamicum*, i.e. BrnFE [310], and their overexpression significantly improved L-valine overproduction in both hosts. Of the four aforementioned proteins analyzed via BLAST [339], only BrnF shared significant similarity with any *B. subtilis* proteins. Specifically, BrnF and AzlC, a component of the 4-azaleucine transporter AzlCD (encoded by *azlCD*) from *B. subtilis* [328], are 31% identical (76% coverage; score 83.6). However, mutation of *azlCD* did not significantly affect the expression of CodY-regulated genes in the presence of BCAAs, suggesting that it does not play a significant role in the maintenance of cellular L-valine levels [328]. On the other hand, *bcaP* is among the most highly CodY-regulated genes in *B. subtilis*, and CodY activity is modulated in a negative feedback loop by the expression of *bcaP* in minimal medium containing only BCAAs [328]. In spite of the fact that BcaP is the most efficient permease for the uptake of L-valine, our attempts to improve L-valine overproduction through promoter engineering to enhance *bcaP* expression were unsuccessful. Perhaps secretion

of L-valine is naturally efficient enough in *B. subtilis* to service the production capacity of our engineered strains. CodY should be highly active in L-valine overproducing strains, such that *bcaP* expression from its native promoter should be severely diminished. Accordingly, BcaP may not serve as a permease for the facilitated export of L-valine, and a currently unidentified exporter(s) of BCAAs may perform this function. Alternatively, based on the hydrophobicity of L-valine and its observed water/lipid phase partition coefficients, it is plausible that L-valine can passively diffuse across the cell membrane at significant rates [340]. Clearly, further investigation is required to clarify the dominant mechanism by which excess L-valine is secreted from the cell to potentially enhance overproduction, which may be achieved by overexpressing a dedicated BCAA exporter, or through engineering or chemical treatment of the cell membrane to enhance permeability.

It is evident from our results that pyruvate availability is limiting L-valine overproduction in *B. subtilis*, which is also the case in *C. glutamicum* [301]. On other hand, pyruvate may not be as scarce in *E. coli* as inactivating the pyruvate dehydrogenase complex did not increase L-valine overproduction to the same degree as reported here [304, 305]. The severe pyruvate limitation in *B. subtilis* is not surprising as its metabolism is suboptimal in the presence of preferred carbon sources due to regulatory mechanisms designed to carefully control metabolic fluxes at the expense of biomass accumulation, enabling a rapid response to environmental changes [240]. To circumvent the rigid flux distribution at the glucose-6-P and fructose-6-P nodes, where glycolysis, the PPP, and cell wall biosynthesis diverge, we successfully applied CRISPRi to reduce the expression of enzymes at the branch points of these central metabolic pathways, in turn, significantly enhancing heterologous HA production in *B. subtilis*. This approach may also prove effective in diverting additional pyruvate or 2-ketoisovalerate from competing metabolic

pathways toward L-valine overproduction. For example, we were unsuccessful in mutating *panB*, encoding ketopantoate hydroxymethyltransferase (PanB) which converts 2-ketosiovalerate to 2-dehydropantoate during pantothenate biosynthesis, in our engineered strains, such that it may be an appropriate target for transcriptional repression to improve L-valine overproduction. One potentially beneficial aspect of the *B. subtilis* metabolism for L-valine overproduction is the general excess of intracellular NADPH that exists due to strict flux partitioning at the glucose-6-P node [240, 341]. The biosynthesis of one mol L-valine requires two mol NADPH (Figure 7.1), such that a natural overabundance of NADPH is potentially a major advantage during L-valine overproduction. Finally, the substantial increase in the L-valine titer in cultures of AW016-5, compared to AW015-5 (Figure 7.5B), due to the simultaneous mutation of *leuA* and *ilvA* is a similar phenomenon to that observed upon the mutation of *alaT*, encoding an aminotransferase that converts pyruvate and L-glutamate to L-alanine and 2-ketoglutarate (AlaT), and *ilvA* in *C. glutamicum* [310]. In our study, mutating *leuA* is essential as *ilvBHC* and *leuABCD* comprise a single operon, such that significant L-leucine production is inevitable in strains in which $P_{ilv\text{-}leu}$ has been replaced to relieve transcriptional regulation. On the other hand, abolished L-isoleucine biosynthesis should contribute less to the improved flux into L-valine overproduction as the expression of *ilvA* is repressed by CodY [318], which is likely active under our cultivation conditions.

To generate AW013-5, we successfully replaced three promoters and their corresponding transcriptional regulatory elements (i.e. $P_{ilv\text{-}leu}$, P_{als}, and P_{bcaP}), chromosomally integrated two expression cassettes (i.e. P_{grac}::*ybgE*:*ywaA* Δ*amyE* and P_{grac}::*ilvD* Δ*wprA*), mutated six genes (i.e. *bcd*, *leuA*, *ilvA*, *alsD*, *sigF*, and *pdhA*), and introduced four point mutations into a single ORF to generate the engineered protein $IlvH^{*}$, over nine successive rounds of editing to generate

AW013-5, demonstrating the efficacy of our CRISPR-Cas9 toolkit for advanced strain engineering. While we were consistently able to generate two mutations simultaneously, our attempt to replace $P_{ilv\text{-}leu,}$ and mutate *bcd* and *leuA* in a single round of editing was unsuccessful. An assessment of the individual editing and transformation efficiencies of all three targets revealed that the replacement of $P_{ilv\text{-}leu}$ with P_{grac} (~70% of 5×10^3 CFU μg_{DNA}^{-1}) was significantly less efficient then the mutation of *leuA* (~100% of ~10^4 CFU μg_{DNA}^{-1}) or *bcd* (~100% of ~10^5 CFU μg_{DNA}^{-1}) (Note that 50% of ~2×10^3 CFU μg_{DNA}^{-1} contained both P_{grac} in place of $P_{ilv\text{-}leu}$ and the *bcd* mutation when generating AW002-5). The editing and transformation efficiencies for different genomic targets can vary significantly due to the frequency of recombination events at respective loci [263], and the ratio of the sizes of the inserted and replaced DNA fragments significantly affects recombination efficiency [86]. These respective observations may explain the particularly low transformation efficiency for the simultaneous mutation of *leuA* and *ilvA* (~2×10^2 CFU μg_{DNA}^{-1}), and the generally lower editing and transformation efficiencies observed when chromosomally inserting genes, compared to gene mutations, in the present study. Accordingly, recombination appears to be the limiting step in applying the CRISPR-Cas9 system to genome editing in *B. subtilis*, and efforts to bolster its natural recombination efficiency are currently underway.

Chapter 8

Original contributions and recommendations

8.1 Original contributions

8.1.1 A comprehensive CRISPR-Cas9 toolkit

The most comprehensive and efficient CRISPR-Cas9 toolkit reported to date for *B. subtilis* was developed. At the same time this work was published, CRISPRi [342] and genome editing [216, 343] with the CRISPR-Cas9 system were reported in *B. subtilis*. However, the singe plasmid CRISPR-Cas9 systems developed by other groups are not suited to multiplexing or CRISPRi, which are two of the most important applications of this technology, such that their application to scalable strain engineering will be limited. On the other hand, we have demonstrated highly efficient gene mutations and insertions, continuous editing, multiplexing, and transcriptional interference with our toolkit, and have successfully applied it to advanced strain engineering through various case studies. Since the initial report, components of the toolkit have been distributed through Addgene, a nonprofit global plasmid repository.

8.1.2 Novel B. subtilis strains for high-level HA production

Using our toolkit, in combination with improved cloning methods (i.e. superior auto-evicting counter-selectable integration cassettes, and high-efficiency natural and artificial transformation protocols), we engineered the cell membrane of HA-producing *B. subtilis* strains to enhance the functional expression of heterologously expressed SeHAS, in turn, significantly improving HA production. These novel strains may be of industrial utility as microbial HA production replaces extraction from animal and avian sources, and our results suggest that

membrane engineering may be a broadly effective strategy to enhance the functional expression of transmembrane proteins. Moreover, removal of certain lipids from the membrane of HA-producing *B. subtilis* has shed new light on the lipid dependence for functional expression of SeHAS.

Similarly, we reduced the expression of *zwf* and *pfkA*, whose respective gene products are enzymes at the branchpoints of the PPP and glycolysis with cell wall biosynthesis, to divert carbon flux from central metabolism into HA biosynthesis. Individual repression of *zwf* and *pfkA* expression typically improved the HA titer at the expense of the MW. On the other hand, multiplexed repression of *zwf* and *pfkA* expression further enhanced the HA titer while modestly increasing the MW, compared to the control strain, resulting in the generation of potentially industrially relevant HA-producing *B. subtilis* strains. Accordingly, this strain engineering strategy is superior to the traditional approach of upregulating genes in the HA biosynthetic pathway, such that it can serve as a paradigm for the future development of heterologous and natural HA production strains, as well as those engineered to produce other metabolites. Moreover, we have provided new insight into the mechanism of HA biosynthesis by SeHAS in *B. subtilis* by artificially altering the supply of the precursors GlcUA and GlcNAc.

8.1.3 Bioprocess development for heterologous HA production in B. subtilis using oxygen vectors

We have identified several hydrocarbons and perfluorocarbons as oxygen vectors to enhance culture performance for heterologous HA production in *B. subtilis*. In particular, the addition of *n*-hexadecane, perfluoro-1,3-dimethylcyclohexane, and perfluoromethyldecalin resulted in significant enhancements to cell growth and HA production, albeit without notable

changes to the MW. We also observed that, in contrast to cultures of group C streptococci, higher shear rates may increase carbon flux through the HA biosynthetic pathway without negatively affecting the MW of produced HA, and that certain vectors may alter the functional expression of Class I HAS in *B. subtilis*. Taken together, the results of this study provide valuable insight for future bioprocess development in microbial HA production.

8.1.4 Novel B. subtilis strains for L-valine overproduction

Using our toolkit, we engineered the natural L-valine biosynthetic pathway to relieve transcriptional and allosteric inhibition in the presence of excess amino acids, resulting in a >14-fold increase in L-valine production relative to the wild-type strain. Further strain engineering revealed that pyruvate availability and competing amino acid biosynthetic pathways were limiting L-valine overproduction in *B. subtilis*, and combinatorial gene mutations to relieve these bottlenecks resulted in an ~50-fold increase in the L-valine titer, compared to the wild-type strain. While bioprocess development is required to reach production levels comparable to those obtained with *E. coli* and *C. glutamicum*, our strains show promise as biomanufacturing platforms for L-valine overproduction. Moreover, this case study has identified recombination efficiency as the limiting factor for the application of the CRISPR-Cas9 system in *B. subtilis*, providing us with a full assessment of and future direction to improve toolkit performance.

8.2 Recommendations

1. The toolkit described herein has proven to be an invaluable resource for advanced strain engineering as outlined in this thesis, and should find widespread use in the engineering of *B. subtilis* strains. While the multiplexing efficiency for two targets was consistently

high in this work, our success in higher order multiplexing has been limited. Editing three or more targets at once would require prior knowledge of the targets as being highly recombination-susceptible, which is likely a rare situation in real applications. Accordingly, enhancements to the natural recombination system of *B. subtilis*, or the introduction of viral recombination proteins may increase the multiplexing capacity of the toolkit. Highly efficient genome editing mediated by the SPP1 phage-derived GP35 recombinase was demonstrated in *B. subtilis* using phosphorothioated lagging-strand-targeting ssDNA as the editing template [344]. Another simple approach may be to overexpress proteins of the native *B. subtilis* recombination machinery (e.g. RecA) to enhance recombination efficiency, and both of these strategies are currently under investigation in our laboratory.

2. The major limitation of *B. subtilis* as a host for heterologous HA production is the inherently lower MW of the produced HA, compared to that of group C streptococci, which is the case for all non-native producers. We have employed two markedly different approaches to improve heterologous HA production in *B. subtilis*, i.e. cell membrane engineering and metabolic engineering to divert carbon flux into HA biosynthesis, in addition to the application of oxygen vectors to reduce shear stress without oxygen limitation, yet only modest improvements to the MW were obtained in all scenarios. On the other hand, supplementing cultures with GlcUA and, in particular, GlcNAc dramatically improved the MW of HA produced by AW006-3, such that improving the precursor supply ratio should be a primary focus. As previously discussed in Section 5.4, initial attempts to improve UDP-GlcNAc levels via repression of *tagO* or *murAA* expression resulted in growth defects, such that lower levels of CRISPRi-mediated

transcriptional repression of *tagO* and *murAA*, and potentially *murAB* and *mnaA*, should be explored as a means to improve the MW of HA produced by AW018-3 and AW019-3. Additionally, a better understanding of the adaptations of naturally producing streptococcal strains may provide opportunities to improve the MW of HA produced in engineered *B. subtilis*.

3. Based on our assessment of potential oxygen vectors, it appears that the effects of structurally similar compounds on HA production can differ significantly. For example, perfluorodecalin and perfluoromethyldecalin differ by only a single methyl group, yet perfluoromethyldecalin supplementation dramatically improved HA production compared to its unmethylated counterpart. As such, predictions of the performance of a given compound as an oxygen vector based on the results obtained with similar compounds may be inaccurate, and the assessment of additional hydrocarbons and perfluorocarbons as potential oxygen vectors is likely necessary to identify superior compounds to further enhance culture performance. Thus, it is recommended that additional compounds be evaluated as potential oxygen vectors, including those that have been successfully applied elsewhere. For example, enhanced HA production was observed in *S. zooepidemicus* cultures supplemented with *n*-dodecane [262], and forane F66E was shown to significantly improve oxygen transfer in *Enterobacter aerogenes* cultures [141]. Moreover, the evaluation of oxygen vectors in medium-cell-density fed-batch cultivations for HA production is of interest as oxygen limitation quickly ensues, necessitating excessively high agitation rates and oxygen supplementation to maintain culture performance.

4. To relieve the pyruvate limitation in our engineered L-valine-overproducing strains, we inactivated the pyruvate dehydrogenase complex via mutation of *pdhA*, necessitating the supplementation of acetate to maintain growth in cultures of Δ*pdhA* mutants. A preliminary assessment of L-valine overproduction in fed-batch cultures revealed that acetate metabolism is poor in our strains, which is not surprising given that *B. subtilis* does not possess an active glyoxylate shunt [345]. Furthermore, both CcpA and CodY repress the expression of *acsA* [318, 346], encoding acetyl-CoA synthetase that converts acetate to acetyl-CoA to initiate acetate metabolism, in nutrient-rich medium. Accordingly, activation of the glyoxylate shunt via expression of *aceB*, encoding isocitrate lyase, and *aceA*, encoding malate synthase, from *Bacillus licheniformis*, which was previously demonstrated in *B. subtilis* [345], and replacement of the *acsA* promoter and its corresponding regulatory elements with a strong constitutive promoter (e.g. $P_{grac.UPmod}$) should significantly improve acetate utilization in Δ*pdhA* mutants. These combined strategies may ultimately be necessary to achieve sufficient growth and, in turn, high-level L-valine overproduction in engineered *B. subtilis*, and are currently being explored in our laboratory.
5. The extension of amino acid biosynthetic pathways for the production of non-native alcohols has been reported, for example [347-349]. In particular, isobutanol was produced in *B. subtilis* by the conversion of 2-ketoisovalerate to isobutyraldehyde, via keto-acid decarboxylase, which is subsequently converted to isobutanol by alcohol dehydrogenase. As 2-ketoisovalerate is the direct precursor of L-valine, our engineered L-valine-overproducing strains should serve as ideal base strains from which to derive superior isobutanol-producing *B. subtilis* strains. In addition, we have identified a novel

pathway for the conversion of 2-ketoisovalerate to 1-butanol that exploits the native L-valine degradation pathway of *B. subtilis*. Currently, strain engineering for isobutanol and 1-butanol production in *B. subtilis* are underway in our laboratory.

References

[1] M. Schallmey, A. Singh, and O. P. Ward, "Developments in the use of *Bacillus* species for industrial production," *Canadian Journal of Microbiology,* vol. 50, pp. 1-17, 2004/01/01 2004.

[2] L. Westers, H. Westers, and W. J. Quax, "*Bacillus subtilis* as cell factory for pharmaceutical proteins: a biotechnological approach to optimize the host organism," *Biochimica et Biophysica Acta (BBA) - Molecular Cell Research,* vol. 1694, pp. 299-310, 11/11/ 2004.

[3] G. Walsh, "Biopharmaceutical benchmarks 2010," *Nat Biotech,* vol. 28, pp. 917-924, 2010.

[4] S. Sabri, L. K. Nielsen, and C. E. Vickers, "Molecular control of sucrose utilization in *Escherichia coli* W, an efficient sucrose-utilizing strain," *Applied and Environmental Microbiology,* vol. 79, pp. 478-487, January 15, 2013 2013.

[5] B. Widner, R. Behr, S. Von Dollen, M. Tang, T. Heu, A. Sloma, *et al.*, "Hyaluronic acid production in *Bacillus subtilis*," *Applied and environmental microbiology,* vol. 71, pp. 3747-3752, 2005.

[6] Z. Mao, H.-D. Shin, and R. Chen, "A recombinant *E. coli* bioprocess for hyaluronan synthesis," *Applied Microbiology and Biotechnology,* vol. 84, pp. 63-69, 2009/08/01 2009.

[7] C. R. Fischer, D. Klein-Marcuschamer, and G. Stephanopoulos, "Selection and optimization of microbial hosts for biofuels production," *Metabolic Engineering,* vol. 10, pp. 295-304, 11// 2008.

[8] C. R. Harwood and S. M. Cutting, *Molecular biological methods for Bacillus*. Chichester; New York: Wiley, 1990.

[9] H. D. Nguyen, Q. A. Nguyen, R. C. Ferreira, L. C. S. Ferreira, L. T. Tran, and W. Schumann, "Construction of plasmid-based expression vectors for *Bacillus subtilis* exhibiting full structural stability," *Plasmid,* vol. 54, pp. 241-248, 11// 2005.

[10] B. Sarrouh, T. M. Santos, Miyoshi, Anderson, R. Dias, and V. Azevedo, "Up-to-date insight on industrial enzymes applications and global market," *Journal of Bioprocessing & Biotechniques,* vol. S4:002, 2012.

[11] J. D. Keasling, "Manufacturing molecules through metabolic engineering," *Science,* vol. 330, pp. 1355-1358, December 3, 2010 2010.

[12] H. Dong and D. Zhang, "Current development in genetic engineering strategies of *Bacillus* species," *Microbial Cell Factories,* vol. 13, pp. 1-11, 2014.

[13] X.-Z. Zhang, X. Yan, Z.-L. Cui, Q. Hong, and S.-P. Li, "*mazF*, a novel counter-selectable marker for unmarked chromosomal manipulation in *Bacillus subtilis*," *Nucleic Acids Research,* vol. 34, pp. e71-e71, 05/19

[14] C. Fabret, S. Dusko Ehrlich, and P. Noirot, "A new mutation delivery system for genome-scale approaches in *Bacillus subtilis*," *Molecular Microbiology,* vol. 46, pp. 25-36, 2002.

[15] X. Yan, H.-J. Yu, Q. Hong, and S.-P. Li, "Cre/*lox* system and PCR-based genome engineering in *Bacillus subtilis*," *Applied and Environmental Microbiology,* vol. 74, pp. 5556-5562, September 1, 2008 2008.

[16] P. T. Chen, J.-F. Shaw, Y.-P. Chao, T.-H. David Ho, and S.-M. Yu, "Construction of chromosomally located T7 expression system for production of heterologous secreted

proteins in *Bacillus subtilis*," *Journal of Agricultural and Food Chemistry,* vol. 58, pp. 5392-5399, 2010/05/12 2010.

[17] Y. Ishino, H. Shinagawa, K. Makino, M. Amemura, and A. Nakata, "Nucleotide sequence of the iap gene, responsible for alkaline phosphatase isozyme conversion in *Escherichia coli,* and identification of the gene product," *Journal of Bacteriology,* vol. 169, pp. 5429-5433, December 1, 1987 1987.

[18] R. Barrangou, C. Fremaux, H. Deveau, M. Richards, P. Boyaval, S. Moineau, *et al.*, "CRISPR provides acquired resistance against viruses in prokaryotes," *Science,* vol. 315, pp. 1709-1712, March 23, 2007 2007.

[19] Y. Li, Z. Lin, C. Huang, Y. Zhang, Z. Wang, Y.-j. Tang, *et al.*, "Metabolic engineering of *Escherichia coli* using CRISPR–Cas9 meditated genome editing," *Metabolic Engineering,* vol. 31, pp. 13-21, 9// 2015.

[20] Y. Jiang, B. Chen, C. Duan, B. Sun, J. Yang, and S. Yang, "Multigene editing in the *Escherichia coli* genome via the CRISPR-Cas9 system," *Applied and Environmental Microbiology,* vol. 81, pp. 2506-2514, April 1, 2015 2015.

[21] Andrew A. Horwitz, Jessica M. Walter, Max G. Schubert, Stephanie H. Kung, K. Hawkins, Darren M. Platt, *et al.*, "Efficient multiplexed integration of synergistic alleles and metabolic pathways in yeasts via crispr-cas," *Cell Systems,* vol. 1, pp. 88-96, 7/29/ 2015.

[22] Z. Bao, H. Xiao, J. Liang, L. Zhang, X. Xiong, N. Sun, *et al.*, "Homology-integrated CRISPR–Cas (HI-CRISPR) system for one-step multigene disruption in *Saccharomyces cerevisiae*," *ACS Synthetic Biology,* 2014/09/10 2014.

[23] Lei S. Qi, Matthew H. Larson, Luke A. Gilbert, Jennifer A. Doudna, Jonathan S. Weissman, Adam P. Arkin, *et al.*, "Repurposing CRISPR as an RNA-guided platform for sequence-specific control of gene expression," *Cell,* vol. 152, pp. 1173-1183, 2013.

[24] J. M. van Dijl and M. Hecker, "*Bacillus subtilis*: from soil bacterium to super-secreting cell factory," *Microbial Cell Factories,* vol. 12, p. 3, 2013.

[25] F. Kawamura and R. H. Doi, "Construction of a *Bacillus subtilis* double mutant deficient in extracellular alkaline and neutral proteases," *Journal of Bacteriology,* vol. 160, pp. 442-444, October 1, 1984 1984.

[26] S.-C. Wu, J. C. Yeung, Y. Duan, R. Ye, S. J. Szarka, H. R. Habibi, *et al.*, "Functional production and characterization of a fibrin-specific single-chain antibody fragment from *Bacillus subtilis*: effects of molecular chaperones and a wall-bound protease on antibody fragment production," *Applied and Environmental Microbiology,* vol. 68, pp. 3261-3269.

[27] K. Stephenson, S. Bron, and C. R. Harwood, "Cellular lysis in *Bacillus subtilis*; the affect of multiple extracellular protease deficiencies," *Letters in Applied Microbiology,* vol. 29, pp. 141-145, 1999.

[28] S.-C. Wu, R. Ye, X.-C. Wu, S.-C. Ng, and S.-L. Wong, "Enhanced secretory production of a single-chain antibody fragment from *Bacillus subtilis* by coproduction of molecular chaperones," *Journal of Bacteriology,* vol. 180, pp. 2830-2835, June 1, 1998 1998.

[29] C. P. Chou, "Engineering cell physiology to enhance recombinant protein production in *Escherichia coli*," *Applied Microbiology and Biotechnology,* vol. 76, pp. 521-532, 2007/09/01 2007.

[30] H. Leonhardt and J. C. Alonso, "Parameters affecting plasmid stability in *Bacillus subtilis*," *Gene,* vol. 103, pp. 107-111, 1991/07/15 1991.

[31] S. Bron, S. Holsappel, G. Venema, and B. H. Peeters, "Plasmid deletion formation between short direct repeats in *Bacillus subtilis* is stimulated by single-stranded rolling-circle replication intermediates," *Molecular and General Genetics MGG,* vol. 226, pp. 88-96, 1991/04/01 1991.
[32] S. Bron, W. Meijer, S. Holsappel, and P. Haima, "Plasmid instability and molecular cloning in *Bacillus subtilis*," *Research in Microbiology,* vol. 142, pp. 875-883, // 1991.
[33] L. Jannière, C. Bruand, and S. Dusko Ehrlich, "Structurally stable *Bacillus subtilis* cloning vectors," *Gene,* vol. 87, pp. 53-61, 3/1/ 1990.
[34] G. del Solar, R. Giraldo, M. J. Ruiz-Echevarría, M. Espinosa, and R. Díaz-Orejas, "Replication and control of circular bacterial plasmids," *Microbiology and Molecular Biology Reviews,* vol. 62, pp. 434-464, June 1, 1998 1998.
[35] S. D. Ehrlich, C. Bruand, S. Sozhamannan, P. Dabert, M. F. Gros, L. Jannière, *et al.*, "Plasmid replication and structural stability in *Bacillus subtilis*," *Research in Microbiology,* vol. 142, pp. 869-873, 1991/01/01 1991.
[36] W. J. J. Meijer, A. J. d. Boer, S. v. Tongeren, G. Venema, and S. Bron, "Characterization of the replication region of the *Bacillus subtilis* plasmid pLS20: a noval type to replicon," *Nucleic Acids Research,* vol. 23, pp. 3214-3223, August 25, 1995 1995.
[37] T. Tanaka and M. Ogura, "A novel Bacillus natto plasmid pLS32 capable of replication in *Bacillus subtilis*," *FEBS Letters,* vol. 422, pp. 243-246, 1/30/ 1998.
[38] M. A. Titok, J. Chapuis, Y. V. Selezneva, A. V. Lagodich, V. A. Prokulevich, S. D. Ehrlich, *et al.*, "*Bacillus subtilis* soil isolates: plasmid replicon analysis and construction of a new theta-replicating vector," *Plasmid,* vol. 49, pp. 53-62, 1// 2003.
[39] T. T. P. Phan, H. D. Nguyen, and W. Schumann, "Novel plasmid-based expression vectors for intra- and extracellular production of recombinant proteins in *Bacillus subtilis*," *Protein Expression and Purification,* vol. 46, pp. 189-195, 4// 2006.
[40] T. T. P. Phan, H. D. Nguyen, and W. Schumann, "Development of a strong intracellular expression system for *Bacillus subtilis* by optimizing promoter elements," *Journal of Biotechnology,* vol. 157, pp. 167-172, 1// 2012.
[41] S. C. Makrides, "Strategies for achieving high-level expression of genes in *Escherichia coli*," *Microbiological Reviews,* vol. 60, pp. 512-38, September 1, 1996 1996.
[42] N. Cavallarin, "Single chain antibody fragment production and metabolic engineering of hyaluronic acid in *Bacillus* and *Escherichia coli*," PhD, Veterinary Sciences, Experimental Veterinary Science, University of Padova, Padua, Italy, 2011.
[43] P. Nicolas, U. Mäder, E. Dervyn, T. Rochat, A. Leduc, N. Pigeonneau, *et al.*, "Condition-dependent transcriptome reveals high-level regulatory architecture in *Bacillus subtilis*," *Science,* vol. 335, pp. 1103-1106, March 2, 2012 2012.
[44] J. Spizizen, "Transformation of biochemically deficient strains of *Bacillus subtilis* by deoxyribonucleate," *Proceedings of the National Academy of Sciences of the United States of America,* vol. 44, pp. 1072-1078, 1958.
[45] R. M. Berka, J. Hahn, M. Albano, I. Draskovic, M. Persuh, X. Cui, *et al.*, "Microarray analysis of the *Bacillus subtilis* K-state: genome-wide expression changes dependent on ComK," *Molecular Microbiology,* vol. 43, pp. 1331-1345, // 2002.
[46] M. Ogura, H. Yamaguchi, K. Kobayashi, N. Ogasawara, Y. Fujita, and T. Tanaka, "Whole-genome analysis of genes regulated by the *Bacillus subtilis* competence transcription factor ComK," *Journal of Bacteriology,* vol. 184, pp. 2344-2351, May 1, 2002 2002.

[47] J. M. Solomon, R. Magnuson, A. Srivastava, and A. D. Grossman, "Convergent sensing pathways mediate response to two extracellular competence factors in *Bacillus subtilis*," *Genes & Development,* vol. 9, pp. 547-558, March 1, 1995 1995.
[48] C. D'Souza, M. M. Nakano, and P. Zuber, "Identification of *comS*, a gene of the *srfA* operon that regulates the establishment of genetic competence in *Bacillus subtilis*," *Proceedings of the National Academy of Sciences of the United States of America,* vol. 91, pp. 9397-9401, 1994.
[49] H. Maamar and D. Dubnau, "Bistability in the *Bacillus subtilis* K-state (competence) system requires a positive feedback loop," *Molecular microbiology,* vol. 56, pp. 10.1111/j.1365-2958.2005.04592.x, 2005.
[50] B. J. Haijema, L. W. Hamoen, J. Kooistra, G. Venema, and D. van Sinderen, "Expression of the ATP-dependent deoxyribonuclease of *Bacillus subtilis* is under competence-mediated control," *Molecular Microbiology,* vol. 15, pp. 203-211, 1995.
[51] B. J. Haijema, D. van Sinderen, K. Winterling, J. Kooistra, G. Venema, and L. W. Hamoen, "Regulated expression of the *dinR* and *recA* genes during competence development and SOS induction in *Bacillus subtilis*," *Molecular Microbiology,* vol. 22, pp. 75-85, 1996.
[52] I. Chen and D. Dubnau, "DNA uptake during bacterial transformation," *Nat Rev Micro,* vol. 2, pp. 241-249, 03//print 2004.
[53] R. Provvedi and D. Dubnau, "ComEA is a DNA receptor for transformation of competent *Bacillus subtilis*," *Molecular Microbiology,* vol. 31, pp. 271-280, 1999.
[54] J. Hahn, B. Maier, B. J. Haijema, M. Sheetz, and D. Dubnau, "Transformation proteins and DNA uptake localize to the cell poles in *Bacillus subtilis*," *Cell,* vol. 122, pp. 59-71, 7/15/ 2005.
[55] M. Kaufenstein, M. van der Laan, and P. L. Graumann, "The three-layered DNA uptake machinery at the cell pole in competent *Bacillus subtilis* cells is a stable complex," *Journal of Bacteriology,* vol. 193, pp. 1633-1642, April 1, 2011 2011.
[56] J. A. Londoño-Vallejo and D. Dubnau, "Mutation of the putative nucleotide binding site of the *Bacillus subtilis* membrane protein ComFA abolishes the uptake of DNA during transformation," *Journal of Bacteriology,* vol. 176, pp. 4642-4645, August 1, 1994 1994.
[57] T. Yadav, B. Carrasco, J. Hejna, Y. Suzuki, K. Takeyasu, and J. C. Alonso, "*Bacillus subtilis* DprA Recruits RecA onto Single-stranded DNA and Mediates Annealing of Complementary Strands Coated by SsbB and SsbA," *Journal of Biological Chemistry,* vol. 288, pp. 22437-22450, August 2, 2013 2013.
[58] T. Yadav, B. Carrasco, A. R. Myers, N. P. George, J. L. Keck, and J. C. Alonso, "Genetic recombination in *Bacillus subtilis*: a division of labor between two single-strand DNA-binding proteins," *Nucleic Acids Research,* vol. 40, pp. 5546-5559, July 1, 2012 2012.
[59] C. Manfredi, Y. Suzuki, T. Yadav, K. Takeyasu, and J. C. Alonso, "RecO-mediated DNA homology search and annealing is facilitated by SsbA," *Nucleic Acids Research,* vol. 38, pp. 6920-6929, November 1, 2010 2010.
[60] B. Carrasco, T. Yadav, E. Serrano, and J. C. Alonso, "*Bacillus subtilis* RecO and SsbA are crucial for RecA-mediated recombinational DNA repair," *Nucleic Acids Research,* May 22, 2015 2015.
[61] B. Carrasco, C. Manfredi, S. Ayora, and J. C. Alonso, "*Bacillus subtilis* SsbA and dATP regulate RecA nucleation onto single-stranded DNA," *DNA Repair,* vol. 7, pp. 990-996, 6/1/ 2008.

[62] C. Anagnostopoulos and J. Spizizen, "Requirements for transformation in *Bacillus subtilis*," *Journal of Bacteriology,* vol. 81, pp. 741-746, 1961.
[63] R. E. Yasbin, G. A. Wilson, and F. E. Young, "Transformation and transfection in lysogenic strains of *Bacillus subtilis*: evidence for selective induction of prophage in competent cells," *Journal of Bacteriology,* vol. 121, pp. 296-304, 1975.
[64] T. Shi, G. Wang, Z. Wang, J. Fu, T. Chen, and X. Zhao, "Establishment of a markerless mutation delivery system in *Bacillus subtilis* stimulated by a double-strand break in the chromosome," *PLoS ONE,* vol. 8, p. e81370, 2013.
[65] R. Rahmer, K. M. Heravi, and J. Altenbuchner, "Construction of a super-competent Bacillus subtilis 168 using the PmtlA-comKS inducible cassette," *Frontiers in microbiology,* vol. 6, 2015.
[66] J. T. Heap, M. Ehsaan, C. M. Cooksley, Y.-K. Ng, S. T. Cartman, K. Winzer, *et al.*, "Integration of DNA into bacterial chromosomes from plasmids without a counter-selection marker," *Nucleic Acids Research,* vol. 40, pp. e59-e59, 01/18
[67] A. Brans, P. Filée, A. Chevigné, A. Claessens, and B. Joris, "New Integrative method to generate *Bacillus subtilis* recombinant strains free of selection markers," *Applied and Environmental Microbiology,* vol. 70, pp. 7241-7250, December 1, 2004 2004.
[68] S. Turan, J. Kuehle, A. Schambach, C. Baum, and J. Bode, "Multiplexing RMCE: versatile extensions of the Flp-recombinase-mediated cassette-exchange technology," *Journal of Molecular Biology,* vol. 402, pp. 52-69, 9/10/ 2010.
[69] H. P. Schweizer, "Applications of the *Saccharomyces cerevisiae* Flp-*FRT* System in Bacterial Genetics," *Journal of Molecular Microbiology and Biotechnology,* vol. 5, pp. 67-77, 2003.
[70] Y. Wang, J. Weng, R. Waseem, X. Yin, R. Zhang, and Q. Shen, "*Bacillus subtilis* genome editing using ssDNA with short homology regions," *Nucleic Acids Research,* vol. 40, p. e91, July 1, 2012 2012.
[71] K. S. Makarova, L. Aravind, N. V. Grishin, I. B. Rogozin, and E. V. Koonin, "A DNA repair system specific for thermophilic Archaea and bacteria predicted by genomic context analysis," *Nucleic Acids Research,* vol. 30, pp. 482-496, January 15, 2002 2002.
[72] F. J. M. Mojica, C. Díez-Villaseñor, E. Soria, and G. Juez, "Biological significance of a family of regularly spaced repeats in the genomes of Archaea, Bacteria and mitochondria," *Molecular Microbiology,* vol. 36, pp. 244-246, 2000.
[73] A. Bolotin, B. Quinquis, A. Sorokin, and S. D. Ehrlich, "Clustered regularly interspaced short palindrome repeats (CRISPRs) have spacers of extrachromosomal origin," *Microbiology,* vol. 151, pp. 2551-2561, 2005.
[74] C. Pourcel, G. Salvignol, and G. Vergnaud, "CRISPR elements in *Yersinia pestis* acquire new repeats by preferential uptake of bacteriophage DNA, and provide additional tools for evolutionary studies," *Microbiology,* vol. 151, pp. 653-663, 2005.
[75] K. S. Makarova, D. H. Haft, R. Barrangou, S. J. J. Brouns, E. Charpentier, P. Horvath, *et al.*, "Evolution and classification of the CRISPR–Cas systems," *Nat Rev Micro,* vol. 9, pp. 467-477, 06//print 2011.
[76] J. van der Oost, E. R. Westra, R. N. Jackson, and B. Wiedenheft, "Unravelling the structural and mechanistic basis of CRISPR-Cas systems," *Nat Rev Micro,* vol. 12, pp. 479-492, 07//print 2014.
[77] J. A. Doudna and E. Charpentier, "The new frontier of genome engineering with CRISPR-Cas9," *Science,* vol. 346, November 28, 2014 2014.

[78] E. Deltcheva, K. Chylinski, C. M. Sharma, K. Gonzales, Y. Chao, Z. A. Pirzada, *et al.*, "CRISPR RNA maturation by trans-encoded small RNA and host factor RNase III," *Nature,* vol. 471, pp. 602-607, 03/31/print 2011.
[79] M. Jinek, K. Chylinski, I. Fonfara, M. Hauer, J. A. Doudna, and E. Charpentier, "A programmable dual-RNA–guided DNA endonuclease in adaptive bacterial immunity," *Science,* vol. 337, pp. 816-821, August 17, 2012 2012.
[80] M. Jinek, F. Jiang, D. W. Taylor, S. H. Sternberg, E. Kaya, E. Ma, *et al.*, "Structures of Cas9 endonucleases reveal RNA-mediated conformational activation," *Science,* vol. 343, March 14, 2014 2014.
[81] S. H. Sternberg, S. Redding, M. Jinek, E. C. Greene, and J. A. Doudna, "DNA interrogation by the CRISPR RNA-guided endonuclease Cas9," *Nature,* vol. 507, pp. 62-67, 03/06/print 2014.
[82] W. Jiang, D. Bikard, D. Cox, F. Zhang, and L. A. Marraffini, "RNA-guided editing of bacterial genomes using CRISPR-Cas systems," *Nat Biotech,* vol. 31, pp. 233-239, 03//print 2013.
[83] C. Anders, O. Niewoehner, A. Duerst, and M. Jinek, "Structural basis of PAM-dependent target DNA recognition by the Cas9 endonuclease," *Nature,* vol. 513, pp. 569-573, 09/25/print 2014.
[84] P. Mali, L. Yang, K. M. Esvelt, J. Aach, M. Guell, J. E. DiCarlo, *et al.*, "RNA-Guided human genome engineering via Cas9," *Science,* vol. 339, pp. 823-826, February 15, 2013 2013.
[85] L. Cong, F. A. Ran, D. Cox, S. Lin, R. Barretto, N. Habib, *et al.*, "Multiplex genome engineering using CRISPR/Cas systems," *Science,* vol. 339, pp. 819-823, February 15, 2013 2013.
[86] M. E. Pyne, M. Moo-Young, D. A. Chung, and C. P. Chou, "Coupling the CRISPR/Cas9 system to lambda Red recombineering enables simplified chromosomal gene replacement in *Escherichia coli*," *Applied and Environmental Microbiology,* May 22, 2015 2015.
[87] H. Huang, G. Zheng, W. Jiang, H. Hu, and Y. Lu, "One-step high-efficiency CRISPR/Cas9-mediated genome editing in *Streptomyces*," *Acta Biochimica et Biophysica Sinica,* vol. 47, pp. 231-243, April 1, 2015 2015.
[88] J.-H. Oh and J.-P. van Pijkeren, "CRISPR–Cas9-assisted recombineering in *Lactobacillus reuteri*," *Nucleic Acids Research,* vol. 42, p. e131, September 29, 2014 2014.
[89] Y. Wang, Z.-T. Zhang, S.-O. Seo, K. Choi, T. Lu, Y.-S. Jin, *et al.*, "Markerless chromosomal gene deletion in *Clostridium beijerinckii* using CRISPR/Cas9 system," *Journal of Biotechnology,* vol. 200, pp. 1-5, 4/20/ 2015.
[90] J. Z. Jacobs, K. M. Ciccaglione, V. Tournier, and M. Zaratiegui, "Implementation of the CRISPR-Cas9 system in fission yeast," *Nat Commun,* vol. 5, 10/29/online 2014.
[91] Andrew R. Bassett, C. Tibbit, Chris P. Ponting, and J.-L. Liu, "Highly efficient targeted mutagenesis of drosophila with the CRISPR/Cas9 system," *Cell Reports,* vol. 4, pp. 220-228, 7/11/ 2013.
[92] W. Y. Hwang, Y. Fu, D. Reyon, M. L. Maeder, S. Q. Tsai, J. D. Sander, *et al.*, "Efficient genome editing in zebrafish using a CRISPR-Cas system," *Nat Biotech,* vol. 31, pp. 227-229, 03//print 2013.
[93] J.-F. Li, J. E. Norville, J. Aach, M. McCormack, D. Zhang, J. Bush, *et al.*, "Multiplex and homologous recombination-mediated genome editing in *Arabidopsis* and *Nicotiana*

benthamiana using guide RNA and Cas9," *Nat Biotech,* vol. 31, pp. 688-691, 08//print 2013.

[94] H. Kim, T. Ishidate, K. S. Ghanta, M. Seth, D. Conte, M. Shirayama, *et al.*, "A Co-CRISPR Strategy for Efficient Genome Editing in *Caenorhabditis elegans*," *Genetics,* vol. 197, pp. 1069-1080, 2014-08-01 00:00:00 2014.

[95] F. J. Isaacs, D. J. Dwyer, C. Ding, D. D. Pervouchine, C. R. Cantor, and J. J. Collins, "Engineered riboregulators enable post-transcriptional control of gene expression," *Nat Biotech,* vol. 22, pp. 841-847, 07//print 2004.

[96] D. Na, S. M. Yoo, H. Chung, H. Park, J. H. Park, and S. Y. Lee, "Metabolic engineering of *Escherichia coli* using synthetic small regulatory RNAs," *Nat Biotech,* vol. 31, pp. 170-174, 02//print 2013.

[97] S. Man, R. Cheng, C. Miao, Q. Gong, Y. Gu, X. Lu, *et al.*, "Artificial trans-encoded small non-coding RNAs specifically silence the selected gene expression in bacteria," *Nucleic Acids Research,* vol. 39, p. e50, April 1, 2011 2011.

[98] R. P. Desai and E. T. Papoutsakis, "Antisense RNA Strategies for Metabolic Engineering of *Clostridium acetobutylicum*," *Applied and Environmental Microbiology,* vol. 65, pp. 936-945, March 1, 1999 1999.

[99] J. Y. H. Kim and H. J. Cha, "Down-regulation of acetate pathway through antisense strategy in *Escherichia coli*: Improved foreign protein production," *Biotechnology and Bioengineering,* vol. 83, pp. 841-853, 2003.

[100] Luke A. Gilbert, Matthew H. Larson, L. Morsut, Z. Liu, Gloria A. Brar, Sandra E. Torres, *et al.*, "CRISPR-mediated modular rna-guided regulation of transcription in eukaryotes," *Cell,* vol. 154, pp. 442-451.

[101] Luke A. Gilbert, Max A. Horlbeck, B. Adamson, Jacqueline E. Villalta, Y. Chen, Evan H. Whitehead, *et al.*, "Genome-scale CRISPR-mediated control of gene repression and activation," *Cell,* vol. 159, pp. 647-661, 10/23/ 2014.

[102] S. Konermann, M. D. Brigham, A. E. Trevino, J. Joung, O. O. Abudayyeh, C. Barcena, *et al.*, "Genome-scale transcriptional activation by an engineered CRISPR-Cas9 complex," *Nature,* vol. 517, pp. 583-588, 01/29/print 2015.

[103] L. Lv, Y.-L. Ren, J.-C. Chen, Q. Wu, and G.-Q. Chen, "Application of CRISPRi for prokaryotic metabolic engineering involving multiple genes, a case study: Controllable P(3HB-co-4HB) biosynthesis," *Metabolic Engineering,* vol. 29, pp. 160-168, 5// 2015.

[104] K. Goa and P. Benfield, "Hyaluronic acid," *Drugs,* vol. 47, pp. 536-566, 1994/03/01 1994.

[105] L. Liu, Y. Liu, J. Li, G. Du, and J. Chen, "Microbial production of hyaluronic acid: current state, challenges, and perspectives," *Microbial Cell Factories,* vol. 10, p. 99, 2011.

[106] B. Chong, L. Blank, R. McLaughlin, and L. Nielsen, "Microbial hyaluronic acid production," *Applied Microbiology and Biotechnology,* vol. 66, pp. 341-351, 2005/01/01 2005.

[107] P. L. DeAngelis, J. Papaconstantinou, and P. H. Weigel, "Molecular cloning, identification, and sequence of the hyaluronan synthase gene from group A *Streptococcus pyogenes*," *Journal of Biological Chemistry,* vol. 268, pp. 19181-19184, September 15, 1993 1993.

[108] K. Kumari and P. H. Weigel, "Molecular cloning, expression, and characterization of the authentic hyaluronan synthase from group C *Streptococcus equisimilis*," *Journal of Biological Chemistry,* vol. 272, pp. 32539-32546, December 19, 1997 1997.
[109] P. L. DeAngelis, W. Jing, R. R. Drake, and A. M. Achyuthan, "Identification and molecular cloning of a unique hyaluronan synthase from *Pasteurella multocida*," *Journal of Biological Chemistry,* vol. 273, pp. 8454-8458, April 3, 1998 1998.
[110] P. H. Weigel, V. C. Hascall, and M. Tammi, "Hyaluronan synthases," *Journal of Biological Chemistry,* vol. 272, pp. 13997-14000, May 30, 1997 1997.
[111] P. H. Weigel and P. L. DeAngelis, "Hyaluronan synthases: A decade-plus of novel glycosyltransferases," *Journal of Biological Chemistry,* vol. 282, pp. 36777-36781, December 21, 2007 2007.
[112] W. Jing and P. L. DeAngelis, "Dissection of the two transferase activities of the *Pasteurella multocida* hyaluronan synthase: two active sites exist in one polypeptide," *Glycobiology,* vol. 10, pp. 883-889, September 1, 2000 2000.
[113] C. Heldermon, P. L. DeAngelis, and P. H. Weigel, "Topological organization of the hyaluronan synthase from *Streptococcus pyogenes*," *Journal of Biological Chemistry,* vol. 276, pp. 2037-2046, January 19, 2001 2001.
[114] N. Itano and K. Kimata, "Mammalian hyaluronan synthases," *IUBMB Life,* vol. 54, pp. 195-199, 2002.
[115] P. H. Weigel, "Functional characteristics and catalytic mechanisms of the bacterial hyaluronan synthases," *IUBMB Life,* vol. 54, pp. 201-211, 2002.
[116] G. Ouskova, B. Spellerberg, and P. Prehm, "Hyaluronan release from *Streptococcus pyogenes*: export by an ABC transporter," *Glycobiology,* vol. 14, pp. 931-938, October 1, 2004 2004.
[117] A. Medina, J. Lin, and P. Weigel, "Hyaluronan synthase mediates dye translocation across liposomal membranes," *BMC Biochemistry,* vol. 13, p. 2, 2012.
[118] C. Hubbard, J. T. McNamara, C. Azumaya, M. S. Patel, and J. Zimmer, "The hyaluronan synthase catalyzes the synthesis and membrane translocation of hyaluronan," *Journal of Molecular Biology,* vol. 418, pp. 21-31, 4/20/ 2012.
[119] V. L. Tlapak-Simmons, E. S. Kempner, B. A. Baggenstoss, and P. H. Weigel, "The Active Streptococcal Hyaluronan Synthases (HASs) Contain a Single HAS Monomer and Multiple Cardiolipin Molecules," *Journal of Biological Chemistry,* vol. 273, pp. 26100-26109, October 2, 1998 1998.
[120] M. X. Triscott and I. van de Rijn, "Solubilization of hyaluronic acid synthetic activity from streptococci and its activation with phospholipids," *Journal of Biological Chemistry,* vol. 261, pp. 6004-6009, May 5, 1986 1986.
[121] V. L. Tlapak-Simmons, B. A. Baggenstoss, T. Clyne, and P. H. Weigel, "Purification and lipid dependence of the recombinant hyaluronan synthases from *Streptococcus pyogenes* and *Streptococcus equisimilis*," *Journal of Biological Chemistry,* vol. 274, pp. 4239-4245, February 12, 1999 1999.
[122] V. L. Tlapak-Simmons, C. A. Baron, and P. H. Weigel, "Characterization of the purified hyaluronan synthase from *Streptococcus equisimilis*," *Biochemistry,* vol. 43, pp. 9234-9242, 2004.
[123] P. H. Weigel, Z. Kyossev, and L. C. Torres, "Phospholipid dependence and liposome reconstitution of purified hyaluronan synthase," *Journal of Biological Chemistry,* vol. 281, pp. 36542-36551, December 1, 2006 2006.

[124] J.-H. Im, J.-M. Song, J.-H. Kang, and D.-J. Kang, "Optimization of medium components for high-molecular-weight hyaluronic acid production by *Streptococcus* sp. ID9102 via a statistical approach," *Journal of Industrial Microbiology & Biotechnology,* vol. 36, pp. 1337-1344, 2009/11/01 2009.
[125] J.-H. Kim, S.-J. Yoo, D.-K. Oh, Y.-G. Kweon, D.-W. Park, C.-H. Lee, *et al.*, "Selection of a *Streptococcus equi*. mutant and optimization of culture conditions for the production of high molecular weight hyaluronic acid," *Enzyme and Microbial Technology,* vol. 19, pp. 440-445, 11/1/ 1996.
[126] D. L. Crater and I. van de Rijn, "Hyaluronic acid synthesis operon (*has*) expression in group A streptococci," *Journal of Biological Chemistry,* vol. 270, pp. 18452-18458, August 4, 1995 1995.
[127] B. Soldo, V. Lazarevic, M. Pagni, and D. Karamata, "Teichuronic acid operon of *Bacillus subtilis* 168," *Molecular Microbiology,* vol. 31, pp. 795-805, 1999.
[128] L.-J. Chien and C.-K. Lee, "Enhanced hyaluronic acid production in *Bacillus subtilis* by coexpressing bacterial hemoglobin," *Biotechnology Progress,* vol. 23, pp. 1017-1022, 2007.
[129] Y. Jia, J. Zhu, X. Chen, D. Tang, D. Su, W. Yao, *et al.*, "Metabolic engineering of *Bacillus subtilis* for the efficient biosynthesis of uniform hyaluronic acid with controlled molecular weights," *Bioresource Technology,* vol. 132, pp. 427-431, 3// 2013.
[130] P. Jin, Z. Kang, P. Yuan, G. Du, and J. Chen, "Production of specific-molecular-weight hyaluronan by metabolically engineered *Bacillus subtilis* 168," *Metabolic Engineering,* vol. 35, pp. 21-30, 5// 2016.
[131] L.-J. Chien and C.-K. Lee, "Hyaluronic acid production by recombinant *Lactococcus lactis*," *Applied Microbiology and Biotechnology,* vol. 77, pp. 339-346, 2007/11/01 2007.
[132] S. Prasad, G. Jayaraman, and K. B. Ramachandran, "Hyaluronic acid production is enhanced by the additional co-expression of UDP-glucose pyrophosphorylase in *Lactococcus lactis*," *Applied Microbiology and Biotechnology,* vol. 86, pp. 273-283, 2010/03/01 2010.
[133] T. Yoshimura, N. Shibata, Y. Hamano, and K. Yamanaka, "Heterologous production of hyaluronic acid in an ε-poly-L-lysine producer, *Streptomyces albulus*," *Applied and Environmental Microbiology,* vol. 81, pp. 3631-3640, June 1, 2015 2015.
[134] H. Yu and G. Stephanopoulos, "Metabolic engineering of *Escherichia coli* for biosynthesis of hyaluronic acid," *Metabolic Engineering,* vol. 10, pp. 24-32, 1// 2008.
[135] Z. Mao and R. R. Chen, "Recombinant synthesis of hyaluronan by *Agrobacterium* sp.," *Biotechnology Progress,* vol. 23, pp. 1038-1042, 2007.
[136] X.-J. Duan, L. Yang, X. Zhang, and W.-S. Tan, "Effect of oxygen and shear stress on molecular weight of hyaluronic acid," *Journal of Microbiology and Biotechnology,* vol. 18, pp. 718-724, 2008.
[137] T. L. da Silva, V. Calado, N. Silva, R. L. Mendes, S. S. Alves, J. M. T. Vasconcelos, *et al.*, "Effects of hydrocarbon additions on gas-liquid mass transfer coefficients in biphasic bioreactors," *Biotechnology and Bioprocess Engineering,* vol. 11, pp. 245-250, 2006.
[138] J. L. Rols, J. S. Condoret, C. Fonade, and G. Goma, "Modeling of oxygen transfer in water through emulsified organic liquids," *Chemical Engineering Science,* vol. 46, pp. 1869-1873, 1991/01/01 1991.

[139] G. Quijano, M. Hernandez, S. Villaverde, F. Thalasso, and R. Muñoz, "A step-forward in the characterization and potential applications of solid and liquid oxygen transfer vectors," *Applied Microbiology and Biotechnology,* vol. 85, pp. 543-551, 2010.
[140] L. Liu, G. Du, J. Chen, M. Wang, and J. Sun, "Comparative study on the influence of dissolved oxygen control approaches on the microbial hyaluronic acid production of *Streptococcus zooepidemicus*," *Bioprocess and Biosystems Engineering,* vol. 32, pp. 755-763, 2009.
[141] J. L. Rols, J. S. Condoret, C. Fonade, and G. Goma, "Mechanism of enhanced oxygen transfer in fermentation using emulsified oxygen-vectors," *Biotechnology and Bioengineering,* vol. 35, pp. 427-435, 1990.
[142] M. Elibol, "Improvement of antibiotic production by increased oxygen solubility through the addition of perfluorodecalin," *Journal of Chemical Technology & Biotechnology,* vol. 76, pp. 418-422, 2001.
[143] J. L. Rols and G. Goma, "Enhanced oxygen transfer rates in fermentation using soybean oil-in-water dispersions," *Biotechnology Letters,* vol. 13, pp. 7-12, 1991// 1991.
[144] G. Quijano, J. Rocha-Ríos, M. Hernández, S. Villaverde, S. Revah, R. Muñoz, *et al.*, "Determining the effect of solid and liquid vectors on the gaseous interfacial area and oxygen transfer rates in two-phase partitioning bioreactors," *Journal of Hazardous Materials,* vol. 175, pp. 1085-1089, 3/15/ 2010.
[145] J. V. Littlejohns and A. J. Daugulis, "Oxygen transfer in a gas–liquid system containing solids of varying oxygen affinity," *Chemical Engineering Journal,* vol. 129, pp. 67-74, 2007.
[146] J. L. Rols, J. S. Condoret, C. Fonade, and G. Goma, "Mechanism of Enhanced Oxygen Transfer in Fermentation Using Emulsified Oxygen-Vectors," *BIOTECHNOLOGY AND BIOENGINEERING* vol. 35, February 1990 1990.
[147] J. D. McMillan and D. I. C. Wang, "Mechanisms of Oxygen Transfer Enhancement during Submerged Cultivation in Perfluorochemical-in-Water Dispersions," *Annals of the New York Academy of Sciences,* vol. 589, pp. 283-300, 1990.
[148] E. Dumont and H. Delmas, "Mass transfer enhancement of gas absorption in oil-in-water systems: a review," *Chemical Engineering and Processing: Process Intensification,* vol. 42, pp. 419-438, 6// 2003.
[149] P. Chen, "ChE 612 course notes, S2016," ed. University of Waterloo, 2016.
[150] D. W. F. Brilman, "Mass transfer and chemical reaction in gas-liquid-liquid systems," PhD, Chemical Engineering, University of Twente, Enschede, The Netherlands, 1998.
[151] J. Stauft, "J. T. Davies und E. K. Rideal. Interfacial Phenomena. Academic Press, New York und London 1961. 474 S. Preis: $ 14,—," *Zeitschrift für Elektrochemie, Berichte der Bunsengesellschaft für physikalische Chemie,* vol. 66, pp. 453-453, 1962.
[152] Z.-W. Lai, R. A. Rahim, A. B. Ariff, and R. Mohamad, "Biosynthesis of high molecular weight hyaluronic acid by *Streptococcus zooepidemicus* using oxygen vector and optimum impeller tip speed," *Journal of Bioscience and Bioengineering,* vol. 114, pp. 286-291, 9// 2012.
[153] D. Zhang, X. Feng, S. Li, F. Chen, and H. Xu, "Effects of oxygen vectors on the synthesis and molecular weight of poly(γ-glutamic acid) and the metabolic characterization of *Bacillus subtilis* NX-2," *Process Biochemistry,* vol. 47, pp. 2103-2109, 12// 2012.

[154] Z. Xu, F. Bo, J. Xia, Z. Sun, S. Li, X. Feng, *et al.*, "Effects of oxygen-vectors on the synthesis of epsilon-poly-lysine and the metabolic characterization of Streptomyces albulus PD-1," *Biochemical Engineering Journal,* vol. 94, pp. 58-64, 2/15/ 2015.
[155] C. J. Van Ede, R. Van Houten, and A. A. C. M. Beenackers, "Enhancement of gas to water mass transfer rates by a dispersed organic phase," *Chemical Engineering Science,* vol. 50, pp. 2911-2922, 1995/09/01 1995.
[156] L. D. C. Correia, C. Aldrich, and K. G. Clarke, "Interfacial gas–liquid transfer area in alkane–aqueous dispersions and its impact on the overall volumetric oxygen transfer coefficient," *Biochemical Engineering Journal,* vol. 49, pp. 133-137, 3/15/ 2010.
[157] C. I. Castro and J. C. Briceno, "Perfluorocarbon-Based Oxygen Carriers: Review of Products and Trials," *Artificial Organs,* vol. 34, pp. 622-634, 2010.
[158] H. J. Reich, "8.1 Relaxation in NMR Spectroscopy, Chem 605 Course Notes," ed. University of Wisconsin, 2010.
[159] M. H. A. Hamza, G. Serratrice, M. J. Stebe, and J. J. Delpuech, "Solute-solvent interactions in perfluorocarbon solutions of oxygen. An NMR study," *Journal of the American Chemical Society,* vol. 103, pp. 3733-3738, 1981/07/01 1981.
[160] M. J. Stebe, G. Serratrice, and J. J. Delpuech, "Fluorocarbons as oxygen carriers. An NMR study of nonionic fluorinated microemulsions and of their oxygen solutions," *The Journal of Physical Chemistry,* vol. 89, pp. 2837-2843, 1985/06/01 1985.
[161] M. H. Ali Hamza, G. Serratrice, M.-J. Stébé, and J.-J. Delpuech, "Fluorocarbons as oxygen carriers. II. An NMR study of partially or totally fluorinated alkanes and alkenes," *Journal of Magnetic Resonance (1969),* vol. 42, pp. 227-241, 1981/02/01 1981.
[162] G. D. Zhang, W. F. Cai, C. J. Xu, and M. Zhou, "A general enhancement factor model of the physical absorption of gases in multiphase systems," *Chemical Engineering Science,* vol. 61, pp. 558-568, 1// 2006.
[163] J. V. Littlejohns and A. J. Daugulis, "Oxygen transfer in a gas–liquid system containing solids of varying oxygen affinity," *Chemical Engineering Journal,* vol. 129, pp. 67-74, 5/1/ 2007.
[164] T. R. Das, A. Bandopadhyay, R. Parthasarathy, and R. Kumar, "Gas—liquid interfacial area in stirred vessels: The effect of an immiscible liquid phase," *Chemical Engineering Science,* vol. 40, pp. 209-214, 1985/01/01 1985.
[165] A. H. G. Cents, D. W. F. Brilman, and G. F. Versteeg, "Gas absorption in an agitated gas–liquid–liquid system," *Chemical Engineering Science,* vol. 56, pp. 1075-1083, 2// 2001.
[166] I. T. M. Hassan and C. W. Robinson, "Oxygen transfer in mechanically agitated aqueous systems containing dispersed hydrocarbon," *Biotechnology and Bioengineering,* vol. 19, pp. 661-682, 1977.
[167] F. Yoshida, T. Yamane, and Y. Miyamoto, "Oxygen absorption into oil-in-water emulsions. A study on hydrocarbon fermentors," *Industrial & Engineering Chemistry Process Design and Development,* vol. 9, pp. 570-577, 1970/10/01 1970.
[168] V. Linek and P. Beneš, "A study of the mechanism of gas absorption into oil-water emulsions," *Chemical Engineering Science,* vol. 31, pp. 1037-1046, 1976/01/01 1976.
[169] J. W. Lee, D. Na, J. M. Park, J. Lee, S. Choi, and S. Y. Lee, "Systems metabolic engineering of microorganisms for natural and non-natural chemicals," *Nat Chem Biol,* vol. 8, pp. 536-546, 06//print 2012.

[170] S. J. J. Brouns, M. M. Jore, M. Lundgren, E. R. Westra, R. J. H. Slijkhuis, A. P. L. Snijders, *et al.*, "Small CRISPR RNAs Guide Antiviral Defense in Prokaryotes," *Science,* vol. 321, pp. 960-964, 2008-08-15 00:00:00 2008.
[171] H. Deveau, R. Barrangou, J. E. Garneau, J. Labonté, C. Fremaux, P. Boyaval, *et al.*, "Phage Response to CRISPR-Encoded Resistance in Streptococcus thermophilus," *Journal of Bacteriology,* vol. 190, pp. 1390-1400, February 15, 2008 2008.
[172] F. J. M. Mojica, C. Díez-Villaseñor, J. García-Martínez, and C. Almendros, "Short motif sequences determine the targets of the prokaryotic CRISPR defence system," *Microbiology,* vol. 155, pp. 733-740, 2009.
[173] T. Xu, Y. Li, Z. Shi, C. L. Hemme, Y. Li, Y. Zhu, *et al.*, "Efficient Genome Editing in *Clostridium cellulolyticum* via CRISPR-Cas9 Nickase," *Applied and Environmental Microbiology,* vol. 81, pp. 4423-4431, July 1, 2015 2015.
[174] R. E. Cobb, Y. Wang, and H. Zhao, "High-Efficiency Multiplex Genome Editing of Streptomyces Species Using an Engineered CRISPR/Cas System," *ACS Synthetic Biology,* vol. 4, pp. 723-728, 2015/06/19 2015.
[175] R. B. Vercoe, J. T. Chang, R. L. Dy, C. Taylor, T. Gristwood, J. S. Clulow, *et al.*, "Cytotoxic Chromosomal Targeting by CRISPR/Cas Systems Can Reshape Bacterial Genomes and Expel or Remodel Pathogenicity Islands," *PLoS Genet,* vol. 9, p. e1003454, 2013.
[176] C. R. Reisch and K. L. J. Prather, "The no-SCAR (Scarless Cas9 Assisted Recombineering) system for genome editing in Escherichia coli," *Scientific Reports,* vol. 5, p. 15096, 10/14/online 2015.
[177] J. Xia, L. Wang, J.-b. Zhu, C.-j. Sun, M.-g. Zheng, L. Zheng, *et al.*, "Expression of Shewanella frigidimarina fatty acid metabolic genes in E. coli by CRISPR/cas9-coupled lambda Red recombineering," *Biotechnology Letters,* vol. 38, pp. 117-122, 2015.
[178] H. Zeng, S. Wen, W. Xu, Z. He, G. Zhai, Y. Liu, *et al.*, "Highly efficient editing of the actinorhodin polyketide chain length factor gene in *Streptomyces coelicolor* M145 using CRISPR/Cas9-CodA(sm) combined system," *Applied Microbiology and Biotechnology,* vol. 99, pp. 10575-10585, 2015.
[179] Y. Tong, P. Charusanti, L. Zhang, T. Weber, and S. Y. Lee, "CRISPR-Cas9 Based Engineering of Actinomycetal Genomes," *ACS Synthetic Biology,* vol. 4, pp. 1020-1029, 2015/09/18 2015.
[180] D. Bikard, W. Jiang, P. Samai, A. Hochschild, F. Zhang, and L. A. Marraffini, "Programmable repression and activation of bacterial gene expression using an engineered CRISPR-Cas system," *Nucleic Acids Research,* vol. 41, pp. 7429-7437, August 1, 2013 2013.
[181] J. Wu, G. Du, J. Chen, and J. Zhou, "Enhancing flavonoid production by systematically tuning the central metabolic pathways based on a CRISPR interference system in Escherichia coli," *Scientific Reports,* vol. 5, p. 13477, 09/01/online 2015.
[182] S. Cleto, J. V. K. Jensen, V. F. Wendisch, and T. K. Lu, "Corynebacterium glutamicum Metabolic Engineering with CRISPR Interference (CRISPRi)," *ACS Synthetic Biology,* 2016/02/01 2016.
[183] E. Choudhary, P. Thakur, M. Pareek, and N. Agarwal, "Gene silencing by CRISPR interference in mycobacteria," *Nat Commun,* vol. 6, 02/25/online 2015.
[184] S. Li, J. Wen, and X. Jia, "Engineering *Bacillus subtilis* for isobutanol production by heterologous Ehrlich pathway construction and the biosynthetic 2-ketoisovalerate

precursor pathway overexpression," *Applied Microbiology and Biotechnology,* vol. 91, pp. 577-589, 2011/08/01 2011.
[185] J. C. Zweers, I. Barák, D. Becher, A. J. Driessen, M. Hecker, V. P. Kontinen, *et al.*, "Towards the development of *Bacillus subtilis* as a cell factory for membrane proteins and protein complexes," *Microbial Cell Factories,* vol. 7, pp. 1-20, 2008.
[186] T. Shi, G. Wang, Z. Wang, J. Fu, T. Chen, and X. Zhao, "Establishment of a Markerless Mutation Delivery System in <italic>Bacillus subtilis</italic> Stimulated by a Double-Strand Break in the Chromosome," *PLoS ONE,* vol. 8, p. e81370, 2013.
[187] J. Sambrook and D. Russell, *Molecular cloning: a laboratory manual*: Cold Spring Harbor Laboratory Press, 2001.
[188] A.-M. Guérout-Fleury, N. Frandsen, and P. Stragier, "Plasmids for ectopic integration in *Bacillus subtilis*," *Gene,* vol. 180, pp. 57-61, // 1996.
[189] B. Härtl, W. Wehrl, T. Wiegert, G. Homuth, and W. Schumann, "Development of a New Integration Site within theBacillus subtilis Chromosome and Construction of Compatible Expression Cassettes," *Journal of Bacteriology,* vol. 183, pp. 2696-2699, April 15, 2001 2001.
[190] J. M. Inácio, C. Costa, and I. de Sá-Nogueira, "Distinct molecular mechanisms involved in carbon catabolite repression of the arabinose regulon in *Bacillus subtilis*," *Microbiology,* vol. 149, pp. 2345-2355, 2003.
[191] T. Bitter and H. M. Muir, "A modified uronic acid carbazole reaction," *Analytical Biochemistry,* vol. 4, pp. 330-334, 1962/10/01 1962.
[192] M. K. Cowman, C. C. Chen, M. Pandya, H. Yuan, D. Ramkishun, J. LoBello, *et al.*, "Improved agarose gel electrophoresis method and molecular mass calculation for high molecular mass hyaluronan," *Analytical Biochemistry,* vol. 417, pp. 50-56, 10/1/ 2011.
[193] C. A. Schneider, W. S. Rasband, and K. W. Eliceiri, "NIH Image to ImageJ: 25 years of image analysis," *Nat Meth,* vol. 9, pp. 671-675, 07//print 2012.
[194] J. H. Miller, *Experiments in molecular genetics*: Cold Spring Harbor Laboratory, 1972.
[195] J. M. Ruijter, C. Ramakers, W. M. H. Hoogaars, Y. Karlen, O. Bakker, M. J. B. van den Hoff, *et al.*, "Amplification efficiency: linking baseline and bias in the analysis of quantitative PCR data," *Nucleic Acids Research,* vol. 37, p. e45, April 1, 2009 2009.
[196] T. Wang, J. J. Wei, D. M. Sabatini, and E. S. Lander, "Genetic screens in human cells using the CRISPR-Cas9 system," *Science,* vol. 343, pp. 80-84, January 3, 2014 2014.
[197] M. H. Larson, L. A. Gilbert, X. Wang, W. A. Lim, J. S. Weissman, and L. S. Qi, "CRISPR interference (CRISPRi) for sequence-specific control of gene expression," *Nat. Protocols,* vol. 8, pp. 2180-2196, 11//print 2013.
[198] D. Gärtner, M. Geissendörfer, and W. Hillen, "Expression of the *Bacillus subtilis* xyl operon is repressed at the level of transcription and is induced by xylose," *Journal of Bacteriology,* vol. 170, pp. 3102-3109, July 1, 1988 1988.
[199] R. Shetty, D. Endy, and T. Knight, "Engineering BioBrick vectors from BioBrick parts," *Journal of Biological Engineering,* vol. 2, p. 5, 2008.
[200] C. R. Harwood, "*Bacillus subtilis* and its relatives: molecular biological and industrial workhorses," *Trends in Biotechnology,* vol. 10, pp. 247-256, // 1992.
[201] X. Z. Zhang and Y. H. P. Zhang, "Simple, fast and high-efficiency transformation system for directed evolution of cellulase in *Bacillus subtilis*," *Microbial biotechnology,* vol. 4, pp. 98-105, 12/23

[202] T. Rygus, A. Scheler, R. Allmansberger, and W. Hillen, "Molecular cloning, structure, promoters and regulatory elements for transcription of the *Bacillus megaterium* encoded regulon for xylose utilization," *Archives of Microbiology,* vol. 155, pp. 535-542, 1991/06/01 1991.
[203] N. A. Shevchuk, A. V. Bryksin, Y. A. Nusinovich, F. C. Cabello, M. Sutherland, and S. Ladisch, "Construction of long DNA molecules using long PCR-based fusion of several fragments simultaneously," *Nucleic Acids Research,* vol. 32, p. e19, January 16, 2004 2004.
[204] S. H. Kung, A. C. Retchless, J. Y. Kwan, and R. P. P. Almeida, "Effects of DNA size on transformation and recombination efficiencies in *Xylella fastidiosa*," *Applied and Environmental Microbiology,* vol. 79, pp. 1712-1717, March 1, 2013 2013.
[205] K. Kumari, B. A. Baggenstoss, A. L. Parker, and P. H. Weigel, "Mutation of Two Intramembrane Polar Residues Conserved within the Hyaluronan Synthase Family Alters Hyaluronan Product Size," *Journal of Biological Chemistry,* vol. 281, pp. 11755-11760, April 28, 2006 2006.
[206] L. I. Salzberg and J. D. Helmann, "Phenotypic and transcriptomic characterization of *Bacillus subtilis* mutants with grossly altered membrane composition," *Journal of Bacteriology,* vol. 190, pp. 7797-7807, December 1, 2008 2008.
[207] F. Kawai, H. Hara, H. Takamatsu, K. Watabe, and K. Matsumoto, "Cardiolipin enrichment in spore membranes and its involvement in germination of *Bacillus subtilis* Marburg," *Genes & Genetic Systems,* vol. 81, pp. 69-76, 2006.
[208] F. Kawai, M. Shoda, R. Harashima, Y. Sadaie, H. Hara, and K. Matsumoto, "Cardiolipin domains in *Bacillus subtilis* Marburg membranes," *Journal of Bacteriology,* vol. 186, pp. 1475-1483, March 1, 2004 2004.
[209] A. Nishibori, J. Kusaka, H. Hara, M. Umeda, and K. Matsumoto, "Phosphatidylethanolamine domains and localization of phospholipid synthases in *Bacillus subtilis* membranes," *Journal of Bacteriology,* vol. 187, pp. 2163-2174, March 15, 2005 2005.
[210] W. Dowhan, "Molecular basis for membrane phospholipid diversity: why are there so many lipids?," *Annual review of biochemistry,* vol. 66, pp. 199-232, 1997.
[211] P. H. Weigel and B. A. Baggenstoss, "Hyaluronan synthase polymerizing activity and control of product size are discrete enzyme functions that can be uncoupled by mutagenesis of conserved cysteines," *Glycobiology,* vol. 22, pp. 1302-1310, 2012.
[212] R. Chen, "Permeability issues in whole-cell bioprocesses and cellular membrane engineering," *Applied Microbiology and Biotechnology,* vol. 74, pp. 730-738, 2007/03/01 2007.
[213] H. Cao, A. J. Heel, H. Ahmed, M. Mols, and O. P. Kuipers, "Cell surface engineering of Bacillus subtilis improves production yields of heterologously expressed α-amylases," *Microbial Cell Factories,* vol. 16, p. 56, 2017.
[214] A. W. Westbrook, M. Moo-Young, and C. P. Chou, "Development of a CRISPR-Cas9 toolkit for comprehensive engineering of *Bacillus subtilis*," *Applied and Environmental Microbiology,* June 3, 2016 2016.
[215] H. Nguyen, T. Phan, and W. Schumann, "Expression vectors for the rapid purification of recombinant proteins in *Bacillus subtilis*," *Current Microbiology,* vol. 55, pp. 89-93, 2007/08/01 2007.

[216] K. Zhang, X. Duan, and J. Wu, "Multigene disruption in undomesticated Bacillus subtilis ATCC 6051a using the CRISPR/Cas9 system," *Scientific reports,* vol. 6, p. 27943, 2016.
[217] J. W. Rosch, F. F. Hsu, and M. G. Caparon, "Anionic lipids enriched at the ExPortal of *Streptococcus pyogenes*," *Journal of bacteriology,* vol. 189, pp. 801-806, 2007.
[218] J.-H. Kim, S.-J. Yoo, D.-K. Oh, Y.-G. Kweon, D.-W. Park, C.-H. Lee, *et al.*, "Selection of a *Streptococcus equi* mutant and optimization of culture conditions for the production of high molecular weight hyaluronic acid," *Enzyme and Microbial Technology,* vol. 19, pp. 440-445, 1996.
[219] J. A. Vázquez, M. I. Montemayor, J. Fraguas, and M. A. Murado, "Hyaluronic acid production by Streptococcus zooepidemicus in marine by-products media from mussel processing wastewaters and tuna peptone viscera," *Microbial Cell Factories,* vol. 9, pp. 1-10, 2010// 2010.
[220] E. Jeong, W. Y. Shim, and J. H. Kim, "Metabolic engineering of *Pichia pastoris* for production of hyaluronic acid with high molecular weight," *Journal of biotechnology,* vol. 185, pp. 28-36, 2014.
[221] M. Ahmad, M. Hirz, H. Pichler, and H. Schwab, "Protein expression in *Pichia pastoris*: recent achievements and perspectives for heterologous protein production," *Applied microbiology and biotechnology,* vol. 98, pp. 5301-5317, 2014.
[222] U. Mamat, K. Wilke, D. Bramhill, A. B. Schromm, B. Lindner, T. A. Kohl, *et al.*, "Detoxifying Escherichia coli for endotoxin-free production of recombinant proteins," *Microbial cell factories,* vol. 14, p. 57, 2015.
[223] M. E. MacGilvray, J. D. Lapek Jr, A. E. Friedman, and R. G. Quivey Jr, "Cardiolipin biosynthesis in *Streptococcus mutans* is regulated in response to external pH," *Microbiology,* vol. 158, pp. 2133-2143, 2012.
[224] C. S. Lopez, A. F. Alice, H. Heras, E. A. Rivas, and C. Sanchez-Rivas, "Role of anionic phospholipids in the adaptation of *Bacillus subtilis* to high salinity," *Microbiology,* vol. 152, pp. 605-616, 2006.
[225] W.-C. Huang, S.-J. Chen, and T.-L. Chen, "The role of dissolved oxygen and function of agitation in hyaluronic acid fermentation," *Biochemical Engineering Journal,* vol. 32, pp. 239-243, 2006.
[226] B. Monterroso, R. Ahijado-Guzmán, B. Reija, C. Alfonso, S. Zorrilla, A. P. Minton, *et al.*, "Mg^{2+}-linked self-assembly of FtsZ in the presence of GTP or a GTP analog involves the concerted formation of a narrow size distribution of oligomeric species," *Biochemistry,* vol. 51, p. 4541, 2012.
[227] L. G. Monahan, I. V. Hajduk, S. P. Blaber, I. G. Charles, and E. J. Harry, "Coordinating bacterial cell division with nutrient availability: a role for glycolysis," *MBio,* vol. 5, pp. e00935-14, 2014.
[228] E. Mileykovskaya and W. Dowhan, "Visualization of phospholipid domains in *Escherichia coli* by using the cardiolipin-specific fluorescent dye 10-N-nonyl acridine orange," *Journal of bacteriology,* vol. 182, pp. 1172-1175, 2000.
[229] K. Kobayashi, S. D. Ehrlich, A. Albertini, G. Amati, K. K. Andersen, M. Arnaud, *et al.*, "Essential *Bacillus subtilis* genes," *Proceedings of the National Academy of Sciences,* vol. 100, pp. 4678-4683, April 15, 2003 2003.
[230] M. G. Percy and A. Gründling, "Lipoteichoic acid synthesis and function in gram-positive bacteria," *Annual review of microbiology,* vol. 68, pp. 81-100, 2014.

[231] D. Shiomi and W. Margolin, "A sweet sensor for size-conscious bacteria," *Cell*, vol. 130, pp. 216-218, 2007.
[232] E. A. Boyle, J. O. Andreasson, L. M. Chircus, S. H. Sternberg, M. J. Wu, C. K. Guegler, *et al.*, "High-throughput biochemical profiling reveals sequence determinants of dCas9 off-target binding and unbinding," *Proceedings of the National Academy of Sciences*, p. 201700557, 2017.
[233] O. Kennard, "Structural studies of DNA fragments: the G· T wobble base pair in A, B and Z DNA; the G· A base pair in B-DNA," *Journal of Biomolecular Structure and Dynamics*, vol. 3, pp. 205-226, 1985.
[234] E. Nudler, M. Kashlev, V. Nikiforov, and A. Goldfarb, "Coupling between transcription termination and RNA polymerase inchworming," *Cell*, vol. 81, pp. 351-357, 1995.
[235] H. Abe and H. Aiba, "Differential contributions of two elements of rho-independent terminator to transcription termination and mRNA stabilization," *Biochimie*, vol. 78, pp. 1035-1042, 1996.
[236] A. Pagano, M. Castelnuovo, F. Tortelli, R. Ferrari, G. Dieci, and R. Cancedda, "New small nuclear RNA gene-like transcriptional units as sources of regulatory transcripts," *PLoS Genet*, vol. 3, p. e1, 2007.
[237] J. W. Lee, D. Na, J. M. Park, J. Lee, S. Choi, and S. Y. Lee, "Systems metabolic engineering of microorganisms for natural and non-natural chemicals," *Nature Chemical Biology*, vol. 8, pp. 536-546, 06//print 2012.
[238] A. W. Westbrook, M. Moo-Young, and C. P. Chou, "Development of a CRISPR-Cas9 tool kit for comprehensive engineering of *Bacillus subtilis*," *Applied and Environmental Microbiology*, vol. 82, pp. 4876-95, Aug 15 2016.
[239] A. W. Westbrook, X. Ren, M. Moo-Young, and C. P. Chou, "Engineering of cell membrane to enhance heterologous production of hyaluronic acid in Bacillus subtilis," *Biotechnology and Bioengineering*, 2017.
[240] E. Fischer and U. Sauer, "Large-scale in vivo flux analysis shows rigidity and suboptimal performance of *Bacillus subtilis* metabolism," *Nature Genetics*, vol. 37, pp. 636-640, 06//print 2005.
[241] K. R. Choi and S. Y. Lee, "CRISPR technologies for bacterial systems: current achievements and future directions," *Biotechnology Advances*, vol. 34, pp. 1180-1209, 2016.
[242] I. Mougiakos, E. F. Bosma, W. M. de Vos, R. van Kranenburg, and J. van der Oost, "Next generation prokaryotic engineering: the CRISPR-Cas toolkit," *Trends in biotechnology*, vol. 34, pp. 575-587, 2016.
[243] O. Krispin and R. Allmansberger, "The *Bacillus subtilis* AraE Protein Displays a Broad Substrate Specificity for Several Different Sugars," *Journal of Bacteriology*, vol. 180, pp. 3250-3252, June 15, 1998 1998.
[244] C. A. Schneider, W. S. Rasband, and K. W. Eliceiri, "NIH Image to ImageJ: 25 years of image analysis," *Nature Methods*, vol. 9, pp. 671-675, 07//print 2012.
[245] W. Y. Chen, E. Marcellin, J. Hung, and L. K. Nielsen, "Hyaluronan molecular weight is controlled by UDP-N-acetylglucosamine concentration in Streptococcus zooepidemicus," *Journal of Biological Chemistry*, vol. 284, pp. 18007-18014, 2009.
[246] I. Sá-Nogueira and S. S. Ramos, "Cloning, functional analysis, and transcriptional regulation of the Bacillus subtilis araE gene involved in L-arabinose utilization," *Journal of bacteriology*, vol. 179, pp. 7705-7711, 1997.

[247] S. Jagannath and K. Ramachandran, "Influence of competing metabolic processes on the molecular weight of hyaluronic acid synthesized by Streptococcus zooepidemicus," *Biochemical Engineering Journal,* vol. 48, pp. 148-158, 2010.
[248] V. L. Tlapak-Simmons, B. A. Baggenstoss, K. Kumari, C. Heldermon, and P. H. Weigel, "Kinetic characterization of the recombinant hyaluronan synthases from Streptococcus pyogenes and Streptococcus equisimilis," *Journal of Biological Chemistry,* vol. 274, pp. 4246-4253, 1999.
[249] I. Gaugué, J. Oberto, H. Putzer, and J. Plumbridge, "The use of amino sugars by Bacillus subtilis: presence of a unique operon for the catabolism of glucosamine," *PLoS One,* vol. 8, p. e63025, 2013.
[250] J. A. Collins, I. Irnov, S. Baker, and W. C. Winkler, "Mechanism of mRNA destabilization by the glmS ribozyme," *Genes & development,* vol. 21, pp. 3356-3368, 2007.
[251] C. Wittmann and A. De Graaf, "Metabolic Flux Analysis in *Corynebacterium glutamicum*," in *Handbook of Corynebacterium glutamicum*, L. Eggeling and M. Bott, Eds., ed Boca Raton, FL: CRC, Taylor & Francis, 2005, pp. 277-300.
[252] A. K. Gombert, M. M. dos Santos, B. Christensen, and J. Nielsen, "Network identification and flux quantification in the central metabolism of Saccharomyces cerevisiae under different conditions of glucose repression," *Journal of bacteriology,* vol. 183, pp. 1441-1451, 2001.
[253] F. Garcia-Ochoa and E. Gomez, "Bioreactor scale-up and oxygen transfer rate in microbial processes: an overview," *Biotechnology advances,* vol. 27, pp. 153-176, 2009.
[254] G. Ming and D. Zhenhao, "Prediction of oxygen solubility in pure water and brines up to high temperatures and pressures," *Geochimica et Cosmochimica Acta,* vol. 74, pp. 5631-5640, 2010.
[255] J. A. Mueller and W. C. Boyle, "Relative importance of viscosity and oxygen solubility on oxygen transfer rates in glucose solutions," *Environmental Science & Technology,* vol. 1, pp. 578-579, 1967/07/01 1967.
[256] H. Gao, J. Chen, G. Du, Y. Zhang, J. Chen, and G. Chen, "Effect of agitation and mixing on hyaluronic acid production by *Streptococcus zooepidemicus*," *JOURNAL OF CHEMICAL INDUSTRY AND ENGINEERING-CHINA-,* vol. 54, pp. 350-356, 2003.
[257] S. B. Farr and T. Kogoma, "Oxidative stress responses in *Escherichia coli* and *Salmonella typhimurium*," *Microbiological Reviews,* vol. 55, pp. 561-585, December 1, 1991 1991.
[258] A. Slavica, I. Dib, and B. Nidetzky, "Single-site oxidation, cysteine 108 to cysteine sulfinic acid, in d-amino acid oxidase from *Trigonopsis variabilis* and its structural and functional consequences," *Applied and Environmental Microbiology,* vol. 71, pp. 8061-8068, December 1, 2005 2005.
[259] R. T. Dean, S. Fu, R. Stocker, and M. J. Davies, "Biochemistry and pathology of radical-mediated protein oxidation.," *Biochemical Journal,* vol. 324, pp. 1-18, 1997.
[260] H. Chaumat, A. M. Billet, and H. Delmas, "Hydrodynamics and mass transfer in bubble column: Influence of liquid phase surface tension," *Chemical Engineering Science,* vol. 62, pp. 7378-7390, 12// 2007.
[261] H. Hristov, R. Mann, V. Lossev, S. D. Vlaev, and P. Seichter, "A 3-D analysis of gas-liquid mixing, mass transfer and bioreaction in a stirred bio-reactor," *Food and Bioproducts Processing,* vol. 79, pp. 232-241, 2001.

[262] L. Liu, H. Q. Yang, D. X. Zhang, G. C. Du, J. Chen, M. Wang, *et al.*, "Enhancement of hyaluronic acid production by batch culture of *Streptococcus zooepidemicus* via the addition of n-dodecane as an oxygen vector," *Journal of microbiology and biotechnology,* vol. 19, pp. 596-603, 2009.
[263] A. W. Westbrook, M. Moo-Young, and C. P. Chou, "Development of a CRISPR-Cas9 tool kit for comprehensive engineering of *Bacillus subtilis*," *Appl Environ Microbiol,* vol. 82, pp. 4876-95, Aug 15 2016.
[264] K. Van't Riet, "Review of measuring methods and results in nonviscous gas-liquid mass transfer in stirred vessels," *Industrial & Engineering Chemistry Process Design and Development,* vol. 18, pp. 357-364, 1979.
[265] M. I. Aralaguppi, T. M. Aminabhavi, R. H. Balundgi, and S. S. Joshi, "Thermodynamic interactions in mixtures of bromoform with hydrocarbons," *The Journal of Physical Chemistry,* vol. 95, pp. 5299-5308, 1991.
[266] L. K. Ju and C. S. Ho, "Oxygen diffusion coefficient and solubility in *n*-hexadecane," *Biotechnology and bioengineering,* vol. 34, pp. 1221-1224, 1989.
[267] E. Michailidou, M. J. Assael, M. L. Huber, I. M. Abdulagatov, and R. A. Perkins, "Reference correlation of the viscosity of *n*-heptane from the triple point to 600 K and up to 248 MPa," *Journal of Physical and Chemical Reference Data,* vol. 43, p. 023103, 2014.
[268] A. B. McKeown and R. Hibbard, "Determination of dissolved oxygen in hydrocarbons," *Analytical Chemistry,* vol. 28, pp. 1490-1492, 1956.
[269] P. J. Hesse, R. Battino, P. Scharlin, and E. Wilhelm, "Solubility of gases in liquids. 21. Solubility of He, Ne, Ar, Kr, N 2, O 2, CH 4, CF 4, and SF 6 in 2, 2, 4-trimethylpentane atT= 298.15 K," *The Journal of Chemical Thermodynamics,* vol. 31, pp. 1175-1181, 1999.
[270] A. Pádua, J. Fareleira, J. Calado, and W. Wakeham, "Density and viscosity measurements of 2, 2, 4-trimethylpentane (isooctane) from 198 K to 348 K and up to 100 MPa," *Journal of Chemical & Engineering Data,* vol. 41, pp. 1488-1494, 1996.
[271] J. Deschamps, D.-H. Menz, A. A. H. Padua, and M. F. C. Gomes, "Low pressure solubility and thermodynamics of solvation of oxygen, carbon dioxide, and carbon onoxide in fluorinated liqids," *Elsevier,* November 29 2006 2006.
[272] A. Weber, R. Pockelmann, and C.-P. Klages, "Electrical and optical properties of amorphous fluorocarbon films prepared by plasma polymerization of perfluoro-1,3-dimethylcyclohexane," *Journal of Vaccum Science & Technology A Vaccum Surfaces and Films,* vol. 16, 1998.
[273] M.-J. Jeng, S.-S. Yang, M. R. Wolfson, and T. H. Shaffer, "Perfluorochemical (PFC) combinations for acute lung injury: an in vitro and in vivo study in juvenile rabbits," *Pediatric research,* vol. 53, pp. 81-88, 2003.
[274] M. F. Refojo, J. Friend, and F.-L. Leong, "Perfluoro-1-methyldecalin as a potential oxygen carrier with fluid scleral lenses," *Current eye research,* vol. 4, pp. 732-733, 1985.
[275] M. G. Freire, A. G. Ferreira, I. M. Fonseca, I. M. Marrucho, and J. A. Coutinho, "Viscosities of liquid fluorocompounds," *Journal of Chemical & Engineering Data,* vol. 53, pp. 538-542, 2008.
[276] A. Dias, A. Caço, J. Coutinho, L. Santos, M. Pineiro, L. Vega, *et al.*, "Thermodynamic properties of perfluoro-*n*-octane," *Fluid phase equilibria,* vol. 225, pp. 39-47, 2004.

[277] A. Kang and M. W. Chang, "Identification and reconstitution of genetic regulatory networks for improved microbial tolerance to isooctane," *Molecular BioSystems,* vol. 8, pp. 1350-1358, 2012.
[278] T. H. Ngo and A. Schumpe, "Oxygen absorption into stirred emulsions of *n*-alkanes," *International Journal of Chemical Engineering,* vol. 2012, 2012.
[279] S. S. Alves and H. J. Pinho, "Gas absorption in stirred gas-liquid-liquid systems: effect of transferred solute solubility and oil phase spreading characteristics," *Chemical Engineering Communications,* vol. 200, pp. 1425-1442, 2013.
[280] A. Kundu, E. Dumont, A. M. Duquenne, and H. Delmas, "Mass transfer characteristics in gas-liquid-liquid system," *The canadian journal of chemical engineering,* vol. 81, pp. 640-646, 2003.
[281] M. Elibol and F. Mavituna, "A remedy to oxygen limitation problem in antibiotic production: addition of perfluorocarbon," *Biochemical engineering journal,* vol. 3, pp. 1-7, 1999.
[282] M. Elibol, "Mass transfer characteristics of yeast fermentation broth in the presence of pluronic F-68," *Process biochemistry,* vol. 34, pp. 557-561, 1999.
[283] T. Hoffmann, B. Troup, A. Szabo, C. Hungerer, and D. Jahn, "The anaerobic life of Bacillus subtilis: cloning of the genes encoding the respiratory nitrate reductase system," *FEMS microbiology letters,* vol. 131, pp. 219-225, 1995.
[284] H. C. Ramos, L. Boursier, I. Moszer, F. Kunst, A. Danchin, and P. Glaser, "Anaerobic transcription activation in Bacillus subtilis: identification of distinct FNR-dependent and-independent regulatory mechanisms," *The EMBO journal,* vol. 14, p. 5984, 1995.
[285] F. Zhu, J. Cai, X. Wu, J. Huang, L. Huang, J. Zhu, *et al.*, "The main byproducts and metabolic flux profiling of γ-PGA-producing strain B. subtilis ZJU-7 under different pH values," *Journal of biotechnology,* vol. 164, pp. 67-74, 2013.
[286] J. Sikkema, J. De Bont, and B. Poolman, "Mechanisms of membrane toxicity of hydrocarbons," *Microbiological reviews,* vol. 59, pp. 201-222, 1995.
[287] T. McIntosh, S. Simon, and R. MacDonald, "The organization of n-alkanes in lipid bilayers," *Biochimica et Biophysica Acta (BBA)-Biomembranes,* vol. 597, pp. 445-463, 1980.
[288] S. Paterson, K. Butler, P. Huang, J. Labelle, I. C. Smith, and H. Schneider, "The effects of alcohols on lipid bilayers: a spin label study," *Biochimica et Biophysica Acta (BBA)-Biomembranes,* vol. 266, pp. 597-602, 1972.
[289] C. Grisham and R. Barnett, "The effects of long-chain alcohols on membrane lipids and the (Na++ K+)-ATPase," *Biochimica et Biophysica Acta (BBA)-Biomembranes,* vol. 311, pp. 417-422, 1973.
[290] L. Ingram, "Adaptation of membrane lipids to alcohols," *Journal of Bacteriology,* vol. 125, pp. 670-678, 1976.
[291] L. Ingram, "Changes in lipid composition of *Escherichia coli* resulting from growth with organic solvents and with food additives," *Applied and environmental microbiology,* vol. 33, pp. 1233-1236, 1977.
[292] H. J. Pinho and S. S. Alves, "Effect of spreading coefficient on gas-liquid mass transfer in gas-liquid-liquid dispersions in a stirred tank," *Chemical Engineering Communications,* vol. 197, pp. 1515-1526, 2010.

[293] I. Hassan and C. W. Robinson, "Oxygen transfer in mechanically agitated aqueous systems containing dispersed hydrocarbon," *Biotechnology and Bioengineering,* vol. 19, pp. 661-682, 1977.
[294] Y. H. Mori, N. Tsui, and M. Kiyomiya, "Surface and interfacial tensions and their combined properties in seven binary, immiscible liquid-liquid-vapor systems," *Journal of Chemical and Engineering Data,* vol. 29, pp. 407-412, 1984.
[295] H.-J. Lehmler, "Anti-inflammatory effects of perfluorocarbon compounds," *Expert review of respiratory medicine,* vol. 2, pp. 273-289, 2008.
[296] R. Bronnenmeier and H. Märkl, "Hydrodynamic stress capacity of microorganisms," *Biotechnology and bioengineering,* vol. 24, pp. 553-578, 1982.
[297] M. Toma, M. Ruklisha, J. Vanags, M. Zeltina, M. Lelte, N. Galinine, *et al.*, "Inhibition of microbial growth and metabolism by excess turbulence," *Biotechnology and bioengineering,* vol. 38, pp. 552-556, 1991.
[298] S. Sahoo, R. K. Verma, A. Suresh, K. K. Rao, J. Bellare, and G. Suraishkumar, "Macro-level and genetic-level responses of *Bacillus subtilis* to shear stress," *Biotechnology progress,* vol. 19, pp. 1689-1696, 2003.
[299] T. Candela and A. Fouet, "Poly-gamma-glutamate in bacteria," *Molecular microbiology,* vol. 60, pp. 1091-1098, 2006.
[300] A. Karau and I. Grayson, "Amino Acids in Human and Animal Nutrition," in *Biotechnology of Food and Feed Additives*, H. Zorn and P. Czermak, Eds., ed Berlin, Heidelberg: Springer Berlin Heidelberg, 2014, pp. 189-228.
[301] M. Oldiges, B. J. Eikmanns, and B. Blombach, "Application of metabolic engineering for the biotechnological production of L-valine," *Applied microbiology and biotechnology,* vol. 98, pp. 5859-5870, 2014.
[302] N.-Z. Xie, H. Liang, R.-B. Huang, and P. Xu, "Biotechnological production of muconic acid: current status and future prospects," *Biotechnology advances,* vol. 32, pp. 615-622, 2014.
[303] J. H. Park, Y. S. Jang, J. W. Lee, and S. Y. Lee, "Escherichia coli W as a new platform strain for the enhanced production of L-Valine by systems metabolic engineering," *Biotechnology and bioengineering,* vol. 108, pp. 1140-1147, 2011.
[304] J. H. Park, T. Y. Kim, K. H. Lee, and S. Y. Lee, "Fed-batch culture of Escherichia coli for L-valine production based on in silico flux response analysis," *Biotechnology and bioengineering,* vol. 108, pp. 934-946, 2011.
[305] J. H. Park, K. H. Lee, T. Y. Kim, and S. Y. Lee, "Metabolic engineering of Escherichia coli for the production of L-valine based on transcriptome analysis and in silico gene knockout simulation," *Proceedings of the National Academy of Sciences,* vol. 104, pp. 7797-7802, 2007.
[306] B. Blombach, M. E. Schreiner, T. Bartek, M. Oldiges, and B. J. Eikmanns, "Corynebacterium glutamicum tailored for high-yield L-valine production," *Applied microbiology and biotechnology,* vol. 79, pp. 471-479, 2008.
[307] S. Hasegawa, M. Suda, K. Uematsu, Y. Natsuma, K. Hiraga, T. Jojima, *et al.*, "Engineering of Corynebacterium glutamicum for high-yield L-valine production under oxygen deprivation conditions," *Applied and environmental microbiology,* vol. 79, pp. 1250-1257, 2013.
[308] V. Elišáková, M. Pátek, J. Holátko, J. Nešvera, D. Leyval, J.-L. Goergen, *et al.*, "Feedback-resistant acetohydroxy acid synthase increases valine production in

Corynebacterium glutamicum," *Applied and environmental microbiology,* vol. 71, pp. 207-213, 2005.
[309] E. Radmacher, A. Vaitsikova, U. Burger, K. Krumbach, H. Sahm, and L. Eggeling, "Linking central metabolism with increased pathway flux: L-valine accumulation by Corynebacterium glutamicum," *Applied and environmental microbiology,* vol. 68, pp. 2246-2250, 2002.
[310] C. Chen, Y. Li, J. Hu, X. Dong, and X. Wang, "Metabolic engineering of Corynebacterium glutamicum ATCC13869 for L-valine production," *Metabolic engineering,* vol. 29, pp. 66-75, 2015.
[311] T. Yang, Z. Rao, B. G. Kimani, M. Xu, X. Zhang, and S.-T. Yang, "Two-step production of gamma-aminobutyric acid from cassava powder using Corynebacterium glutamicum and Lactobacillus plantarum," *Journal of Industrial Microbiology & Biotechnology,* vol. 42, pp. 1157-1165, August 01 2015.
[312] J. S. Cho, K. R. Choi, C. P. S. Prabowo, J. H. Shin, D. Yang, J. Jang, *et al.*, "CRISPR/Cas9-coupled recombineering for metabolic engineering of Corynebacterium glutamicum," *Metabolic engineering,* vol. 42, pp. 157-167, 2017.
[313] T. Yoneda, Y. Miyota, K. Furuya, and T. Tsuzuki, "Production process of surfactin," ed: Google Patents, 2006.
[314] S. Li, D. Huang, Y. Li, J. Wen, and X. Jia, "Rational improvement of the engineered isobutanol-producing Bacillus subtilis by elementary mode analysis," *Microbial cell factories,* vol. 11, p. 101, 2012.
[315] M. C. Renna, N. Najimudin, L. Winik, and S. Zahler, "Regulation of the Bacillus subtilis alsS, alsD, and alsR genes involved in post-exponential-phase production of acetoin," *Journal of Bacteriology,* vol. 175, pp. 3863-3875, 1993.
[316] D. Chipman, Z. e. Barak, and J. V. Schloss, "Biosynthesis of 2-aceto-2-hydroxy acids: acetolactate synthases and acetohydroxyacid synthases," *Biochimica et Biophysica Acta (BBA)-Protein Structure and Molecular Enzymology,* vol. 1385, pp. 401-419, 1998.
[317] U. Mäder, S. Hennig, M. Hecker, and G. Homuth, "Transcriptional organization and posttranscriptional regulation of the Bacillus subtilis branched-chain amino acid biosynthesis genes," *Journal of bacteriology,* vol. 186, pp. 2240-2252, 2004.
[318] V. Molle, Y. Nakaura, R. P. Shivers, H. Yamaguchi, R. Losick, Y. Fujita, *et al.*, "Additional targets of the Bacillus subtilis global regulator CodY identified by chromatin immunoprecipitation and genome-wide transcript analysis," *Journal of bacteriology,* vol. 185, pp. 1911-1922, 2003.
[319] A. L. Sonenshein, "Control of key metabolic intersections in Bacillus subtilis," *Nature Reviews Microbiology,* vol. 5, pp. 917-927, 2007.
[320] S. R. Brinsmade, E. L. Alexander, J. Livny, A. I. Stettner, D. Segrè, K. Y. Rhee, *et al.*, "Hierarchical expression of genes controlled by the Bacillus subtilis global regulatory protein CodY," *Proceedings of the National Academy of Sciences,* vol. 111, pp. 8227-8232, 2014.
[321] Y. Fujita, T. Satomura, S. Tojo, and K. Hirooka, "CcpA-mediated catabolite activation of the Bacillus subtilis ilv-leu operon and its negation by either CodY-or TnrA-mediated negative regulation," *Journal of bacteriology,* vol. 196, pp. 3793-3806, 2014.
[322] R. P. Shivers and A. L. Sonenshein, "Activation of the Bacillus subtilis global regulator CodY by direct interaction with branched-chain amino acids," *Molecular microbiology,* vol. 53, pp. 599-611, 2004.

[323] S. Tojo, T. Satomura, K. Morisaki, K.-I. Yoshida, K. Hirooka, and Y. Fujita, "Negative transcriptional regulation of the ilv-leu operon for biosynthesis of branched-chain amino acids through the Bacillus subtilis global regulator TnrA," *Journal of bacteriology,* vol. 186, pp. 7971-7979, 2004.
[324] J. Grandoni, S. Fulmer, V. Brizzio, S. Zahler, and J. Calvo, "Regions of the Bacillus subtilis ilv-leu operon involved in regulation by leucine," *Journal of bacteriology,* vol. 175, pp. 7581-7593, 1993.
[325] C. Frädrich, A. March, K. Fiege, A. Hartmann, D. Jahn, and E. Härtig, "The transcription factor AlsR binds and regulates the promoter of the alsSD operon responsible for acetoin formation in Bacillus subtilis," *Journal of bacteriology,* vol. 194, pp. 1100-1112, 2012.
[326] H. Reents, R. Münch, T. Dammeyer, D. Jahn, and E. Härtig, "The Fnr regulon of Bacillus subtilis," *Journal of bacteriology,* vol. 188, pp. 1103-1112, 2006.
[327] M. Debarbouille, R. Gardan, M. Arnaud, and G. Rapoport, "Role of BkdR, a Transcriptional Activator of the SigL-Dependent Isoleucine and Valine Degradation Pathway inBacillus subtilis," *Journal of bacteriology,* vol. 181, pp. 2059-2066, 1999.
[328] B. R. Belitsky, "Role of branched-chain amino acid transport in Bacillus subtilis CodY activity," *Journal of bacteriology,* vol. 197, pp. 1330-1338, 2015.
[329] B. R. Belitsky and A. L. Sonenshein, "Contributions of multiple binding sites and effector-independent binding to CodY-mediated regulation in Bacillus subtilis," *Journal of bacteriology,* vol. 193, pp. 473-484, 2011.
[330] B. Härtl, W. Wehrl, T. Wiegert, G. Homuth, and W. Schumann, "Development of a new integration site within the *Bacillus subtilis* chromosome and construction of compatible expression cassettes," *Journal of Bacteriology,* vol. 183, pp. 2696-2699, April 15, 2001 2001.
[331] S. Ulusoy, H. I. Ulusoy, D. Pleissner, and N. T. Eriksen, "Nitrosation and analysis of amino acid derivatives by isocratic HPLC," *RSC Advances,* vol. 6, pp. 13120-13128, 2016.
[332] S. Mendel, T. Elkayam, C. Sella, V. Vinogradov, M. Vyazmensky, D. M. Chipman, *et al.*, "Acetohydroxyacid synthase: a proposed structure for regulatory subunits supported by evidence from mutagenesis," *Journal of molecular biology,* vol. 307, pp. 465-477, 2001.
[333] V. A. Livshits, V. G. Doroshenko, N. V. Gorshkova, A. V. Belaryeva, L. V. Ivanovskaya, E. M. Khourges, *et al.*, "Mutant ilvH gene and method for producing L-valine," ed: Google Patents, 2004.
[334] A. Kaplun, M. Vyazmensky, Y. Zherdev, I. Belenky, A. Slutzker, S. Mendel, *et al.*, "Structure of the regulatory subunit of acetohydroxyacid synthase isozyme III from Escherichia coli," *Journal of molecular biology,* vol. 357, pp. 951-963, 2006.
[335] K. M. Heravi, M. Wenzel, and J. Altenbuchner, "Regulation of mtl operon promoter of Bacillus subtilis: requirements of its use in expression vectors," *Microbial cell factories,* vol. 10, p. 83, 2011.
[336] J. Errington, "Regulation of endospore formation in Bacillus subtilis," *Nature Reviews Microbiology,* vol. 1, pp. 117-126, 2003.
[337] D. Leyval, D. Uy, S. Delaunay, J. Goergen, and J. Engasser, "Characterisation of the enzyme activities involved in the valine biosynthetic pathway in a valine-producing strain of Corynebacterium glutamicum," *Journal of biotechnology,* vol. 104, pp. 241-252, 2003.

[338] E. A. Kutukova, V. A. Livshits, I. P. Altman, L. R. Ptitsyn, M. H. Zyiatdinov, I. L. Tokmakova, *et al.*, "The yeaS (leuE) gene of Escherichia coli encodes an exporter of leucine, and the Lrp protein regulates its expression," *FEBS letters*, vol. 579, pp. 4629-4634, 2005.
[339] M. Johnson, I. Zaretskaya, Y. Raytselis, Y. Merezhuk, S. McGinnis, and T. L. Madden, "NCBI BLAST: a better web interface," *Nucleic acids research*, vol. 36, pp. W5-W9, 2008.
[340] R. Krämer, "Secretion of amino acids by bacteria: physiology and mechanism," *FEMS Microbiology Reviews*, vol. 13, pp. 75-93, 1994.
[341] N. Zamboni, E. Fischer, A. Muffler, M. Wyss, H. P. Hohmann, and U. Sauer, "Transient expression and flux changes during a shift from high to low riboflavin production in continuous cultures of Bacillus subtilis," *Biotechnology and bioengineering*, vol. 89, pp. 219-232, 2005.
[342] J. M. Peters, A. Colavin, H. Shi, T. L. Czarny, M. H. Larson, S. Wong, *et al.*, "A comprehensive, CRISPR-based functional analysis of essential genes in bacteria," *Cell*, vol. 165, pp. 1493-1506, 2016.
[343] J. Altenbuchner, "Editing of the Bacillus subtilis genome by the CRISPR-Cas9 system," *Applied and environmental microbiology*, vol. 82, pp. 5421-5427, 2016.
[344] Z. Sun, A. Deng, T. Hu, J. Wu, Q. Sun, H. Bai, *et al.*, "A high-efficiency recombineering system with PCR-based ssDNA in *Bacillus subtilis* mediated by the native phage recombinase GP35," *Applied Microbiology and Biotechnology*, vol. 99, pp. 5151-5162, 2015/06/01 2015.
[345] J. Kabisch, I. Pratzka, H. Meyer, D. Albrecht, M. Lalk, A. Ehrenreich, *et al.*, "Metabolic engineering of Bacillus subtilis for growth on overflow metabolites," *Microbial cell factories*, vol. 12, p. 72, 2013.
[346] F. J. Grundy, D. A. Waters, T. Y. Takova, and T. M. Henkin, "Identification of genes involved in utilization of acetate and acetoin in Bacillus subtilis," *Molecular microbiology*, vol. 10, pp. 259-271, 1993.
[347] X. Jia, S. Li, S. Xie, and J. Wen, "Engineering a metabolic pathway for isobutanol biosynthesis in Bacillus subtilis," *Applied biochemistry and biotechnology*, vol. 168, pp. 1-9, 2012.
[348] K. Zhang, M. R. Sawaya, D. S. Eisenberg, and J. C. Liao, "Expanding metabolism for biosynthesis of nonnatural alcohols," *Proceedings of the National Academy of Sciences*, vol. 105, pp. 20653-20658, 2008.
[349] Y. J. Choi, J. H. Park, T. Y. Kim, and S. Y. Lee, "Metabolic engineering of Escherichia coli for the production of 1-propanol," *Metabolic engineering*, vol. 14, pp. 477-486, 2012.
[350] M. Wolf, A. Geczi, O. Simon, and R. Borriss, "Genes encoding xylan and β-glucan hydrolysing enzymes in *Bacillus subtilis*: characterization, mapping and construction of strains deficient in lichenase, cellulase and xylanase," *Microbiology*, vol. 141, pp. 281-290, 1995.
[351] P. R. Burkholder and N. H. Giles Jr, "Induced biochemical mutations in *Bacillus subtilis*," *American Journal of Botany*, pp. 345-348, 1947.

Appendices

Appendix A. Supplementary tables

Table S3.1. Strains, plasmids, and primers used in Chapter 3

Strain or plasmid	*Characteristics*‡	Source
E. coli		
HI-Control™ 10G	*mcrA* Δ(*mrr-hsdRMS-mcrBC*) *endA1 recA1* ϕ80d*lacZ*ΔM15 Δ*lacX74 araD139* Δ (*ara,leu*)7697*galU galK rpsL* (StrR) *nupG* λ− *tonA* Mini-F *lacIq1* (Gent^R)	Lucigen
B. subtilis		
1A751	*his npr*R2 *npr*E18 Δ*aprA*3 Δ*eglS*102 Δ*bglT bglS*RV	[350]
AW009	1A751 *amyE*::(P$_{grac.UPmod}$::*seHas*:*tuaD*, Neo^R)	This work
AW001-2	1A751 *lacA*::(*cas9*, tracrRNA, Erm^R)	This work
AW002-2	1A751 *lacA*::(*cas9*, tracrRNA, Erm^R), *thrC*::(P$_{xylA.SphI+1}$::*ugtP*-gRNA.P395T, P$_{araE}$::*mazF*, Spc^R), Δ*ugtP*	This work
AW003-2	1A751 *lacA*::(*cas9*, tracrRNA, Erm^R), *thrC*::(*ugtP*-CRISPRa.P395T, P$_{araE}$::*mazF*, Spc^R), Δ*ugtP*	This work
AW004-2	1A751 *lacA*::(*cas9*, tracrRNA, Erm^R), *amyE*::P$_{grac}$::*seHas*:*tuaD*, *thrC*::(P$_{xylA.SphI+1}$::*amyE*-gRNA.P636T, P$_{araE}$::*mazF*, Spc^R)	This work
AW005-2	1A751 *lacA*::(*cas9*, tracrRNA, Erm^R), *amyE*::P$_{grac}$::*seHas*:*tuaD*, *thrC*$^+$	This work
AW006-2	1A751 *lacA*::(*cas9*, tracrRNA, Erm^R), *amyE*::P$_{grac}$::Δ*seHas*:*tuaD*, *thrC*::(P$_{xylA.SphI+1}$::*seHas*-gRNA.P394T, P$_{araE}$::*mazF*, Spc^R)	This work
AW007-2	1A751 *lacA*::(*cas9*, tracrRNA, Erm^R), *amyE*::P$_{grac}$::Δ*seHas*:*tuaD*, *thrC*$^+$	This work
AW008-2	1A751 *lacA*::(*cas9*, tracrRNA, Erm^R), *amyE*::P$_{grac}$::Δ*seHas*:*tuaD*, *thrC*::(P$_{xylA.SphI+1}$::*ugtP*-gRNA.P395T, P$_{araE}$::*mazF*, Spc^R), Δ*ugtP*	This work
AW009-2	1A751 *lacA*::(*cas9*, tracrRNA, Erm^R), *thrC*::(P$_{xylA.SphI+1}$::*amyE*-gRNA.P636T, P$_{xylA.SphI+1}$::*ugtP*-gRNA.P395T, P$_{araE}$::*mazF*, Spc^R), Δ*amyE*, Δ*ugtP*	This work
AW010-2	1A751 *lacA*::(*cas9*, tracrRNA, Erm^R), *thrC*::(P$_{xylA.SphI+1}$::*amyE*-gRNA.P636T, P$_{araE}$::*mazF*, Spc^R), Δ*amyE*	This work
AW011-2	1A751 *lacA*::(*cas9*, tracrRNA, Erm^R), *thrC*::(P$_{xylA.SphI+1}$::*amyE*-gRNA.P25NT, P$_{araE}$::*mazF*, Spc^R), Δ*amyE*	This work

AW012-2	1A751 *lacA*::(*cas9*, tracrRNA, Erm^R), *thrC*::($P_{xylA.SphI+1}$::*amyE*-gRNA.P330T, P_{araE}::*mazF*, Spc^R), Δ*amyE*	This work
AW013-2	1A751 *lacA*::(*cas9*, tracrRNA, Erm^R), *thrC*::($P_{xylA.SphI+1}$::*amyE*-gRNA.P1344T, P_{araE}::*mazF*, Spc^R), Δ*amyE*	This work
AW014-2	1A751 *amyE*::($P_{grac.UPmod}$::*seHas*:*tuaD*, Neo^R) *lacA*::($P_{xylA, Bm}$::*dcas9*, *xylR*, Erm^R)	This work
AW015-2	1A751 *amyE*::($P_{grac.UPmod}$::*seHas*:*tuaD*, Neo^R) *lacA*::($P_{xylA, Bm}$::*dcas9*, *xylR*, Erm^R), *wprA*::$P_{xylA.SphI+1}$::*lacZ*-gRNA.P28NT)	This work
AW016-2	1A751 *amyE*::($P_{grac.UPmod}$::*seHas*:*tuaD*, Neo^R) *lacA*::($P_{xylA, Bm}$::*dcas9*, *xylR*, Erm^R), *wprA*::$P_{xylA.SphI+1}$::*lacZ*-gRNA.P28NT, *ugtP*::(*lacI*, P_{grac}::*lacZ*, Spc^R)	This work
Plasmids		
pIEFBPR	P_{spac}::*mazF*, *lacI*, Amp^R, Spc^R, *B. subtilis* auto-evicting counter-selectable *bpr* integration vector	[13]
pDG1731	*B. subtilis thrC* integration vector	[188]
pAX01	$P_{xylA, Bm}$, *xylR*, Amp^R, Erm^R, *B. subtilis lacA* integration vector	[330]
pCRISPR	*E. coli* plasmid for CRISPRa transcription	[82]
pCas9	*E. coli* plasmid for expression of Cas9	[82]
pgRNA-bacteria	*E. coli* plasmid for gRNA transcription	[23]
pdCas9-bacteria	*E. coli* plasmid for expression of dCas9	[23]
pAW008	P_{grac}::*seHas*:*tuaD*, Neo^R, *B. subtilis amyE* integration vector	This work
pAW016	P_{grac}::*lacZ*, *lacI*, Spc^R, Erm^R, *B. subtilis ugtP* integration vector	This work
pAW001-2	P_{spac}::*mazF*, *lacI*, Spc^R, Amp^R, *B. subtilis* auto-evicting counter-selectable *thrC* integration vector	This work
pAW002-2	P_{spac}::*mazF*, *lacI*, Spc^R, Erm^R, *B. subtilis* auto-evicting counter-selectable *thrC* integration vector	This work
pAW003-2	$P_{xylA,Bm}$::*mazF*, *xylR*, Spc^R, Erm^R, *B. subtilis* auto-evicting counter-selectable *thrC* integration vector	This work
pAW004-2	P_{araE}::*mazF*, *araR*, Spc^R, Erm^R, *B. subtilis* auto-evicting counter-selectable *thrC* integration vector	This work
pAW005-2	$P_{xylA.SphI+1}$, P_{araE}::*mazF*, *araR*, Spc^R, Erm^R, *B. subtilis* counter-selectable *thrC* integration vector	This work
pAW006-2	$P_{xylA.SphI+1}$::*ugtP*-gRNA.P395T , P_{araE}::*mazF*, *araR*, Spc^R, Erm^R, *B. subtilis* counter-selectable *thrC* integration vector	This work
pAW007-2	$P_{xylA.SphI+1}$::*amyE*-gRNA.P25NT , P_{araE}::*mazF*, *araR*, Spc^R, Erm^R, *B. subtilis* counter-selectable *thrC* integration vector	This work

pAW008-2	$P_{xylA.SphI+1}$::*amyE*-gRNA.P330T , P_{araE}::*mazF*, *araR*, Spc^R, Erm^R, *B. subtilis* counter-selectable *thrC* integration vector	This work
pAW009-2	$P_{xylA.SphI+1}$::*amyE*-gRNA.P636T , P_{araE}::*mazF*, *araR*, Spc^R, Erm^R, *B. subtilis* counter-selectable *thrC* integration vector	This work
pAW010-2	$P_{xylA.SphI+1}$::*amyE*-gRNA.P1344T , P_{araE}::*mazF*, *araR*, Spc^R, Erm^R, *B. subtilis* counter-selectable *thrC* integration vector	This work
pAW011-2	$P_{xylA.SphI+1}$::*seHas*-gRNA.P394T , P_{araE}::*mazF*, *araR*, Spc^R, Erm^R, *B. subtilis* counter-selectable *thrC* integration vector	This work
pAW012-2	CRISPRa, P_{araE}::*mazF*, *araR*, Spc^R, Erm^R, *B. subtilis* counter-selectable *thrC* integration vector	This work
pAW013-2	*ugtP*-CRISPRa.P395T, P_{araE}::*mazF*, *araR*, Spc^R, Erm^R, *B. subtilis* counter-selectable *thrC* integration vector	This work
pAW014-2	(BglII) $P_{xylA.SphI+1}$::*ugtP*-gRNA.P395T (NcoI), P_{araE}::*mazF*, *araR*, Spc^R, Erm^R, *B. subtilis* multi-gRNA counter-selectable *thrC* integration vector	This work
pAW015-2	(BglII) $P_{xylA.SphI+1}$::*amyE*-gRNA.P636T, $P_{xylA.SphI+1}$::*ugtP*-gRNA.P395T (NcoI), P_{araE}::*mazF*, *araR*, Spc^R, Erm^R, *B. subtilis* multi-gRNA counter-selectable *thrC* integration vector	This work
pAW016-2	*cas9*, tracrRNA, Amp^R, Erm^R, *B. subtilis lacA* integration vector	This work
pAW017-2	$P_{xylA.SphI+1}$, P_{araE}::*mazF*, *araR*, Spc^R, Erm^R, *B. subtilis* auto-evicting counter-selectable *wprA* integration vector	This work
pAW018-2	$P_{xylA.SphI+1}$::*lacZ*-gRNA.P28NT, P_{araE}::*mazF*, *araR*, Spc^R, Erm^R, *B. subtilis* auto-evicting counter-selectable *wprA* integration vector	This work
pAW019-2	$P_{xylA,\ Bm}$::*dcas9*, *xylR*, Amp^R, Erm^R, *B. subtilis lacA* integration vector	This work
pAW020-2	P_{grac}::*seHas*:*tuaD*, Amp^R, ET for insertion of the HA biosynthetic operon into the *amyE* locus at *amyE*.P636T	This work
pAW021-2	*seHas*-ET-1330bp-P394T, Amp^R, editing template for KO of *seHas* at *seHas*.P394T	This work
pAW022-2	*amyE*-ET-1330bp-P636T, Amp^R, editing template for KO of *amyE* at *amyE*.P636T	This work

primer	**sequence (5'-3')**[#]
P3.1	tctactttgacctgcaggaagtcatgtaaaagatgaggttggttcattctc
P3.2	cagattgagctagcgaaggcagcagtttttggcc
P3.3	gtgactgacccgggg*ggcgcgcc*ctcgaggccttccgaaaatgc
P3.4	gtcactgaactagt*accggt*aattccggcgactgtttctgtttcag
P3.5	ctctacttgagctctaaagcctggggtgcctaatga
P3.6	gctaaagaggtccctaga*agcgct*aaggatctaggtgaagatccttttgataa

P3.7 *agcgct*tctagggacctctttagctccttg

P3.8 ctactttgagccggctgaagcatttatcagggttattgtctcatg

P3.9 catacctgcttcctccttaa*agatct*catttccccctttgatttttagat

P3.10 ctctatgacaattggctcctaacttatagggtaacacttaa

P3.11 cagattgaggatccctacccaatcagtacgttaattttggc

P3.12 *agatct*taaggaggaagcaggtatggtaagc

P3.13 catacctgcttcctccttaa*agatct*atgttgagtaaagcgttttcatttaaaccttc

P3.14 cactttgagaattcttattcattcagttttcgtgcggactg

P3.15 gtcattgagctagccataaaaaactaaaaaaaatattga

P3.16 gacattggatcctgacatcagttaca*gcatgc*atcttatataacctcgtcagtattt

P3.17 tatgatgcatgc**aaggaaaaactgctggagat**gttttagagctagaaatagcaagttaaa

P3.18 tatgatgcatgc**agcgaataacggcagtaaag**gttttagagctagaaatagcaagttaaa

P3.19 tatgatgcatgc**cagccgacatcgtatcaaat**gttttagagctagaaatagcaagttaaa

P3.20 tatgatgcatgc**gcattgaatgacggggcaga**gttttagagctagaaatagcaagttaaa

P3.21 tatgatgcatgc**ggttcatttcaagtgaacga**gttttagagctagaaatagcaagttaaa

P3.22 tatgatgcatgc**caagcaatgtcattgttcat**gttttagagctagaaatagcaagttaaa

P3.23 gctcatgaggatccaaaaaaagcaccgactcggt

P3.24 gagacttggctagctatttcttaataactaaaaatatggtataatactc

P3.25 cagattgaggatccatgagttcaactcaac

P3.26 aaac**agattacgtgaaggaaaaactgctggagat**g

P3.27 aaaac**atctccagcagtttttccttcacgtaatct**

P3.28 ggaactgctagctgaatcatac*agatct*cataaaaaactaaaaaaaatattgaaaatact

P3.29 ttaacgtactgattgggtag*ccatgg*aaaaaaagcaccgactcggt

P3.30 *ccatgg*ctacccaatcagtacgttaattttgg

P3.31 gctcatgaggatcctaaggaggaagcaggtatgg

P3.32 gctattgaccatggaaaaaaagcaccgactcggt

P3.33 gctcatgaggatccaaaaaaagcaccga

P3.34 gtgttagatctagataatgcggtagtttatcacagttaaattgc

P3.35 ctaagatatctagatcagtcacctcctagctgactcaaatc

P3.36 gctattgacctgcaggtcgtgatgagcagctgagcc

P3.37 agtattttcaatatttttttagtttttatg*gctagc*caggctcatatttcacatccgc

P3.38 *gctagc*cataaaaaactaaaaaaaatattgaaaatactg

P3.39 gtgttaccatgg*cctagg*tagattga*gcatgc*cttattttcatcttatataacctcgtca

P3.40 gacttagaggcgcgccgtcgcaggcattattgcagc

P3.41 gtgattgaaccggtttcctctgacagctgtttgagtg

P3.42 gcattagcatgc**gtcacgacgttgtaaaacga**gttttagagctagaaatagcaagttaaa

P3.43 gctattgaactagtaaaggaggtatcaagtatggataagaaatactcaataggcttagct

P3.44 gacattgaagatct*cctgcagg*ataaaacgaaaggcccagtctttc
P3.45 acaagaggtttgacggcatgattatc
P3.46 gatttttacattgcttggatgtcatgattatcacagcagtttttccttcacgtaatctg
P3.47 tgataa*tcatga*catccaagcaatgtaaaaatcacagg
P3.48 cgcagctatggatgataaagacttg
P3.49 cctaccttcaacgttatgactg
P3.50 actttttttgtttggtgaaagattgtac
P3.51 ctcaatcgggaaacagttttatcg
P3.52 atcaatgcgctccacatagc
P3.53 cattgaggtgaatttacttgaatacc
P3.54 ggaagtgactgactcgaga
P3.55 cgtttaccaagaaactccttatgaatg
P3.56 tcaaaagaagggcaagttcc
P3.57 acattcttaccgcatcaaaggaagc
P3.58 ccatctccttcgatagctgtgaag
P3.59 *gctagc*ctgatctcgaccatcgaattcttagtgg
P3.60 ccaatgattcggattttgatagccgatggt
P3.61 gtgattgaccatggttgtttggaaagcgagggaagcgttc
P3.62 ggtctattgctagctgtgtgtttccatgtgtccagtttgg
P3.63 ggctttttgaacgatagattgcaccag
P3.64 tcaagcaatgtcattgtttaataagagctcgtcaatcaaggaaagcgtcatgcacag
P3.65 gagctcttattaaacaatgacattgcttgataggtcacc
P3.66 caatgattcggattttgatagccgatgg
P3.67 cgggaggaaggtcatgaataatctgc
P3.68 ggcggcatcaaatcgaaattaagtactttatcaattcaatgccctgtctaagaaccg
P3.69 tgataaagtacttaatttcgatttgatgccgccaaacatataga
P3.70 ggaagagaaccgcttaagcccg
P3.71 ccatacattcttcgcttggctg
P3.72 gttacaccatcactgttcgttcc
P3.73 ttgccgccagcggtattcc
P3.74 tccagcgaataacggttactcgagttatttgaatcgttttgcaaacattcttgacactc
P3.75 taactcgagtaaccgttattcgctggatttttattgc
P3.76 aagaggcgtactgcctgaacg
P3.77 aaatctggtcggagattgggatgatagc
P3.78 cttgttcagtacctaagtaacgtcattactcgagatacgatgtcggctgatacagcc
P3.79 ctcgagtaatgacgttacttaggtactgaacaagaatttaaagaaatg
P3.80 ttcacttgaaatgaacccgctcca

P3.81	gcaaccgttacttaggtactgaacaag
P3.82	gatcgtgcctgtcagtcattaggatcccacttgaaatgaacccgctccag
P3.83	ggatcctaatgactgacaggcacgatcaatgccag
P3.84	gatgttttgaccggttgtggcg
P3.85	cgaagcgaaggaaaatggatgc
P3.86	ggtcaaagcgtctacttcacaatgag
P3.87	tgtatgaacggtctggtctttgcc
P3.88	caggtattcgctggtcacttcgatg
P3.89	gaaacggcaaaacgttctgg
P3.90	gtgttgggttcacaatgtcg
P3.138	ggttcacaacgatggcagctc
P3.139	actgatctggatccatgagaacattaaaaaacctcataactgttgtg
P3.140	gattgatctagattagtggtgatgatggtggtgtaataatttttacgtgttccccagtc
P3.141	acaagcttcctttagcaccaaagagat
P3.142	agagggatttttgactccgaagtaagtc
P3.143	acgcaaatgcataactgcttccaaca

[‡]: *amyE*: α-amylase; *lacA* (*ganA*): β-galactosidase; *cas9*: CRISPR-associated protein 9 (Cas9; *Streptococcus pyogenes*); *mazF*: endoribonuclease (*Escherichia coli*); *thrC*: threonine synthase; *ugtP*: UDP-glucose diacylglyceroltransferase; *seHas*: hyaluronan synthase (*Streptococcus equisimilis*); *tuaD*: UDP-glucose 6-dehydrogenase; *xylR*: xylose operon repressor (*Bacillus megaterium*); *wprA*: cell wall-associated protease; *dcas9*: dead Cas9 (derived from *S. pyogenes*); *lacZ*: β-galactosidase (*E. coli*); *lacI*: lactose operon repressor (*E. coli*); *bpr*: bacillopeptidase F; *araR*: repressor of arabinose operons; Neo^R: neomycin resistance cassette; Erm^R: erythromycin resistance cassette; Spc^R: spectinomycin resistance cassette; Amp^R: ampicillin resistance cassette; [#]: restriction sites used for cloning are underlined; inserted restriction sites are italicized; protospacer sequences are in bold font

Table S3.2. Results from two-tailed t-tests of data presented in Chapter 3

Comparison	Relevant figure(s)	Result
Editing efficiency between pAW006-2 and pAW013-2 (1330 bp HL ugtP ET; ugtP KO) obtained without modified competence protocol	3.7B	NS
Editing efficiency between HA operon KI (pAW009-2/pAW020-2) and *seHas* KO (pAW011-2/pAW021-2)	3.7C	S
Editing efficiency between HA operon KI (pAW009-2/pAW020-2) and *ugtP* KO (pAW006-2-2/1330 bp HL *ugtP* ET)	3.7C	S
Editing efficiency between *seHas* KO (pAW011-2/pAW021-2) and *ugtP* KO (pAW006-2-2/1330 bp HL *ugtP* ET)	3.7C	S
Editing efficiency between original and modified competence protocols (pAW006-2/1330 bp HL ugtP ET; *ugtP* KO)	3.7B, 3.7C	S
Editing efficiency between *amyE* (pAW009-2/1330 bp HL *amyE* ET) and *ugtP* (pAW006-2/1330 bp HL ugtP ET) KOs	3.9A	S
Editing efficiency between PCR product (1330 bp HL *amyE* editing template) and pAW022-2 (pAW009-2; *amyE* KO)	3.9B	NS
Transformation efficiency between PCR product (1330 bp HL *amyE* editing template) and pAW022-2 (pAW009-2; *amyE* KO)	3.9B	S
Editing efficiency between 300 and 500 bp HL editing templates (pAW006-2; *ugtP* KO)	3.9C	S
Editing efficiency between 300 and 750 bp HL editing templates (pAW006-2; *ugtP* KO)	3.9C	S
Editing efficiency between 300 and 1000 bp HL editing templates (pAW006-2; *ugtP* KO)	3.9C	S
Editing efficiency between 300 and 1330 bp HL editing templates (pAW006-2; *ugtP* KO)	3.9C	S
Editing efficiency between 500 and 750 bp HL editing templates (pAW006-2; *ugtP* KO)	3.9C	NS
Editing efficiency between 500 and 1000 bp HL editing templates (pAW006-2; *ugtP* KO)	3.9C	S
Editing efficiency between 500 and 1330 bp HL editing templates (pAW006-2; *ugtP* KO)	3.9C	NS
Editing efficiency between 750 and 1000 bp HL editing templates (pAW006-2; *ugtP* KO)	3.9C	S
Editing efficiency between 750 and 1330 bp HL editing templates (pAW006-2; *ugtP* KO)	3.9C	NS
Editing efficiency between 1000 and 1330 bp HL editing templates (pAW006-2; *ugtP* KO)	3.9C	NS

Transformation efficiency between 300 and 500 bp HL editing templates (pAW006-2; *ugtP* KO)	3.9C	S
Transformation efficiency between 300 and 750 bp HL editing templates (pAW006-2; *ugtP* KO)	3.9C	S
Transformation efficiency between 300 and 1000 bp HL editing templates (pAW006-2; *ugtP* KO)	3.9C	S
Transformation efficiency between 300 and 1330 bp HL editing templates (pAW006-2; *ugtP* KO)	3.9C	S
Transformation efficiency between 500 and 750 bp HL editing templates (pAW006-2; *ugtP* KO)	3.9C	S
Transformation efficiency between 500 and 1000 bp HL editing templates (pAW006-2; *ugtP* KO)	3.9C	S
Transformation efficiency between 500 and 1330 bp HL editing templates (pAW006-2; *ugtP* KO)	3.9C	S
Transformation efficiency between 750 and 1000 bp HL editing templates (pAW006-2; *ugtP* KO)	3.9C	S
Transformation efficiency between 750 and 1330 bp HL editing templates (pAW006-2; *ugtP* KO)	3.9C	NS
Transformation efficiency between 1000 and 1330 bp HL editing templates (pAW006-2; *ugtP* KO)	3.9C	S
Editing efficiency between P25NT (pAW007-2) and P330T (pAW008-2) (1000 bp HL editing templates; *amyE* KO)	3.9D	NS
Editing efficiency between P25NT (pAW007-2) and P636T (pAW009-2) (1000 bp HL editing templates; *amyE* KO)	3.9D	S
Editing efficiency between P25NT (pAW007-2) and P1344T (pAW0010-2) (1000 bp HL editing templates; *amyE* KO)	3.9D	S
Editing efficiency between P330T (pAW008-2) and P636T (pAW009-2) (1000 bp HL editing templates; *amyE* KO)	3.9D	S
Editing efficiency between P330T (pAW008-2) and P1344T (pAW0010-2) (1000 bp HL editing templates; *amyE* KO)	3.9D	S
Editing efficiency between P636T (pAW009-2) and P1344T (pAW0010-2) (1000 bp HL editing templates; *amyE* KO)	3.9D	S
Transformation efficiency between P25NT (pAW007-2) and P330T (pAW008-2) (1000 bp HL editing templates; *amyE* KO)	3.9D	NS
Transformation efficiency between P25NT (pAW007-2) and P636T (pAW009-2) (1000 bp HL editing templates; *amyE* KO)	3.9D	NS
Transformation efficiency between P25NT (pAW007-2) and P1344T (pAW0010-2) (1000 bp HL editing templates; *amyE* KO)	3.9D	NS
Transformation efficiency between P330T (pAW008-2) and P636T (pAW009-2) (1000 bp HL editing templates; *amyE* KO)	3.9D	NS

Transformation efficiency between P330T (pAW008-2) and P1344T (pAW0010-2) (1000 bp HL editing templates; *amyE* KO)	3.9D	NS
Editing efficiency between P636T (pAW009-2) and P1344T (pAW0010-2) (1000 bp HL editing templates; *amyE* KO)	3.9D	NS
Editing efficiency between *amyE* (pAW009-2) and *ugtP* (pAW006-2) KOs (editing template combination 1)	3.9F	NS
Editing efficiency between *amyE* (pAW009-2) and *ugtP* (pAW006-2) KOs (editing template combination 2)	3.9G	NS
Editing efficiency between 1330 bp HL editing template and 1000 bp HL ET (pAW009-2; *amyE* KO)	3.9A, 3.9F	NS
Editing efficiency between 1330 bp HL editing template and pAW022-2 (pAW009-2; *amyE* KO)	3.9A, 3.9G	S
Editing efficiency between 1000 bp HL editing template and pAW022-2 (pAW009-2; *amyE* KO)	3.9F, 3.9G	S
Multiplexing efficiency between initial demonstration (1330 bp HL editing templates) and editing template combination 1 (pAW006-2 (*ugtP*) and pAW009-2 (*amyE*))	3.9A, 3.9F	NS
Multiplexing efficiency between initial demonstration (1330 bp HL editing templates) and editing template combination 2 (pAW006-2 (*ugtP*) and pAW009-2 (*amyE*))	3.9A, 3.9G	S
Multiplexing efficiency between editing template combinations 1 and 2 (pAW006-2 (*ugtP*) and pAW009-2 (*amyE*))	3.9F, 3.9G	S
Transcription of *lacZ* mRNA between induced and uninduced cultures of AW016-2	3.10	S
Expression of β-galactosidase between induced and uninduced cultures of AW016-2	3.10	S

($\alpha = 0.05$; unequal variances assumed). S: significant; NS: not significant

Table S4.1. Strains, plasmids, and primers used in Chapter 4

Strain or plasmid	Characteristics‡	Source
E. coli		
HI-Control™ 10G	*mcrA* Δ(*mrr-hsdRMS-mcrBC*) *endA1 recA1* ϕ80d*lacZ*ΔM15 Δ*lacX74 araD139* Δ (*ara,leu*)7697*galU galK rpsL* (StrR) *nupG* λ− *tonA* Mini-F *lacIq1* (Gent^R)	Lucigen
B. subtilis		
168/1A1	*trpC*2	[351]
1A786	*amyE*::*cat* Cm *lacA*::*spec leuB*8 *metA*4 Sp *hsd*(*RI*)R+M-	[330]
1A751	*his npr*R2 *npr*E18 Δ*aprA*3 Δ*eglS*102 Δ*bglT bgl*SRV	[350]
AW008	1A751 *amyE*::(P$_{grac}$::*seHas*:*tuaD*, Neo^R)	This work
AW001-4	1A751 *amyE*::(P$_{grac}$::*seHas*:*tuaD*, Neo^R), *thrC*::(P$_{grac}$::*pgsA*:*clsA*)	This work
AW002-4	1A751 *amyE*::(P$_{grac}$::*seHas*:*tuaD*, Neo^R), *lacA*::(P$_{xylA,\ Bm}$::d*cas9*, *xylR*, Erm^R)	This work
AW003-4	1A751 *amyE*::(P$_{grac}$::*seHas*:*tuaD*, Neo^R), *lacA*::(P$_{xylA,\ Bm}$::d*cas9*, *xylR*, Erm^R), *thrC*::(P$_{grac}$::*pgsA*:*clsA*)	This work
AW004-4	1A751 *amyE*::(P$_{grac}$::*seHas*:*tuaD*, Neo^R), *lacA*::(P$_{xylA,\ Bm}$::d*cas9*, *xylR*, Erm^R), *thrC*::(P$_{grac}$::*pgsA*:*clsA*), *wprA*::(P$_{xylA.SphI+1}$::*ftsZ*-gRNA.P79NT(15C-U))	This work
AW005-4	1A751 *amyE*::(P$_{grac}$::*seHas*:*tuaD*, Neo^R), *lacA*::(P$_{xylA,\ Bm}$::d*cas9*, *xylR*, Erm^R), *wprA*::(P$_{xylA.SphI+1}$::*ftsZ*-gRNA.P79NT(15C-U))	This work
AW006-4	1A751 *amyE*::(P$_{grac}$::*seHas*:*tuaD*, Neo^R), *lacA*::(P$_{xylA,\ Bm}$::d*cas9*, *xylR*, Erm^R), *wprA*::(P$_{xylA.SphI+1}$::*ftsZ*-gRNA.P244NT)	This work
AW007-4	1A751 *amyE*::(P$_{grac}$::*seHas*:*tuaD*, Neo^R), *lacA*::(P$_{xylA,\ Bm}$::d*cas9*, *xylR*, Erm^R), *thrC*::(P$_{grac.UPmod}$::*pgsA*:*clsA*)	This work
AW008-4	1A751 *amyE*::(P$_{grac}$::*seHas*:*tuaD*, Neo^R), *lacA*::(P$_{xylA,\ Bm}$::d*cas9*, *xylR*, Erm^R), *thrC*::(P$_{grac.UPmod}$::*pgsA*:*clsA*), *wprA*::(P$_{xylA.SphI+1}$::*ftsZ*-gRNA.P79NT(15C-U))	This work
AW009-4	1A751 *amyE*::(P$_{grac}$::*seHas*:*tuaD*, Neo^R), *lacA*::(P$_{xylA,\ Bm}$::d*cas9*, *xylR*, Erm^R), *thrC*::(P$_{grac.UPmod}$::*pgsA*:*clsA*), *wprA*::(P$_{xylA.SphI+1}$::*ftsZ*-gRNA.P244NT)	This work

AW010-4	1A751 *amyE*::(P_{grac}::*seHas*:*tuaD*, Neo^R), *lacA*::($P_{xylA,\ Bm}$::d*cas9*, *xylR*, Erm^R), *thrC*::($P_{grac.UPmod}$::*pgsA*:*clsA*), *wprA*::($P_{xylA.SphI+1}$::*ftsZ*-gRNA.P244NT(15C-A))	This work
AW011-4	1A751 *amyE*::(P_{grac}::*seHas*:*tuaD*, Neo^R), *lacA*::($P_{xylA,\ Bm}$::d*cas9*, *xylR*, Erm^R), *thrC*::($P_{grac.UPmod}$::*pgsA*:*clsA*), *wprA*::($P_{xylA.SphI+1}$::*ftsZ*-gRNA.P533NT)	This work
AW012-4	1A751 *amyE*::(P_{grac}::*seHas*:*tuaD*, Neo^R), Δ*pssA*	This work
AW013-4	1A751 *amyE*::(P_{grac}::*seHas*:*tuaD*, Neo^R), Δ*ugtP*	This work

Plasmids

pAW004-2	P_{araE}::*mazF*, *araR*, Spc^R, Erm^R, *B. subtilis* auto-evicting counter-selectable *thrC* integration vector	[214]
pAW017-2	$P_{xylA.SphI+1}$, P_{araE}::*mazF*, *araR*, Spc^R, Erm^R, *B. subtilis* auto-evicting counter-selectable *wprA* integration vector	[214]
pAW019-2	$P_{xylA,\ Bm}$::*dcas9*, *xylR*, Amp^R, Erm^R, *B. subtilis lacA* integration vector	[214]
pAW005	*lacI*, P_{grac}, MCS, Cat^R, Amp^R, *B. subtilis* replicating shuttle vector	This work
pAW008	P_{grac}::*seHas*:*tuaD*, Neo^R, Amp^R, *B. subtilis amyE* integration vector	[214]
pAW001-4	*lacI*, P_{grac}::*pgsA*:*clsA*, MCS, Cat^R, Amp^R, *B. subtilis* replicating shuttle vector	This work
pAW002-4	P_{grac}::*pgsA*:*clsA*, P_{araE}::*mazF*, *araR*, Spc^R, Erm^R, *B. subtilis* auto-evicting counter-selectable *thrC* integration vector	This work
pAW003-4	$P_{grac.UPmod}$::*pgsA*:*clsA*, P_{araE}::*mazF*, *araR*, Spc^R, Erm^R, *B. subtilis* auto-evicting counter-selectable *thrC* integration vector	This work
pAW004-4	$P_{xylA.SphI+1}$::*ftsZ*-gRNA.P79NT, P_{araE}::*mazF*, *araR*, Spc^R, Erm^R, *B. subtilis* auto-evicting counter-selectable *wprA* integration vector	This work
pAW005-4	$P_{xylA.SphI+1}$::*ftsZ*-gRNA.P79NT(10A-G), P_{araE}::*mazF*, *araR*, Spc^R, Erm^R, *B. subtilis* auto-evicting counter-selectable *wprA* integration vector	This work
pAW006-4	$P_{xylA.SphI+1}$::*ftsZ*-gRNA.P79NT(15C-U), P_{araE}::*mazF*, *araR*, Spc^R, Erm^R, *B. subtilis* auto-evicting counter-selectable *wprA* integration vector	This work
pAW007-4	$P_{xylA.SphI+1}$::*ftsZ*-gRNA.P244NT, P_{araE}::*mazF*, *araR*, Spc^R, Erm^R, *B. subtilis* auto-evicting counter-selectable *wprA* integration vector	This work

pAW008-4	$P_{xylA.SphI+1}$::*ftsZ*-gRNA.P244NT(15C-A), P_{araE}::*mazF*, *araR*, Spc^R, Erm^R, *B. subtilis* auto-evicting counter-selectable *wprA* integration vector	This work
pAW009-4	$P_{xylA.SphI+1}$::*ftsZ*-gRNA.P533NT, P_{araE}::*mazF*, *araR*, Spc^R, Erm^R, *B. subtilis* auto-evicting counter-selectable *wprA* integration vector	This work
pAW010-4	P_{araE}::*mazF*, *araR*, Spc^R, Erm^R, *B. subtilis* counter-selectable *pssA* integration vector	This work
pAW011-4	P_{araE}::*mazF*, *araR*, Spc^R, Erm^R, *B. subtilis* counter-selectable *ugtP* integration vector	This work

primer	**sequence (5'-3')**[#]
P4.32	gctattgaccatggaaaaaaagcaccgactcggt
P4.122	cagattgaggatccatgtttaacttaccaaataaaatcacacta
P4.123	ctcttatcctcctttt*gtaca*gattgcttagttagatgtttttaacgcttccca
P4.124	gcaatc*tgtaca*aaaggaggataagagaatgagtatttcttccatccttttatcac
P4.125	agtaactaactagtttataagatcggcgacaacag
P4.126	ggtcatggatccgcaatatgcactgacgtctattctcc
P4.127	tggtgcataggtcccgggataa
P4.128	ggatctatgcaaccgttttttcgg
P4.129	cacagattgagctagcttctctccatggacgcgtgac
P4.130	gctattgacctgcaggaattcatgtaaaagatgag
P4.131	ccttccgaaaaaacggttgcatagatccgaaggcagcagttttttggcc
P4.132	*atcgat*ggatcactagaaaatttttatcttatcacttgaaattgg
P4.133	gataagataaaaaatttttctagtgatccatcgatgaaggcagcagttttttggcc
P4.134	tatgatgcatgc**attttcaatcattcggttaa**gttttagagctagaaatagcaagttaaa
P4.135	cgcgtggcatgc**attttcaatcgttcggttaa**gttttagagctagaaatagcaagttaaa
P4.136	gcacctgcatgc**atttttaatcattcggttaa**gttttagagctagaaatagcaagttaaa
P4.137	tatgatgcatgc**ctgctctttgctttcttcag**gttttagagctagaaatagcaagttaaa
P4.138	tatgatgcatgc**ctgctatttgctttcttcag**gttttagagctagaaatagcaagttaaa
P4.139	tggaatgcatgc**tcgcggaatgcttcaagcat**gttttagagctagaaatagcaagttaaa
P4.140	ctctacgacctgcaggatcaagtggatcacaggcgac
P4.141	cagattgagctagcccccatatcagaaacggcattcag
P4.142	gtctactgggcgcgccgacgtacagcatttgcggaat
P4.143	cagacagaaccggtatgaataatccctataacccttccgattgt
P4.144	ctcactgacctgcaggtttgcaaaaggcagcaacgagc
P4.145	cagattgagctagccttccagttcggcgtctgtattcc

P4.146	gtgactgaggcgcgccatgtggagcgcattgatgagc
P4.147	cagattgaaccggttttgtatccatctccttcgatagctgt
MCS*	gcaatatgcact*gacgtc*tattct*cctgcagg*cattggatgcgc*ggcgcgcc* ***gaaaagaatgatggatcactagaaaatttttttaaaaaatctcttgacattgg*** ***aagggagatatgttattataagaattgcggaattgtgagcggataacaatt*** ***cccaattaaaggagg***aa*actagt*tcatcacagttg*gccggc*aactaaagt gcg*gcggccgc*cccggttgctgc*gcgatcgc*ttgggaccataa*accggt*t tatgacgttatcccgggacctatgcacca

‡: *amyE*: α-amylase; *clsA*: cardiolipin synthase; *ftsZ*: cell division initiation protein; *lacA* (*ganA*): β-galactosidase; *mazF*: endoribonuclease (*Escherichia coli*); *pgsA*: phosphatidylglycerophosphate synthase; *thrC*: threonine synthase; *ugtP*: UDP-glucose diacylglyceroltransferase; *seHas*: hyaluronan synthase (*Streptococcus equisimilis*); *tuaD*: UDP-glucose-6 dehydrogenase; *xylR*: xylose operon repressor (*Bacillus megaterium*); *wprA*: cell wall-associated protease; d*cas9*: dead Cas9 (derived from *S. pyogenes*); *lacI*: lactose operon repressor (*E. coli*); *araR*: repressor of arabinose operons; *pssA*: phosphatidylserine synthase; Neo^R: neomycin resistance cassette; Erm^R: erythromycin resistance cassette; Spc^R: spectinomycin resistance cassette; Amp^R: ampicillin resistance cassette; #: restriction sites used for cloning are underlined; inserted restriction sites are italicized; protospacer sequences are in bold font; substitutions in protospacers are in bold font and underlined; $P_{grac.max}$ and downstream ribosome binding site are in bold and italicized font; *: synthesized as double-stranded DNA

Table S5.1. Strains, plasmids, and primers used in Chapter 5

Strain or plasmid	***Characteristics*** ǂ	**Source**
E. coli		
HI-Control™ 10G	*mcrA* Δ(*mrr-hsdRMS-mcrBC*) *endA1 recA1* ϕ80d*lacZ*ΔM15 Δ*lacX74 araD139* Δ (*ara,leu*)7697*galU galK rpsL* (StrR) *nupG* λ− *tonA* Mini-F *lacIq1* (Gent^R)	Lucigen
B. subtilis		
1A751	*his npr*R2 *npr*E18 Δ*aprA*3 Δ*eglS*102 Δ*bglT bglS*RV	[350]
AW008	1A751 *amyE*::(P$_{grac}$::*seHas*:*tuaD*, Neo^R)	[239]
AW009	1A751 *amyE*::(P$_{grac.UPmod}$::*seHas*:*tuaD*, Neo^R),	This work
AW014-2	1A751 *amyE*::(P$_{grac.UPmod}$::*seHas*:*tuaD*, Neo^R) *lacA*::(P$_{xylA,Bm}$::*dcas9*, *xylR*, Erm^R)	[238]
AW016-2	1A751 *amyE*::(P$_{grac.UPmod}$::*seHas*:*tuaD*, Neo^R) *lacA*::(P$_{xylA,Bm}$::*dcas9*, *xylR*, Erm^R), *wprA*::(P$_{xylA.SphI+1}$::*lacZ*-gRNA.P28NT), *ugtP*::(*lacI*, P$_{grac}$::*lacZ*, Spc^R)	[238]
AW001-3	1A751 *amyE*::(P$_{grac.UPmod}$::*seHas*:*tuaD*, Neo^R) *lacA*::(P$_{xylA,Bm}$::*dcas9*, *xylR*, Erm^R) *vpr*::(P$_{grac.UPmod}$::*araE*)	This work
AW002-3	1A751 *amyE*::(P$_{grac.UPmod}$::*seHas*:*tuaD*, Neo^R) *lacA*::(P$_{xylA,Bm}$::*dcas9*, *xylR*, Erm^R) *vpr*::(P$_{grac.ΔUP}$::*araE*)	This work
AW003-3	1A751 *amyE*::(P$_{grac.UPmod}$::*seHas*:*tuaD*, Neo^R) *lacA*::(P$_{xylA,Bm}$::*dcas9*, *xylR*, Erm^R) *vpr*::(P$_{grac.ΔUP}$::*araE*) *wprA*::(P$_{xylA.SphI+1}$::*lacZ*-gRNA.P28NT)	This work
AW004-3	1A751 *amyE*::(P$_{grac.UPmod}$::*seHas*:*tuaD*, Neo^R) *lacA*::(P$_{xylA,Bm}$::*dcas9*, *xylR*, Erm^R) *vpr*::(P$_{grac.ΔUP}$::*araE*) *wprA*::(P$_{xylA.SphI+1}$::*lacZ*-gRNA.P28NT) *ugtP*::(*lacI*, P$_{grac}$::*lacZ*, Spc^R)	This work
AW005-3	1A751 *amyE*::(P$_{grac.UPmod}$::*seHas*:*tuaD*, Neo^R) *lacA*::(P$_{xylA,Bm}$::*dcas9*, *xylR*, Erm^R) *vpr*::(P$_{grac.ΔUP}$::*araE*) *wprA*::(P$_{xylA.SphI+1}$::*pfkA*-gRNA.P41NT, *araR*, P$_{araE}$::*mazF*, Spc^R)	This work
AW006-3	1A751 *amyE*::(P$_{grac.UPmod}$::*seHas*:*tuaD*, Neo^R) *lacA*::(P$_{xylA,Bm}$::*dcas9*, *xylR*, Erm^R) *vpr*::(P$_{grac.ΔUP}$::*araE*) *wprA*::(P$_{xylA.SphI+1}$::*pfkA*-gRNA.P41NT(10C-A), *araR*, P$_{araE}$::*mazF*, Spc^R)	This work
AW007-3	1A751 *amyE*::(P$_{grac.UPmod}$::*seHas*:*tuaD*, Neo^R) *lacA*::(P$_{xylA,Bm}$::*dcas9*, *xylR*, Erm^R) *vpr*::(P$_{grac.ΔUP}$::*araE*) *wprA*::(P$_{xylA.SphI+1}$::*pfkA*-gRNA.P41NT(15U-C), *araR*, P$_{araE}$::*mazF*, Spc^R)	This work
AW008-3	1A751 *amyE*::(P$_{grac.UPmod}$::*seHas*:*tuaD*, Neo^R) *lacA*::(P$_{xylA,Bm}$::*dcas9*, *xylR*, Erm^R) *vpr*::(P$_{grac.ΔUP}$::*araE*)	This work

	wprA::($P_{xylA.SphI+1}$::*pfkA*-gRNA.P315NT(10G-A), *araR*, P_{araE}::*mazF*, Spc^R)	
AW009-3	1A751 *amyE*::($P_{grac.UPmod}$::*seHas*:*tuaD*, Neo^R) *lacA*::($P_{xylA,Bm}$::*dcas9*, *xylR*, Erm^R) *vpr*::($P_{grac.\Delta UP}$::*araE*) *wprA*::($P_{xylA.SphI+1}$::*pfkA*-gRNA.P315NT(15U-G), *araR*, P_{araE}::*mazF*, Spc^R)	This work
AW010-3	1A751 *amyE*::($P_{grac.UPmod}$::*seHas*:*tuaD*, Neo^R) *lacA*::($P_{xylA,Bm}$::*dcas9*, *xylR*, Erm^R) *vpr*::($P_{grac.\Delta UP}$::*araE*) *wprA*::($P_{xylA.SphI+1}$::*pfkA*-gRNA.P610NT(10G-A), *araR*, P_{araE}::*mazF*, Spc^R)	This work
AW011-3	1A751 *amyE*::($P_{grac.UPmod}$::*seHas*:*tuaD*, Neo^R) *lacA*::($P_{xylA,Bm}$::*dcas9*, *xylR*, Erm^R) *vpr*::($P_{grac.\Delta UP}$::*araE*) *wprA*::($P_{xylA.SphI+1}$::*pfkA*-gRNA.P610NT(15U-C), *araR*, P_{araE}::*mazF*, Spc^R)	This work
AW012-3	1A751 *amyE*::($P_{grac.UPmod}$::*seHas*:*tuaD*, Neo^R) *lacA*::($P_{xylA,Bm}$::*dcas9*, *xylR*, Erm^R) *vpr*::($P_{grac.\Delta UP}$::*araE*) *wprA*::($P_{xylA.SphI+1}$::*zwf*-gRNA.P92NT, *araR*, P_{araE}::*mazF*, Spc^R)	This work
AW013-3	1A751 *amyE*::($P_{grac.UPmod}$::*seHas*:*tuaD*, Neo^R) *lacA*::($P_{xylA,Bm}$::*dcas9*, *xylR*, Erm^R) *vpr*::($P_{grac.\Delta UP}$::*araE*) *wprA*::($P_{xylA.SphI+1}$::*zwf*-gRNA.P92NT(10U-G), *araR*, P_{araE}::*mazF*, Spc^R)	This work
AW014-3	1A751 *amyE*::($P_{grac.UPmod}$::*seHas*:*tuaD*, Neo^R) *lacA*::($P_{xylA,Bm}$::*dcas9*, *xylR*, Erm^R) *vpr*::($P_{grac.\Delta UP}$::*araE*) *wprA*::($P_{xylA.SphI+1}$::*zwf*-gRNA.P92NT(15C-A), *araR*, P_{araE}::*mazF*, Spc^R)	This work
AW015-3	1A751 *amyE*::($P_{grac.UPmod}$::*seHas*:*tuaD*, Neo^R) *lacA*::($P_{xylA,Bm}$::*dcas9*, *xylR*, Erm^R) *vpr*::($P_{grac.\Delta UP}$::*araE*) *wprA*::($P_{xylA.SphI+1}$::*zwf*-gRNA.P603NT, *araR*, P_{araE}::*mazF*, Spc^R)	This work
AW016-3	1A751 *amyE*::($P_{grac.UPmod}$::*seHas*:*tuaD*, Neo^R) *lacA*::($P_{xylA,Bm}$::*dcas9*, *xylR*, Erm^R) *vpr*::($P_{grac.\Delta UP}$::*araE*) *wprA*::($P_{xylA.SphI+1}$::*zwf*-gRNA.P603NT(10U-C), *araR*, P_{araE}::*mazF*, Spc^R)	This work
AW017-3	1A751 *amyE*::($P_{grac.UPmod}$::*seHas*:*tuaD*, Neo^R) *lacA*::($P_{xylA,Bm}$::*dcas9*, *xylR*, Erm^R) *vpr*::($P_{grac.\Delta UP}$::*araE*) *wprA*::($P_{xylA.SphI+1}$::*zwf*-gRNA.P603NT(15G-U), *araR*, P_{araE}::*mazF*, Spc^R)	This work
AW018-3	1A751 *amyE*::($P_{grac.UPmod}$::*seHas*:*tuaD*, Neo^R) *lacA*::($P_{xylA,Bm}$::*dcas9*, *xylR*, Erm^R) *vpr*::($P_{grac.\Delta UP}$::*araE*) *wprA*::($P_{xylA.SphI+1}$::*zwf*-gRNA.P603NT(10U-C), $P_{xylA.SphI+1}$::*pfkA*-gRNA.P41NT, *araR*, P_{araE}::*mazF*, Spc^R)	This work
AW019-3	1A751 *amyE*::($P_{grac.UPmod}$::*seHas*:*tuaD*, Neo^R) *lacA*::($P_{xylA,Bm}$::*dcas9*, *xylR*, Erm^R) *vpr*::($P_{grac.\Delta UP}$::*araE*)	This work

	wprA::($P_{xylA.SphI+1}$::*zwf*-gRNA.P603NT(10U-C), $P_{xylA.SphI+1}$::*pfkA*-gRNA.P41NT(10C-A), *araR*, P_{araE}::*mazF*, Spc^R)	
AW020-3	1A751 *amyE*::($P_{grac.UPmod}$::*seHas*:*tuaD*, Neo^R) *thrC*::(P_{grac}::*pgcA*)	This work
AW021-3	1A751 *amyE*::($P_{grac.UPmod}$::*seHas*:*tuaD*, Neo^R) *thrC*::(P_{grac}::*glmS*)	This work
AW022-3	1A751 *amyE*::($P_{grac.UPmod}$::*seHas*:*tuaD*, Neo^R) *thrC*::(P_{grac}::*pgcA*:*glmS*)	This work
Plasmids		
pHT01	*lacI*, P_{grac}, Cat^R, Amp^R, *B. subtilis* replicating shuttle vector	[215]
pAW008	P_{grac}::*seHas*:*tuaD*, Neo^R, *B. subtilis amyE* integration vector	[238]
pAW009	$P_{grac.UPmod}$::*seHas*:*tuaD*, Neo^R, *B. subtilis amyE* integration vector	This work
pAW016	P_{grac}::*lacZ*, *lacI*, Spc^R, Erm^R, *B. subtilis ugtP* integration vector	[238]
pAW017-2	$P_{xylA.SphI+1}$, P_{araE}::*mazF*, *araR*, Spc^R, Erm^R, *B. subtilis* auto-evicting counter-selectable *wprA* integration vector	[238]
pAW018-2	$P_{xylA.SphI+1}$::*lacZ*-gRNA.P28NT, P_{araE}::*mazF*, *araR*, Spc^R, Erm^R, *B. subtilis* auto-evicting counter-selectable *wprA* integration vector	[238]
pAW019-2	$P_{xylA, Bm}$::*dcas9*, *xylR*, Amp^R, Erm^R, *B. subtilis lacA* integration vector	[238]
pAW002-4	P_{grac}::*pgsA*:*clsA*, P_{araE}::*mazF*, *araR*, Spc^R, Erm^R, *B. subtilis* auto-evicting counter-selectable *thrC* integration vector	[239]
pAW001-3	$P_{grac.UPmod}$::*araE*, P_{araE}::*mazF*, *araR*, Spc^R, Erm^R, *B. subtilis* auto-evicting counter-selectable *vpr* integration vector	This work
pAW002-3	$P_{grac.\Delta UP}$::*araE*, P_{araE}::*mazF*, *araR*, Spc^R, Erm^R, *B. subtilis* auto-evicting counter-selectable *vpr* integration vector	This work
pAW003-3	$P_{xylA.SphI+1}$::*pfkA*-gRNA.P41NT, P_{araE}::*mazF*, *araR*, Spc^R, Erm^R, *B. subtilis* auto-evicting counter-selectable *wprA* integration vector	This work
pAW004-3	$P_{xylA.SphI+1}$::*pfkA*-gRNA.P41NT(10C-A), P_{araE}::*mazF*, *araR*, Spc^R, Erm^R, *B. subtilis* auto-evicting counter-selectable *wprA* integration vector	This work
pAW005-3	$P_{xylA.SphI+1}$::*pfkA*-gRNA.P41NT(15U-C), P_{araE}::*mazF*, *araR*, Spc^R, Erm^R, *B. subtilis* auto-evicting counter-selectable *wprA* integration vector	This work
pAW006-3	$P_{xylA.SphI+1}$::*pfkA*-gRNA.P315NT(10G-A), P_{araE}::*mazF*, *araR*, Spc^R, Erm^R, *B. subtilis* auto-evicting counter-selectable *wprA* integration vector	This work

pAW007-3	$P_{xylA.SphI+1}$::*pfkA*-gRNA.P315NT(15U-G), P_{araE}::*mazF*, *araR*, Spc^R, Erm^R, *B. subtilis* auto-evicting counter-selectable *wprA* integration vector	This work
pAW008-3	$P_{xylA.SphI+1}$::*pfkA*-gRNA.P610NT(10G-A), P_{araE}::*mazF*, *araR*, Spc^R, Erm^R, *B. subtilis* auto-evicting counter-selectable *wprA* integration vector	This work
pAW009-3	$P_{xylA.SphI+1}$::*pfkA*-gRNA.P610NT(15U-C), P_{araE}::*mazF*, *araR*, Spc^R, Erm^R, *B. subtilis* auto-evicting counter-selectable *wprA* integration vector	This work
pAW010-3	$P_{xylA.SphI+1}$::*zwf*-gRNA.P92NT, P_{araE}::*mazF*, *araR*, Spc^R, Erm^R, *B. subtilis* auto-evicting counter-selectable *wprA* integration vector	This work
pAW011-3	$P_{xylA.SphI+1}$::*zwf*-gRNA.P92NT(10U-G), P_{araE}::*mazF*, *araR*, Spc^R, Erm^R, *B. subtilis* auto-evicting counter-selectable *wprA* integration vector	This work
pAW012-3	$P_{xylA.SphI+1}$::*zwf*-gRNA.P92NT(15C-A), P_{araE}::*mazF*, *araR*, Spc^R, Erm^R, *B. subtilis* auto-evicting counter-selectable *wprA* integration vector	This work
pAW013-3	$P_{xylA.SphI+1}$::*zwf*-gRNA.P603NT , P_{araE}::*mazF*, *araR*, Spc^R, Erm^R, *B. subtilis* auto-evicting counter-selectable *wprA* integration vector	This work
pAW014-3	$P_{xylA.SphI+1}$::*zwf*-gRNA.P603NT(10U-C), P_{araE}::*mazF*, *araR*, Spc^R, Erm^R, *B. subtilis* auto-evicting counter-selectable *wprA* integration vector	This work
pAW015-3	$P_{xylA.SphI+1}$::*zwf*-gRNA.P603NT(15G-U), P_{araE}::*mazF*, *araR*, Spc^R, Erm^R, *B. subtilis* auto-evicting counter-selectable *wprA* integration vector	This work
pAW016-3	(BglII) $P_{xylA.SphI+1}$, P_{araE}::*mazF*, *araR*, Spc^R, Erm^R, *B. subtilis* multi-gRNA counter-selectable *wprA* integration vector	This work
pAW017-3	(BglII) $P_{xylA.SphI+1}$::*zwf*-gRNA.P603NT(10U-C), $P_{xylA.SphI+1}$::*pfkA*-gRNA.P41NT, P_{araE}::*mazF*, *araR*, Spc^R, Erm^R, *B. subtilis* multi-gRNA counter-selectable *wprA* integration vector	This work
pAW018-3	(BglII) $P_{xylA.SphI+1}$::*zwf*-gRNA.P603NT(10U-C), $P_{xylA.SphI+1}$::*pfkA*-gRNA.P41NT(10C-A), P_{araE}::*mazF*, *araR*, Spc^R, Erm^R, *B. subtilis* multi-gRNA counter-selectable *wprA* integration vector	This work
pAW019-3	P_{grac}::*pgcA*, P_{araE}::*mazF*, *araR*, Spc^R, Erm^R, *B. subtilis* auto-evicting counter-selectable *thrC* integration vector	This work
pAW020-3	P_{grac}::*glmS*, P_{araE}::*mazF*, *araR*, Spc^R, Erm^R, *B. subtilis* auto-evicting counter-selectable *thrC* integration vector	This work
pAW021-3	P_{grac}::*pgcA*:*glmS*, P_{araE}::*mazF*, *araR*, Spc^R, Erm^R, *B. subtilis* auto-evicting counter-selectable *thrC* integration vector	This work

primer	sequence (5'-3')[#]
P5.28	ggaactgctagctgaatcatac*agatct*cataaaaaactaaaaaaaatattgaaaatact
P5.31	gctcatgaggatcctaaggaggaagcaggtatgg
P5.32	gctattgaccatggaaaaaaagcaccgactcggt
P5.33	gctcatgaggatccaaaaaaagcaccga
P5.97	cagattgagtcgacggatcactagaaaatttttatcttatcacttgaaattgg
P5.98	gcacttgaggatccttcctcctttaattggg
P5.107	tatgatgcatgc**cgaactgctgcgttcattcc**gttttagagctagaaatagcaagttaaa
P5.108	cgcgtggcatgc**cgaactgctgagttcattcc**gttttagagctagaaatagcaagttaaa
P5.109	gatcctgcatgc**cgaaccgctgcgttcattcc**gttttagagctagaaatagcaagttaaa
P5.110	gtgttagcatgc**taatttttca**cacccatatgttttagagctagaaatagcaagttaaa
P5.111	tcaatcgcatgc**taattgtttcgcacccatat**gttttagagctagaaatagcaagttaaa
P5.112	atgttagcatgc**gttcgtggccacgttttaag**gttttagagctagaaatagcaagttaaa
P5.113	atgttcgcatgc**gttcgcggccgcgttttaag**gttttagagctagaaatagcaagttaaa
P5.114	*cctagg*ggatcactagaaaatttttatcttatcacttg
P5.115	ctaattgagttggagtattcttcat*gcatgc*ttcctcctttaattgggaattgttatc
P5.116	*gcatgc*atgaagaatactccaactcaattagaacca
P5.117	gagacaatgcgatcgctcattttatccaaagcttttcaatttc
P5.118	gctattgacctgcaggcggaaaagtaaaccgggaatatgag
P5.119	agataaaaaattttctagtgatcc*cctagg*gaaagtgacggcgtattcattgag
P5.120	ctatttgaggcgcgccgccctgaaagctggtgagaca
P5.121	gagacaatactagtggcttggcctgcgaaatcaag
P5.150	cagattgacctaggttgaaattggaagggagattctttattat
P5.151	gtgattgagcatgcttcctcctttaattgggaattgttatc
P5.152	tggaatgcatgc**tttgtccgttttgatataaa**gttttagagctagaaatagcaagttaaa
P5.153	tggaatgcatgc**tttgtccgttgtgatataaa**gttttagagctagaaatagcaagttaaa
P5.154	agtgtggcatgc**tttgtacgttttgatataaa**gttttagagctagaaatagcaagttaaa
P5.155	tggaatgcatgc**atgtagcggtttgtccaaag**gttttagagctagaaatagcaagttaaa
P5.156	gaaattgcatgc**atgtagcggtctgtccaaag**gttttagagctagaaatagcaagttaaa
P5.157	tggaatgcatgc**atgtatcggtttgtccaaag**gttttagagctagaaatagcaagttaaa
P5.158	ccaaaattaacgtactgattgggtaggcggtttaaactccggaga
P5.159	ctacccaatcagtacgttaattttgg
P5.160	gctattgacctgcaggaagtcatgtaaaagatgag
P5.161	atagctctttctccaagtcat*gcatgc*ttcctcctttaattgggaattgttatc
P5.162	*gcatgc*atgacttggagaaagagctatgaacg
P5.163	gacattgagcgatcgctctactgtca*atcgat*ttattttgctgttgactcaacaatttc

P5.164	acctacgattccacacat*gcatgc*ttcctcctttaattgggaattgttatc
P5.165	*gcatgc*atgtgtggaatcgtaggttatatcggt
P5.166	gtgattgagcgatcgcttactccacagtaacactcttcgcaag
P5.167	gctattcaatcgataaaggaggtatcaagtatgtgtggaatcgtaggttatatcggt

[‡] *amyE*: α-amylase; *araE*: transporter of L-arabinose and D-xylose; *araR*: repressor of arabinose operons; d*cas9*: dead Cas9 (derived from *S. pyogenes*); *glmS*: L-glutamine-D-fructose-6-phosphate amidotransferase; *lacA* (*ganA*): β-galactosidase; *lacI*: lactose operon repressor (*E. coli*); *lacZ*: β-galactosidase (*E. coli*); *mazF*: endoribonuclease (*Escherichia coli*); *pfkA*: 6-phosphofructokinase; *pgcA*: phosphoglucomutase; *thrC*: threonine synthase; *ugtP*: UDP-glucose diacylglyceroltransferase; *seHas*: hyaluronan synthase (*Streptococcus equisimilis*); *tuaD*: UDP-glucose 6-dehydrogenase; *xylR*: xylose operon repressor (*Bacillus megaterium*); *wprA*: cell wall-associated protease; *zwf*: glucose-6-phosphate 1-dehydrogenase; Neo^R: neomycin resistance cassette; Erm^R: erythromycin resistance cassette; Spc^R: spectinomycin resistance cassette; Amp^R: ampicillin resistance cassette; [#]: restriction sites used for cloning are underlined; inserted restriction sites are italicized; protospacer sequences are in bold font; substitutions in protospacers are in bold font and underlined

Table S6.1. Results from ANOVA for experimental data presented in Chapter 6

Comparison	Relevant figure	Result
HA titer in cultures containing various oxygen vectors (4 h)	6.1A	S
HA MW in cultures containing various oxygen vectors (4 h)	6.1B	S
Cell density in cultures containing various oxygen vectors (4 h)	6.1C	S
HA titer in cultures containing various oxygen vectors (6 h)	6.1A	S
HA MW in cultures containing various oxygen vectors (6 h)	6.1B	S
Cell density in cultures containing various oxygen vectors (6 h)	6.1C	S
HA titer in cultures containing various oxygen vectors (8 h)	6.1A	S
HA MW in cultures containing various oxygen vectors (8 h)	6.1B	NS
Cell density in cultures containing various oxygen vectors (8 h)	6.1C	S
HA titer in cultures containing various oxygen vectors (10 h)	6.1A	S
HA MW in cultures containing various oxygen vectors (10 h)	6.1B	S
Cell density in cultures containing various oxygen vectors (10 h)	6.1C	S
HA titer in cultures containing various oxygen vectors (12 h)	6.1A	S
HA MW in cultures containing various oxygen vectors (12 h)	6.1B	S
Cell density in cultures containing various oxygen vectors (12 h)	6.1C	S
HA titer in cultures in which *n*-hexadecane was added at 0 h or 2 h after inoculation (4 h)	6.2A	S
HA MW in cultures in which *n*-hexadecane was added at 0 h or 2 h after inoculation (4 h)	6.2B	NS
Cell density in cultures in which *n*-hexadecane was added at 0 h or 2 h after inoculation (4 h)	6.2C	NS
HA titer in cultures in which *n*-hexadecane was added at 0 h or 2 h after inoculation (6 h)	6.2A	NS
HA MW in cultures in which *n*-hexadecane was added at 0 h or 2 h after inoculation (6 h)	6.2B	NS
Cell density in cultures in which *n*-hexadecane was added at 0 h or 2 h after inoculation (6 h)	6.2C	S
HA titer in cultures in which *n*-hexadecane was added at 0 h or 2 h after inoculation (8 h)	6.2A	NS
HA MW in cultures in which *n*-hexadecane was added at 0 h or 2 h after inoculation (8 h)	6.2B	S
Cell density in cultures in which *n*-hexadecane was added at 0 h or 2 h after inoculation (8 h)	6.2C	NS
HA titer in cultures in which *n*-hexadecane was added at 0 h or 2 h after inoculation (10 h)	6.2A	S
HA MW in cultures in which *n*-hexadecane was added at 0 h or 2 h after inoculation (10 h)	6.2B	S

Cell density in cultures in which *n*-hexadecane was added at 0 h or 2 h after inoculation (10 h)	6.2C	NS
HA titer in cultures in which *n*-hexadecane was added at 0 h or 2 h after inoculation (12 h)	6.2A	NS
HA MW in cultures in which *n*-hexadecane was added at 0 h or 2 h after inoculation (12 h)	6.2B	S
Cell density in cultures in which *n*-hexadecane was added at 0 h or 2 h after inoculation (12 h)	6.2C	S
HA titer in cultures in which perfluoro-1,3-dimethylcyclohexane was added at 0 h or 2 h after inoculation (4 h)	6.2A	S
HA MW in cultures in which perfluoro-1,3-dimethylcyclohexane was added at 0 h or 2 h after inoculation (4 h)	6.2B	S
Cell density in cultures in which perfluoro-1,3-dimethylcyclohexane was added at 0 h or 2 h after inoculation (4 h)	6.2C	NS
HA titer in cultures in which perfluoro-1,3-dimethylcyclohexane was added at 0 h or 2 h after inoculation (6 h)	6.2A	NS
HA MW in cultures in which perfluoro-1,3-dimethylcyclohexane was added at 0 h or 2 h after inoculation (6 h)	6.2B	S
Cell density in cultures in which perfluoro-1,3-dimethylcyclohexane was added at 0 h or 2 h after inoculation (6 h)	6.2C	S
HA titer in cultures in which perfluoro-1,3-dimethylcyclohexane was added at 0 h or 2 h after inoculation (8 h)	6.2A	NS
HA MW in cultures in which perfluoro-1,3-dimethylcyclohexane was added at 0 h or 2 h after inoculation (8 h)	6.2B	NS
Cell density in cultures in which perfluoro-1,3-dimethylcyclohexane was added at 0 h or 2 h after inoculation (8 h)	6.2C	NS
HA titer in cultures in which perfluoro-1,3-dimethylcyclohexane was added at 0 h or 2 h after inoculation (10 h)	6.2A	S
HA MW in cultures in which perfluoro-1,3-dimethylcyclohexane was added at 0 h or 2 h after inoculation (10 h)	6.2B	NS
Cell density in cultures in which perfluoro-1,3-dimethylcyclohexane was added at 0 h or 2 h after inoculation (10 h)	6.2C	NS
HA titer in cultures in which perfluoro-1,3-dimethylcyclohexane was added at 0 h or 2 h after inoculation (12 h)	6.2A	NS
HA MW in cultures in which perfluoro-1,3-dimethylcyclohexane was added at 0 h or 2 h after inoculation (12 h)	6.2B	NS
Cell density in cultures in which perfluoro-1,3-dimethylcyclohexane was added at 0 h or 2 h after inoculation (12 h)	6.2C	S
HA titer in cultures containing various concentrations of *n*-hexadecane (4 h)	6.3A	S
HA MW in cultures containing various concentrations of *n*-hexadecane (4 h)	6.3B	S
Cell density in cultures containing various concentrations of *n*-hexadecane (4 h)	6.3C	S
HA titer in cultures containing various concentrations of *n*-hexadecane (6 h)	6.3A	S
HA MW in cultures containing various concentrations of *n*-hexadecane (6 h)	6.3B	NS

Cell density in cultures containing various concentrations of *n*-hexadecane (6 h)	6.3C	S
HA titer in cultures containing various concentrations of *n*-hexadecane (8 h)	6.3A	S
HA MW in cultures containing various concentrations of *n*-hexadecane (8 h)	6.3B	S
Cell density in cultures containing various concentrations of *n*-hexadecane (8 h)	6.3C	S
HA titer in cultures containing various concentrations of *n*-hexadecane (10 h)	6.3A	S
HA MW in cultures containing various concentrations of *n*-hexadecane (10 h)	6.3B	S
Cell density in cultures containing various concentrations of *n*-hexadecane (10 h)	6.3C	S
HA titer in cultures containing various concentrations of *n*-hexadecane (12 h)	6.3A	S
HA MW in cultures containing various concentrations of *n*-hexadecane (12 h)	6.3B	NS
Cell density in cultures containing various concentrations of *n*-hexadecane (12 h)	6.3C	S
HA titer in cultures containing various concentrations of *n*-heptane (4 h)	6.4A	S
HA MW in cultures containing various concentrations of *n*-heptane (4 h)	6.4B	S
Cell density in cultures containing various concentrations of *n*-heptane (4 h)	6.4C	S
HA titer in cultures containing various concentrations of *n*-heptane (6 h)	6.4A	S
HA MW in cultures containing various concentrations of *n*-heptane (6 h)	6.4B	NS
Cell density in cultures containing various concentrations of *n*-heptane (6 h)	6.4C	S
HA titer in cultures containing various concentrations of *n*-heptane (8 h)	6.4A	S
HA MW in cultures containing various concentrations of *n*-heptane (8 h)	6.4B	NS
Cell density in cultures containing various concentrations of *n*-heptane (8 h)	6.4C	S
HA titer in cultures containing various concentrations of *n*-heptane (10 h)	6.4A	S
HA MW in cultures containing various concentrations of *n*-heptane (10 h)	6.4B	S
Cell density in cultures containing various concentrations of *n*-heptane (10 h)	6.4C	S
HA titer in cultures containing various concentrations of *n*-heptane (12 h)	6.4A	NS
HA MW in cultures containing various concentrations of *n*-heptane (12 h)	6.4B	NS
Cell density in cultures containing various concentrations of *n*-heptane (12 h)	6.4C	NS
HA titer in cultures containing various concentrations of perfluoromethyldecalin (4 h)	6.5A	S
HA MW in cultures containing various concentrations of perfluoromethyldecalin (4 h)	6.5B	S
Cell density in cultures containing various concentrations of perfluoromethyldecalin (4 h)	6.5C	S
HA titer in cultures containing various concentrations of perfluoromethyldecalin (6 h)	6.5A	S
HA MW in cultures containing various concentrations of perfluoromethyldecalin (6 h)	6.5B	NS
Cell density in cultures containing various concentrations of perfluoromethyldecalin (6 h)	6.5C	S
HA titer in cultures containing various concentrations of perfluoromethyldecalin (8 h)	6.5A	S
HA MW in cultures containing various concentrations of perfluoromethyldecalin (8 h)	6.5B	S

Cell density in cultures containing various concentrations of perfluoromethyldecalin (8 h)	6.5C	S
HA titer in cultures containing various concentrations of perfluoromethyldecalin (10 h)	6.5A	S
HA MW in cultures containing various concentrations of perfluoromethyldecalin (10 h)	6.5B	S
Cell density in cultures containing various concentrations of perfluoromethyldecalin (10 h)	6.5C	S
HA titer in cultures containing various concentrations of perfluoromethyldecalin (12 h)	6.5A	S
HA MW in cultures containing various concentrations of perfluoromethyldecalin (12 h)	6.5B	S
Cell density in cultures containing various concentrations of perfluoromethyldecalin (12 h)	6.5C	S
k_La in cultures containing various concentrations of *n*-hexadecane	6.6A	S
k_La in cultures containing various concentrations of *n*-heptane	6.6B	S
k_La in cultures containing various concentrations of perfluoromethyldecalin	6.6C	S
Lactate titer in cultures with or without 0.5% v/v *n*-hexadecane operated at an agitation rate of 300 rpm (4 h)	6.7A	NS
Lactate titer in cultures with or without 0.5% v/v *n*-hexadecane operated at an agitation rate of 300 rpm (6 h)	6.7A	S
Lactate titer in cultures with or without 0.5% v/v *n*-hexadecane operated at an agitation rate of 300 rpm (8 h)	6.7A	NS
Lactate titer in cultures with or without 0.5% v/v *n*-hexadecane operated at an agitation rate of 300 rpm (10 h)	6.7A	NS
Lactate titer in cultures with or without 0.5% v/v *n*-hexadecane operated at an agitation rate of 300 rpm (12 h)	6.7A	NS
Acetate titer in cultures with or without 0.5% v/v *n*-hexadecane operated at an agitation rate of 300 rpm (4 h)	6.7B	NS
Acetate titer in cultures with or without 0.5% v/v *n*-hexadecane operated at an agitation rate of 300 rpm (6 h)	6.7B	NS
Acetate titer in cultures with or without 0.5% v/v *n*-hexadecane operated at an agitation rate of 300 rpm (8 h)	6.7B	NS
Acetate titer in cultures with or without 0.5% v/v *n*-hexadecane operated at an agitation rate of 300 rpm (10 h)	6.7B	NS
Acetate titer in cultures with or without 0.5% v/v *n*-hexadecane operated at an agitation rate of 300 rpm (12 h)	6.7B	NS
2,3-BDO titer in cultures with or without 0.5% v/v *n*-hexadecane operated at an agitation rate of 300 rpm (4 h)	6.7C	S
2,3-BDO titer in cultures with or without 0.5% v/v *n*-hexadecane operated at an agitation rate of 300 rpm (6 h)	6.7C	S
2,3-BDO titer in cultures with or without 0.5% v/v *n*-hexadecane operated at an agitation rate of 300 rpm (8 h)	6.7C	S

2,3-BDO titer in cultures with or without 0.5% v/v *n*-hexadecane operated at an agitation rate of 300 rpm (10 h)	6.7C	S
2,3-BDO titer in cultures with or without 0.5% v/v *n*-hexadecane operated at an agitation rate of 300 rpm (12 h)	6.7C	S
HA titer in cultures operated at an agitation rate of 600 rpm without vector, with *n*-hexadecane, or with perfluoromethyldecalin, or 300 rpm without vector and with supplemental oxygen (4 h)	6.8A	S
HA MW in cultures operated at an agitation rate of 600 rpm without vector, with *n*-hexadecane, or with perfluoromethyldecalin, or 300 rpm without vector and with supplemental oxygen (4 h)	6.8B	NS
Cell density in cultures operated at an agitation rate of 600 rpm without vector, with *n*-hexadecane, or with perfluoromethyldecalin, or 300 rpm without vector and with supplemental oxygen (4 h)	6.8C	S
HA titer in cultures operated at an agitation rate of 600 rpm without vector, with *n*-hexadecane, or with perfluoromethyldecalin, or 300 rpm without vector and with supplemental oxygen (6 h)	6.8A	S
HA MW in cultures operated at an agitation rate of 600 rpm without vector, with *n*-hexadecane, or with perfluoromethyldecalin, or 300 rpm without vector and with supplemental oxygen (6 h)	6.8B	S
Cell density in cultures operated at an agitation rate of 600 rpm without vector, with *n*-hexadecane, or with perfluoromethyldecalin, or 300 rpm without vector and with supplemental oxygen (6 h)	6.8C	S
HA titer in cultures operated at an agitation rate of 600 rpm without vector, with *n*-hexadecane, or with perfluoromethyldecalin, or 300 rpm without vector and with supplemental oxygen (8 h)	6.8A	S
HA MW in cultures operated at an agitation rate of 600 rpm without vector, with *n*-hexadecane, or with perfluoromethyldecalin, or 300 rpm without vector and with supplemental oxygen (8 h)	6.8B	S
Cell density in cultures operated at an agitation rate of 600 rpm without vector, with *n*-hexadecane, or with perfluoromethyldecalin, or 300 rpm without vector and with supplemental oxygen (8 h)	6.8C	S
HA titer in cultures operated at an agitation rate of 600 rpm without vector, with *n*-hexadecane, or with perfluoromethyldecalin, or 300 rpm without vector and with supplemental oxygen (10 h)	6.8A	S
HA MW in cultures operated at an agitation rate of 600 rpm without vector, with *n*-hexadecane, or with perfluoromethyldecalin, or 300 rpm without vector and with supplemental oxygen (10 h)	6.8B	S
Cell density in cultures operated at an agitation rate of 600 rpm without vector, with *n*-hexadecane, or with perfluoromethyldecalin, or 300 rpm without vector and with supplemental oxygen (10 h)	6.8C	S

S: significant; NS: not significant

Table S7.1. Strains, plasmids, and primers used in Chapter 7

Strain or plasmid	*Characteristics*‡	Source
E. coli		
HI-Control™ 10G	*mcrA* Δ(*mrr-hsdRMS-mcrBC*) *endA1 recA1* ϕ80d*lacZ*ΔM15 Δ*lacX74 araD139* Δ (*ara,leu*)7697*galU galK rpsL* (StrR) *nupG* λ− *tonA* Mini-F *lacIq1* (Gent^{R})	Lucigen
B. subtilis		
1A751	*his npr*R2 *npr*E18 Δ*aprA*3 Δ*eglS*102 Δ*bglT bglS*RV	[350]
AW001-2	1A751 *lacA*::(*cas9*, tracrRNA, Erm^{R})	[263]
AW001-5	1A751 *lacA*::(*cas9*, tracrRNA, Erm^{R}), *bpr*::(P$_{xylA,\ Bm}$::*comK*:*comS*, *xylR*)	This work
AW002-5	1A751 *lacA*::(*cas9*, tracrRNA, Erm^{R}), *bpr*::(P$_{xylA,\ Bm}$::*comK*:*comS*, *xylR*), P$_{grac}$::*ilvBHC*, Δ*bcd*	This work
AW003-5	1A751 *lacA*::(*cas9*, tracrRNA, Erm^{R}), *bpr*::(P$_{xylA,\ Bm}$::*comK*:*comS*, *xylR*), P$_{grac}$::*ilvBHC*, Δ*bcd*, *amyE*::P$_{grac}$::*ybgE*:*ywaA*	This work
AW004-5	1A751 *lacA*::(*cas9*, tracrRNA, Erm^{R}), *bpr*::(P$_{xylA,\ Bm}$::*comK*:*comS*, *xylR*), P$_{grac}$::*ilvBHC*, Δ*bcd*, *amyE*::P$_{grac}$::*ybgE*:*ywaA*, *wprA*::P$_{grac}$::*ilvD*	This work
AW005-5	1A751 *lacA*::(*cas9*, tracrRNA, Erm^{R}), *bpr*::(P$_{xylA,\ Bm}$::*comK*:*comS*, *xylR*), P$_{grac}$::*ilvBH***C*, Δ*bcd*, *amyE*::P$_{grac}$::*ybgE*:*ywaA*, *wprA*::P$_{grac}$::*ilvD*	This work
AW006-5	1A751 *lacA*::(*cas9*, tracrRNA, Erm^{R}), *bpr*::(P$_{xylA,\ Bm}$::*comK*:*comS*, *xylR*), P$_{grac}$::*ilvBHC*, Δ*bcd*, *amyE*::P$_{grac}$::*ybgE*:*ywaA*, *wprA*::P$_{grac}$::*ilvD*, P$_{grac.UPmod}$::*als*, Δ*ilvB*	This work
AW007-5	1A751 *lacA*::(*cas9*, tracrRNA, Erm^{R}), *bpr*::(P$_{xylA,\ Bm}$::*comK*:*comS*, *xylR*), P$_{grac}$::*ilvBH***C*, Δ*bcd*, *amyE*::P$_{grac}$::*ybgE*:*ywaA*, *wprA*::P$_{grac}$::*ilvD*, Δ*leuA*, Δ*ilvA*	This work
AW008-5	1A751 *lacA*::(*cas9*, tracrRNA, Erm^{R}), *bpr*::(P$_{xylA,\ Bm}$::*comK*:*comS*, *xylR*), P$_{grac}$::*ilvBH***C*, Δ*bcd*, *amyE*::P$_{grac}$::*ybgE*:*ywaA*, *wprA*::P$_{grac}$::*ilvD*, Δ*leuA*, Δ*ilvA*, P$_{grac.UPmod}$::*als*	This work
AW009-5	1A751 *lacA*::(*cas9*, tracrRNA, Erm^{R}), *bpr*::(P$_{xylA,\ Bm}$::*comK*:*comS*, *xylR*), P$_{grac}$::*ilvBH***C*, Δ*bcd*, *amyE*::P$_{grac}$::*ybgE*:*ywaA*, *wprA*::P$_{grac}$::*ilvD*, Δ*leuA*, Δ*ilvA*, P$_{mtlA}$::*als*	This work
AW010-5	1A751 *lacA*::(*cas9*, tracrRNA, Erm^{R}), *bpr*::(P$_{xylA,\ Bm}$::*comK*:*comS*, *xylR*), P$_{grac}$::*ilvBH***C*, Δ*bcd*, *amyE*::P$_{grac}$::*ybgE*:*ywaA*, *wprA*::P$_{grac}$::*ilvD*, Δ*leuA*, Δ*ilvA*, P$_{mtlA}$::*als*, Δ*alsD*	This work
AW011-5	1A751 *lacA*::(*cas9*, tracrRNA, Erm^{R}), *bpr*::(P$_{xylA,\ Bm}$::*comK*:*comS*, *xylR*), P$_{grac}$::*ilvBH***C*, Δ*bcd*,	This work

	amyE::P_{grac}::*ybgE*:*ywaA*, *wprA*::P_{grac}::*ilvD*, Δ*leuA*, Δ*ilvA*, P_{mtlA}::*als*, Δ*alsD*, $P_{grac.UPmod}$::*bcaP*	
AW012-5	1A751 *lacA*::(*cas9*, tracrRNA, Erm^R), *bpr*::($P_{xylA,Bm}$::*comK*:*comS*, *xylR*), P_{grac}::*ilvBH***C*, Δ*bcd*, *amyE*::P_{grac}::*ybgE*:*ywaA*, *wprA*::P_{grac}::*ilvD*, Δ*leuA*, Δ*ilvA*, P_{mtlA}::*als*, Δ*alsD*, $P_{grac.UPmod}$::*bcaP*, Δ*sigF*	This work
AW013-5	1A751 *lacA*::(*cas9*, tracrRNA, Erm^R), *bpr*::($P_{xylA,Bm}$::*comK*:*comS*, *xylR*), P_{grac}::*ilvBH***C*, Δ*bcd*, *amyE*::P_{grac}::*ybgE*:*ywaA*, *wprA*::P_{grac}::*ilvD*, Δ*leuA*, Δ*ilvA*, P_{mtlA}::*als*, Δ*alsD*, $P_{grac.UPmod}$::*bcaP*, Δ*sigF*, Δ*pdhA*	This work
AW014-5	1A751 *lacA*::(*cas9*, tracrRNA, Erm^R), *bpr*::($P_{xylA,Bm}$::*comK*:*comS*, *xylR*), P_{grac}::*ilvBHC*, Δ*bcd*, *amyE*::P_{grac}::*ybgE*:*ywaA*, *wprA*::P_{grac}::*ilvD*, Δ*pdhA*	This work
AW015-5	1A751 *lacA*::(*cas9*, tracrRNA, Erm^R), *bpr*::($P_{xylA,Bm}$::*comK*:*comS*, *xylR*), P_{grac}::*ilvBH***C*, Δ*bcd*, *amyE*::P_{grac}::*ybgE*:*ywaA*, *wprA*::P_{grac}::*ilvD*, Δ*pdhA*	This work
AW016-5	1A751 *lacA*::(*cas9*, tracrRNA, Erm^R), *bpr*::($P_{xylA,Bm}$::*comK*:*comS*, *xylR*), P_{grac}::*ilvBH***C*, Δ*bcd*, *amyE*::P_{grac}::*ybgE*:*ywaA*, *wprA*::P_{grac}::*ilvD*, Δ*leuA*, Δ*ilvA*, Δ*pdhA*	This work
AW017-5	1A751 *lacA*::(*cas9*, tracrRNA, Erm^R), *bpr*::($P_{xylA,Bm}$::*comK*:*comS*, *xylR*), P_{grac}::*ilvBH***C*, Δ*bcd*, *amyE*::P_{grac}::*ybgE*:*ywaA*, *wprA*::P_{grac}::*ilvD*, Δ*leuA*, Δ*ilvA*, P_{mtlA}::*als*, Δ*pdhA*	This work
AW018-5	1A751 *lacA*::(*cas9*, tracrRNA, Erm^R), *bpr*::($P_{xylA,Bm}$::*comK*:*comS*, *xylR*), P_{grac}::*ilvBH***C*, Δ*bcd*, *amyE*::P_{grac}::*ybgE*:*ywaA*, *wprA*::P_{grac}::*ilvD*, Δ*leuA*, Δ*ilvA*, P_{mtlA}::*als*, Δ*alsD*, Δ*pdhA*	This work
AW019-5	1A751 *lacA*::(*cas9*, tracrRNA, Erm^R), *bpr*::($P_{xylA,Bm}$::*comK*:*comS*, *xylR*), P_{grac}::*ilvBH***C*, Δ*bcd*, *amyE*::P_{grac}::*ybgE*:*ywaA*, *wprA*::P_{grac}::*ilvD*, Δ*leuA*, Δ*ilvA*, P_{mtlA}::*als*, Δ*alsD*, $P_{grac.UPmod}$::*bcaP*, Δ*pdhA*	This work
AW020-5	1A751 *lacA*::(*cas9*, tracrRNA, Erm^R), *bpr*::($P_{xylA,Bm}$::*comK*:*comS*, *xylR*), P_{grac}::*ilvBH***C*, Δ*bcd*, *amyE*::P_{grac}::*ybgE*:*ywaA*, *wprA*::P_{grac}::*ilvD*, Δ*leuA*, Δ*ilvA*, Δ*pdhA*, Δ*sigF*	This work
AW021-5	1A751 *lacA*::(*cas9*, tracrRNA, Erm^R), *bpr*::($P_{xylA,Bm}$::*comK*:*comS*, *xylR*), P_{grac}::*ilvBHC*, Δ*bcd*, *amyE*::P_{grac}::*ybgE*:*ywaA*, *wprA*::P_{grac}::*ilvD*, Δ*pdhA*, Δ*leuA*, Δ*ilvA*	This work
Plasmids		
pAX01	$P_{xylA,Bm}$, *xylR*, Amp^R, Erm^R, *B. subtilis lacA* integration vector	[330]
pgRNA-bacteria	*E. coli* plasmid for gRNA transcription	[23]
pAW008	P_{grac}::*seHas*:*tuaD*, Neo^R, *B. subtilis amyE* integration vector	[263]

pAW004-2	P_{araE}::*mazF*, *araR*, Spc^R, Erm^R, *B. subtilis* auto-evicting counter-selectable *thrC* integration vector	[263]
pAW014-2	(BglII) $P_{xylA.SphI+1}$::*ugtP*-gRNA.P395T (NcoI), P_{araE}::*mazF*, *araR*, Spc^R, Erm^R, *B. subtilis* multi-gRNA counter-selectable *thrC* integration vector	[263]
pAW020-2	P_{grac}::*seHas*:*tuaD*, Amp^R, ET for insertion of the HA biosynthetic operon into the *amyE* locus at *amyE*.P636T	[263]
pAW001-5	$P_{xylA,\ Bm}$::*comK*, *xylR*, P_{araE}::*mazF*, *araR*, Spc^R, Erm^R, *B. subtilis* counter-selectable *bpr* integration vector	This work
pAW002-5	$P_{xylA,\ Bm}$::*comK*:*comS*, *xylR*, P_{araE}::*mazF*, *araR*, Spc^R, Erm^R, *B. subtilis* counter-selectable *bpr* integration vector	This work
pAW003-5	$P_{xylA.SphI+1}$::P_{grac}::*ilvBHC*-gRNA, P_{araE}::*mazF*, *araR*, Spc^R, Erm^R, *B. subtilis* counter-selectable *thrC* integration vector	This work
pAW004-5	$P_{xylA.SphI+1}$::*bcd*-gRNA.P585T, $P_{xylA.SphI+1}$::P_{grac}::*ilvBHC*-gRNA, P_{araE}::*mazF*, *araR*, Spc^R, Erm^R, *B. subtilis* counter-selectable *thrC* integration vector	This work
pAW005-5	$P_{xylA.SphI+1}$::*leuA*-gRNA.P764NT, $P_{xylA.SphI+1}$::*bcd*-gRNA.P585T, $P_{xylA.SphI+1}$::P_{grac}::*ilvBHC*-gRNA, P_{araE}::*mazF*, *araR*, Spc^R, Erm^R, *B. subtilis* counter-selectable *thrC* integration vector	This work
pAW006-5	$P_{xylA.SphI+1}$::*amyE*-gRNA.P636T, P_{araE}::*mazF*, *araR*, Spc^R, Erm^R, *B. subtilis* counter-selectable *thrC* integration vector	This work
pAW007-5	$P_{xylA.SphI+1}$::*wprA*-gRNA.P1419T, $P_{xylA.SphI+1}$::*amyE*-gRNA.P636T, P_{araE}::*mazF*, *araR*, Spc^R, Erm^R, *B. subtilis* counter-selectable *thrC* integration vector	This work
pAW008-5	$P_{xylA.SphI+1}$::$P_{grac.UPmod}$::*als*-gRNA, P_{araE}::*mazF*, *araR*, Spc^R, Erm^R, *B. subtilis* counter-selectable *thrC* integration vector	This work
pAW009-5	$P_{xylA.SphI+1}$::*ilvB*-gRNA.P1101NT, $P_{xylA.SphI+1}$::$P_{grac.UPmod}$::*als*-gRNA, P_{araE}::*mazF*, *araR*, Spc^R, Erm^R, *B. subtilis* counter-selectable *thrC* integration vector	This work
pAW010-5	$P_{xylA.SphI+1}$::*ilvA*-gRNA.P581NT, $P_{xylA.SphI+1}$::*leuA*-gRNA.P764NT, $P_{xylA.SphI+1}$::*bcd*-gRNA.P585T, $P_{xylA.SphI+1}$::P_{grac}::*ilvBHC*-gRNA, P_{araE}::*mazF*, *araR*, Spc^R, Erm^R, *B. subtilis* counter-selectable *thrC* integration vector	This work
pAW011-5	$P_{xylA.SphI+1}$::$P_{grac.UPmod}$::*bcaP*-gRNA, P_{araE}::*mazF*, *araR*, Spc^R, Erm^R, *B. subtilis* counter-selectable *thrC* integration vector	This work
pAW012-5	$P_{xylA.SphI+1}$::*sigF*-gRNA.P371T, $P_{xylA.SphI+1}$::$P_{grac.UPmod}$::*bcaP*-gRNA, P_{araE}::*mazF*, *araR*, Spc^R, Erm^R, *B. subtilis* counter-selectable *thrC* integration vector	This work
pAW013-5	$P_{xylA.SphI+1}$::*ilvH*-gRNA.P40T, P_{araE}::*mazF*, *araR*, Spc^R, Erm^R, *B. subtilis* counter-selectable *thrC* integration vector	This work
pAW014-5	$P_{xylA.SphI+1}$::*alsD*-gRNA.P99T, P_{araE}::*mazF*, *araR*, Spc^R, Erm^R, *B. subtilis* counter-selectable *thrC* integration vector	This work
pAW015-5	$P_{xylA.SphI+1}$::*pdhA*-gRNA.P116T, P_{araE}::*mazF*, *araR*, Spc^R, Erm^R, *B. subtilis* counter-selectable *thrC* integration vector	This work
pAW016-5	$P_{xylA.SphI+1}$::*sigF*-gRNA.P371T, P_{araE}::*mazF*, *araR*, Spc^R, Erm^R, *B. subtilis* counter-selectable *thrC* integration vector	This work

pAW017-5	P_{grac}::*ilvBHC* editing template, Amp^R	This work
pAW018-5	mut.*bcd*.P585T editing template, Amp^R	This work
pAW019-5	mut.*leuA*.P764NT editing template, Amp^R	This work
pAW020-5	P_{grac}::*ybgE*:*ywaA*, Amp^R, *B. subtilis amyE* integration vector	This work
pAW021-5	P_{grac}::*ilvD*, Amp^R, *B. subtilis wprA* integration vector	This work
pAW022-5	IlvH(N11A,G14D,N17F,N29H) editing template, Amp^R	This work
pAW023-5	$P_{grac.UPmod}$::*als* editing template, Amp^R	This work
pAW024-5	P_{mtlA}::*als* editing template, Amp^R	This work
pAW025-5	mut.*ilvB*.P1101NT editing template, Amp^R	This work
pAW026-5	mut.*ilvA*.P581NT editing template, Amp^R	This work
pAW027-5	mut.*alsD*.P99T editing template, Amp^R	This work
pAW028-5	$P_{grac.UPmod}$::*bcaP* editing template, Amp^R	This work
pAW029-5	mut.*sigF*.P371T editing template, Amp^R	This work
pAW030-5	mut.*pdhA*.P116T editing template, Amp^R	This work
pAW031-5	editing template to restore *thrC*, Amp^R	This work

primers	**sequence (5'-3')**[#]
P7.1	*gcatgc*ctaacttataggggtaacacttaaaaaaga
P7.2	gttttctgactcat*atcgat*ttcctcctttcatttccccctttgatttttagat
P7.3	aaaggaggaa*atcgat*atgagtcagaaaacagacgcacct
P7.4	gcagatgagctagcctaataccgttccccaagctcacg
P7.5	gctattgacctgcaggacaagagaaggacgtgacgaag
P7.6	ttaagtgttacccctataagttag*gcatgc*ttaaatttaatcagaaaagtcgttttttct
P7.7	ctacttgaggcgcgccaactggcagtatatagatggaaagtggc
P7.8	cagattgaaccggtatctaaatcctcagcgcttgagaaagc
P7.9	gcgtatcagctagcaaaggaggtatcaagtatgaaccgatcaggcaagcatc
P7.10	cgtgaccagcggccgcttacttctccctccagcagaagtacagc
P7.11	ggtcatgcatgc**tgattcactcgttactaaag**gttttagagctagaaatagcaagttaaa
P7.12	gctattgaccatggaaaaaaagcaccgactcggt
P7.13	ggaactgctagctgaatcatac*agatct*cataaaaaactaaaaaaaatattgaaaatact
P7.14	ctaaaactcttcatgcaggtggcggcagcatgcatcttatataacctcgtc
P7.15	**tgccgccacctgcatgaaga**gttttagagctagaaatagcaagttaaa

P7.16 gctcatgaggatccaaaaaaagcaccgactcggt
P7.17 gctctaaaacagtcgaaacaggtattacgcgcatgcatcttatataacctcgtc
P7.18 **gcgtaatacctgtttcgact**gttttagagctagaaatagcaagttaaa
P7.19 tatgatgcatgc**gcattgaatgacggggcaga**gttttagagctagaaatagcaagttaaa
P7.20 taaaactttaaatcggcaagcgtgctgcatgcatcttatataacctcgtc
P7.21 **agcacgcttgccgatttaaa**gttttagagctagaaatagcaagttaaa
P7.22 taaaaccactccttattatgcattttgcatgcatcttatataacctcgtc
P7.23 **aaaatgcataataaggagtg**gttttagagctagaaatagcaagttaaa
P7.24 gctctaaaacctctggtatgtagataatgagcatgcatcttatataacctcgtc
P7.25 **tcattatctacataccagag**gttttagagctagaaatagcaagttaaa
P7.26 taaaactctctctggggtaggtacatgcatgcatcttatataacctcgtc
P7.27 **atgtacctaccccagagaga**gttttagagctagaaatagcaagttaaa
P7.28 gctctaaaacttctcctactcaatattatagcatgcatcttatataacctcgtc
P7.29 **tataatattgagtaggagaa**gttttagagctagaaatagcaagttaaa
P7.30 aaaactcgcgcgccggattttgtttgcatgcatcttatataacctcgtc
P7.31 **aaacaaaatccggcgcgcga**gttttagagctagaaatagcaagttaaa
P7.32 ggtcatgcatgc**tgactgtggtgaaccgctcc**gttttagagctagaaatagcaagttaaa
P7.33 gctctaaaactctaatagagaagtcattgtgcatgcatcttatataacctcgtc
P7.34 **acaatgacttctctattaga**gttttagagctagaaatagcaagttaaa
P7.35 aaaaccttcattcacgacttctcccgcatgcatcttatataacctcgtc
P7.36 **gggagaagtcgtgaatgaag**gttttagagctagaaatagcaagttaaa
P7.37 cgcagccagctagttcatcacc
P7.38 *gcatgc*tgtaactgatgtca*ggatcc*gatatggttcgtatatggattgagtctgac
P7.39 aaaggaggaactaaaatggggactaatg
P7.40 gtgtgccacagggatttgctg
P7.41 *ggatcc*tgacatcagttaca*gcatgc*cagctattgtaacataatcggtacgg
P7.42 cattagtccccattttagttcctcctttaattgggaattgttatccgctcac
P7.43 gctgaacagcagcaaatccctgtggcacacgaaccgttgtaggtggcgtg
P7.44 catgggaaggtgatgaactagctggctgcgctcgagccatccggaagatc
P7.45 cttctcgtcccaacaattgaggc
P7.46 cgtaacgattaagtttcatta*gcgcgc*atgcaggtggcggcaaagg
P7.45 *gcgcgc*taatgaaacttaatcgttacggatatcaacaaacaatctg
P7.48 cctcttgcgcagactgcatc
P7.49 ttcaaagtttgatgcagtctgcgcaagagggaaccgttgtaggtggcgtg
P7.50 attgccggcctcaattgttgggacgagaagctcgagccatccggaagatc
P7.51 caatccgctcatattcgactgg
P7.52 cataccagaaaagat*gcgcgc*tgataagaaacaggtattacgctgaacgag
P7.53 ttatca*gcgcgc*atcttttctggtatggagggctacg
P7.54 tttcgatacgacgcttcgtgatgg
P7.55 tgttcaccatcacgaagcgtcgtatcgaaagaaccgttgtaggtggcgtg
P7.56 ttggttttccagtcgaatatgagcggattgctcgagccatccggaagatc
P7.57 gcagcccgcctaatgagcgggctttttgctagctgtgtgtttccatgtg
P7.58 cgttcaataagcttattcattctagattcctcctttaattgggaattgttatcc
P7.59 taacaattcccaattaaaggaggaa*tctaga*atgaataagcttattgaacgagaaaaaac
P7.60 cattatcttatcctcctttgagctctcacacttccactgtccagttaaac
P7.61 *gagctc*aaaggaggataagataatgactaaacaaacaattcgcgttg

P7.62 aaaaaagcccgctcattaggcgggctgc*accggt*ttacttgctttcagtcagcgctg
P7.63 cgccagatcttccggatggctcgagtcgtgatgagcagctgagcc
P7.64 cccgtaccgattatgttacaatagctggctagccaggctcatatttcacatc
P7.65 gcagcccgcctaatgagcgggctttttgtcgcaggcattattgcagc
P7.66 gagaataaaagaagaacatcgattttcttcctctgacagctgtttgagtg
P7.67 gcggatgtgaaatatgagcctggctagccagctattgtaacataatcggtacgg
P7.68 cctcctttaattgttatccgctcacaattccac
P7.69 aattgtgagcggataacaattaaaggaggaaagataatggcagaattacgcagtaatatg
P7.70 aaaagcccgctcattaggcgggctgc*ggatcc*ttagattttcataataccgccgg
P7.71 caaacagctgtcagaggaagaaaatcgatgttcttcttttattctctcaag
P7.72 tgtttggctcagctgctcatcacgactcgagccatccggaagatc
P7.73 acagattcctgtagtcggagacag
P7.74 atagaccggtgatccggaataacacatcgga*gcgcgc*caccacagtcaatgtgataattc
P7.75 tgtgttattccggatcaccggtctattcacaaaaaggcattaccacattgaaagcattac
P7.76 cctgctgtcaattcatctttgatttcag
P7.77 cgccagatcttccggatggctcgagcattctgcattaagctgtatttggtcc
P7.78 aagataaaaaattttctagtgatcc*ctcgag*tcgcagtagccgaagagcttc
P7.79 taacaattcccaattaaaggaggaaactaaaatgacaaaagcaacaaaagaaca
P7.80 gaaaacccacgccacctacaacggttcggaacaaaccgatacggc
P7.81 gaagctcttcggctactgcga*ctcgag*ggatcactagaaaatttttatcttatcacttg
P7.82 tttgttcttttgttgcttttgtcattttagtttcctccttttaattgggaattgttatcc
P7.83 atattttggccgtatcggtttgttccgaaccgttgtaggtggcgtg
P7.84 gaccaaatacagcttaatgcagaatgctcgagccatccggaagatc
P7.85 gaagcatcattctctgaacatatttcccaattaaaggaggaaactaaaatgac
P7.86 gtttcaggagccttttctctttcctcctcgagtcgcagtagccgaag
P7.87 gaagctcttcggctactgcgactcgaggaggaaagagaaaaggctcctg
P7.88 cattttagtttcctcctttaattgggaaatatgttcagagaatgatgcttcc
P7.89 gccagatcttccggatggctcgagcgtctttacagggcaggtagc
P7.90 ttcattatctac*gctagc*ttattaatactcttctttccattctgcgagc
P7.91 aaagaagagtattaataa*gctagc*gtagataatgaagaagaaggttttaaacc
P7.92 aacccacgccacctacaacggttcaccttcaacatgaacgacg
P7.93 accttcgtcgttcatgttgaaggtgaaccgttgtaggtggcgtg
P7.94 gttgctacctgccctgtaaagacgctcgagccatccggaagatc
P7.95 cgccagatcttccggatggctcgagtcttggctctgcaggataatgg
P7.96 ttcaaatatgtacctaccc*gcgcgc*ttattagccgcctccgacacttgc
P7.97 ttgcaagtgtcggaggcggctaataa*gcgcgc*ggggtaggtacatatttgaaaaacg
P7.98 aaacccacgccacctacaacggttcctctaggcttttgagtaacaagctatc
P7.99 tagcttgttactcaaaagcctagaggaaccgttgtaggtggcgtg
P7.100 caaccattatcctgcagagccaagactcgagccatccggaagatc
P7.101 cgccagatcttccggatggctcgagcagattggaaatcagacagagc
P7.102 tcaaaatctccgtctta*gctggg*tcataatagagaagtcattgttgatacttgataaatc
P7.103 caacaatgacttctctattatga*cccagc*taagacggagattttgaactgtcag
P7.104 aaacccacgccacctacaacggttcttcatcagaccacacctttactg
P7.105 aacagtaaaggtgtggtctgatgaagaaccgttgtaggtggcgtg
P7.106 tgcgctctgtctgatttccaatctgctcgagccatccggaagatc
P7.107 cgccagatcttccggatggctcgagcgatcattactggaggcgacag

P7.108	gataaaaaattttctagtgatcc*ctcgag*acaaaaaaccagctcttgagctgg
P7.109	aacaattcccaattaaaggaggaaactaaaatgaaagggagcgtttttaggaag
P7.110	gaaaacccacgccacctacaacggttcatgcctttaggcagatccttcg
P7.111	gctcaagagctggttttttgt*ctcgag*ggatcactagaaaatttttttatcttatcacttg
P7.112	cttcctaaaaacgctccctttcattttagtttcctcctttaattgggaattgttatcc
P7.113	ccgcgaaggatctgcctaaaggcatgaaccgttgtaggtggcgtg
P7.114	ccgctgtcgcctccagtaatgatcgctcgagccatccggaagatc
P7.115	cgccagatcttccggatggctcgaggaatcgttcgcccgtgtgac
P7.116	ctgcccagtgttttcgaaagtca*cctagg*ttagcgccggattttgtttccaag
P7.117	cttggaaacaaaatccggcgctaa*cctagg*tgactttcgaaaacactgggcagag
P7.118	gaaaacccacgccacctacaacggttcggtttctgctccgcctacg
P7.119	caaaccgtaggcggagcagaaaccgaaccgttgtaggtggcgtg
P7.120	caactgtcacacgggcgaacgattcctcgagccatccggaagatc
P7.121	cgccagatcttccggatggctcgagccgcagcaaaccatatgg
P7.122	tgatcatcagttaaatcaggtcatta*tctaga*attcacgacttctccctttttc
P7.123	aaagggagaagtcgtgaat*tctaga*taatgacctgatttaactgatgatcaattaaaag
P7.124	gaaaacccacgccacctacaacggttcaaggaacgcacggaaacg
P7.125	gcttgtacgtttccgtgcgttccttgaaccgttgtaggtggcgtg
P7.126	cttttctccatatggtttgctgcggctcgagccatccggaagatc
P7.127	cgaagcgaaggaaaatggatgc
P7.128	ggtcaaagcgtctacttcacaatgag

‡: *alsD*, acetolactate decarboxylase; *alsS*, acetolactate synthase; *amyE*, α-amylase; *araR*, repressor of arabinose operons; *bcaP*, BCAA permease; *bcd*, BCAA dehydrogenase; *bpr*, bacillopeptidase F; *cas9*, CRISPR-associated protein 9 (Cas9; *Streptococcus pyogenes*); *comK*, master competence regulator; *comS*, competence protein S; *ilvA*, L-threonine dehydratase; *ilvB*, acetohydroxy-acid synthase catalytic subunit; *ilvC*, acetohydroxy-acid isomeroreductase; *ilvD*, dihydroxy-acid dehydratase; *ilvH*, native acetohydroxy-acid synthase regulatory subunit, *ilvH**, engineered acetohydroxy-acid synthase regulatory subunit; *lacA*, β-galactosidase; *leuA*, 2-isopropylmalate synthase; *mazF*, endoribonuclease (*Escherichia coli*); *pdhA*, E1α subunit of the pyruvate dehydrogenase complex; *sigF*, sporulation-specific transcription factor σ^F; *thrC*, threonine synthase; tracrRNA, trans-activating CRISPR RNA; *wprA*, cell wall-associated protease; *xylR*, xylose operon repressor (*Bacillus megaterium*); *ybgE*, BCAA aminotransferase; *ywaA*; BCAA aminotransferase; Neo^R, neomycin resistance cassette; Erm^R, erythromycin resistance cassette; Spc^R, spectinomycin resistance cassette; Amp^R, ampicillin resistance cassette.

Appendix B. Supplementary figures

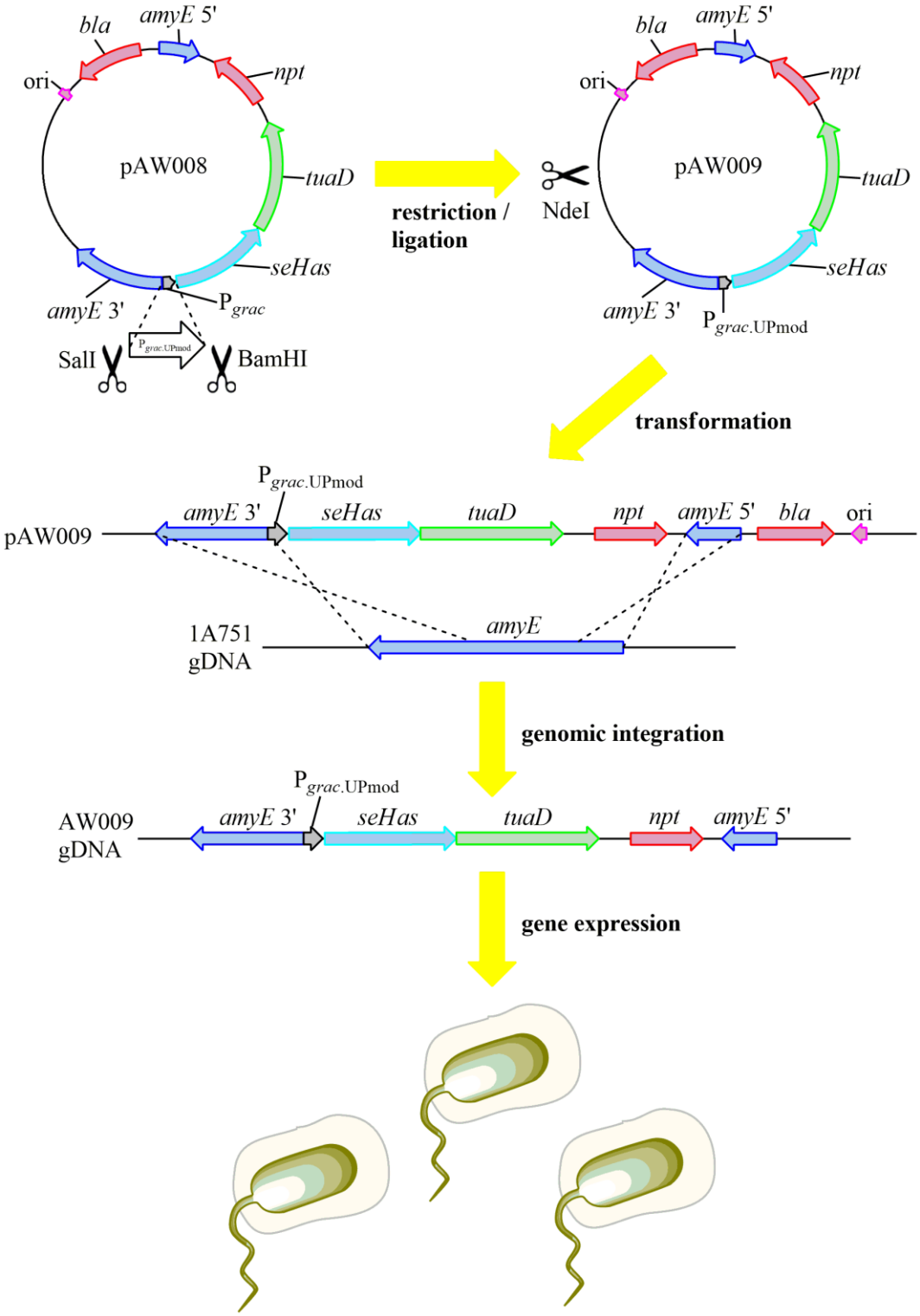

Figure S6.1. The derivation of an improved strain of *B. subtilis* for heterologous HA production. Genomic integration vector pAW009 was constructed by amplifying promoter $P_{grac.UPmod}$ from pHT01, followed by insertion into SalI/BamHI-digested pAW008. $P_{grac.UPmod}$ is a weaker derivative of promoter P_{grac} that has a modified upstream promoter element (UP) that reduces the relative promoter strength by approximately half. AW009 was constructed via transformation by natural competence of 1A751 with NdeI-linearized pAW009, resulting in the integration of a $P_{grac.UPmod}$::*seHas*:*tuaD* expression cassette and neomycin resistance marker (i.e. *npt*, encoding neomycin phosphotransferase) at the *amyE* locus. AW009 constitutively expresses *seHas* and *tuaD*, respectively encoding hyaluronan synthase from *S. zooepidemicus* (SeHAS) and native UDP-glucose-6 dehydrogenase (TuaD), resulting in the production of high MW HA and, in turn, encapsulation of AW009. AW009 produced approximately twice as much HA as our previous production strain, i.e. AW008, which was constructed via transformation of 1A751 with NdeI-linearized pAW008. Other genes and abbreviations: *bla* encodes β-lactamase for selection of *E. coli* on ampicillin; *amyE* encodes native α-amylase; origin of replication (ori); genomic DNA (gDNA)